Synthesis and Non-Covalent Interactions of Novel Phosphonium-Containing Polymers

Emily Baird Anderson

Dissertation submitted to the faculty of the Virginia Polytechnic Institute and State University in partial fulfillment of the requirements for the degree of
Doctor of Philosophy
in
Chemistry

Timothy E. Long, Chair
Richey M. Davis
Thomas C. Ward
Judy S. Riffle
S. Richard Turner

August 18, 2010
Blacksburg, Virginia

Keywords: phosphonium, imdiazolium, step-growth polymerization, ionomers, non-covalent interactions, Michael addition, multi-walled carbon nanotubes, ionic liquids, polyurethanes, polyesters, methacrylates

Synthesis and Non-Covalent Interactions of Novel Phosphonium-Containing Polymers

Emily Baird Anderson

Abstract

Phosphonium ions readily compare to ammonium ions in regards to their aggregate characteristics, thermal stability, and antibacterial activity. Ionic aggregation in phosphonium-based polymers provides thermoreversible crosslinks, ideal for reversible self-assembly, self-healing, and smart response. In polymers, these ionic functionalities aggregate, providing improved moduli, and altering the size and structure of ionic aggregates regulates polymer melt processability.

This dissertation highlights phosphonium-based chemistry for the synthesis of novel step-growth ionomers and structure-property relationships in ionic polymers. The synthesis of phosphonium endcapping reagents for melt polyester reactions afforded a thermally stable ionic functionality that controlled molecular weight. Weak association was present with phosphonium ions at low ion concentrations below 7.7 mole %. The use of novel ionic bisacetoacetate monomers in the formation of networks from Michael addition reactions led to the synthesis of ionic networks with increased and broadened glass transitions and improved tensile stresses at break and strains at break compared to those in the non-ionic networks. The first electrospun fibers from Michael addition crosslinking reactions are reported, and equilibrium ionic liquid uptake experimental results indicated that ionic functional networks absorb close to three times the amount of ionic liquid as non-ionic, poly(ethylene glycol)-based films. Chain-extending polyurethanes with a phosphonium diol and subsequently varying the hard segment content led to changes in ionic aggregation, crystallinity, and thermal transitions in the polymers.

Additionally, novel phosphonium-based methacrylate monomers incorporated into diblock copolymers with styrene exhibited microphase separation. Overall, the inclusion of phosphonium ions pendant to or in the main chain of various types of polymers led to changes in morphology, improved tensile properties, enhanced moduli, broadened transitions, changes in crystalline melting points, changes in solubility, and appearance of ionic aggregation.

Acknowledgements

First and foremost, I would like to thank my advisor Dr. Timothy E. Long for providing me with a well-rounded knowledge of polymer chemistry. He has provided me with a wealth of opportunities for which I am sincerely grateful. I would also like to thank Dr. Thomas C. Ward for his contribution in my recent obtainment of a post-doctoral position and all of his encouragement throughout the years. Teaching his short course experiments under his guidance and taking his viscoelasticity class have both profoundly influenced my career, and he has been one of single-best influences in my life for my future aspirations. I also am extremely thankful for Dr. S. Richard Turner, who also aided in my procurement of a post-doctoral position and who has been a great support and teacher the last five years. He always had an open door for me, and I am grateful for all of his guidance. I would also like to thank Dr. Judy S. Riffle for providing me with a phenomenal foundation in synthetic polymer chemistry my first year and her continued encouragement over my career at Virginia Tech. I would like to sincerely thank both Dr. Turner and Dr. Riffle for their tremendous help in revising my thesis and papers. They have donated a great deal of their time generously, despite their busy schedules. I also would like to thank Dr. Rick Davis for insightful discussions and supporting me as one of my committee members. I also thank Dr. Joseph S. Merola for his time and tremendous dedication to my degree. He has served as a valuable contributor to my degree this past year, and he spent a great deal of time working on my behalf regardless of his busy schedule. I sincerely appreciate all his efforts.

Many additional professors have contributed to my experience and research accomplishments at Virginia Tech, and I would especially like to thank Dr. Paul Deck, Dr. Robert B. Moore, Dr. David Dillard, Dr. James McGrath, Dr. Harry W. Gibson, and Dr. Garth L. Wilkes for their valuable time and assistance. I also thank Dr. Fredrick L. Beyer from the Army Research Labs for TEM training and for many helpful discussions over the years. I additionally thank ARL for their financial support and leadership. From Kodak, I would like to acknowledge Dr. Douglas R. Robello who provided me with a wonderful summer internship that has expanded my horizons and my knowledge of organic polymer synthesis and organic chemistry. He introduced me to the industrial world. I gained a wealth of experience from his leadership, and I am very grateful for the opportunity to meet and work for such a phenomenal organic polymer chemist.

I also would like to thank Mary Jane Smith, Angie Miller, Tammy Jo Hiner, Laurie Goode, and Millie Ryan who have helped me countless times for various tasks throughout the years. They were always there to help in any situation, and I greatly appreciated their time and consideration. Additionally, I thank Dr. Robert B. Moore, Jong K. Park, Steve McCartney, John MacIntosh, Tom Glass, Geno Innoa, and Victoria Long for their patience and analytical expertise.

I have had an amazing time getting to know my co-workers and now friends at Virginia Tech, and I want to especially thank Karina Kizjakina, Sampada Karkare, Nipa Deora, Amber Nicole Hancock, Dr. Susan Mitroka, Dr. Brian Mather, Dr. Kalpana Viswanathan, Dr. Sharlene R. Williams, Dr. Gozde Ozturk, Dr. Serkan Unal, Dr. Rebecca H. Brown, Dr. Qin Lin, Dr. Takeo Suga, Dr. John Layman, Dr. Tomonori Saito, Steve June, Matthew Green, Matthew Hunley, Nancy Zhang, Mana Tamami, Renlong Gao, and Jenny B. England for their help over the years.

I have had two great labmates in Hahn 3007, Dr. Brian Mather and Shijing Cheng who truly are the best labmates one could have. Thank you all for being my family over the last few years. I also want to thank Dr. Philippe Bissel, Dr. Kevin Miller, and Dr. Erin Murphy for their thoughtful scientific discussions, their expertise, and their guidance through writing and finishing my degree. I also want to thank Dr. Michael Rubinstein and Dr. Joseph M. DeSimone, two of my great inspirations who are the reasons that I am in the field of polymer chemistry.

I am also ever-indebted to my amazing fiancé, Dr. Kamal Idrisi. His support, love, and friendship make everything worthwhile. He believes in making all my dreams come true and reaching for that Nobel Prize, and I am forever grateful for his patience these past years while finishing my degree. In all my life, I never thought I would meet such a wonderful, loving, brilliant man. He is my number-one inspiration, and I dedicate my entire future to our happiness and success together in life. I am forever indebted to him for waiting on the other side of the world for me, come what may. He truly has defined our love for the storybooks.

Finally, I thank my father and mother, Douglas and Lee Anderson, who have made me who I am today and raised me with such unconditional love and support in all of my life's endeavors. They provided me with an amazing childhood and guidance, and my father truly is the sweetest, most-patience man. He is the best businessman I know, and I am thankful for his love and hard work which have made all my dreams come true. He was determined to give me everything I ever desired, and I am eternally grateful. My mother is also my best friend, and I would not be here without her. She is always there for me no matter what. I additionally thank my wonderful sister and brother, Keeley Anderson Pollard and Douglas Anderson, and all the rest of my extended family for their love and friendship. To anyone else who has known me and helped over the years, thank you. I am very blessed.

Attributions

Prof. Timothy E. Long – Ph.D. (Department of Chemistry, Virginia Tech) is the primary research advisor.

Rebecca H. Brown – Ph.D. (Department of Chemistry, Virginia Tech) conducted SEC experiments for PET-based polyesters for chapter 3.

Serkan Unal – Ph.D. (Department of Chemistry, Virginia Tech), aided in phosphonium-based polyester and phosphonium-based methacrylate experiments in chapters 3 and 7.

Matthew T. Hunley – Ph.D. (Department of Chemistry, Virginia Tech) aided with electrospinning networks from Michael addition reactions in chapter 4.

Steve M. June – Ph.D. candidate (Department of Chemistry, Virginia Tech) aided in AFM experiments in chapter 4 and 7.

Robert B. Moore – Ph.D. (Department of Chemistry, Virginia Tech) conducted all SAXS experiments on polyurethanes in chapter 6.

Jong K. Park – Ph.D. (Department of Chemistry, Virginia Tech) conducted all SAXS experiments on polyurethanes in chapter 6.

Steve McCartney – technician (Virginia Tech) aided in TEM and AFM experiments in chapter 6 and 7.

Jenny B. England – M.S. candidate (Department of Chemistry, Virginia Tech) aided with syntheses of imidazolium-based polyesters in chapter 10.

Mike Allen – Ph.D. candidate (Department of Chemistry, Virginia Tech), conducted all MTT assays in chapter 10.

Table of Contents

List of Figures

List of Tables

List of Equations

List of Abbreviations

Chapter 1: Introduction

1.1 Dissertation Overview

Ionomers are classically defined as polymers with 15 mole percent or less ionic groups, yet the ionic aggregation in isolated locations in the polymer governs thermal, mechanical, and morphological properties.[1] Ion-containing polymers attract much industrial attention due to their capability to dramatically improve bulk polymer properties with small changes in the type and percent of ionic functionalities. Physical crosslinking in the polymer due to ionic aggregation provides moduli and tensile improvements, reinforces the polymer, and regulates thermal stability and miscibility with inorganic additives.[1] They function as smart materials, providing improved actuation as transducers, and they improve the uptake of ionic liquid in polymers to generate enhanced conductivity in electro-active devices.[2-4] Ionomers also are known to have self-healing capability.[5] Ionomers often have their own ionic transition temperature where these ionic aggregates dissociate and reform, and energy transferred as heat upon impact and ionic aggregate thermoreversibility provide healing as physical crosslinks break and reconnect.[1,5]

Most ionomers reported in the literature have anionic groups attached to the polymer backbone and possess random placement of the ionic functionalities along the polymer chains.[1] In this research, we investigate cationic groups attached to the polymer backbone as well as regular placement of these functionalities. Phosphonium salts are particularly attractive due to their enhanced thermal stability[6] and antimicrobial ability[7] compared to widely-commercialized ammonium salts. The large phosphorus cation allows for weak ionic associations in the polymer that provide improved performance without detrimental effects on processing. Various phosphonium-containing monomers and endcapping reagents to include in high performance

polyesters, networks from Michael addition reactions, polyurethanes, and diblock copolymers were synthesized.

In chapter 3 of this dissertation, the thermal stability and control of molecular weight with phosphonium-containing endcapping reagents were investigated in high-temperature melt reactions to make telechelic polyesters. In chapter 4, novel phosphonium-based, imidazolium-based, and non-ionic crosslinking reagents were synthesized for Michael addition reactions and facilitated a study of the influence of ionic aggregation and ionic content on thermal, mechanical, and morphological properties of crosslinked films. We report the first electrospun fibers synthesized from Michael addition crosslinking reactions for both ionic and non-ionic networks. In chapter 5, carbon nanotube incorporation, tensile improvements, and resistivities were examined for non-ionic and ionic networks. In chapter 6, a novel phosphonium-based chain extender was used to regularly place phosphonium groups in the hard segment of polyurethanes. Additionally in chapter 7, novel methacrylate phosphonium-containing ionic liquid monomers were synthesized and incorporated into diblock copolymers with styrene. In chapter 8, phosphonium-based bisphenol monomers were prepared and their potential for use in syntheses of functional polysulfones was investigated. In chapter 9, imidazolium-based polymers are reviewed. In chapter 10, syntheses and cytotoxicities of several main-chain imidazolium-based polyesters are discussed. Overall, the thermal, mechanical, rheological, and morphological properties of various polyesters, polyurethanes, networks, and block copolymers containing phosphonium groups have been investigated in hopes to inspire future research on polymers that contain phosphonium chemistry.

1.2 References

1. Eisenberg, A., Kim, J. S. *Introduction to Ionomers*. Wiley: New York, 1998.
2. Duncan, A. J.; Akle, B. J.; Long, T. E., Leo, D. J. *Smart Mater. Struct.* **2009**, *18*, 104005.
3. Duncan, A. J.; Leo, D. J.; Long, T. E. *Macromolecules* **2008**, *41(21)*, 7765-7775.
4. Brown, R. H.; Duncan, A. J.; Choi, J.-H.; Park, J. K.; Wu, T.; Leo, D. J.; Winey, K. I.; Moore, R. B.; Long, T. E. *Macromolecules* **2010**, *43(2)*, 790-796.
5. Kalista, S. J.; Ward, T. C. *J. R. Soc. Interface* **2007**, *4(13)*, 405-411.
6. Xie, W.; Xie, R.; Pan, W.; Hunter, D.; Koene, B.; Tan, L.; Vaia, R., *Chem. Mater.* **2002**, *14*, 4837-4845.
7. Kanazawa, A.; Ikeda, T.; Endo, T., *Journal of Polymer Science: Part A: Polymer Chemistry* **1993**, *31*, 335-343.

Chapter 2: Molecular Design of Phosphonium-Containing Macromolecular and Supramolecular Structures

2.1 Abstract

Non-covalent interactions in polymers provide smart, reversible, and dynamic physical networks to afford directed self-assembly, self-healing, electro-activity, enhanced mechanical performance, unique morphologies, and other physical properties. Ionomers, or polymers containing 15 mole percent or less ionic functionality, advantageously allow for vast changes in physical polymer attributes with small modifications in the amount, type, and topological location of ionic functionalities. Alkyl ammonium-containing polymers are ubiquitous throughout the present literature, but their low thermal stability due to the Hofmann elimination presents difficulties in industrial applications and high-temperature processing. Unlike the ammonium cations, sodiosulfonate ionomers possess high thermal stability; however, their strong non-covalent associations often remain above thermal degradation temperatures and prevent processing. Utilizing a large cation with weak ionic associations may improve processability and provide valuable physical crosslinking interactions to impart control over physical polymer properties. The large phosphonium cation is ideal for these applications, for it provides weak, reversible associations yet is comparable to the ubiquitous sodiosulfonate- and ammonium-based derivatives. However, the field of phosphonium-containing polymers is relatively unexplored. This review elucidates the advantages of the phosphonium functionality as a means to obtain reversible, self-assembled, and physically-crosslinked macromolecular structures. Due to the limited literature on phosphonium-containing polymers, we hope to inspire

future research employing phosphonium-based polymers in electro-active devices, self-healing, and self-assembly.

2.2 Scientific Rationale

Phosphonium cations are readily compared to ammonium groups due to their aggregation,[1] phase transfer capability,[2] thermal stability,[3] antibacterial activity,[4] and electrostatic properties. The phosphonium functionality is attractive predominantly because of its higher thermal stability[3] and greater antimicrobial activity[4] compared to widely-commercialized ammonium derivatives. Phosphonium salts are also used as stabilizers[5, 6] and for adsorption onto substrates[7, 8] and find application in smart materials[9-13] and self-assembly.[14] Although using these salts presents several advantages, expense is a common reason for using the ammonium over the phosphonium functionality.[1] Also, alkyl phosphines are often pyrophoric and demand more cautious laboratory techniques.[15] Although phosphonium salts are ubiquitous in the literature, the study of phosphonium-based polymers is a relatively unexplored field.

For many applications, polymers offer benefits over small molecules, including non-volatility, improved chemical stability, low permeability through the skin, and recycling potential.[16, 17] Using polymeric phosphonium salts may also improve catalytic[2] and antimicrobial action[4] as well as better disperse silicate nanoparticles in a macromolecular matrix. The Wittig reaction is one case where polymer-supported phosphonium salts are growing more popular (Figure 2.1).[18,19] For example, Hodge and Waterhouse treated chloromethylated polystyrene in 1% or 2% crosslinked beads with triphenylphosphine for 60 hours at reflux in chlorobenzene.[19] The reaction produced quantitative conversion of all chloromethyl groups into phosphonium functionalities. Exposure of these phosphonium-containing beads to ambient conditions of

various aldehydes, solvent, and sodium hydroxide resulted in alkene-containing polystyrene beads. The various aldehydes included ferrocen-2-carboxaldehyde, formaldehyde, thiophen-2-aldehyde, and others.[19]

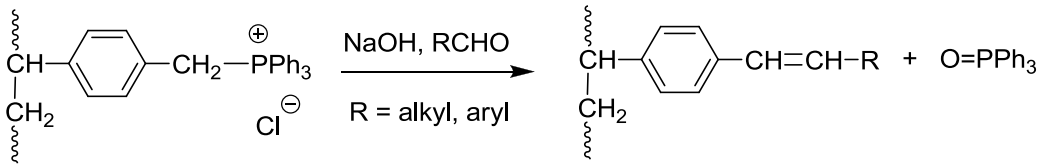

Figure 2.1. The Wittig Reaction with polymer-supported phosphonium salts;[19] Adapted from *Polymer*, 22, P. Hodge, J. Waterhouse, Chemical Modification of chloromethylated crosslinked polystyrene via phase transfer catalyzed Wittig reactions, 1153-1154, Copyright (1981), with permission from Elsevier

Phosphonium cations may improve the thermal stability of polymers,[3] help facilitate aggregation,[20] or aid in matrix reinforcement of ionomers.[21-24] Due to the enhanced thermal stability of phosphonium versus ammonium cations, phosphonium-containing polymers have many new or potential applications.

2.3 Phosphonium versus Ammonium Ions: Structure and Bonding

The strength of cation, anion, and conjugative interactions plays a role in the final structure and properties of phosphonium-based molecules. Phosphonium cations exhibit tetrahedral geometry with four two-electron bonds. Phosphorus often exists as the omnipresent phosphine oxide, phosphate, or phosphonate functionalities since the phosphorus 3d orbital and large size of the atom allow for additional bonding beyond satisfaction of its octet.[15] Phosphonium cations are synthesized from quaternization of phosphines. Due to a downfield

resonance shift from phosphine to phosphonium functionality, ^{31}P NMR is commonly employed to monitor phosphonium synthesis from precursor phosphines.

The greater electronegativity and smaller size of nitrogen compared to phosphorus leads to vast differences in the strength and dissociation of ionic interactions.[25-28] Electrostatic interactions decrease from phosphorus to nitrogen due to the larger size of the phosphorus atom and its capability to distribute charge on its surface. Nitrogen also possess shorter bond lengths with carbon, namely 1.53 Å, compared to P-C bonds at 1.81 Å.[28] Furthermore, the smaller ammonium atom facilitates tighter ion pairs than phosphonium functionalities, and the alpha-methylene protons for ammonium cations are more acidic than alpha-methylene protons for phosphonium cations due to inductive effects.[28] Hydrogen-bonding and anion contact is enhanced for ammonium over phosphonium salts, and all these combined effects elucidate the lower melting points for phosphonium salts compared to ammonium analogues. Many phosphonium salts exist as ionic liquids while ammonium molecules do not and more easily form a crystalline lattice. Melting points of phosphonium salts increase as the alkyl chain lengths on phosphorus are increased, but ammonium salts do not show a dramatic trend.[28] A delicate balance of packing forces between chains, electrostatic interactions, and lypophilic interactions exists. Phosphonium compounds, however, are more thermally stable and thus may be preferable for long-term use applications.[3,29]

2.4 Thermal Stability of Phosphonium versus Ammonium Salts

Phosphonium compounds possess thermal stabilities up to 70 to 80 °C higher than similar ammonium molecules by thermogravimetric analysis (TGA) ramps to 1000 °C at 2 °C/min under nitrogen.[3] Although phosphonium salts may thermally decompose through various mechanisms

compared to ammonium salts, the Hofmann elimination, its tight ion-pair association, and the increased acidity of β-protons prevent ammonium functionalities from reaching high thermal stability. However, anion basicity and sterics both play a vital role in final decomposition temperatures.[3]

In polymer chemistry, thermal stability is especially important for melt processing[23] as well as composite compounding.[30] Pan, Vaia, and co-workers examined thermal decomposition mechanisms of montmorillonite nanocomposites including phosphonium salts and mapped decomposition pathways for both alkyl and aryl salts compared to ammonium analogues.[3] Single-step decomposition was distinguished for the phosphonium salts alone, but incorporation into silicates added multiple decomposition steps.[3]

Pan and Vaia et al. outlined the many decomposition pathways for alkyl phosphonium compounds (Figure 2.2).[3]

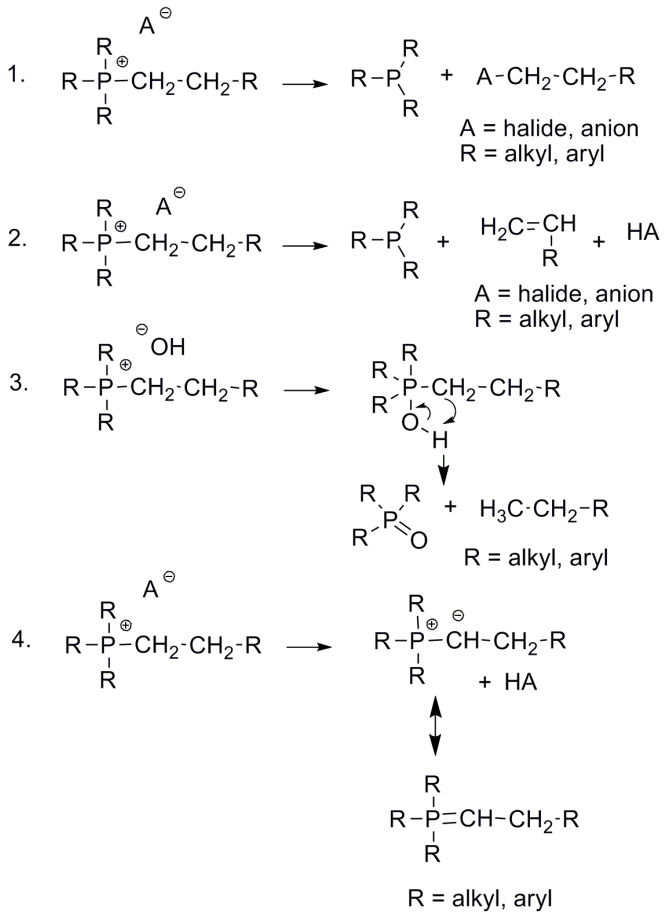

Figure 2.2. Thermal decomposition pathways for phosphonium groups in montmorillonite nanocomposites:[3] (1) reductive elimination, (2) β-elimination, (3) substitution and oxidation, (4) α-proton abstraction and formation of Wittig reagents; Adapted with permission from Xie, W.; Xie, R.; Pan, W.; Hunter, D.; Koene, B.; Tan, L.; Vaia, R. *Chem. Mater.* **2002**, *14*, 4837-4845. Copyright 2002 American Chemical Society

First, elimination can occur to produce starting material, phosphines, and alkyl halides. Second, proton β-elimination, or Hofmann elimination, creates phosphines, protonated halides, and alkenes. However, the Hofmann elimination in phosphonium versus ammonium functionalities occurs at much higher temperatures. Third, anion substitution with strong hydroxyl anions can promote oxidation to phosphine oxides and alkanes. This decomposition reaction especially

limits phosphonium applications in high-temperature or hydroxide-containing fuel cell applications. Fourth, a strong base, typically alkyl lithium, abstracts α-protons to produce phosphonium ylides and Wittig reagents. Reductive elimination, β-elimination, and substitution with a five-coordinate intermediate were the most common mechanisms seen with high-temperature thermal degradation since abstraction of α-protons requires the presence of a strong base.[3] Varying long alkyl chain lengths on phosphonium salts of 14 to 18 carbons showed no change in thermal stability, yet symmetric, long-chain alkyl phosphonium salts had higher thermal stability than short-chain, non-symmetric salts. Stability for long-chain alkyl salts and aryl salts was attributed to steric hindrance for the decomposition mechanisms listed.[3]

The aryl phosphonium salts also have a more limited scope of mechanisms for thermal decomposition through radical homolysis at temperatures exceeding 300 °C.[3] The aryl salts are particularly attractive due to high thermal stability, but synthesis of these salts often includes use of difficult-to-remove catalysts like nickel(II) bromide.[23, 24] The alkyl or aryl phosphonium cation's superior thermal stability of over 70 to 80 °C relative to ammonium ions by TGA ramps at 2 °C/min up to 1000 °C under nitrogen, and the control of stability with varying composition make application of these salts highly desired, yet synthetic strategies to polymeric phosphonium salts have received only moderate exploration.[3]

2.5 Current Synthetic Strategies for Phosphonium-Containing Macromolecules

2.5.1 Chemical Modification of Polymers with Alkyl and Aryl Phosphines

The vast majority of literature cites the use of chemical modification of polymers to create phosphonium-containing macromolecules. These modifications include: (1) polymerization of chlorine- and bromine-containing monomers followed by quaternization with

phosphines,[2,16] (2) chloromethylation or chlorination and bromination reactions on polymers followed by quaternization with phosphines,[20,31-32] (3) reduction of poly(phosphine oxides) followed by quaternization with alkyl or aryl halides,[33-34] and (4) transquaternization of ammonium to phosphonium salts with phosphines.[35]

Chemical modification of polymers can lead to heterogeneity in the polymer matrix (Figure 2.3).[36]

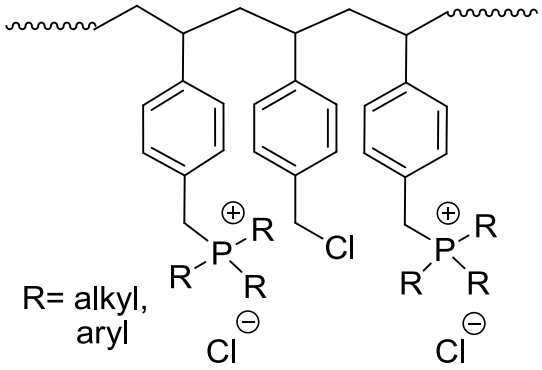

Figure 2.3. Incomplete quaternization due to neighboring group effects

Ionic aggregation and steric and electronic repulsion in a polymer can alter the kinetics and mechanisms of substitution reactions on the polymer chain, and the utilization of solvents to disperse the chains may not fully disrupt associations. Small changes in the amount of ionic functionality can lead to large changes in polymer properties including crystallinity, morphology, thermal transitions and mechanical performance.[21] All these polymer attributes depend on highly reproducible syntheses of polymers containing specified ionic functionalities, and precise percentages of chemical modification reactions can be difficult to reproduce.[36] Quaternization reactions on polymers proceed through second-order reactions where the conversion of neighboring groups slows the reaction rate through electronic repulsion and steric effects.[36] Retardation reactions can lead to isolated, unreacted groups along the chain (Figure 2.3).

Additionally as the polymer changes from neutral to a polyelectrolyte, solvation and aggregation present challenging problems, and conversion is typically less than 100%. Parent et al. studied the reaction kinetics and conversion of brominated poly(isobutylene-*co*-isoprene) polymers.[20] When using a 3-fold excess of triphenylphosphine at 100 °C, deceleration occurred due to neighboring group effects during conversion, and a 1:1 ratio of phosphine to alkyl bromide resulted in even slower rates.[20]

Using a large excess of phosphine increased reaction rates for chloromethylated or alkyl-halide-containing polymers reacted with phosphines. Alternatively, the use of alkyl instead of aryl phosphines and methyl iodide can lead to more quantitative yields.[15,33] High pressure and high temperature improves reactions with secondary alkyl halides.[15] The most common route to phosphonium-containing polymers remains quaternization of chloromethylated polymers with air-stable phosphines like triphenylphosphine. The reactivity of alkyl phosphines is dependent on steric hindrance. As the number of carbons in the alkyl chains attached to phosphorus is increased, the reactivity towards chloromethyl groups decreases.[7,37] Nishikubo et al. modified polychloromethylstyrene with tripropylphosphine and achieved 96.6% conversion to phosphonium groups.[7] Conversion with trihexylphosphine peaked at 87.8% for uncrosslinked and 72.1% for crosslinked polymers. Crosslinked polymers showed significantly lower conversions via chemical modification reactions.[7]

Coupling reactions catalyzed with nickel(II) bromide are a less common route, possibly due to extensive catalyst removal steps required after the synthesis is complete.[23, 24] McGrath et al. synthesized poly(arylene ether) phosphonium ionomers in good yield from standard aryl halide coupling reactions using nickel(II) bromide and a polyphosphine (Figure 2.4).[33] Horner's standard procedure was used.[33, 38]

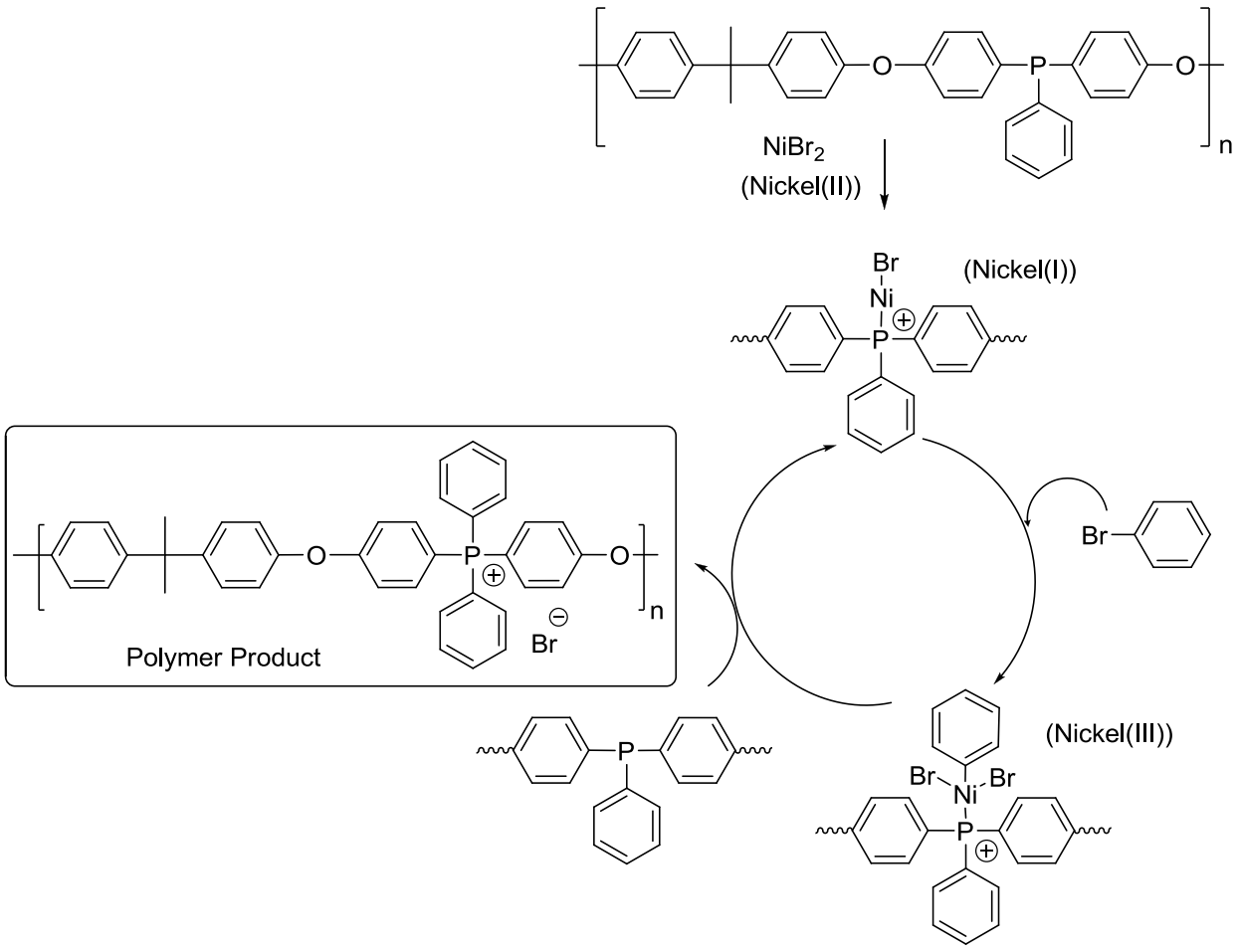

Figure 2.4. Nickel(II) bromide coupling reaction on poly(arylene ether phosphines)[15,33,38] H. Ghassemi; D. J. Riley; M. Curtis; E. Bonaplata; J. E. McGrath: Main-Chain Poly(arylene ether) Phosphonium Ionomers. *Appl. Organometal. Chem.* 1998. Volume 12. Pages 781-785. Copyright John Wiley and Sons. Adapted with permission. L. Horner; G. Mummenthey; H. Moser; P. Beck: Phosphororganische Verbindungen, 51. Die Einführung von Arylresten in tertiäre Phosphine mit Hilfe von Komplexen der übergangsmetalle (Komplexsalzmethode). *Chemische Berichte.* 1966. Volume 99, Issue 9. Pages 2782-2788. Copyright Wiley-VCH Verlag GmbH & Co. KGaA. Adapted with permission

2.5.2 Synthesis of Phosphonium-Containing Monomers and Endcapping Reagents

Few reports of phosphonium-containing monomer syntheses exist. Phosphonium derivatives of vinylbenzyl monomers,[4,39-40] brominated phenylacetylene,[41] bis(bromoalkyl) diacetylene monomers,[42] and diallylphosphonium halides[43] culminate the list of phosphonium containing monomers. Due to the nature of currently employed quaternization reactions on polymers, expansion of phosphonium-containing monomer syntheses solves many issues with reproducibility and high conversion. Many of these monomers also possess properties of common ionic liquids.

Endo et al. synthesized several 3-and 4-(vinylbenzyl)phosphonium chlorides.[4] He and his colleagues synthesized phosphonium monomers through reaction of triethylphosphine, tributylphosphine, triphenylphosphine, and trioctylphosphines with chloromethylstyrene.[4] Dimethyldecyl, dimethyltetradecyl, or dimethyloctadecyl(4-vinylbenzyl)phosphonium chloride monomers were also prepared using similar methods and then compared to 4-ethylbenzyl derivatives.[4,39] These quaternization reactions proceeded at room temperature as opposed to chemical modification on polymers at 100 °C or greater.[4,20] Characterization of these monomers was limited in the manuscript, although rapid absorption of water was noted on their contact with air.[4]

To date, solution phase, free-radical polymerization reactions initiated with 2,2'-azobis-2-amidinopropane·HCl or azobisisobutyronitrile (AIBN) are the most common methods used to polymerize vinyl phosphonium salt monomers. Endo et al. found stringent removal of air necessary for polymerization, and reaction tubes were degassed with three freeze-pump-thaw cycles, sealed, and then polymerized at constant temperature.[4] Nitrogen was used in the synthesis of all phosphonium monomers, and no detail of the type of seal for the polymerization tube was

described.[4] Polydispersity data is often not provided for phosphonium-based polymers due to high ionic aggregation or insolubility.[4,40]

Blumstein et al. and Wherrett et al. functionalized acetylene monomers.[41,42] They successfully quaternized brominated phenylacetylenes with phosphines. Blumstein et al. discovered that unlike ammonium-based acetylenes, phosphonium-based acetylenes would not spontaneously polymerize under ambient conditions.[41,42] High electron affinity of phosphorus aided in the stabilization of the acetylene monomer. Brominated polyacetylene was first prepared, followed with addition into phosphine solutions.[41] ^{13}C, ^{31}P, and ^{1}H NMR spectra, UV Vis spectra, and FTIR spectra confirmed the structure and that the phosphorus center was connected directly to a carbon in the polymer's double bond.[41] Phosphonium salts tailored the structure, reactivity, and stability of final polymers.

Blumstein et al. utilized pyridine or heat to initiate the polymerization of phosphonium-containing acetylenes.[41] The authors synthesized black, lustrous, phosphonium-based polymers, and it was reported that steric hindrances in the final polymer induced unique polymer thermal instability compared to the thermal stability of the monomers.[41] Post reactions on these materials resulted in complete quaternization as confirmed with ^{1}H NMR spectra, ^{31}P NMR spectra, and IR spectra. Interestingly, the authors proposed the reaction followed a zwitterionic-anionic mechanism similar to the theory of Balogh and Blumstein (Figure 2.5).[41,42,44]

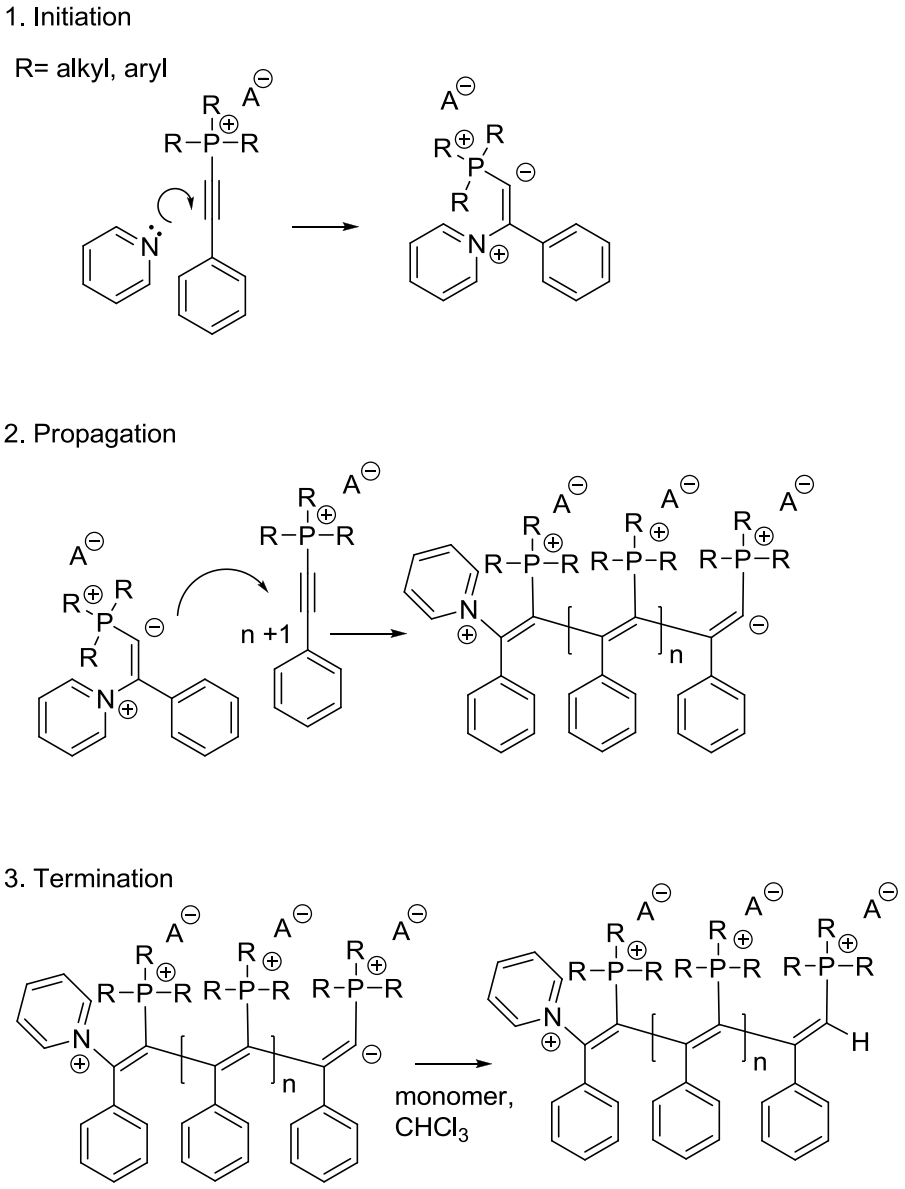

Figure 2.5. Zwitterionic mechanism of phosphonium-based polyacetylene propagation;[41] Adapted from *Polymer*, 38/3, P. Zhou, A. Blumstein. Conjugated phosphonium polyacetylenes, 595-604, Copyright (1997), with permission from Elsevier

In this mechanism, pyridine attacks the acetylene monomer at the phenyl-substituted carbon. Quaternization results, and the phosphonium-substituted carbanion is formed. The zwitterionic monomer propagates due to attack of the anionic carbon on more phosphonium-based

phenylacetylene monomer. Polymerization occurs with initiation, propagation, and termination steps. Low degrees of polymerization resulted from ionic aggregation and termination through proton transfer from chloroform or monomer.[41] However, Blumstein et al. reported one of the first phosphonium-based alkynes and phosphonium-containing zwitterionic polymerizations.

Seyferth et al. reported cyclopolymerization of diallyldiphenylphosphonium halide (Figure 2.6).[43]

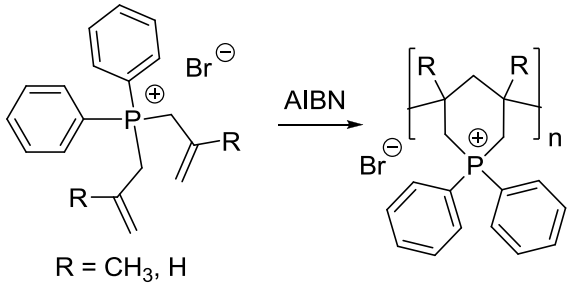

Figure 2.6. Cyclopolymerization of diallyldiphenylphosphonium halide;[43] Adapted with permission from Seyferth, D.; Masterman, T. C. *Macromolecules* **1995**, *28,* 3055-3066. Copyright 1995 American Chemical Society

High initiator and monomer concentrations were required for polymerization to proceed, and allylic hydrogens on the monomer caused degradative chain transfer. The authors note that the high initiator concentrations required were not consistent with typical polymerization procedures to achieve high molecular weights. Solubility issues were mentioned in the experimental for the initiator and polymer. Perhaps better selection of initiator and solvent is needed. As confirmed by ^{31}P NMR spectra, both 5-membered and predominately 6-membered rings were formed during the reaction. The resultant polymer was amorphous and hygroscopic, forming a hydrate with 0.5 equivalents of water per phosphonium group as determined by Karl Fischer titrations. Heating the polymer at 100 °C for one week still did not dry the polymer.[43]

2.5.3 Synthesis of Phosphonium-Endcapped Polymers

The synthesis of phosphonium endcapping reagents for polymers allows control of size and spacing of ionic aggregates and adds molecular weight control for step growth reactions. Soutar et al. and Long et al. exercised this method to produce functionalized phosphonium-based polymers.[23, 24, 45]

Phosphorus-terminated poly(1,3-butadiene) was first synthesized with Soutar et al.[45] Anionic methods were used to synthesize 2,000 to 10,000 g/mole polybutadiene oligomers terminated with "living" butadienyllithium endgroups. Chlorodiphenylphosphine, chlorodiethylphosphine, and chlorodicyclohexylphosphine endcapped the living polymers with phosphine functionality, and quaternization reactions *in situ* with iodomethane followed. Quaternization was quantitative. However, endcapping the polymers with chlorophosphines yielded only 50-93% phosphorus-endcapped polymer. Radical coupling of chains was evident due to the appearance of a coupled byproduct with two phosphine ends, and a single electron transfer mechanism was suggested as a possible culprit. Polymer dispersities were 1.17 to 1.25.[45]

To study the microstructure of the polymer termini, 5,5-dimethylhex-2-enyllithium (neopentylallyllithium) was prepared from t-butyllithium and butadiene.[45] A model reaction of this reagent with chlorophosphines $PClR_2$, where R equaled phenyl, ethyl, or cyclohexyl groups, followed with methyl idodide resulted in phosphonium-based alkenes with three configurations, 1,4-cis (Z), 1,4-trans (E), and 1,2. These model compounds were used to determine the ^{31}P NMR resonances for the polymer termini. Subsequently, the authors used ^{31}P NMR on their polymers compared to these model compounds to show preference for 1,4-cis (Z) configuration of the phosphonium-containing alkene at the terminus, followed with trans and then 1,2.[45] Dynamic

mechanical analysis (DMA) also confirmed a thermal transition related to dissociation of the ionic aggregates for each polymer between 73 to 120 °C.[45]

Our research group previously investigated the synthesis of a monofunctional phosphonium-containing endcapping reagent, *p*-carboxyphenyl trioctylphosphonium bromide for use in high-temperature melt polyesterifications (Figure 2.7).[23,24]

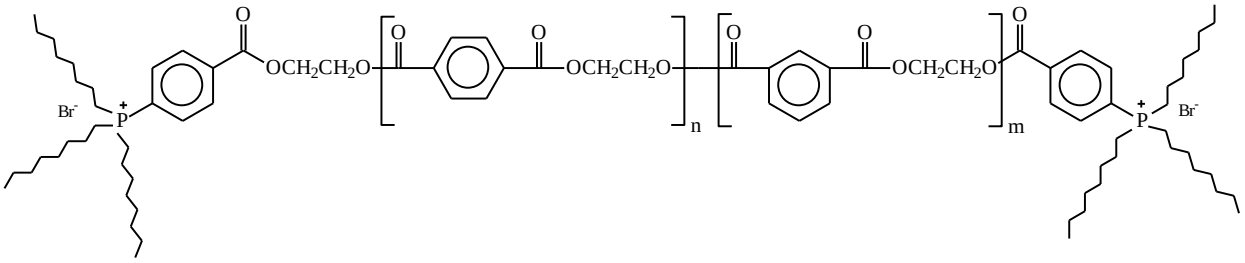

Figure 2.7. Phosphonium-endcapped polyesters;[23-24] Reproduced with permission from Unal, S. Synthesis and Characterization of Branched Macromolecules for High Performance Elastomers, Fibers, and Films. Ph.D. Thesis, Virginia Polytechnic and State University, Blacksburg, VA, 2005.

Synthesis of the endcapping reagent involved nickel(II) bromide catalyzed coupling of 4-bromobenzoic acid and trioctylphosphine at 170 °C over 24 hours under argon. Several washing steps and five recrystallization steps were required to purify the compound and remove nickel(II) bromide. Synthesis of linear and branched poly(ethylene terephthalate)-*co*-poly(ethylene isophthalate) (PET-*co*-PEI) with typical melt polymerization conditions produced oligomeric polyesters. The endcapping reagent was added with continued polymerization under reduced pressure at 220 °C to 275 °C for 2-3 hours, but discolored products resulted.[23, 24]

Allyl phosphonium salts, phosphonium ylides, and benzyl triphenylphosphonium salts initiate polymerization.[46-48] These reactions present future ways to endcap polymers while controlling molecular weight and dispersity. For example, photopolymerization of ethyl cyanoacrylate through a zwitterionic mechanism was reported through the use of benzyl triphenylphosphonium hexafluoroantimonate or (anthracen-9-ylmethyl)triphenylphosphonium hexafluoroantimonate.[47] Yagci et al. used anion exchange to enhance salt activation with light absorption, and homolytic and heterolytic cleavage of phosphonium molecules resulted in benzyl radicals, triphenylphosphonium radical cations, benzyl cations, and triphenylphosphine.[47] Triphenylphosphine initiated polymerization of ethyl cyanoacrylate. Addition of triphenylphosphine to the vinyl group creates a zwitterionic molecule that polymerizes through a zwitterionic mechanism. The stabilized anionic alpha carbon attached to the ester and the cyano groups facilitates polymerization to produce a phosphonium endcapped product. Initiation of methyl methacrylate (MMA) did not occur due to the less electrophilic character of the monomer.[47] However, a free radical mechanism of initiation was cited for MMA polymerization with benzyl triphenylphosphonium bromide due to photolysis of the benzyl triphenylphosphonium bromide into the phosphonium radical cation and the benzyl radical.[51] Bajpai et al. proposed that the benzyl radical caused subsequent initiation, and the phosphonium radical cation underwent various side reactions and terminated polymer chains.[51]

Yagci et. al reported that allyl phosphonium salts rapidly produced phosphonium-based radical cations through reaction with radical initiators and an addition-fragmentation mechanism.[46] The authors suggested that subsequent polymerization of cyclohexene oxide and other cationic-polymerized monomers occurred due to proton abstraction from the solvent or monomer to generate H^+ or due to direct initiation from the phosphonium-based radical cations

themselves (Figure 2.8).[46, 52] Further and future investigation of initiation and termination steps was suggested.

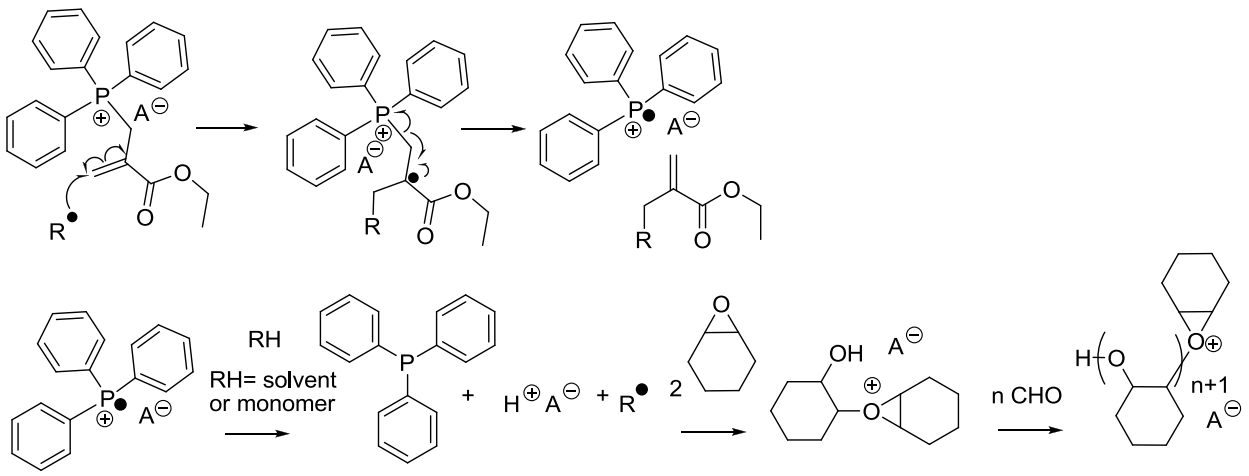

Figure 2.8. Addition and fragmentation of an allyl phosphonium salt with a radical initiator and cationic polymerization of cyclohexene oxide;[46, 52] Adapted from *Polymer*, 41/16, L. Atmaca, I. Kayihan, Y. Yagci, Photochemically and thermally induced radical promoted cationic polymerization using allyl phosphonium salts, 6035-6041, Copyright (2000), with permission from Elsevier. Adapted from *Polymer*, 37/13, Dietmar Dossow, Qin Qin Zhu, Gürkan Hizal, Yusuf Yaci, Wolfram Schnabel, Photosensitized cationic polymerization of cyclohexene oxide: A mechanistic study concerning the use of pyridinium-type salts, 2821-2826, Copyright (1996), with permission from Elsevier

Radicals first added to the vinyl group on the phosphonium molecule, then phosphonium radical cations were generated through decomposition. This radical cation initiates polymerization or acts as a chain transfer agent through abstracting hydrogens. Triphenylphosphine radical also endcaps and terminates chains.[46] Phosphonium initiators, endcapping reagents, and ionic liquids facilitate regulation of reaction rate, chain transfer, and functional chain ends.[46-53]

2.6 Physical Properties and Applications of Phosphonium Salts

2.6.1 Phosphonium-Containing Composites and Thermal Stability

Phosphonium salts find application as flame retardants,[54] thermal stabilizers,[30, 54] mass transport aids,[55] and compatibilizers[6] in polymer composites. In specifically layered silicate nanocomposites, either of two levels of compounded structure exist including exfoliated and intercalated structure.[30] Exfoliated silicate layered nanocomposites have dispersed silicate in the polymer, and intercalated layered nanocomposites have a stratum of polymer and silicate. Microcomposites are a different type of nanocomposites with a fine distribution of silicate. Phosphonium compounds are attractive because composite mixing, processing, and formation require high temperatures, and phosphonium salts have higher thermal stability than commonly used ammonium salts. For example, ammonium bentonite decomposes 70 °C lower than phosphonium bentonite due to Hofmann elimination.[30] Thermal stability is particularly critical for processing of composite materials. Pan and Vaia et al. studied the mechanisms of decomposition for both ammonium- and phosphonium-containing montmorillonites using thermogravimetric analysis (TGA), pyrolysis GC-MS, high-temperature X-ray diffraction, and FTIR.[3] Phosphonium salts decomposed through various pathways compared to ammonium salts; however, ammonium-containing montmorillonites were overall less thermally stable than phosphonium-modified compounds.[3]

Faroq et al. utilized the thermal stability of phosphonium salts in flame retardant applications.[54] Treatment with flame-retardant phosphonium salts such as phosphonium salt-urea-ammonia polycondensates reduced flammability of cotton textiles. Faroq and colleagues found that phosphonium salts raised the activation energy required for ignition compared to

cotton without any treatment. Diffusion control contributed to their higher activation energies, since the salts presented a diffusion barrier and insulator to prevent loss of volatiles.[54]

Phosphonium salts also find applications as compatibilizers and stabilizers.[6,30,54] Aggregated rather than uniformly distributed silicate stiffens the polymer matrix and decreases elastomeric properties, but incorporation of hydrophilic and ionic polymer endgroups promotes adhesion to the silicates.[6] Transmission electron microscopy (TEM), wide-angle X-ray scattering (WAXS), and NMR techniques were utilized to evaluate the effects of phosphonium salts on nucleation and distribution. TEM imaging confirmed that phosphonium salts performed better than ammonium salts in dispersing bentonite in an epoxy matrix.[30] The phosphonium bentonite also possessed improved fire resistance compared to ammonium compounds.[30] Phosphonium and ammonium surfactant absorption on silica nanocomposites was examined with electron spin echo techniques.[56] Electron spin echo techniques were used to show interaction between the surfactant, polymer, and nanocomposite material. Morphologies were assessed based on excess surfactant, stoichiometric amounts, and limiting values. Multiple morphologies were seen with excess or limiting amounts of surfactant.[56] Tributylhexadecylphosphonium bromide (HTBP) had a small transition in the composite at approximately 30 °C, and this transition was around 20 °C in the surfactant alone. These transitions represent dissociation of aggregates and surfactant layers.[56]

Parent et al. employed one of the first phosphonium-containing polymers as a matrix for composite materials.[6] Polyisobutylene ionomers formed elastomeric composite materials due to improved exfoliation of ammonium ion-exchanged montmorillonite clay in the polymer matrix and enhanced strength compared to analogous non-ionic polyisobutylene composites.[6] Also, tensile and mechanical properties of zinc-oxide-cured polyisobuylene were compared to the ionic

polymers. The authors indicated that polyisobutylene crosslinked with ZnO provided composites testable with tensile techniques and similar in structure to the ionic polymers due to the ionic physical crosslinking of phosphonium groups. Viscosity and ^{1}H NMR spin relaxation studies confirmed ion-pair aggregation in the phosphonium-containing polymer.[20] Compounding at 100 °C did not result in significant degradation of phosphonium endgroups.[6] Modulus and tensile strength improvement in ionic polyisobutylenes were also observed compared to nonionic, crosslinked and uncrosslinked polyisobutylenes. Low loadings of clay for non-ionic crosslinked polyisobutylene showed no improvement on tensile and mechanical properties, and high loadings only decreased performance. For the phosphonium-based polymers, the clay instead acted as a reinforcing filler for up to 30 weight percent clay with little agglomeration of the filler, but tensile and mechanical experiments showed clay agglomeration at all loading levels for the non-ionic analogs.[6]

Minteer et al. studied ion-exchanged Nafion® for specifically mass transport properties to determine if increasing the pore size of Nafion® would allow the transport of large molecules in redox or biological entrapment applications.[55] Minteer et al. also has shown that ionic-modified Nafion® traps small redox couples, allowing larger redox couples to transport to the electrodes and increase electrochemical flux.[57] Nafion® modified with phosphonium salts maintained greater sulfonic acid proton exchange with the cations than membranes modified with ammonium salts.[55] The protons on sulfonic acid groups exchange with $X^{+}A^{-}$ to form $-SO_3X$ and $H^{+}A^{-}$ where A^{-} is the anion and X^{+} is the cation. Casting Nafion® with phosphonium salts with a higher hydrophobicity than ammonium salts produced larger pore sizes than the ammonium-modified polymers. Thus, membranes with phosphonium-containing polymers showed greater transport of large molecules. Overall, phosphonium compounds were able to improve diffusive

mass transport with minimal effect on the proton exchange compared to ammonium salts due to the greater hydrophobicity of the phosphonium cation and less agglomeration with the sulfonic acid exchange sites. Hydrophobic interactions are also important in trapping and transport of ions and neutral material in Nafion® membranes.[55] Alkyl chain length may influence diffusive mass transport more than the effects of using ammonium versus phosphonium cations and should also be investigated.

2.6.2 Phosphonium-Containing Ionomers, Ionic Aggregates, and Self-Assembly

Ionomers are commonly described as polymers with less than ~15 mole percent ionic sites, and they are attractive for their capacity to reinforce a polymer matrix.[21] Ionic content in a polymer can serve as thermoreversible crosslink points to facilitate processing at high temperatures.[21] At ambient conditions, low molecular weight polymers containing thermoreversible crosslinks and could have properties similar to high molecular weight analogs.

Morphological and rheological characterization is critical to examining potential thermoreversible properties of phosphonium-based ionomers. Eisenberg, Hird, and Moore proposed a morphological model of random ionomers based on small angle X-ray scattering (SAXS) and DMA.[22] In this theory, ionic material in a polymer existed as aggregates or small groupings called multiplets, and this was dependent on the ion content.[22] Polymer chains wrapped around and surrounded the multiplets, and agglomeration could be controlled by the type and amount of charged material. These aggregates can be large enough to produce a SAXS ionic peak, and they can phase separate. DMA or differential scanning calorimetry (DSC) can measure the glass transition temperatures of phase separated ionic domains.[22] Soutar et al. showed that phosphonium-terminated polybutadiene polymers between 2,000 and 10,000 g/mole

have an ionic transition between 70 and 102 °C for polymers with diethylmethyl and dicyclohexylmethyl phosphonium endgroups.[45]

Residual catalyst and mobile ionic sites serve as nucleation sites for crystal growth.[58] Xin et al. showed that mixing polystyrene and polyethylene ionomers with poly(ethylene terephthalate) (PET) increased the crystallization rate.[59] However, ionic aggregation that persists in the melt hinders chain mobility and prevents full availability of the ionic sites, which in-turn has countering effect on the crystallization rate. Long et al. showed that telechelic PET sodiosulfonate ionomers displayed a slower crystallization rate compared to polymer without ionic content.[60] In these sodiosulfonate telechelic polyesters, the ionic aggregates persisted even above 150 °C, and increased viscosity accounted for the slower crystallization rates.[60] Colonna et al. discovered the same thing for sodiosulfonate-based telechelic poly(butylene terephthalate) (PBT) ionomers.[61] The ionic groups retarded mobility, leading to slower crystallization rates.[61]

SAXS is used to confirm ionic aggregation, and DMA is used to confirm the thermoreversibility of ionic aggregates with a transition indicating the dissociation and/or association of them. However, other techniques show that phosphonium groups hinder mobility and mechanically reinforce polymers through their ionic aggregates. Viscosity measurements and melt rheology are commonly used examples. In rheological studies, the melt viscosity of sodiosulfonate-terminated PET was shown to be higher than dodecanol-endcapped analogs, indicating ionic reinforcement in the polymer matrix.[60]

More interestingly, ionic aggregation has led to broadened ^{1}H NMR peaks in polyisobutylene ionomers. ^{1}H spin-spin relaxation measurements quantified local and chain mobility.[20] Measurement of spin-spin relaxation requires a 90 degree pulse with successive 180 degree pulses. T_2 values, the time required to randomize spins of local protons in the transverse

plane, are recorded. In polyisobutylene ionomers, T_2 values of isobutylene resonances showed equal mobility for phosphonium-based polymers with random attachment of phosphonium groups compared to brominated, non-ionic polyisobutylene with random attachment of bromine along the polymer chain.[20] However, unlike the other isobutylene resonances, the T_2 values of the allylic hydrogens of phosphonium-containing polymers relaxed faster than bromine-containing controls.[20] Ion-pairs restricted mobility of the allylic groups, and this finding supported the existence of ionic aggregation.[20, 22] Spin-spin relaxation experiments is useful to measure diffusion coefficients and local environment restrictions not previously quantified. Viscosity measurements of the phosphonium-containing polymers showed an increase in intrinsic viscosity as the methanol content was increased in chloroform/methanol polymer solutions, suggesting that addition of methanol disrupted the ionic aggregates. With increasing methanol in chloroform/methanol solutions, ^{1}H NMR resonance positions shifted, and the resonances had widths and positions similar to model compounds.[20]

Proton spin-lattice relaxation times and spin-spin relaxation can also be utilized to analyze electrostatic and non-electrostatic forces in small molecule phosphonium and ammonium salts.[26] Spin-lattice relaxation times of local protons are measured with a 180 degree pulse followed by a 90 degree pulse. Free induction decay signals are monitored and used to calculate T_1, the spin-lattice relaxation time. Neutron scattering and diffraction studies also indicated that electrostatic forces were not the only forces affecting structure and movement.[26, 62-63]

2.6.3 Phosphonium-Based Polyelectrolytes, Surfactants, and Self-Assembly

Phosphonium-based polyelectrolytes find potential application as stabilizers,[6] smart materials,[9-13] and antimicrobial agents.[40, 64] Gene therapy and chemotherapeutics are other

potential future applications.[65-68] Ikeda et al. reviewed physical applications of phosphonium ions as antimicrobial agents and liquid-crystalline molecules.[69] The authors tried to link physical state and morphology with antimicrobial behavior, explaining that the availability of ionic sites due to ionic aggregation and morphology was critical to antibacterial activity. They describe ionic structure, morphology, and micelle formation all as important regulators of antimicrobial activity. Large aggregates limited antimicrobial behavior, and the authors pointed out that most long-alkyl-containing phosphonium salts readily aggregated and were also liquid crystalline. They investigated trimethyl or dimethylphosphonium salts with respectively one or two long 10-, 14-, or 18-carbon chains. With long alkyl groups, these phosphonium molecules had liquid-crystalline properties.[69] Organizational ability of phosphonium salts was found superior to ammonium analogs, but this higher organizational activity is not well understood.[69]

Phosphonium-containing polyacetylene is currently under investigation as a smart material. Control of chain conjugation length in phosphonium-based polymers governs switching action catalyzed with light, heat, or solvent. Dichroism and helix-to-coil transitions in polydiacetylenes are facilitated with this smart response.[9-13] Calvin-Lewis analysis using (λ^2_{max} = kn) where n is the conjugation length and λ is the wavelength of the ultraviolet absorption of the polymer can be utilized to calculate extended chain lengths.[41] Conjugated phosphonium-containing polyacetylenes possess much longer conjugated lengths or extended chain structures than non-ionic analogs due to electrostatic repulsion of phosphonium groups in the chain (Figure 2.5).[41]

Nishikubo et al. studied polymeric photosensitizers containing both pendant photosensitizing groups (-NO_2) and also pendant phosphonium salts.[37] These polymers were used to photoisomerize small molecules in water or hydrophilic solvent. Photochemcial valence

isomerization is important in the storage of solar energy which has utilized the isomerizaiton of norbornadiene to quadricyclane.[37] Hydrophilic interactions between the small molecule reagents and the polymers occurred due to the hydrophilic phosphonium cations. These substrate-attraction interactions directed the small molecule reagents to the pendant photosensitizers. Potassium 3-phenyl-2,5-norbornadiene-2-carboxylate[37] and potassium cinnamate[7,8] both showed enhanced photochemical valence isomerization with the phosphonium-containing polymers compared to non-ionic polymers.

Photosensitizers transfer energy to other molecules to promote isomerization. Self-quenching due to mobility restrictions in polymers compared to small molecules has limited the application of polymeric photosensitizers.[70] The active photosensitizers on the polymer were 4-nitroxyphenoxy groups, but phosphonium salts on the polymer chain were used for self-assembly. Potassium *p*-nitrophenoxide and various phosphines were used to functionalize polychloromethylstyrene.[7] The substrate-attraction of phosphonium groups helped aid the cis/trans photoisomerization by placing the $-NO_2$ groups next to the small molecule reagents, and photosensitizing ability for the photosensitizing groups on phosphonium-containing polymers was larger than ammonium salt analogs.[7] Increasing the alkyl length of the groups attached to phosphorus resulted in decreased photoisomerization rates, perhaps due to aggregation of the ionic polymers. The phosphonium groups effectively blocked self-quenching of photosensitizing nitro groups to allow uniquely higher rates for polymers than small molecule models.[7]

Phosphonium functionalities were more efficient at substrate-attraction in these polymers than ammonium groups, which subsequently aided in photoisomerization.[37] Promotion of isomerization of potassium 3-phenyl-2,5-norbornadiene-2-carboxylate was found in the presence

of both 15 mole % *p*-nitroanisole photosensitizer and phosphonium-containing polymer (Figure 2.9).

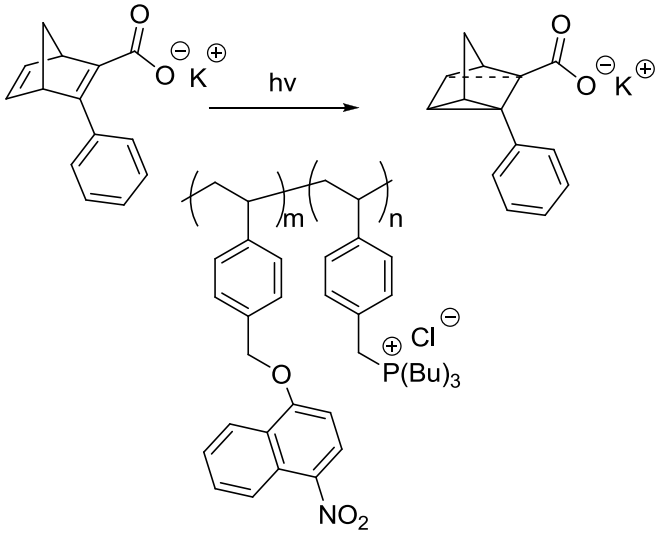

Figure 2.9. Photoisomerization of 3-phenyl-2,5-norbornadiene-2-carboxylate;[37] Adapted with permission from Nishikubo, T.; Kawashima, T.; Inomata, K.; Kameyama, A. *Macromolecules* **1992**, *25*, 2312-2318. Copyright 1992 American Chemical Society

Without phosphonium groups, isomerization was not found. Phosphonium groups attracted 3-phenyl-2,5-norbornadiene-2-carboxylate to the polymer chain, and isomerism was allowed due to energy transfer from nitrate groups on the polymer. Photosensitizing ability was very dependent on polymer composition and the number of photosensitizing groups incorporated in the polymer.[37]

The polarity and structure of phosphonium salts was useful to align nitrate groups with reagents in photosensitizing reactions, but phosphonium salts also find application as gelling reagents; the structure of the phosphonium cation is critical to consider. Abdallah and Weiss investigated small molecule thermoreversible "gelators" with long-chain phosphonium salts (Figure 2.10).[29] The aggregative properties of phosphonium and ammonium salts combined with

Van der Waals attractive forces of long-chain alkyls allowed these unique salts to form a network in a standing liquid. A colloid with a well-mixed portion of both sol and gel is a gelator.[71] Although ammonium gelators retained a network structure for longer times due to stronger ionic interactions, phosphonium gels were reversed to liquids and regelled more times than the ammonium salts due to thermal stability of the phosphonium cation.[28] The phosphonium gelators have lower gelation temperatures and provided homogeneous dispersions. Solubility of the salt also affects the capacity to form a gel in an organic liquid.[28]

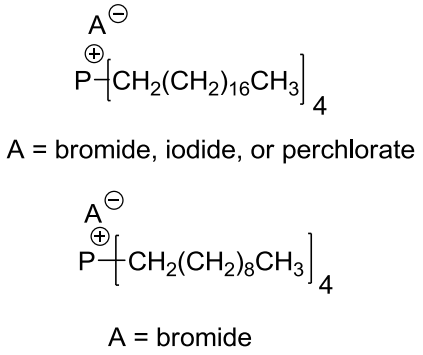

Figure 2.10. Thermoreversible phosphonium salts used to gel organic solvents;[29] Adapted with permission from Abdallah, D. J.; Lu, L.; Weiss, R. G. *Mater. Chem.* **1999**, *11*, 2907. Copyright 2000 American Chemical Society

Self-assembly and stabilization continue to surface as growing fields for phosphonium salts. Solvent polarity, temperature, and salt concentration in solution prove critical to aggregate formation.[1] Phosphonium salt aggregation can control porphyrin self-assembly and DNA binding.[14, 67] Aggregates and micelles of triphenylphosphonium ions with one long alkyl or fluoroalkyl group formed in formamide.[72] Decyl, dodecyl, tetradecyl, and hexadecyltriphenylphosphonium bromide surfactants all micellized.[73]

Critical micelle concentrations (cmc), the concentration of surfactant where self-assembly of amphiphiles into micelles in solution becomes abundant and spontaneous, are measured with conductance versus concentration experiments or microcalorimetry (isothermal titration calorimetry).[72, 73] Abrupt increases in conductance and decreases in surface tension indicate that one has reached the critical micelle concentration. For the conductometry method, small amounts of a solution of known concentration of surfactant in solvent are added sequentially to a large container of solvent with controlled temperature. After each addition, stirring, and temperature equilibration, the conductance is measured. In plots of conductance versus concentration, the critical micelle concentration occurs when an abrupt change in the slope of lines drawn between the values is apparent.[73] In isothermal titration calorimetry, introducing aliquots of surfactant in solvent into pure solvent is associated with the enthalpy of solvation. The heat flow, exothermic, and endothermic transitions are recorded for each dilution, and the differential enthalpies of dilution per injection are plotted against concentration of surfactant. Cmc and enthalpy of dilution are derived.[73]

Isothermal titration calorimetry measures differential heats of dilution at varying temperatures against surfactant concentration.[73] Each injection of surfactant into the pure solvent relates to a change in heat flow due to the exothermic solvation process. Plotting kcal/mole of injectant versus concentration of surfactant results ideally in a step output, indicating a dramatic decrease in kcal/mol of injectant at the cmc that then begins to plateau to a single value beyond this concentration. Moulik et al. evaluated cmc values of monoalkyl (C_{10}-, C_{12}-, C_{14}-, and C_{16}-) triphenylphosphonium bromides in water, but the authors found unique behavior for shorter alkyl triphenylphosphonium salts.[73] For the decyl- and dodecyl-containing triphenylphosphonium salts, heat of dilution versus concentration plots at lower temperatures

(near 298 K) each showed a peak rather than a stepwise drop. These peaks indicated coupled endothermic and exothermic processes, meaning two processes of association existed. Only one exothermic process and a large stepwise drop in the heat of dilution versus concentration plots occurred when evaluating triphenylphosphonium cations with longer monoalkyl lengths or when measurements of the decyl- or dodecyl-containing triphenylphosphonium salts' cmc values were completed at higher temperatures.[73]

Moulik et al. also showed that all four types of triphenylphosphonium salts with varied monoalkyl group length displayed two abrupt slope changes in the conductivity versus concentration plots.[73] Each abrupt change in slope is considered a critical concentration for a type of association. Cmc values from microcalorimetry and from conductivity measurements were similar for decyl-containing triphenylphosphonium and dodecyl-containing triphenylphosphonium salts. The first change in the slope of the conductivity versus concentration plots was the cmc, and the authors related the second slope change to a small secondary change in size, shape, or micelle behavior. The prime association was seen to decrease with temperature. Higher temperatures for cmc minima resulted from lipophilicity of the cation. Low enthalpy of the secondary transition was attributed to a lack of a secondary transition for longer-chain monoalkyl-containing triphenylphosphonium salts. Entropy of aggregation between the different salts varied little, but enthalpy did change. This change in enthalpy was responsible for differences in self-assembly.[73]

Although most cmc studies are completed in water, Lattes et al. studied some water-insoluble triphenylphosphonium salts with one long 4-to-8-carbon alkyl group and their self-assembly in formamide.[72] Formamide solvates large cations and has a higher dielectric constant than water (110 versus 80 respectively).[72] An abrupt change in slope between values of

conductance versus concentration was noted as the cmc. The cmc decreased with increasing alkyl group length. Conductance increased even after the critical micelle concentration was achieved. The authors associated this behavior with imperfect micelle formation due to formamide's high dielectric constant; this behavior is still not fully understood.[72]

2.6.4 Phase Transfer Catalysis

Tomoi et al. employed phosphonium-based salts as phase-transfer catalysts.[34,74-76] Phase-transfer with small molecules is often more efficient than with polymeric phosphonium salts due to solvation of the ions and entropy-driven desolvation of polymer chains.[34] Polymer-supported phosphonium catalysts were used to study phase-transfer reactions of alkyl and aryl halides with sodium cyanide in various solvents.[76] Alkyl halides that could swell catalyst supports had greater efficiency.[76] Rates were enhanced with phosphonium catalytic sites farther from the polystyrene backbones of supported catalysts.[74] Increased hydrophobic character and increased ion exchange were reported for longer spacer lengths.[74]

Through emulsion polymerization, Ruckenstein et al. prepared two types of phosphonium-based phase transfer catalysts.[2] The authors synthesized both poly(vinylbenzyl chloride) (PVBC) by itself and also a core-shell polymer with a core of polystyrene and a shell of PVBC. The core-shell polymer was prepared through first synthesizing polystyrene oligomers and subsequently adding vinylbenzyl chloride to the emulsion polymerization. Crosslinked particles were prepared with divinylbenzene (DVB). The resultant PVBC-containing polymers were quaternized with tributylphosphine, resulting in poly(vinylbenzyltributyl phosphonium chloride) (PVBPC)-containing polymers. Scanning electron microscopy (SEM) of the particles suggested that quaternization did not change the particle size, and core-shell morphology was

observed for polystyrene-PVBPC.[2] Unsupported PVBPC showed increased phase transfer catalysis in the alkylation of isopropylidene malonate due to increased solvation and catalyst availability compared to polystyrene-supported PVBPC. Ammonium analogs, synthesized with tributylamine containing poly(vinylbenzyltributyl ammonium chloride) units, were compared and found to have much less catalytic activity than the phosphonium polymers. Cooperativity effects were noted for controlling and enhancing catalyst activity for supported polymers with higher catalyst content.[2]

Ruckenstein et al. also synthesized the monomers triethylvinylbenzyl phosphonium chloride and tributylvinylbenzyl phosphonium chloride, and these monomers were used in a third method to make core-shell polystyrene-PVBPC.[2] Instead of adding vinylbenzyl chloride, the phosphonium monomer was added in the polymerization step. However, this emulsion polymerization was affected by the concentration of phosphonium salts, where there was a limiting value for salt content to maintain an emulsion. This was attributed to anionic surfactant interactions with phosphonium groups.[2]

Kubisa et al. utilized telechelic triphenylphosphonium-endcapped poly(ethylene glycol) (PEG) in phase transfer catalysis.[77-79] The authors used commercially available PEG diols with degrees of polymerization (DP) from 6 to 34, converted the diol endgroups to bromide endgroups with triphenylphosphine and bromine, and subsequently quaternized the polymers with triphenylphosphine in a separate reaction.[77-78] Measurement of bulk viscosities at ambient temperature was possible due to the low DP values, and in bulk the telechelic PEG had viscosities that were close to 10^6 orders of magnitude higher than PEG diols.[32,79] In chloroform at 25 °C at concentrations below 1 g/100 mL, the telechelic phosphonium-based polymers had lower viscosities than PEG diols with comparable molecular weights.[79] It was reasoned that

cyclic structures were possible since these groups only contained 6 to 34 oxyethylene units in the chain.[32] Phase-transfer of phosphonium catalysts was studied in reactions of sodium phenoxide with 1-bromooctane in 1,4-dioxane. The rate constant of the reactions with phosphonium-based PEG which had a low number of oxyethylene units (6.4 units on average) did not differ from PEG that was hydroxyl terminated. A phase transfer catalyst with a higher degree of polymerization of 23 units and phosphonium endgroups possessed a rate constant that was twice that of the hydroxyl terminated PEG. Cooperative effects with increasing chain length were implicated.[32]

2.7 Biological Applications of Phosphonium-Containing Macromolecules

2.7.1 Overview of Biological Applications of Phosphonium-Containing Polymers

Phosphonium small molecule salts find application as antibacterial agents, as nucleotide carriers, and as directing agents for self-assembly.[4, 66-67] Current employment of phosphonium-containing polymers is limited to antimicrobial agents. Difficult purification and handling of these salts and their precursor phosphines, the pyrophoric trialkylphosphines for example, have restricted the use of phosphonium-based molecules.[39] Most studies have found transquaternization and chemical modification reactions on polymers with phosphines to result in less than 100% conversion.[17,31,35] Antibacterial activity has been found to depend on phosphonium salt concentration.[39] Low molar mass phosphonium molecules may aid in transport of nucleotides across cell membranes.[66] Tetraphenylphosphonium cations have been shown to traverse across mitochondrial inner membranes without ionophore assistance, and build-up of these cations can occur inside the mitochondria.[65] Phosphonium functionalities also facilitate

porphyrin-DNA binding through controlling aggregation and deposition on the surface of DNA.[67]

2.7.2 Antimicrobial Activity: Ammonium versus Phosphonium Polymers and Small Molecule Analogs

Polymeric biocides offer many benefits compared to small molecule antimicrobial agents, including non-volatility, improved chemical stability, low permeability through animal or human skin, and recycling potential.[16,17] Medical implantation requires long lifetimes of the implants and no corrosion or leaching of chemicals into the body, and medical sterilization requires the absence of chemical residues on the sterilized instruments that could penetrate the skin or wear off while the instrument is in use. Small molecule antimicrobial coatings can erode from the implant or instrument surface, but polymer-based antimicrobial agents or crosslinked coatings can provide a safer route. Bacterial cell death from cationic molecules is commonly described in six steps:[4, 80-82] adsorption on the walls of the bacteria, diffusion into and through the cell wall, attachment to the cytoplasmic membrane, rupture of the cytoplasmic membrane, leakage of DNA, RNA, and K^+ as well as other cytoplasmic contents, followed by primarily necrotic cell death. Since activity varies according to the antimicrobial agent's structure and the type of microorganism, selectivity is an issue for both low molar mass compounds and polymers.[16] Small molecules may diffuse through the cell membranes of Gram-negative bacteria. Macromolecules may have difficulty penetrating this extra barrier, yet cationic polymers have greater binding affinity to the negatively charged bacteria. Polymers based on dimethyldecyl, dimethyltetradecyl and dimethyloctadecyl(4-vinylbenzyl)phosphonium chloride monomers were synthesized and compared to 4-ethylbenzyl small molecule analogs. The small molecule model

compounds displayed higher activity against *Escherichia coli* (Gram-negative bacteria) than the corresponding polymers.[39] TEM has been used to study cell wall disfigurement and damage after exposure to phosphonium-based polymers.[16]

Kenawy et al. and Endo et al. have reported that phosphonium-based polymers have higher antimicrobial activity than ammonium analogs.[31,39] Various phosphonium-based antimicrobial macromolecules were synthesized through chemical modification of polymers, through transquaternization reactions on polymers, and through polymerization of phosphonium-based monomers.[31,35,39] Kenawy et al. compared poly(glycidyl methacrylate-*co*-2-hydroxyethyl methacrylate) polymers modified with chloracetyl chloride followed by triphenylphoshine, tributylphosphine, or triethylamine.[31] The tributylphosphonium-substituted copolymer was found to have the highest antimicrobial activity against bacteria and fungi including *Staphylococcus aureus*, *Escherichia coli*, *Bacillus subtilis*, *Aspergillus flavus*, *Fusarium oxysporum* and *Candida albicans*.[31] Endo et al. synthesized various phosphonium- and ammonium-containing polymers from vinylbenzyl phosphonium and ammonium monomers. Model ethylbenzyl phosphonium-based small molecule compounds were also synthesized. Phosphonium polymers had twice as much antimicrobial activity as their ammonium analogs, and polymer antibacterial activity was higher than for model small molecules.[4]

Endo et al. examined the antibacterial activity of copolymers of ammonium- and phosphonium-containing monomers, yet phosphonium-based homopolymers proved more effective than copolymers containing both ammonium and phosphonium units in the macromolecular structure.[40] Including ammonium units into the polymer chain had a negative effect on antimicrobial activity. However, the authors also analyzed the antimicrobial activity of a mixture of two independent homopolymers, poly(tributyl(4-vinylbenzyl)phosphonium

chloride) and poly(tributyl(4-vinylbenzyl)ammonium chloride). When mixing the two homopolymers together in solution, the antimicrobial activity peaked at a phosphonium to ammonium homopolymer ratio of 1:1.[40] This 1:1 mixture possessed greater antibacterial activity than either phosphonium or ammonium homopolymer alone. Mixing the two homopolymers together created a synergistic effect, and the authors proposed that the higher antimicrobial activity was due to greater solubility of bacterial membrane components, phospholipids and proteins, into the polymer micelles.[40] The solubility of bacterial cell components disrupted cell function and contributed to cell death. Structure-dependent micelle formation was expected at low concentrations of these cationic polymers, and mixed micelles were possible for the mixed salt copolymers. Antibacterial activity depended on micelle formation, availability of ionic groups, and solubility of both the antibacterial agent and the contents of the cell.[40] The relationships of aggregation and of micelle formation compared with morphological changes in the cell and antibacterial activity are not fully understood.[64]

Polymeric phosphonium salts with only one long alkyl chain have been studied, and antimicrobial action has been found to be highly dependent on the number of carbons in this chain.[39] Antibacterial activity decreased with increasing alkyl chain length. Decyl-containing polymers at 280 and 28 μM killed all *S. aureus* bacteria in thirty minutes and were still active below 0.28 μM, but tetradecyl- and octadecyl-containing polymers were inactive at concentrations below 0.28 μM.[39] The opposite has been found for small molecule model compounds. The critical micelle concentration (cmc) decreases upon increasing the number of carbons in the alkyl chain, and aggregation may increase local concentration of a salt.[39]

2.7.3 Biological Transport Properties of Low Molar Mass Phosphonium Salts: Nucleotide Transport and Mitochondrial Permeation

Hong et al. discovered that molecular transportation rates across phospholipid membranes are higher for phosphonium-based compounds compared to previously published work on ammonium analogs.[66,83-85] Phosphonium salts are larger and often weakly-associated cations compared to similar ammonium derivatives.[15] Tetraphenylphosphonium cations transport across mitochondrial inner membranes and build-up in the mitochondria.[65] Typically, transport is aided by ionophores, potential and pH gradients, but tetraphenylphosphonium cations do not need this aid. Even charged, these phosphonium salts are fat soluble. The radius of the phosphonium cation center is approximately 4.2 Å, and the radius of hydrophilic Na+ is close to 1 Å.[65] Transportation across phospholipid membranes is facilitated by hydrophobic character, caused by a large radius distributing charge and making local polarization of water less likely. Sodium ions are hydrophilic and do not cross the mitochondrial membrane without ionophore assistance.[65]

Many antiviral drugs, like azidothymidine (AZT) which is used in the treatment of human immunodeficiency virus (HIV), stop virus replication through causing early nucleic acid chain termination in the replication process.[86] They block enzymes and disrupt chain propagation. Although the mechanisms through which some of these drugs inhibit virus replication are not fully understood, much research focuses on synthesizing antiviral drugs from DNA nucleotides in hopes that hydrogen-bonding in complementary nucleobase-pairs will direct transport inside the cell.[66] However, the problem arises with transport of these nucleotide derivatives across phospholipid membranes and into the cells. High charge concentration and hydrophilicity are factors contributing to inefficient transport.[66, 87]

Hong et al. used phosphonium salts covalently attached to nucleobases as carriers to direct the transport of guest molecules adenosine monophosphate (AMP) and guanosine monophosphate (GMP) across the cell membrane.[66] The guest molecules AMP and GMP are both components of RNA, and they contain the nucleobases adenine and guanine, respectively. Non-covalent interactions existed between the nucleobases on the two different types of molecules, carrier and guest, which bound the two together. Additionally, supramolecular interactions between the phosphonium centers and the phosphates also contributed to transport across the cell membranes (Figure 2.11). The nucleobase-containing carriers were synthesized with phosphonium functionalities to help penetrate cell membranes. Studying transport of these molecules across a membrane with source and receiving solutions to extract the molecules contributed to future evaluation of antiviral derivatives and their transport into cells.[66]

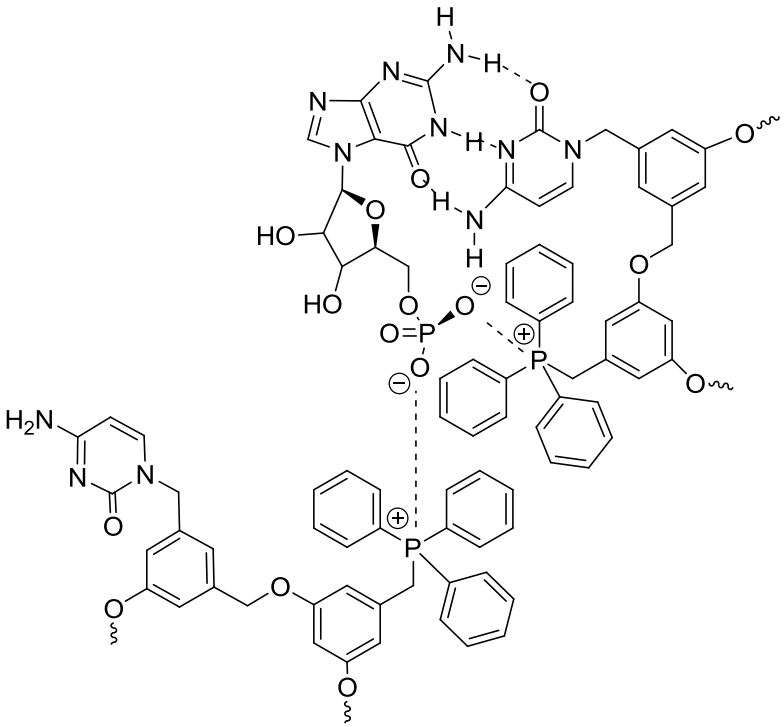

Figure 2.11. Theorized GMP recognition of phosphonium-based nucleobase complex;[66] Jung, Y.; Yeo, W.; Lee, S. B.; Hong, J. *Chem. Commun.* **1997**, 1061-1062. Reproduced by permission of the Royal Society of Chemistry

Hong et al. achieved the best transport rates for the guests AMP and GMP using thymine- and cytosine-based, phosphonium-containing carriers.[66] Nucleobase pairing on the phosphonium-based carrier with the guests AMP or GMP also facilitated transport. Using nucleobases on the phosphonium-based carriers that were complementary to AMP's adenine or GMP's guanine improved transportation rates of AMP and GMP; carriers with non-complementary nucleobases for AMP or GMP provided slower rates. Without phosphonium functionalities on the nucleobases, AMP and GMP were not transported.[66]

2.7.4 Porphyrin-Nucleic Acid Self-Assembly Facilitated with Phosphonium Salt Aggregation

Research on porphyrins has also received much attention due to their anitiviral activity and use as chemotherapeutics.[67] Cleaving DNA or stopping the replication of DNA are antiviral mechanisms for porphyrins. Anzenbacher et al. synthesized phosphonium-based porphyrins to control self-assembly and facilitate porphyrin-DNA binding (Figure 2.12).[67] Porphyrin-DNA binding in aqueous solutions was dictated by porphyrin aggregation on the surface of DNA. Binding affinity was determined through measuring photochemical changes in quantum yields and triplet states that are associated.[67] Phosphonium groups on the porphyrins non-covalently associated with phosphates of nucleic acids in the DNA, and binding affinity to DNA was controlled by the concentration of salts.[14]

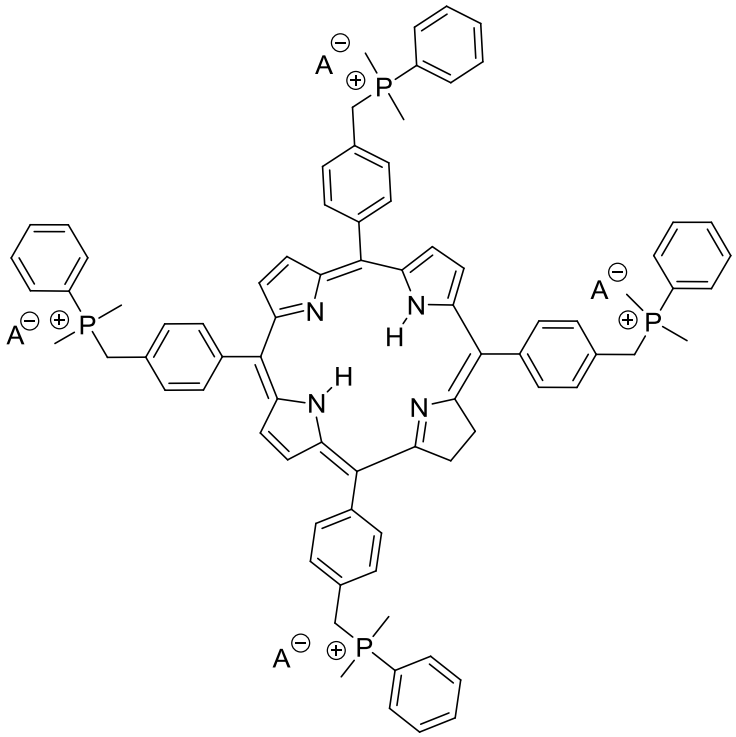

Figure 2.12. A meso-tolylporphyrin with dimethylphenylphosphonium functionalities;[67] Adapted with permission from Kubat, P.; Lang, K.; Kral, V.; Anzenbacher, P. *J. Phys. Chem. B* **2002**, *106*, 6784-6792. Copyright 2002 American Chemical Society

Anzenbacher et al. synthesized several different phosphonium-containing porphyrins.[67] A delicate balance existed between the choice of phosphonium functionality to better direct binding to DNA and aggregation of those phosphonium compounds in solution. Aggregates themselves could deposit on the DNA forming extended assemblies. The aim was to destabilize aggregation of the phosphonium salts in solution yet concurrently facilitate phosphonium group association with the phosphate groups of DNA. Dimethylphenyl, trimethyl, tributyl, and triphenylphosphonium derivatives were synthesized.[67] Small changes in the alkyl or aryl functionalities led to large effects in aggregation in solution. Triphenyl and tributylphosphonium derivatives had the highest propensity to aggregate and they deposited directly on the DNA in

aggregates. Dimethylphenylphosphonium-based porphyrins possessed an equilibrium of aggregates versus single salts in aqueous solution, and trimethylphosphonium-functionalized porphyrins were mostly isolated salts in solution.[67] These two compounds deposited in a more monomeric fashion on the surface of the DNA.[67]

2.8 Future Perspectives

It is hoped that this review will encourage and expound potential research in the field of phosphonium-based polymer chemistry. The limited study of phosphonium-containing polymers in the present literature makes the possibilities boundless. Phosphonium cations offer many advantages due to their antimicrobial activity[4] and thermal stability,[3] and their ionic aggregation is a means to self-assembly, self-healing, and smart materials. These polymers are particularly attractive for both electro-active and biological applications, and the large phosphorus center allows controlled, tunable melt processing and ionic reinforcement through physical crosslinks.

We recently synthesized a uracil-containing phosphonium salt from 6-chloromethyluracil and trioctylphosphine to physically crosslink adenine-containing triblock copolymers.[88] The triblock copolymers were synthesized using nitroxide-mediated polymerization and included a poly(n-butyl acrylate) central block and two poly(9-vinylbenzyladenine) (poly(9-VBA)) external blocks. The uracil functionality hydrogen bonded with the nucleobase-containing polymers, and subsequently the phosphonium groups aggregated creating physical crosslinks between polymer chains. Mixing adenine-based polymers with the uracil-based phosphonium produced clear films, indicating that the uracil-based phosphonium salt was miscible with the polymer. Mixing the uracil-phosphonium compound with poly(*n*-butyl acrylate)s produced cloudy films,

indicating that the nucleobase functionality aided miscibility. H-bonding between uracil and adenine functionalities enhanced miscibility.[88]

This review describes the synthesis of several novel phosphonium-containing monomers that were included in the backbone of various high performance polymers to evaluate structure-property relationships. Tailoring the structure of the phosphonium cation allows one to incorporate the functionality in various forms as pendant chains, backbone monomers, and endcapping groups to control the ionic aggregation and melt processability. Small changes in the ionic content or type of cation resulted in large changes in the bulk polymer attributes, creating a facile method to fabricate polymers with tunable mechanical, morphological, rheological, and thermal properties.

2.9 References

1. Karaman, H.; Barton, R. J.; Robertson, B. E.; Lee, D. G. *J. Org. Chem.* **1984**, *49*, 4509-4516.
2. Hong, L.; Ruckenstein, E., *Polymer* **1992**, *33(9)*, 1968-1975.
3. Xie, W.; Xie, R.; Pan, W.; Hunter, D.; Koene, B.; Tan, L.; Vaia, R. *Chem. Mater.* **2002**, *14*, 4837-4845.
4. Kanazawa, A.; Ikeda, T.; Endo, T. *Journal of Polymer Science: Part A: Polymer Chemistry* **1993**, *31*, 335-343.
5. White, C. K.; Rieke, R. D. *J. Org. Chem.* **1978**, *43(24)*, 4638-4641.
6. Parent, J. S.; Liskova, A.; Resendes, R. *Polymer* **2004**, *45*, 8091-8096.
7. Nishikubo, T.; Koichi, A.; Uchida, J. *Makromol. Chem.* **1989**, *190*, 1471-1482.
8. Nishikubo, T.; Uchida, J.; Matsui, K.; Iizawa, T. *Macromolecules* **1988**, *21*, 1583-1589.
9. Chance, R. R.; Patel, G. N.; Witt, J. D. *J. Chem. Phys.* **1979**, *71*, 206.
10. Chance, R. R. *Macromolecules* **1980**, *13*, 396.
11. Preziosi, A. F.; Bhattacharjee, H. R.; Patel, G. N. *Polym. Prepr., Am. Chem. Soc. Div. Polym. Chem.* **1980**, *21(2)*, 166-167.
12. Bhattacharjee, H. R.; Preziosi, A. F.; Patel, G. N. *Polym. Prepr., Am. Chem. Soc. Div. Polym. Chem.* **1980**, *21(2)*, 168-169.
13. Bhattacharjee, H. R.; Preziosi, A. F.; Patel, G. N. *J. Chem. Phys.* **1980**, *73*, 1478.
14. Jin, R.; Aoki, S.; Shima, K. *Chem. Commun.* **1996**, 1939-1940.
15. Hartley, F. R., John Wiley & Sons: 1994; Vol. 3, p 25-91.
16. Kenawy, E.; Mahmoud, Y. *Macromol. Biosci.* **2003**, *3(2)*, 107-116.

17. Popa, A.; Davidescu, C. M.; Trif, R.; Ilia, G.; Iliescu, S.; Dehelean, G. *Reactive & Functional Polymers* **2003**, *55*, 151-158.
18. Hodge, P.; Khoshdel, E.; Waterhouse, J. *Makromol. Chem.* **1984**, *185*, 489-497.
19. Hodge, P.; Waterhouse, J. *Polymer* **1981**, *22*, 1153-1154.
20. Parent, J. S.; Penciu, A.; Guillen-Castellanos, S. A.; Liskova, A.; Whitney, R. A. *Macromolecules* **2004**, *37*, 7477-7483.
21. Eisenberg, A., Kim, J. S. *Introduction to Ionomers*. Wiley: New York, 1998.
22. Eisenberg, A.; Hird, B.; Moore, R. B. *Macromolecules* **1990**, *23*, 4098-4107.
23. Unal, S. Synthesis and Characterization of Branched Macromolecules for High Performance Elastomers, Fibers, and Films. Ph.D. Thesis, Virginia Polytechnic and State University, Blacksburg, VA, 2005.
24. Unal, S.; McKee, M. G.; Massa, D. J.; Long, T. E. *Polymer Preprints* **2005**, *46(2)*, 1028-1029.
25. Song, K.; Liu, L.; Guo, Q. *J. Org. Chem.* **2003**, *68*, 4604-4607.
26. Tsang, T.; Farrar, T. C. *J. Chem. Phys.* **1968**, *49(10)*, 4403-4406.
27. Wennerstrom, H.; Lindman, B.; Forsen, S. *The Journal of Physical Chemistry* **1971**, *75(19)*, 2936-2942.
28. Abdallah, D. J.; Weiss, R. G., *Chem. Mater.* **2000**, *12*, 406-413.
29. Abdallah, D. J.; Lu, L.; Weiss, R. G. *Mater. Chem.* **1999**, *11*, 2907.
30. Hartwig, A.; Putz, D.; Schartel, B.; Bartholmai, M.; Wendschuh-Josties, M. *Macromol. Chem. Phys.* **2003**, *204*, 2247-2257.
31. Kenawy, E.; Abdel-Hay, F. I.; El-Shanshoury, E. R.; El-Newehy, M. H. *Journal of Polymer Science: Part A: Polymer Chemistry* **2002**, *40*, 2384-2393.
32. Kubisa, P.; Bedron, T. *Reactive & Functional Polymers* **1995**, *27*, 237-241.
33. Ghassemi, H.; Riley, D. J.; Curtis, M.; Bonaplata, E.; McGrath, J. E. *Appl. Organometal. Chem.* **1998**, *12*, 781-785.
34. Kobayashi, S.; Suzuki, M.; T.Sakaya; Saegusa, T. *Makromol. Chem.* **1987**, *188*, 457-462.
35. Popa, A.; Ilia, G.; Iliescu, S.; Dehelean, G.; Pascariu, A.; Bora, A. *Mol. Cryst. Liq. Cryst.* **2004**, *418*, 195-203.
36. Marechal, E., *Comprehensive Polymer Science The Synthesis, Characterization, Reactions & Applications of Polymers*. Pergamon Press: 1989; Vol. 6.
37. Nishikubo, T.; Kawashima, T.; Inomata, K.; Kameyama, A. *Macromolecules* **1992**, *25*, 2312-2318.
38. Horner, L.; Mummenthey, G.; Moser, H.; Beck, P. *Chem. Ber.* **1966**, *99(9)*, 2782.
39. Kanazawa, A.; Ikeda, T.; Endo, T. *Journal of Applied Polymer Science* **1994**, *53*, 1237-1244.
40. Kanazawa, A.; Ikeda, T.; Endo, T. *Journal of Applied Polymer Science* **1994**, *53*, 1245-1249.
41. Zhou, P.; Blumstein, A. *Polymer* **1997**, *38(3)*, 595-604.
42. Jenkins, I. H.; Kar, A. K.; Lindsell, W. E.; Murray, C.; Preston, P. N.; Wang, C.; Wherrett, B. S. *Macromolecules* **1996**, *29(20)*, 6365-6370.
43. Seyferth, D.; Masterman, T. C. *Macromolecules* **1995**, *28*, 3055-3066.
44. Balogh, L.; Blumstein, A. *Macromolecules* **1995**, *28*, 5691.
45. Lindsell, W. E.; Radha, K.; Soutar, I.; Stewart, M. J. *Polymer* **1990**, *31*, 1374-1378.
46. Atmaca, L.; Kayihan, I.; Yagci, Y. *Polymer* **2000**, *41*, 6035-6041.

47. Onen, A.; Arsu, N.; Yagci, Y. *Die Angewandte Makromolekulare Chemie* **1999**, *264*, 56-59.
48. Prajapati, K.; Varshney, A. *Journal of Polymer Research* **2006**, *13*, 97-105.
49. Tang, J. B.; Sun, W. L.; Tang, H. D.; Radosz, M.; Shen, Y. Q. *Macromolecules* **2005**, *38(6)*, 2037-2039.
50. Tang, J.; Tang, H.; Sun, W.; Radosz, M.; Shen, Y. *PMSE Preprints* **2005**, 93, 1006-1007.
51. Bajpai, U. D. N.; Otsu, T. *Eur. Polym. J.* **1993**, *29(4)*, 517-521.
52. Dossow, D.; Zhu, Q. Q.; Hizal, G.; Yagci, Y.; Schnabelt, W. *Polymer* **1996**, *37(13)*, 2821-2826.
53. Pringle, J. M.; MacFarlane, D. R.; Forsyth, M. *Synthetic Metals* **2005**, *155*, 684-689.
54. Faroq, A. A. *Polymer Degradation and Stability* **1994**, *44*, 323-333.
55. Moore, C. M.; Hackman, S.; Brennan, T.; Minteer, S. D. *Journal of Membrane Science* **2005**, *254*, 63-70.
56. Panek, G.; Schleidt, S.; Mao, Q.; Wolkenhauer, M.; Spiess, H. W.; Jeschke, G. *Macromolecules* **2006**, *39*, 2191-2200.
57. Schrenk, M.J.; Villigram, R.E.; Torrence, N.J.; Brancato, S.J.; Minteer, S.D. *J. Membr. Sci.* **2002**, *205(1-2)*, 3-10.
58. *Modern Polyesters*. Scheirs, J.; Long, T. E. eds. John Wiley & Sons, Ltd.: West Sussex, England, 2003.
59. Tang, S.; Xin, Z. *Polymer* **2009**, *50*, 1054–1061.
60. Kang, H.; Lin, Q.; Armentrout, R. S.; Long, T. E. *Macromolecules* **2002**, *35*, 8738-8744.
61. Berti, C.; Colonna, M.; Binassi, E.; Fiorini, M.; Karanam, S.; Brunelle, D. J. *Reactive and Functional Polymers* **2010**, *70(6)*, 366-375.
62. Gutowsky, H. S.; Pake, G. E.; Bersohn, R. *J. Chem. Phys.* **1954**, *22*, 643.
63. Rush, J. J. *J. Chem. Phys.* **1966**, *44*, 1722.
64. Kanazawa, A.; Ikeda, T.; Endo, T. *Antimicrobial Agents and Chemotherapy* **1994**, *38(5)*, 945-952.
65. Ross, M. F.; Kelso, G. F.; Blaikie, F. H.; James, A. M.; Cocheme, H. M.; Flilipovska, A.; Ros, T. D.; Hurd, T. R.; Smith, R. A. J.; Murphy, M. P. *Biochemistry (Moscow)* **2005**, *70(2)*, 222-230.
66. Jung, Y.; Yeo, W.; Lee, S. B.; Hong, J. *Chem. Commun.* **1997**, 1061-1062.
67. Kubat, P.; Lang, K.; Kral, V.; Anzenbacher, P. *J. Phys. Chem. B* **2002**, *106*, 6784-6792.
68. Haraldsson, P.; Karlsson, A.; Wieslander, E.; Guztavsson, H.; Back, S. A. *J. Phys. Med. Biol.* **2006**, *51*, 919-928.
69. Kanazawa, A.; Ikeda, T. *Coordination Chemistry Reviews* **2000**, *198*, 117-131.
70. Paczkowski, J.; Neckers, D. C. *Macromolecules* **1985**, *18*, 2412.
71. Terech, P.; Weiss, R. G. *Chem. Rev.* **1997**, *97*, 3133.
72. Escoula, B.; Hajjaji, N.; Rico, I.; Lattes, A. *J. Chem. Soc. Chem. Commun.* **1984**, 1233-1234.
73. Prasad, M.; Moulik, S. P. *J. Phys. Chem. B* **2004**, *108*, 355-362.
74. Tomoi, M.; Kori, N.; Kakiuchi, H. *Makromol. Chem.* **1986**, *187*, 2753-2761.
75. Ford, W. T.; Lee, J.; Tomoi, M. *Macromolecules* **1982**, *15*, 1246-1251.
76. Tomoi, M.; Nakamura, E.; Hosokawa, Y.; Kakiuchi, H. *Makromol. Chem., Rapid Commun.* **1984**, *5*, 281-285.
77. Kubisa, P.; Biedron, T. *Macromol. Symp.* **1994**, *85*, 129.
78. Kubisa, P.; Biedron, T. *Macromol. Chem. Phys.* **1996**, *197*, 19-30.

79. Kubisa, P.; Biedron, T. *Macromol. Chem. Phys.* **1996**, *197*, 31-40.
80. Hugo, W. B.; Longworth, A. R. *J. Pharm. Pharmacol.* **1966**, *18*, 569-578.
81. Hugo, W. B.; Longworth, A. R. *J. Pharm. Pharmacol.* **1964**, *16*, 655-662.
82. Franklin, T. J.; G. A. Snow, E., *Antiseptics, Antibiotics and the Cell Membrane. in Biochemistry of Antimicrobial Action*. Chapman and Hall: London, 1981; p 58-78.
83. Maruyama, K.; Tsukube, H.; Araki, T. *J. Am. Chem. Soc.* **1982**, *104*, 3197.
84. Behr, J.-P.; Lehn, J.-M. *J. Am. Chem. Soc.* **1973**, *95*, 6108.
85. Tsukube, H. *J. Chem. Soc., Perkin Trans. 1* **1983**, *1*, 29-34.
86. Gschwentner, M.; Susanna, A.; Woll, E.; Ritter, M.; Nagl, U.; Schmarda, A.; Laich, A.; Pinggera, G. M.; Ellemunter, H.; Huemer, H.; Deetjen, P.; Paulmichl, M. *Molecular Medicine* **1995**, *1(4)*, 407-417.
87. *Nucleotide Analogues as Antiviral Agents*, ed. J. C. Martin, American Chemical Society, Washington, D.C., 1989.
88. Mather, B. D.; Baker, M. B., Beyer, F. L.; Green, M. D.; Berg, M. A. G.; Long, T. E. *Macromolecules* **2007**, *40*, 4396-4398.

Chapter 3: Synthesis and Characterization of Phosphonium-Endcapped Poly(ethylene terephthalate-*co*-ethylene isophthalate) Ionomers

3.1 Abstract

Poly(ethylene terephthalate-*co*-ethylene isophthalate) ionomers with 1.3 to 7.7 mole % phosphonium endgroups by ^{1}H NMR were synthesized utilizing a novel cationic endcapping reagent, butyl *p*-carboxyphenyl triphenylphosphonium bromide. The high thermal stability of this phosphonium salt enabled its survival in high temperature syntheses and applications. The phosphonium endcapping reagent was found to be stable up to 317 °C by a TGA ramp to 600 °C at 10 °C/minute under nitrogen. ^{1}H and ^{31}P NMR spectra indicated that no degradation of the phosphonium endcapping reagent occurred during syntheses of linear polyester ionomers at 220 °C. Melt rheological studies suggested that no appreciable ionic aggregation was present above 120 °C for telechelic ionomers endcapped with 7.7 mole % or less of the phosphonium salt. This was attributed to the large, weak phosphonium ions preventing ionic aggregation at 120 °C. The glass transition temperatures were ~65 °C for number-average molecular weights ranging from 5,100 to 9,900 g/mole with 7.7 and 1.3 mole % phosphonium endgroups, respectively.

3.2 Introduction

Ionomers are defined as polymers with less than 15 mole % ionic groups that aggregate and serve as physical crosslinking sites.[1-6] Ionic associations in polymers, even at low concentrations of ionic groups, greatly affect physical properties, increasing both the modulus and the glass transition temperature.[1-6] A thermoreversible transition is associated with the

formation and disruption of ionic aggregates.[1-6] Oligomers with thermoreversible ionic aggregation are proposed to have properties similar to higher molecular weight analogs below the dissociation temperature of the aggregates.[1-6]

Many investigations of ionomers have concentrated on random ionomers[2-8] and anionomers with carboxylate[3-4, 6, 9-11] and sulfonate[5, 12-13] anionic sites pendant to the main chain and with mobile cations (not attached to the chain). In random ionomers, the ionic functionalities are randomly distributed along the polymer chain.[3-4,6] Cationomers with cationic sites on the polymer with mobile anions represent a much smaller class of ionomers, and little is published on phosphonium cationomers.[14-26] The majority of the cationomer literature focuses on quaternary-ammonium-containing polymers.[6, 27-29] Phosphonium cations are readily compared to ammonium groups in regards to their aggregate characteristics,[30-31] thermal stability,[32] and antibacterial activity.[14] Phosphonium-based polymers are attractive predominantly because of their higher thermal stability[32] and greater antimicrobial activity[14] compared to the omnipresent, commercialized ammonium derivatives. They are up to 80 °C[32] or even 166 °C[1] more thermally stable than similar ammonium molecules based on their onset temperatures for thermal degradation by TGA under nitrogen to 1000°C at 2 to 10°C/minute respectively. Therefore, phosphonium salts have potential use in high-temperature melt polyester syntheses and may melt process.

Our research group has completed extensive previous research on PET- and PEI-based polyester oligomers, polymers, and ionomers.[1, 5, 33-45] For example, we recently published the use of sodium salts of 3-sulfobenzoic acid to synthesize telechelic PET ionomers.[5] Since the chain length between ionic sites is well-defined, telechelic ionomers (with terminal ionic groups) can be utilized as model ionomers.[1, 46-47] These sodiosulfonate telechelic polyesters had ionic

aggregation even in the melt phase above 150 °C.[5] Colonna et al. published that sodiosulfonate-based telechelic poly(butylene terephthalate) (PBT) ionomers also had subsisting ionic aggregation.[8] PET is a common packaging material for soft drinks and food that offers exceptional mechanical properties, transparency, and gas barrier performance. PET properties include good thermal stability and high chemical resistance, and PET exhibits strain-induced crystallization and is readily recyclable.[33, 48] These properties all make PET an excellent choice for packaging and fiber formation.[33, 48] However, the necessary high-temperature processing of PET requires significant energy.[33, 48] PET with ionic endgroups that can thermoreversibly aggregate may allow facile and lower-temperature melt processing.[1] Phosphonium-based polyester ionomers with only weak ionic interactions and sterically hindered cations may enable these polymers to have improved mechanical performance while maintaining relatively low melt viscosities that facilitate processing. Our hypothesis is that low molecular weight polymers with thermoreversible ionic aggregation will have properties similar to high molecular weight derivatives below the dissociation temperature of the aggregates.[1,5] An increase in temperature above the ionic dissociation temperature disrupts aggregates to promote polymer flow for molding and shaping.

In this study, synthesis of phosphonium-endcapped poly(ethylene terephthalate)-*co*-poly(ethylene isophthalate) ionomers offer a unique approach to melt processable, model telechelics. We have synthesized mixed terephthalate/isophthalate wholly amorphous copolymers so that we can investigate ionic association of endgroups without the complicating effect of crystallization. This investigation describes the synthesis of telechelic ionomers, with a unique focus on cationic phosphonium-endcapped ionomers. These telechelic ionomers had precise placement of the ionic groups only at the ends of the polymer chains as opposed to

random placement throughout the polymer chains. It was anticipated that this precise placement compared to random placement would simplify the study of ionic aggregation and morphological assembly as related to the polymer structure. Moreover, introducing ionic character through the use of phosphonium-based endcapping reagents in these step-growth polymerizations enabled control over the polymer molecular weights. The ionic concentration increased and polymer molecular weights decreased with the addition of more monofunctional ionic endcapping reagent.

This paper describes the synthesis of a novel, phosphonium-containing endcapping reagent, butyl *p*-carboxyphenyl diphenylphosphonium bromide, and phosphonium-endcapped amorphous polyesters through melt polycondensation reactions. Melt rheological studies have shown that ionic association in these phosphonium endcapped polyesters was absent above 120 °C, thus suggesting that such materials may be amenable to melt processing. Our research strives to expand the limited field of phosphonium-based polymers and demonstrate the advantages of new phosphonium-containing ionomers with high thermal stability and melt processability.

3.3 Experimental

3.3.1 Materials

Anhydrous nickel(II) bromide (99.99^{+}%), 2-bromoethanol (98^{+}%), 6-bromohexanol (97%), trioctylphosphine (TOP) (90%), triphenylphosphine (TPP) (99%), 4-bromobenzoic acid (98%), 4-(diphenylphosphino)benzoic acid (97%), 1-bromobutane (≥99%), dimethyl terephthalate (DMT) (≥99%), dimethyl isophthalate (DMI) (99%), 1-butanol (≥99%), 1-dodecanol (≥95%), chloroform-d (99.96 atom % D), dimethylsulfoxide-d6 (99.96 atom % D), and methanol-d_4 (99.96 atom % D), hydrogen bromide 2 M in H_2O, sodium sulfate (≥99.0%),

and ethylene glycol (EG) (≥99%) were acquired from Aldrich. Anhydrous diethyl ether was purchased from VWR Titanium tetraisopropoxide (99%) was purchased from Aldrich and made into a 0.0098 g/mL solution in 1-butanol. Tetraoctylphosphonium bromide (TOPBr) (97.0%) and tetraoctylammonium bromide (TOABr) (>97.0%) were acquired from TCI America. Acetone and chloroform were purchased from Fisher Scientific and used as received.

3.3.2 Synthesis of (*p*-Carboxyphenyl)trioctyl Phosphonium Bromide (Compound A)

Horner's nickel(II) bromide coupling procedure was used,[49] and this closely followed our previous work.[1] 4-Bromobenzoic acid was dried under reduced pressure overnight at 60 °C. TOP (39.7 g, 107.2 mmol) and 4-bromobenzoic acid (21.2 g, 105.6 mmol) were added under argon to a flame-dried, double-neck, 100-mL, round-bottom flask with an overhead mechanical stirrer. The flask was then charged with anhydrous nickel(II) bromide (2.00 g, 9.15 mmol) from an ampoule, and the reaction was purged with argon for an additional 30 min before the temperature was raised to 170 ºC for 13.5 h. The dark purple product was dissolved in 100 mL of chloroform and filtered to remove a by-product, biphenyl-4,4'-dicarboxylic acid. The dark purple chloroform solution was washed with 44% aq HBr three times to six times until the color changed to light yellow. Water was removed from the product with sodium sulfate. The product was precipitated in approximately 600 mL of hexane. White crystals were dried at 60 ºC under reduced pressure in a vacuum oven overnight before recrystallization from acetone. When no trace of yellow color existed, the white crystals were subsequently dried under reduced pressure at 60 °C in a vacuum oven over 24 h. The yields were around 50%. X-ray photoelectron spectroscopy (XPS) data indicated the absence of residual nickel(II) bromide. ^{1}H NMR (400 MHz, 25 ºC) in DMSO-d_6: δ (ppm) 0.779 (t, 9H), 1.061-1.460 (m, 36H), 2.52-2.742 (m, 6H), 8.064-8.218 (t, 4H), 13.599 (s,

1H). ^{31}P NMR (162 MHz, 25 ºC, referenced to H_3PO_4 external standard) in $CDCl_3$: δ (ppm) 29.5. DSC (20 °C/min, Ramp -10 to 200 °C) mp 151-152 °C.

3.3.3 Synthesis of (*p*-Carboxyphenyl)triphenyl Phosphonium Bromide (Compound B)

p-Carboxyphenyl diphenylphosphine (5.61 g, 18.32 mmol) and 4-bromobenzoic acid (3.74 g, 18.61 mmol) were dried under reduced pressure in a vacuum oven overnight at 60 °C and added under argon to a flame-dried, double-neck, 100-mL, round-bottom flask with an overhead mechanical stirrer. Anhydrous nickel(II) bromide (2.06 g, 9.43 mmol) was added from an ampoule under an argon purge, and then the flask was purged with argon for an additional 30 min. The reaction proceeded at 160 ºC under argon for 15.5 h. The dark green product was dissolved in 50 mL of chloroform and filtered. The product was then washed with 44% aq HBr two times. Residual water was removed with sodium sulfate. The dark green solution was then precipitated in 600 mL of ethyl ether. The product was then purified with a 90/10 chloroform/ methanol column and precipitated in 600 mL of ethyl ether. White crystals was acquired and dried at 60 ºC under reduced pressure in a vacuum oven overnight, and yields were around 20%. XPS data indicated the absence of residual nickel(II) bromide. ^{1}H NMR (400 MHz, 25 ºC) in CD_3OD: δ (ppm) 8.566-9.056 (m, 14H), 9.257-9.549 (m, 3H), 9.558-9.880 (m, 2H). ^{31}P NMR (162 MHz, 25 ºC, referenced to H_3PO_4 external standard) in CD_3OD: δ (ppm) 22.9. DSC (20 °C/min, Ramp -10 to 200 °C) mp 148-150 °C.

3.3.4 Synthesis of (6-Hydroxyhexyl)trioctylphosphonium Bromide (Compound C)

TOP (12.0 g, 33.0 mmol) was added to a flame-dried, 100-mL, double-neck, round-bottom flask with a condenser and an addition funnel. The TOP was purged with argon for 30

min. Then, 6-bromohexanol (5.98 g, 33.0 mmol) was added to the addition funnel under argon. The reaction proceeded at 80 °C for 3 h as 6-bromohexanol was added dropwise. After addition, the temperature was increased to 120 ºC for 5 h. Any residual reagents were removed with vacuum distillation at 120 ºC and approximately 0.3 mmHg. The product was a clear and colorless ionic liquid. Greater than 98% yield was achieved. ^{1}H NMR (400 MHz, 25 ºC) in $CDCl_3$: δ (ppm) 0.834 (t, 9H), 1.151-1.885 (44H), 2.353 (t, 8H), 3.350 (t, 1H), 3.607 (t, 2H). ^{31}P NMR (162 MHz, 25 ºC, referenced to H_3PO_4 external standard) in $CDCl_3$: δ (ppm) 32.9. m/z (+FAB, 100% M^+, Exact mass, Direct Probe) 471.5 g/mol as expected. DSC (20 °C/min, Ramp -80 to 25 °C) mp 12.7-13.0 °C.

3.3.5 Synthesis of (2-Hydroxyethyl)trioctylphosphonium Bromide (Compound D)

This procedure closely followed our previous work.[4] TOP (16.62 g, 44.8 mmol) was added to a flame-dried, 100-mL, double-neck, round-bottom flask with a condenser and an addition funnel. The TOP was purged with argon for 30 min. Then, 2-bromoethanol (5.66 g, 45.3 mmol) was added to the addition funnel under argon. The reaction proceeded at 80 °C for 3 h as 2-bromoethanol was added dropwise over 2 h. After addition, the temperature was increased to 120 ºC for 3 h. Any residual reagents were removed through vacuum distillation at 60 ºC and approximately 0.3 mmHg. The product was a clear and colorless ionic liquid. Greater than 98% yield was achieved. ^{1}H NMR (400 MHz, 25 ºC) in $CDCl_3$: δ (ppm) 0.700 (t, 9H), 0.816-1.715 (36H), 2.205 (t, 6H), 2.506 (t, 2H), 3.87 (t, 2H), 4.473 (s, 1H). ^{31}P NMR (162 MHz, 25 ºC, referenced to H_3PO_4 external standard) in $CDCl_3$: δ (ppm) 32.8. m/z (+FAB, 100% M^+, Exact mass, Direct Probe) 415.4 g/mol as expected. DSC (20 °C/min, Ramp -90 to 30 °C) mp 4.8-5.4 °C.

3.3.6 Synthesis of Butyl *p*-Carboxyphenyl Diphenylphosphonium Bromide (Compound E)

Our method followed closely with a procedure that was reported earlier in the literature.[50] A flame-dried, 250-mL, 2-necked, round-bottomed flask was charged with 10.0 g (0.0326 mol) of 4-diphenylphosphinobenzoic acid. A condenser was attached. The flask was purged with argon for 30 min, and then 36.4 mL (0.339 mol) of 1-bromobutane was added. The reaction mixture was heated in an oil bath adjusted to 110 °C for 18 h. The phosphonium salt product precipitated during the reaction. The product was collected with a fine fritted funnel under aspiration. The product was washed with approximately 50 mL of anhydrous ethyl ether, 5 mL of chloroform, and then with approximately 10 mL of ethyl ether. The collected product was dried overnight in a vacuum oven at 60 °C and stored in a desiccator. A 94% yield was achieved. ^{1}H NMR (400 MHz, 25 ºC) in CD_3OD: δ (ppm) 0.934 (t, 3H), 1.502-1.698 (m, 4H), 3.385-3.490 (m, 2H), 7.691-7.946 (m, 12H), 8.258-8.327 (m, 2H). ^{31}P NMR (162 MHz, 25 ºC, referenced to H_3PO_4 external standard) in $CDCl_3$: δ (ppm) 24.5. m/z (+FAB, 100% M^+, Exact mass, Direct Probe) 363.15 g/mol as expected. DSC (20 °C/min, Ramp -10 to 200 °C) mp 231-237 °C.

3.3.7 Synthesis of Linear Poly(ethylene terephthalate)-*co*-poly(ethylene isophthalate) (PET-co-PEI) Ionomers

This procedure closely followed our previous work.[1] The oligomers were prepared through melt polymerization of DMT (6.08 g, 0.0313 mol), DMI (6.08 g, 0.0313 mol), and EG (5.82 g, 0.0938 mol). Titanium tetraisopropoxide (60 ppm, 0.0098 g/mL in 1-butanol) was used as a catalyst. A three-neck, 100-mL, flame-dried, round-bottom flask was fitted with an overhead mechanical stirrer. A vacuum-distillation condenser with a 100-mL round-bottom receiving flask

was attached. DMT, DMI, and EG were added and degassed with three sets of alternating nitrogen and vacuum cycles, 10 min each. Titanium tetraisopropoxide catalyst was subsequently added. The reactants were stirred and heated to 190 °C under nitrogen. The reaction mixture was polymerized for 2 h at 190 °C with mechanical stirring. After 2 h, the temperature was raised to 220 °C for 2 h, followed by 275 °C for 30 min. Vacuum (0.30 mmHg) was applied for 30 additional min at 275 °C. The product was allowed to cool to room temperature under nitrogen.

Butyl *p*-carboxyphenyl diphenylphosphonium bromide endcapping reagent (1.0 to 7.0 mole % by repeat unit) was added to the oligomers. Mole % targeted was calculated based on the assumption that under reduced pressure at 220-275 °C excess ethylene glycol would be removed and the stoichiometry would be 1 to 1. This calculation was based on 1 equivalent of –OH ends to 1 equivalent of carboxylate groups. After addition of endcapping reagent, the reactants were degassed with nitrogen for 30 min. The mixture was heated under nitrogen with stirring at 220 °C for 30 min. Vacuum (0.30 mmHg) was applied, and the reaction was continued at 220 °C for an additional 2 h. The product was allowed to cool to room temperature under nitrogen.

Mole % incorporation reported was calculated based on ^{1}H NMR integration of the phosphonium endgroup butyl hydrogen resonances versus the other phenyl hydrogen resonances with subtraction of the endcapping reagent phenyl hydrogen resonances. In particular, the butyl –CH_3 or -CH_2-CH_2- units were used from each endcapping reagent. Mole % values achieved were 1.3, 3.9, 5.8, and 7.7 for the targeted mole % values of 1.0, 3.0, 5.0, and 7.0 mole %. The mole % incorporated was slightly higher than the mole % targeted due to loss of some oligomers in addition to the excess ethylene glycol during the synthetic steps under reduced pressure. ^{1}H NMR (400 MHz, 25 ºC) in $CDCl_3$: δ (ppm) 0.829 (-CH_3), 1.464-1.767 (-CH_2-CH_2-), 3.669-3.536 (DEG), 3.724-3.963 (-CH_2-P^+), 4.240-4.338 (DEG), 4.363-4.913 (EG),7.389-7.543 (DMI),

7.582-7.696 (P^+ Phenyl), 7.702-7.858 (P^+ Phenyl), 7.909-8.343 (DMT and DMI), 8.568-8.712 (DMI). ^{31}P NMR (162 MHz in a magnetic field of 9.39 Tesla, 25 ºC, referenced to H_3PO_4external standard) in $CDCl_3$: δ (ppm) 24.5.

3.3.8 Characterization

^{1}H NMR and ^{31}P NMR spectroscopic data were collected in $CDCl_3$ and CD_3OD on a Varian 400 MHz spectrometer operating at 400 MHz and 162 MHz in a magnetic field of 9.39 Tesla respectively. Fast atom bombardment mass spectrometry (FAB MS) was performed on a JEOL JMS-HX-110 instrument in positive mode. A Perkin Elmer Model 5400 with a Mg Kα X-ray source of 1253.8 eV and with an anode operating at 250 W and a take-off angle of 45° was used for XPS. Size-exclusion chromatography (SEC) was conducted in HPLC grade tetrahydrofuran at 40 °C at a rate of 1 mL/min. A size-exclusion chromatograph with 3 in-line 5-μm PLgel MIXED-C columns and a Waters 717 autosampler was used. A Waters 2410 differential refractive index (DRI) detector using 880 nm and a 690 nm Wyatt Technologies miniDAWN (MALLS) multiangle laser-light scattering detector were used. The weight average molecular weights reported are absolute molecular weights from the MALLS detector. DSC was conducted with a Perkin Elmer Pyris 1 under nitrogen at 10 ºC/min. These samples were dried overnight under reduced pressure at 60-70 °C before analysis to remove any residual water that could absorb on contact with air. They were stored in a scintillation vial in a jar surrounded by desiccant for transfer to the DSC. Values from the second heating scan are reported. Samples were melt pressed into thin films before melt rheology only. Melt rheology was obtained with an AR G2 TA Instruments rheometer with 25-mm parallel plates and 5% strain and the measurements were run in oscillatory mode at 120 °C under nitrogen. A Perkin-Elmer TGA 7

was used for thermogravimetric analysis (TGA) under a nitrogen atmosphere and 10°C/min for temperature ramps up to 800°C.

3.4 Results and Discussion

3.4.1 Endcapping Reagent Synthesis and Thermal Properties

One goal of this research was to design a polyester oligomer with phosphonium endgroups where the endcapping reagent and polymer were sufficiently thermally stable to withstand the elevated-temperature melt reaction conditions typically utilized for step-growth polyesters. A series of monofunctional phosphonium endcapping reagents was prepared, and their thermal properties were compared by TGA to choose the most thermally stable one for subsequent polymerization reactions. Our studies focused on carboxylic acid or hydroxyl containing phosphonium salt endcapping reagents that could possibly withstand melt polycondensation reactions at 220 ºC over three hours. Synthesis of all monofunctional phosphonium endcapping reagents proceeded through one of two pathways, a nickel(II) bromide coupling reaction or S_N2 reactions (Figure 3.1).

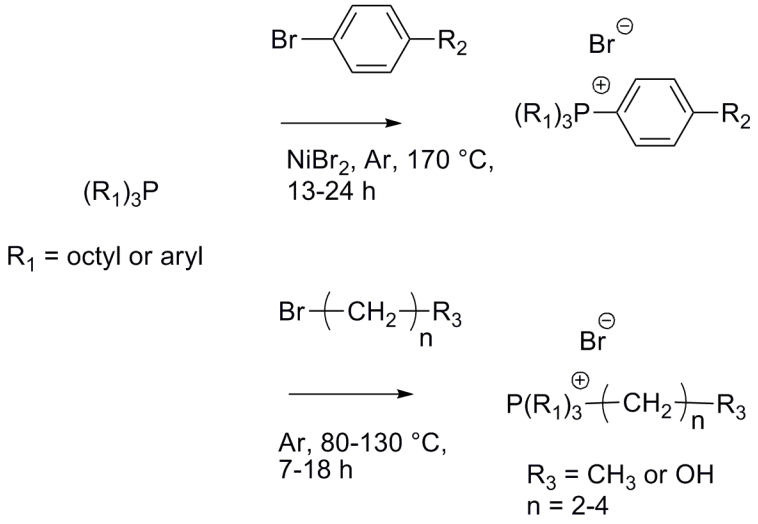

Figure 3.1. Synthesis of phosphonium endcapping agents through a nickel(II) bromide oxidative addition and reductive elimination pathway or through simple S_N2 reactions

Figure 3.2 depicts the series of phosphonium endcapping reagents.

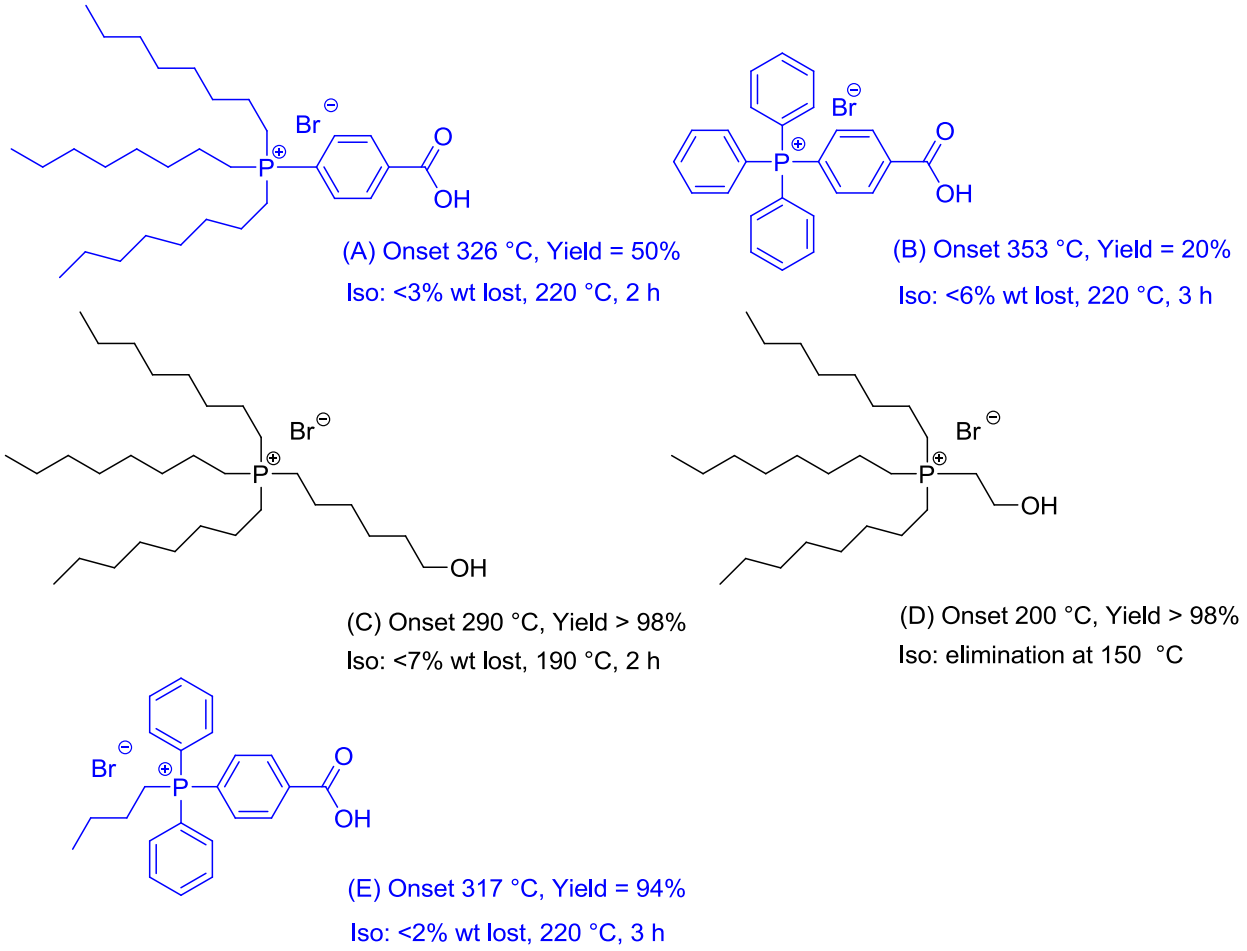

Figure 3.2. Monofunctional phosphonium endcapping reagents, (A)-(E) includes yield, temperature of the onset of degradation (from TGA at 10 °C/minute, N_2); isothermal weight loss (220 or 190 °C, 2 or 3 hours, N_2)

(*p*-Carboxyphenyl)trioctylphosphonium bromide (A) and (*p*-carboxyphenyl)triphenyl phosphonium bromide (B) were synthesized with an oxidative addition and reductive elimination reaction with nickel(II) bromide as a catalyst.[1, 49] These reactions required temperatures around 160-170 °C and long times of 13 to 24 hours. For compound A, a by-product was produced from the coupling of two 4-bromobenzoic acid groups. The nickel(II) bromide reactions were colored: Complexes with TOP produced a dark purple color, and complexes with TPP produced a dark

green color. After extensive catalyst removal steps, yields were around 50% for compound (A) and 20% for compound (B). Retention of nickel(II) bromide limited thermal stability, and nickel(II) bromide is carcinogenic, so removal was imperative.

The endcapping reagents (6-hydroxyhexyl)trioctylphosphonium bromide (C), (2-hydroxyethyl)trioctylphosphonium bromide (D), and butyl (*p*-carboxylphenyl)diphenylphosphonium bromide (E) were synthesized with S_N2 reactions, and their yields were > 94%. These reactions were conducted at <130 °C, produced yields > 94%, and proceeded without a catalyst.

However, butyl (*p*-carboxylphenyl)diphenylphosphonium bromide (E) had both a combination of both good yield and high thermal stability, and thus this chapter focuses on this particular endcapping reagent for polycondensation reactions. It was synthesized through a simple S_N2 reaction without the aid of a catalyst that had to be subsequently removed (Figure 3.3). A large excess of 1-bromobutane was utilized to generate a fast, complete reaction with the aryl phosphine. ^{1}H NMR and ^{31}P NMR spectra indicated that the product had no residual starting reagents (Figure 3.4).

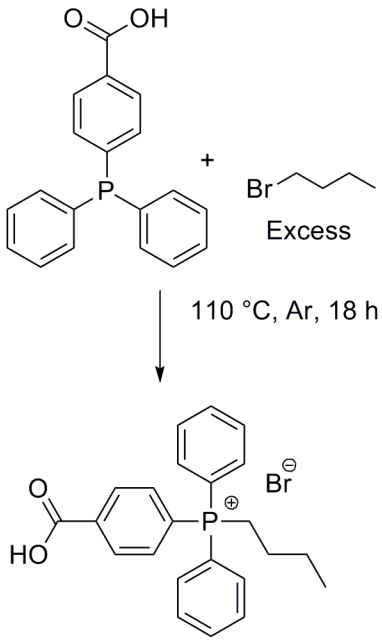

Figure 3.3. Synthesis of butyl (*p*-carboxyphenyl)diphenylphosphonium bromide (E)

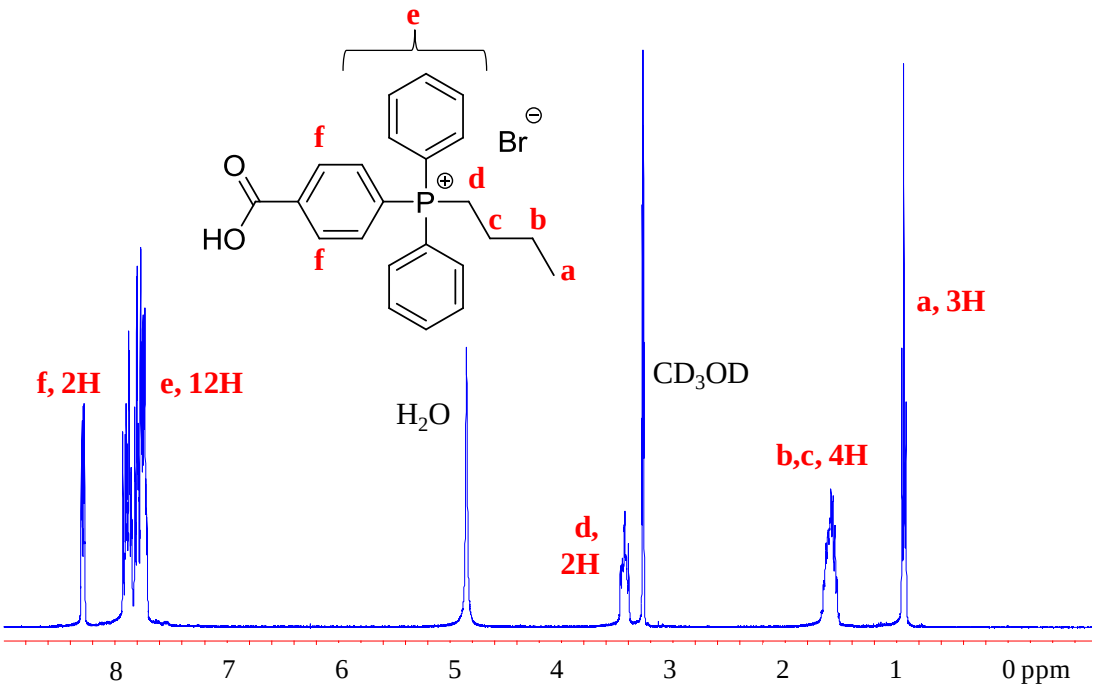

Figure 3.4. ^{1}H NMR spectrum of butyl (*p*-carboxyphenyl)diphenylphosphonium bromide (E); 400 MHz, CD_3OD

Alkylphosphonium salts can degrade through many mechanisms compared to other salts including ammonium compounds which have the Hofmann elimination as their main degradation mechanism.[32] These mechanisms were previously described in chapter 2 and in Figure 2.2. In the absence of oxygen and without any hydroxide anion, the degradation mechanisms with only the bulk sample should not result in phosphine oxide formation. With β-hydrogen abstraction with a bromide anion and subsequent Hofmann elimination, an alkene, a phosphine, and HBr would result.[32, 51] With reduction to phosphine and a bromoalkyls,[32] the TGA should show the loss of the volatile bromoalkanes or bromoalcohols. The α-hydrogen abstraction would form a ylide which can be seen with ^{31}P NMR and HBr.[32, 51] However, typically strong bases, such as alkyl lithium are required to remove the α-hydrogen.[32] In the case of compound (D), the loss of water helps facilitate this elimination.[1,51] The Hofmann elimination is one of the key reactions. Although the Hofmann elimination is a prevalent mechanism for both functionalities, the β-hydrogen elimination occurs at much higher temperatures for the phosphonium salts.[32]

In this thesis, thermal weight loss profiles with temperature of the functional phosphonium endcapping reagents were compared (Figure 3.2). (6-Hydroxyhexyl)trioctylphosphonium bromide (C) and (2-hydroxyethyl)trioctylphosphonium bromide (D) are similar in that they are tetra-alkyl phosphonium ions with one hydroxyl group at the end of one of four alkyls. These salts display onsets of degradation of 290 and 200 °C, respectively. (2-Hydroxyethyl)trioctylphosphonium bromide (D) undergoes elimination to form vinyl trioctylphosphonium bromide and water (Figure 3.5).[1, 51] Formation of vinyls were apparent in the ^{1}H NMR specta with hydrogen resonances of 6.3 to 6.8 ppm.[1]

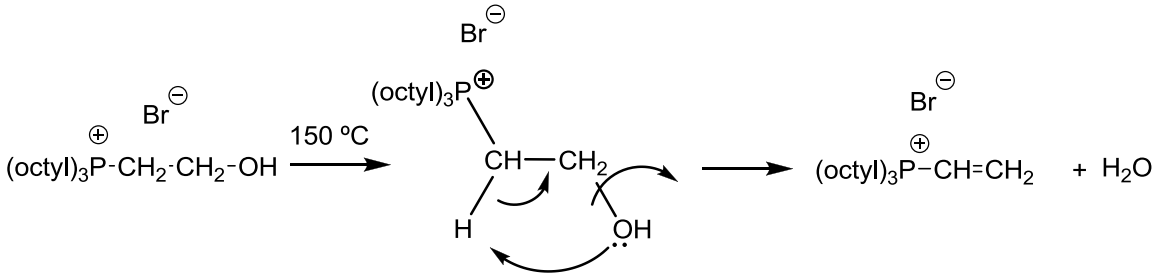

Figure 3.5. The elimination reaction of (2-hydroxylethyl)trioctylphosphonium bromide (D) to form water and trioctyl(vinyl)phosphonium bromide;[1, 51] Adapted with permission from Unal, S. Synthesis and Characterization of Branched Macromolecules for High Performance Elastomers, Fibers, and Films. Ph.D. Thesis, Virginia Polytechnic and State University, Blacksburg, VA, 2005.

Extending the alkyl chain connecting the phosphonium center and the hydroxyl in (C) compared to (D) increased the onset of degradation and the isothermal stability substantially (90 °C according to TGA ramp 10 °C/minute). The longer alkyl chain (C) prevented internal elimination of water which previously formed the trioctyl(vinyl)phosphonium (Figure 3.5). 4-Carboxyphenyl trioctylphosphonium bromide (A) had a higher onset of degradation of 323 °C by TGA under nitrogen at 10 °C/minute than compounds (C) or (D). Therefore, having a carboxylic acid attached directly to the phenyl ring instead of having a long chain with a hydroxyl increased the thermal stability greatly. Butyl (*p*-carboxyphenyl)diphenylphosphonium bromide (E) displays an onset of weight loss at 317 °C by TGA under nitrogen with a 10 °C/minute heating rate. 4-(Carboxylphenyl)triphenylphosphonium bromide (B) with all aryl groups proved to have the highest thermal stability of all salts with an onset of degradation of 353 °C in a TGA ramp at 10 °C/minute under nitrogen.

Isothermal stability studies were performed on the most thermally stable compounds (A), (B), (C), (E) for 2 to 3 hours under nitrogen at 190 or 220 °C in bulk to ensure that no thermal degradation of the endcapping reagent would occur during the course of melt reactions. Compounds (B) and (E) proved highly isothermally stable and lost less than 6 and 2 weight % after 3 hours at 220 °C, respectively. Compound (A) lost less than 3 weight % at 2 hours and had no degradation during those 2 hours, and compound (C) was only thermally stable at 190 °C for 2 hours and lost 7 weight % of its mass. These compounds all readily absorb water upon contact with air, and some mass loss is considered to be from adsorbed water accumulated during transfer. Based on the TGA data, it was reasoned that compounds (A), (B), and (E) were likely sufficiently thermally stable to survive melt polymerization temperatures.

The polyesterifications in this thesis all involve the study of one phosphonium-based endcapping reagent butyl (*p*-carboxyphenyl)diphenylphosphonium bromide (E). This reagent degrades in bulk through elimination of bromobutane to reform the phosphine, the reverse reaction from quaternization (Figure 3.6). The expected mas loss due to bromobutane was 30% and this compares well with the experimental value of 32% between about 317-350 °C observed through TGA.

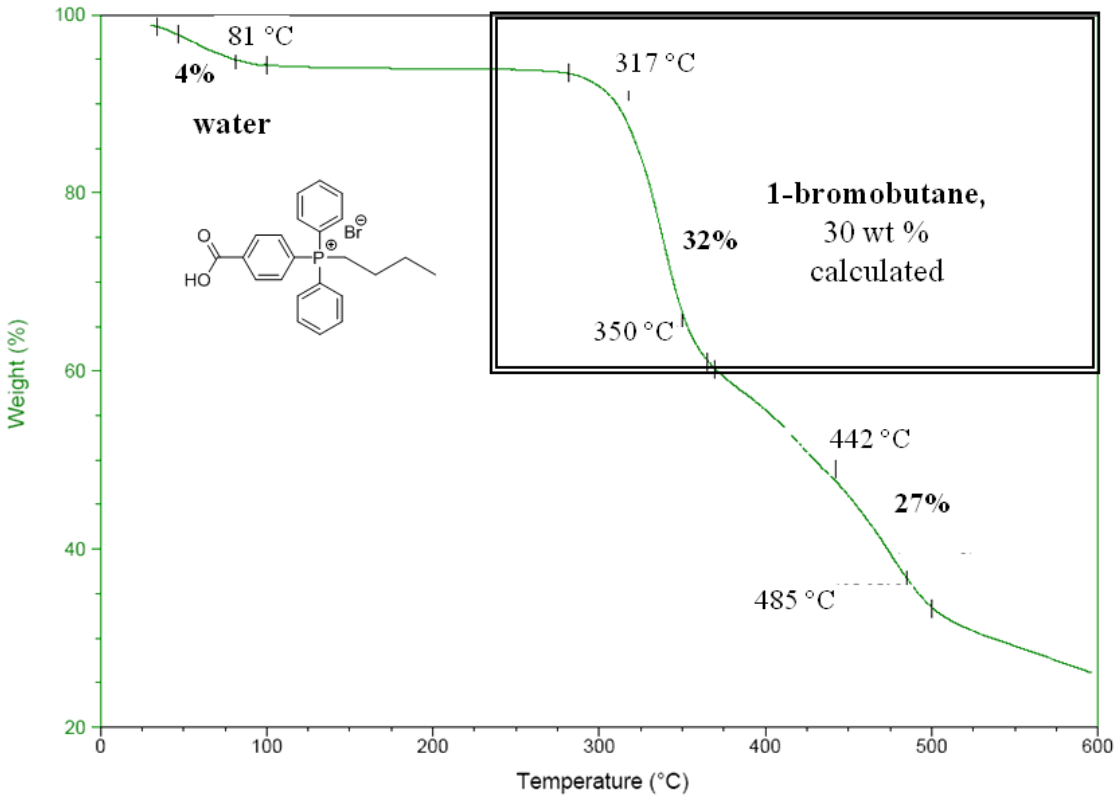

Figure 3.6. Thermal degradation of butyl (*p*-carboxyphenyl)diphenylphosphonium bromide (E), TGA heating rate was 10 °C/minute under nitrogen

3.4.2 Polymer Synthesis

Butyl 4-carboxyphenyl diphenylphosphonium bromide (E) was the focus of our study for the polyester reactions. The synthesis of this reagent was facile with good yield, and (E) exhibited great thermal stability. Polyesterification reactions with this endcapping reagent also resulted in clear, transparent polyesters. Endcapping reagents other than (E) produced discolored polymers, and only compound (E) produced pale yellow, transparent polyesters. A very slight yellow tint was evident in all polymers due to the use of titanium tetra(isopropoxide) catalyst, even in polymers containing only controls with no phosphonium endcapping reagent or just containing 1-dodecanol as the endcapping reagent.

PET-*co*-PEI oligomers were synthesized through typical, multi-step polycondensation conditions (Figure 3.7).[1, 5, 35-45] DMT and DMI were used in a 50/50 ratio for all polymerization reactions to produce amorphous polymers. Synthesizing amorphous polyesters allowed for the study of aggregation and morphology without the complicating effects of crystallization. A series of polymers with various concentrations of phosphonium endcapping reagent were prepared: 1.3, 3.9, 5.8, and 7.7 mole % phosphonium endcapping reagent. These polymers were analyzed with ^{1}H NMR, ^{31}P NMR, SEC, DSC, TGA, and melt rheological measurements. Samples were melt pressed into thin films for rheological studies only, but these films were too brittle for tensile experiments and fractured or cracked immediately during sample handling, cutting, and clamping. These polyesters all had low molecular weights and were, thus, very fragile. Uniform films for DMA in tension mode were difficult to make and keep in-tact during transfer and clamping, and tensile at ambient temperature was not possible.

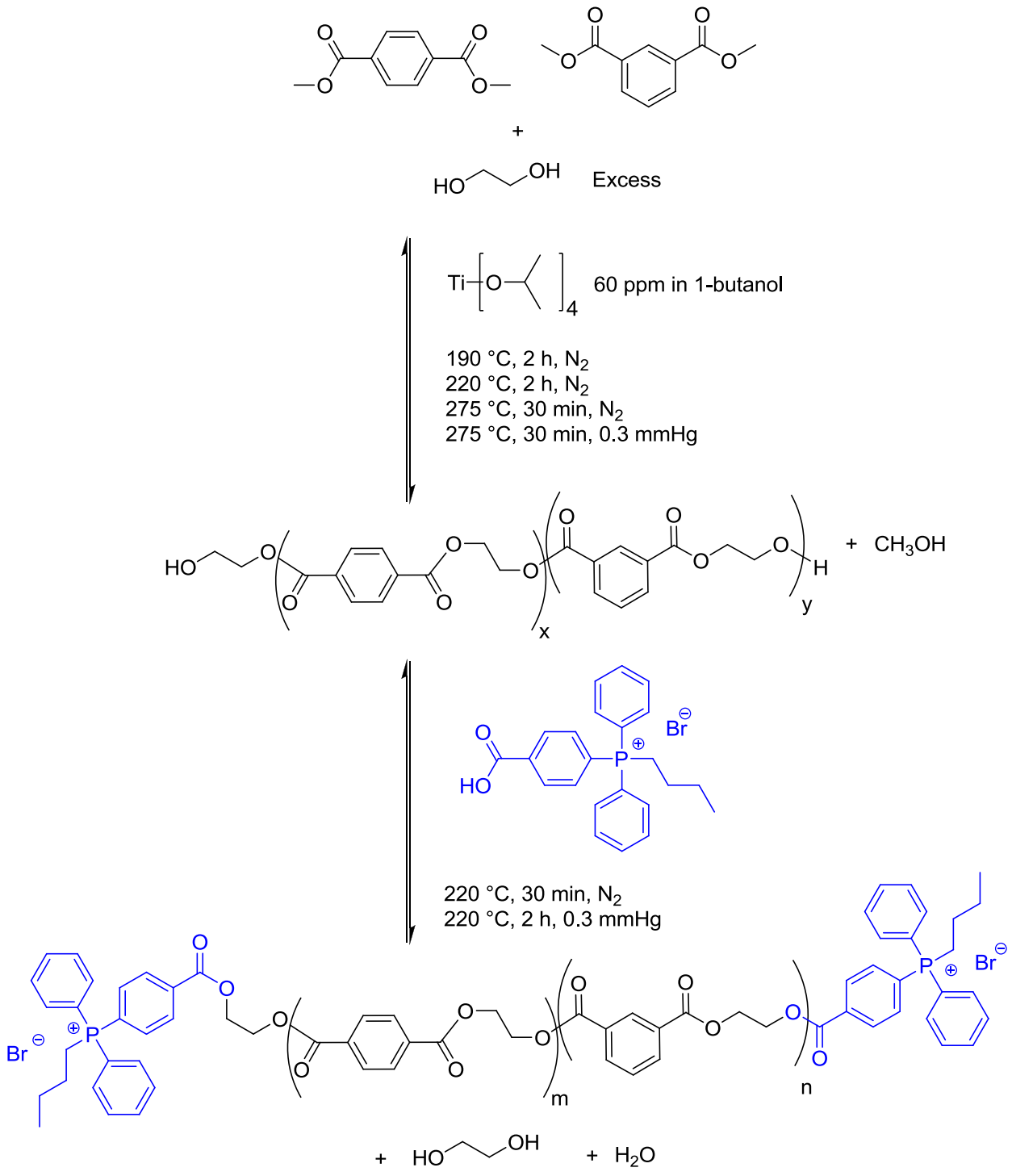

Figure 3.7. Synthesis of linear PET-*co*-PEI oligomers with phosphonium (E) termini

3.4.3 ^{1}H NMR and ^{31}P NMR Analysis

Oligomeric polyester precursors were synthesized to limit the time that the phosphonium salt endcapping reagent was exposed to high temperatures. Shortening the time of high temperature exposure prevented degradation of the phosphonium functionality. ^{1}H NMR resonances relating to the hydrogen resonances of the phosphonium endcapping reagent were evident in the product, and ^{31}P NMR spectra also showed that significant degradation did not occur, including the absence of oxidation and reduction of the cationic center to phosphine oxides or phosphines, respectively (Figure 3.8).

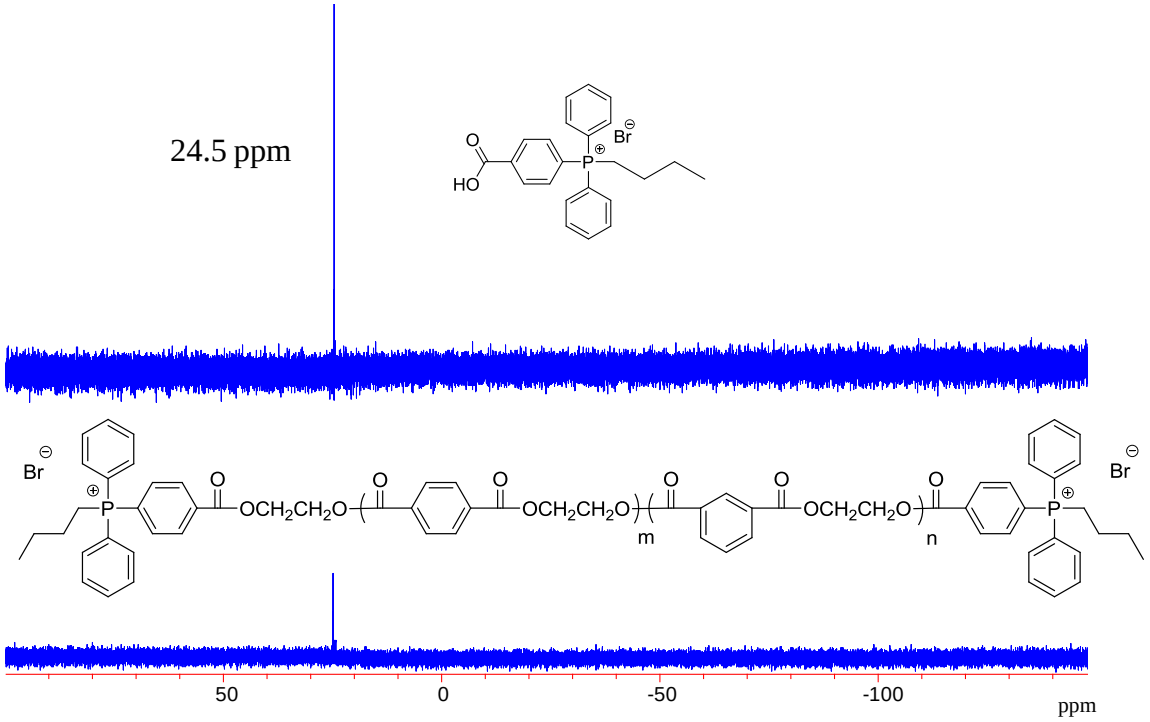

Figure 3.8. ^{31}P NMR spectra of butyl (*p*-carboxyphenyl)diphenylphosphonium bromide and the corresponding endcapped polyester with 5.8 mole % endgroups, NMR: 162 MHz in a magnetic field of 9.39 Tesla, $CDCl_3$

^{1}H NMR spectra showed quantitative incorporation of butyl (*p*-carboxyphenyl)diphenylphosphonium bromide into PET-*co*-PEI. ^{1}H NMR spectra also provided evidence of ionic aggregation in solution for a PET-*co*-PEI polymer endcapped with 7.7 mole % butyl (*p*-carboxyphenyl)diphenylphosphonium bromide (Figure 3.9).

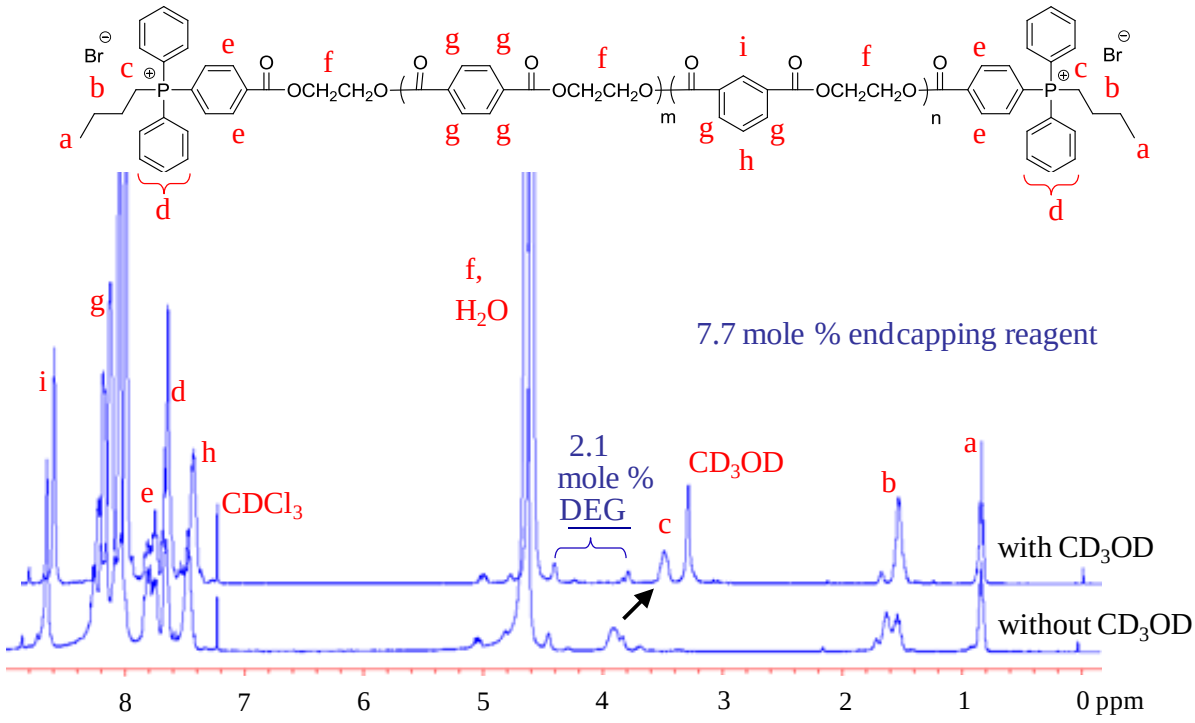

Figure 3.9. ^{1}H NMR spectra of a 7.7 mole % phosphonium endcapped PET-*co*-PEI; 400 MHz in $CDCl_3$ with 6 drops of CD_3OD where indicated

Aggregated phosphonium end groups and subsequently the phosphonium-based butyl groups in $CDCl_3$ may cause additional splitting of butyl protons on methylene units in ^{1}H NMR spectra, compared to shifts in solutions containing a few drops of CD_3OD in $CDCl_3$. Broadening of the butyl methylene proton resonances in the polymer was also evident in $CDCl_3$. Adding 6 drops of

CD_3OD to the NMR tube containing the phosphonium-terminated PET-*co*-PEI in $CDCl_3$ provided a resonance shift in methylene protons next to the phosphonium center. This dramatic movement represents increased mobility of the phosphonium groups as polar solvents help break ionic aggregation. Parent et. al synthesized phosphonium-based poly(isobutylene-*co*-isoprene).[15] Their polymers also exhibited broadening in ^1H NMR in specifically the methylene proton resonances connected to the phosphonium center, and the addition of CD_3OD also resulted in a dramatic resonance shift of these isobutylene protons next to the phosphonium center due to the disruption of ionic aggregation.[15]

^1H NMR was also used to analyze diethylene glycol (DEG) units in the polyesters. The formation of DEG is a typical PET side reaction where elimination of water creates ether linkages, and diethylene glycol units are formed in the polymers.[33] The DEG levels in a control polyester using similar reaction conditions except with a 1-dodecanol endcapping reagent and the reactions containing phosphonium endcapping reagent were compared. A control polyester with a M_n of 6,800 g/mole had 2.4 mole % DEG. Polymers with 1.3, 3.9, 5.8, and 7.7 mole % phosphonium endgroups had DEG levels of 2.3, 3.4, 3.3, and 2.1 mole %. Fiber-grade PET is known to have DEG values ranging from 1.5-2.5%,[33] and polymerization with the phosphonium functionality did not appear to affect this side reaction.

3.4.4 SEC Analysis

The molecular weight of the polymers was reproducibly controlled through the stoichiometry of the phosphonium endcapping reagent (Table 1). As expected, including more endcapping reagent produced a lower molecular weight. Both the number-average and weight-average molecular weights decreased with increased addition of phosphonium endcapping

reagent. Carothers' equation was used to calculate predicted molecular weights.[52-54] The predicted molecular weights were within SEC error of 1000 to 1500 g/mole, except only one value for the highest molecular weight was much lower than predicted. The predicted values assumed that all excess ethylene glycol was removed and that no oligomers were lost under reduced pressure and, thus, these calculations were not a truly-accurate representation of the experiments. The targeted mole % of phosphonium endcapping reagent is greater than expected due to loss of some oligomers under reduced pressure at 220 and 275 °C. The targeted mole % of 1-dodecanol in the control polyester is much lower than expected due to the low boiling point of 1-dodecanol around 260 °C. SEC traces are provided in Figure 3.10 and show the change in molecular weight as endcapping reagent was increased. Increased elution time in SEC correlated with increased mole % phosphonium endcapping reagent in the polyester as calculated with ^{1}H NMR spectra, meaning a lower molecular weight resulted. Overall, control of molecular weight with compound (E) was successfully achieved.

Table 3.1. Compositional analysis of phosphonium (E) endcapped PET-*co*-PEI

Targeted P^+Br^- Salt (mole %)	Incorporated[a] P^+Br^- Salt (mole %)	DEG Levels[a] (mole %)	M_n[b] (g/mole)	M_n[c] (g/mole)	M_w[c] (g/mole)	PDI[c]	T_g[d] (°C)
1.0	1.3	2.3	20,000	9,900	20,000	2.06	65
3.0	3.9	3.4	7,300	6,200	12,000	1.87	65
5.0	5.8	3.3	4,700	6,000	9,300	1.55	65
7.0	7.7	2.1	3,600	5,100	6,900	1.36	65
	Incorporated 1-Dodecanol (mole %)						
5.0	1.2	2.4	---	6,800	14,000	2.09	56

[a] ^{1}H NMR analysis; [b] Predicted M_n: $X_n = (1+r)/(1-r)$ and $r = NA/(NB+2NB')$ assumed excess ethylene glycol removed and 100% conversion;[52-54] [c] SEC analysis, THF, 40 °C, 1 mL/minute; [d] DSC, 10°C/minute, N_2

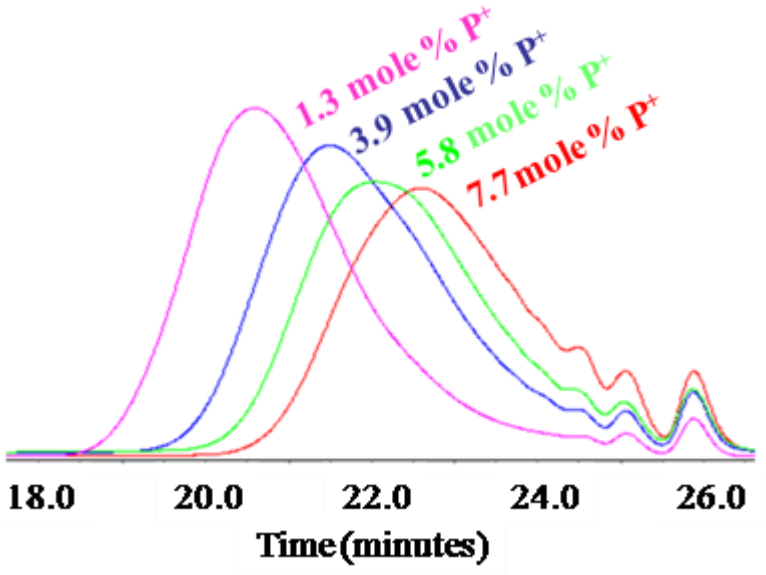

Figure 3.10. SEC traces of phosphonium endcapped polyesters with 1.3 to 7.7 mole % endcapping reagent (E); THF, 40 °C, 1 mL/minute

PDI unexpectedly decreased as the mole % of phosphonium was increased. Lower values than 2.0 may be at least partly attributed to ionic interactions, despite assumedly good resolution in SEC. A small amount of aggregation or column interaction in THF SEC may account for the low PDI values for the two phosphonium-endcapped polyesters containing a high mole % of charge, 5.8 and 7.7 mole %. Polyesters with low amounts of endcapping reagent, 1.3 and 3.9 mole %, produced polymers with typical step-growth PDI values of 2.06 and 1.87, respectively.

3.4.5 Thermal Transitions

Including isophthalate moieties not only creates an amorphous polymer, but it also decreases the T_g of PET. All polymers contained 50% DMI and were expected to have lower glass transitions than PET. The glass transition temperatures were the same for oligomers with number-average molecular weights spanning from 5,100 to 9,900 g/mole with 7.7 to 1.3 mole %

phosphonium endcapping reagent incorporated (Table 1). All phosphonium-endcapped polyesters had a glass transition temperature of 65 °C. DSC data did not indicate a separate ionic transition for any of these amorphous, salt-containing polyesters. A control, 1-dodecanol-endcapped polyester with M_n of 6,800 g/mole and a M_w of 14,000 g/mole produced a glass transition temperature of 56 °C. The number-average and weight-average molecular weights of this control were greater than the 1.3, 3.9, and 5.8 mole % phosphonium-endcapped polyesters, but a T_g of 56 °C for the control is much lower than a T_g of 65 °C.

For most polymers, glass transition temperatures increase significantly with molecular weight when going from very low molecular weights to higher molecular weight, closer to the limiting glass transition value. Ionic aggregation could potentially affect this change and make it less dramatic.[3-4, 6] For example, Eisenberg et al. discussed poly(styrene-*co*-*N*-methyl-4-vinylpyridinium iodide) which had ionic associations that were not stable enough to remain above the T_g, but they increased the T_g with increasing ionic content.[4, 55] In our case, it is hypothesized that ionic aggregation also does not dissociate until above or during the breadth of the glass transition temperature, and the T_g increases or broadens to the same value for all structurally similar polymers. The association of the ionic polymer ends resulted in similar "effective" molecular weights for all of the polymers, and the phosphonium salts dissociate towards the end or just above the glass transition temperature. Ionic aggregates limit the segmental motion of the chain, increasing the glass transition due to physical crosslinking.[3-4, 6] However, weak, large cations are expected to have weak ionic interactions that will dissociate, and the phosphonium ionic aggregates are not expected to exist well above the glass transition in these large cationomers. Changing ionic concentration in polymers with smaller cations, short chain alkyl cations or rigid aryl or ring structures, tends to show large changes in the glass

transition temperature.[2] The phosphonium salts' weak association affords a structural advantage for reversible supramolecular assembly.

3.4.6 Melt Rheology

Melt rheology data indicated only a slight change in viscosity due to ionic association at high temperatures exceeding or equal to 120 °C (Figure 3.11).

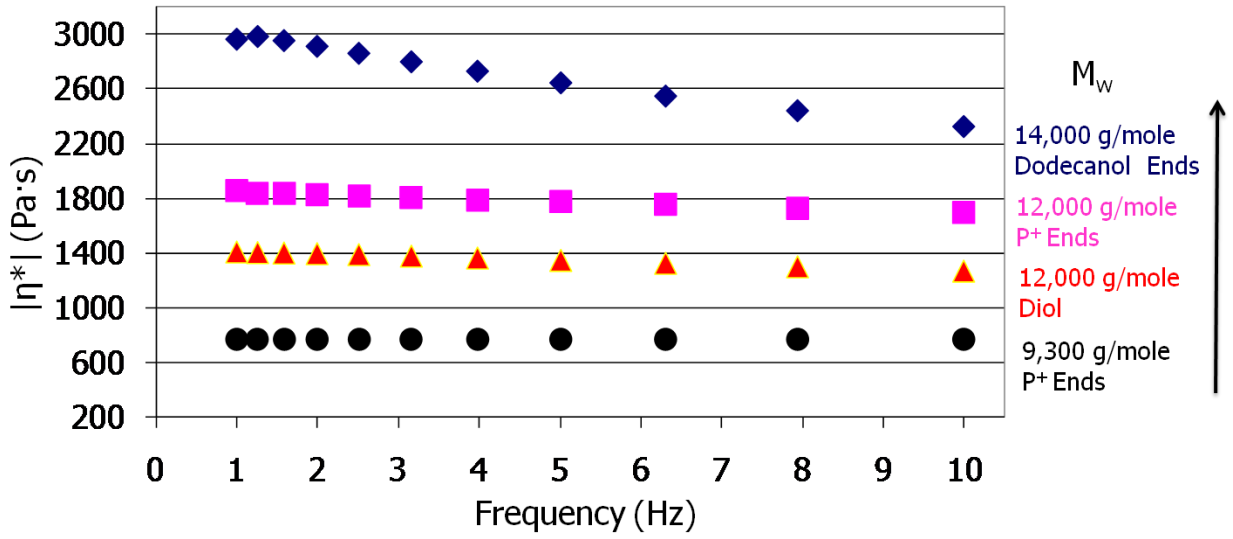

Figure 3.11. Melt rheology of phosphonium-terminated polyesters with 5.8 or 3.9 mole % versus 1-dodecanol endcapped polyesters and polyester diols; rheology was conducted with 25-mm parallel plates at 5% strain in oscillatory mode at 120 °C under nitrogen

Viscosity simply scaled with weight-average molecular weight for all of the polymers. Two controls including a 1-dodecanol endcapped PET-*co*-PEI with a of M_w 14,000 g/mole and a diol endcapped PET-*co*-PEI with a M_w of 12,000 g/mole were compared to two phosphonium-endcapped polymers with 3.9 and 5.8 mole % phosphonium terminal groups and M_w values of

9,300 and 12,000 g/mole respectively. Directly comparing the two polymers with M_w of 12,000 g/mole, the phosphonium endcapped polymer has a slightly higher viscosity. The 1-dodecanol-endcapped control had a M_w of 14,000 g/mole, and the melt viscosity of this control is much higher than the phosphonium-endcapped PET-*co*-PEI. Also, the phosphonium-endcapped polyester with a weight-average molecular weight of 9,300 g/mole had a lower viscosity than the 12,000 g/mole PET-*co*-PEI diol control. Therefore, appreciable ionic association at high temperatures exceeding 120 °C does not exist.

3.4.7 SAXS Analysis

The similarities in the glass transition temperatures in Table 1 for a range of molecular weights suggest that ionic aggregation exists at or below the T_g but may dissociate above the T_g.[4, 55] DSC data did not indicate a separate ionic transition for any of the salt-containing polymers. SAXS analysis did not provide any evidence of an ionic peak, due to the small features and scattering intensity. Due to the low concentrations of ionic content, less than 7.7 mole %, the ionic aggregates should be small, and WAXS analyses may provide valuable information relative to ionic aggregation. WAXS typically is used to observe smaller ionic associations not seen in SAXS, namely multiplets, instead of larger ionic clusters.[2,4] Changing the counter anion may also be a valuable means to probe this ionic aggregation and increase its effects.

3.5 Conclusions

We successfully synthesized an isothermally stable, endcapping reagent, butyl (*p*-carboxyphenyl)diphenylphosphonium bromide (E), and investigated its incorporation as an endcapping reagent for amorphous polyester oligomers. PET-*co*-PEI oligomeric precursors were

synthesized first, then the ionic endcapping reagent was added to limit the amount of time that the phosphonium ionomer was exposed to the elevated temperature synthetic conditions, and avoid thermal degradation of the phosphonium center. ^{1}H spectroscopic analysis confirmed the incorporation of phosphonium endcapping reagent, and ^{31}P NMR spectra showed the absence of any significant degradation of the phosphonium functionality to other phosphorus centers. Molecular weight was successfully controlled with addition of endcapping agent. The glass transition temperatures were 65 °C for number average molecular weights ranging from 5,100 g/mole to 9,900 g/mole with 7.7 to 1.3 mole % phosphonium endcapping reagent, respectively. ^{1}H NMR in solution in $CDCl_3$ and DSC provided evidence of ionic aggregation. DSC showed weak ionic aggregation that increased glass transition temperatures with respect to a control, but all polymers with varied low molecular weights uniquely had the same glass transition temperature. The use of large phosphonium ions prevents strong electrostatic association, and this large cation is unique in that ionic aggregation does not hinder melt processability. In melt rheological studies, low or no appreciable ionic aggregation was apparent above 120 °C in telechelic ionomers endcapped with 7.7 mole % or less phosphonium salt. Ionomers with sodiosulfonate groups have shown aggregation existing greater than degradation temperatures of the polymers, creating polymers that are not melt processable.[10] Weak ionic association could provide a new route to high performance and high strength polymers while maintaining facile melt processing.

3.6 Acknowledgements

Research was sponsored by the Army Research Laboratory and was accomplished under Cooperative Agreement Number W911NF-06-2-0014. The views and conclusions contained in

this document are those of the authors and should not be interpreted as representing official policies, either expressed or implied, of the Army Research Laboratory or the U.S. Government. The U.S. Government is authorized to reproduce and distribute reprints for Government purposes notwithstanding any copyright notation hereon. The authors would like to acknowledge Tom Glass for ^{31}P NMR spectrometry and Fredrick L. Beyer, Jong Keun Park and Steve McCartney for aid with TEM and SAXS analyses. Serkan Unal and Qin Lin are also acknowledged for thoughtful discussions, and Rebecca H. Brown is acknowledged for aid with SEC experiments.

3.7 References

1. Unal, S. Synthesis and Characterization of Branched Macromolecules for High Performance Elastomers, Fibers, and Films. Ph.D. Thesis, Virginia Polytechnic and State University, Blacksburg, VA, 2005.
2. Eisenberg, A.; King, M., *Ion-Containing Polymers*. Academic Press: New York, 1977.
3. Eisenberg, A.; Hird, B.; Moore, R. B. *Macromolecules* **1990**, *23*, 4098-4107.
4. Eisenberg, A.; Kim, J.-S., *Introdcution to Ionomers*. John Wiley & Sons, Inc.: New York, 1998.
5. Kang, H.; Lin, Q.; Armentrout, R. S.; Long, T. E. *Macromolecules* **2002**, *35*, 8738-8744.
6. Tant, M. R.; Mauritz, M. R.; Wilkes, G. L., *Ionomers: Synthesis, Structure, Properties and Applications*. Blackie Academic & Professional: New York, 1997.
7. Grady, B. P. *Polymer Engineering and Science* **2008**, *48(6)*, 1029-1051.
8. Berti, C.; Colonna, M.; Binassi, E.; Fiorini, M.; Karanam, S.; Brunelle, D. J. *Reactive and Functional Polymers* **2010**, *70(6)*, 366-375.
9. Buruiana, T.; Buruiana, E. C. *Journal of Applied Polymer Science* **2005**, *96*, 577–582.
10. Lahor, A.; Nithitanakul, M.; Grady, B. P. *European Polymer Journal* **2004**, *40*, 2409–2420.
11. Ibarra, L.; Alzorriz, M. *Journal of Applied Polymer Science* **2003**, *87(5)*, 805-813.
12. Saito, T., Mather, B. D.; Costanzo, P. J.; Beyer, F. L.; Long, T. E. *Macromolecules* **2008**, *41*, 3503-3512.
13. Paddison ,S. J. *Annual Review of Materials Research* **2003**, 33, 289-319.
14. Kanazawa, A.; Ikeda, T.; Endo, T., *Journal of Polymer Science: Part A: Polymer Chemistry* **1993**, *31*, 335-343.
15. Parent, J. S.; Penciu, A.; Guillen-Castellanos, S. A.; Liskova, A.; Whitney, R. A. *Macromolecules* **2004**, *37*, 7477-7483.
16. Zhou, P.; Blumstein, A. *Polymer* **1997**, *38(3)*, 595-604.
17. Jenkins, I. H.; Kar, A. K.; Lindsell, W. E.; Murray, C.; Preston, P. N.; Wang, C.; Wherrett, B. S. *Macromolecules* **1996**, *29(20)*, 6365-6370.
18. Seyferth, D.; Masterman, T. C. *Macromolecules* **1995**, *28*, 3055-3066.

12. Lindsell, W. E.; Radha, K.; Soutar, I.; Stewart, M. J. *Polymer* **1990**, *31*, 1374-1378.
19. Atmaca, L.; Kayihan, I.; Yagci, Y. *Polymer* **2000**, *41*, 6035-6041.
20. Kanazawa, A.; Ikeda, T. *Coordination Chemistry Reviews* **2000**, *198*, 117-131.
21. Mather, B. D.; Baker, M. B., Beyer, F. L.; Green, M. D.; Berg, M. A. G.; Long, T. E. *Macromolecules* **2007**, *40*, 4396-4398.
22. Nishikubo, T.; Koichi, A.; Uchida, J. *Makromol. Chem.* **1989**, *190*, 1471-1482.
23. Nishikubo, T.; Uchida, J.; Matsui, K.; Iizawa, T. *Macromolecules* **1988**, *21*, 1583-1589.
24. Tomoi, M.; Kori, N.; Kakiuchi, H. *Makromol. Chem.* **1986**, *187*, 2753-2761.
25. Kenawy, E.; Abdel-Hay, F. I.; El-Shanshoury, E. R.; El-Newehy, M. H. *Journal of Polymer Science: Part A: Polymer Chemistry* **2002**, *40*, 2384-2393.
26. Parent, J. S.; Liskova, A.; Resendes, R. *Polymer* **2004**, *45*, 8091-8096.
27. Buruiana, E.C.; Buruiana, T.; Melinte, V.Reactive & Functional Polymers **2006**, *66(10)*, 1132-1140.
28. Pazhanisamy, P., Ariff, M.; Anwaruddin, Q. *Journal of Applied Polymer Science* **2005**, *98(3)*, 1100-1105.
29. Tsou, A. H.; Duvdevani, I.; Agarwal, P. K. **2004**, 45(10), 3163-3173.
30. Karaman, H.; Barton, R. J.; Robertson, B. E.; Lee, D. G. *J. Org. Chem.* **1984**, *49*, 4509-4516.
31. Jin, R. ; Aoki, S. ; Shima, K. *Chem. Commun.* **1996**, 1939-1940.
32. Xie, W.; Xie, R.; Pan, W.; Hunter, D.; Koene, B.; Tan, L.; Vaia, R. *Chem. Mater.* **2002**, *14*, 4837-4845.
33. *Modern Polyesters*. Scheirs, J.; Long, T. E. eds. John Wiley & Sons, Ltd.: West Sussex, England, 2003.
34. McKee, M. G.; Wilkes, G. L.; Colby, R. H.; Long, T. E. *Macromolecules* **2004**, *37*, 1760-1767.
35. Lin, Q.; Pasatta, J.; Wang, Z-H.; Ratta, V.; Wilkes, G. L.; Long, T. E. *Polymer International* **2002**, *51*, 540-546.
36. Lin, Q. Pasatta, J.; Long, T. E. *Journal of Polymer Science: Part A: Polymer Chemistry* **2003**, *41*, 2512-2520.
37. Lin, Q.; Unal, S.; Fornof, A. R.; Wei, Y.; Li, H.; Armentrout, R. S.; Long, T. E. *Macromol. Symp.* **2003**, *199*, 163-172.
38. Lin, Q; Long, T. E. *Macromolecules* **2003**, *36*, 9809-9816.
39. Lin, Q.; Unal, S.; Fornof, A. R.; Armentrout, R. S.; Long, T. E. *Polymer* **2006**, *47*, 4085-4093.
40. Landry, C. J. T.; Massa, D. J.; Teegarden, D. M.; Landry, M. R.Henrichs, P. M.; Colby, R. H.; Long, T. E. *Macromolecules* **1993**, *26*, 6299-6307.
41. Yamauchi, K.; Kanomata, A.; Inoue, T.; Long, T. E. *Macromolecules* **2004**, *37(10)*, 3519-3522.
42. Unal, S.; Ozturk, G.; Sisson, K.; Long, T. E. *Journal of Polymer Science: Part A: Polymer Chemistry* **2008**, *46*, 6285-6295.
43. Unal, S.; Long, T. E. *Macromolecules* **2006**, *39*, 2788-2793.
44. Unal, S.; Lin, Q.; Mourey, T. H.; Long, T. E. *Macromolecules* **2005**, *38*, 3246-3254.
45. Suloff, E. C.; Marcy, J. E.; Blackistone, B. A.; Duncan, S. E.; Long, T. E.; O'Keefe, S. F. *Journal of Food Science* **2003**, *68(6)*, 2028-2033.
46. Broze, G.; Jerome, R.; Teyssie, P.; Marco, G., *Polym. Bull.* **1981,** 4, 241. Broze, G.; Jerome, R.; Teyssie, P.; Gallot, B., *J. Polym. Sci., Polym. Lett. Ed.* **1981,** 19, 415. Broze, G.; Jerome, R.; Teyssie, P., *Macromolecules* **1981,** 14, 224. Broze, G.; Jerome, R.;

Teyssie, P., *Macromolecules* **1982,** 15, 920. Jerome, R., In *Telecheloc Polymers: Synthesis and Applications*, Goethals, E. J., Ed. CRC Press, Inc.: Boca Raton, FL, 1989; p Chapter 11.

47. Boykin, T. C.; Moore, R. B., *Poly. Eng. Sci.* **1998,** 38, 1658. Boykin, T. C.; Moore, R. B., *Polym. Prepr.* **1998,** 39, 393. Barber, G. D.; Carter, C. M.; Moore, R. B., *Polym. Mater. Eng.* **2000,** 82, 241. Ng, C. W. A.; Lindway, M. J.; MacKnignt, W. J., *Macromolecules* **1994,** 27, 7. Ng, C. W. A.; Macnight, W. J., *Macromolecules* **1996,** 29, 2421.
48. Bjorksten Research Laboratories, Inc. *Polyesters and Their Applications*. Reinhold Publishing Corporation: New York, 1956.
49. Horner, H.; Duda, U. M., *Tetrahedron Letters* **1970,** 59, 5177.
50. Russell, M. G.; Warren, S. *J. Chem. Soc., Perkin Trans.* I **2000**, 505-513.
51. Hartley, F. R., John Wiley & Sons: 1994; Vol. 3, p 25-91.
52. Schonberger, F.; Kerres, J. *Journal of Polymer Science: Part A: Polymer Chemistry* **2007**, *45*, 5237–5255.
53. Kunz, M. J.; Hayn, G.; Saf, R.; Binder, W. H. *J Polym Sci Part A: Polym Chem* **2004**, *42*, 661.
54. Jurek, M. J.; McGrath, J. E. Polymer 1989, 30, 1552.
55. Gauthier, S.; Duchesne, D.; Eisenberg, A. *Macromolecules* **1987**, *20*, 753-759.

Chapter 4: Bisphosphonium and Bisimidazolium Cations in the Design of Novel Networks from Michael Addition Reactions

4.1 Abstract

Crosslinking through carbon-Michael addition with bisacetoacetates and diacrylates affords a fast, room-temperature curing reaction under mild, basic conditions. Network formation occurs in minutes with minimal solvent or under neat conditions to high gel fractions, greater than 96 to 98%. This thesis describes the first ionic networks synthesized from Michael addition reactions using either a novel bisphosphonium bisacetoacetate (bisacac) or a novel bisimidazolium bisacac. Incorporation of both ionic bisacac monomers into networks through carbon-Michael addition crosslinking reactions with biocompatible PEG diacrylate resulted in the formation of clear, transparent films. All networks were synthesized using the same mole % of bisacac. A non-ionic bisacac based on 1,4-butanediol was also synthesized. This thesis reports the synthesis and the structure-property relationships in all three types of networks: bisphosphonium-based, bisimidazolium-based, and non-ionic. Incorporation of ionic functionality led to broadened and increased glass transition temperatures, yet all three types of networks had similar plateau moduli measured by DMA, and similar Young's moduli, and crosslink densities. Bisphosphonium networks displayed a higher and broader glass transition temperature than the bisimidazolium networks. Inclusion of the bisphosphonium functionality also imparted greater strains at break and stresses at break for its networks than inclusion of bisimidazolium-based or non-ionic bisacacs. The non-ionic networks had the lowest strains at break and stresses at break. Inclusion of ionic functionalities resulted in improved tensile properties, higher and broadened glass transition temperatures, and greater ionic liquid uptake.

Ionic liquid equilibrium uptake results with 1-ethyl-3-methylethyl imidazolium sulfate showed that bisphosphonium-based versus bisimidazolium-based films did not show preferential uptake for the imidazolium ionic liquid. Uptake was dependent on mole % of ionic character, and both types of ionic networks absorbed 2.5X the amount of ionic liquid compared to the absorption of the non-ionic network. Additionally, we report the first electrospun fibers synthesized through Michael addition crosslinking reactions, both non-ionic and ionic fibers.

4.2 Introduction

The base-catalyzed carbon-Michael addition reaction provides a facile, fast, and room-temperature curing reaction under mild, basic conditions to produce robust networks. The reaction tolerates a wide variety of functional groups, and Long et al. recently reviewed Michael addition reactions in polymer chemistry,[1] elucidating their application as tissue scaffolds,[2-3] crosslinked resins,[4] biodegradable hydrogels,[5] and coatings.[6-7] Carbon-Michael addition reactions are omnipresent throughout polymer chemistry.[1] "Living" anionic polymerization of methyl methacrylate and other methacrylates, for example, also proceeds through the carbon-Michael addition mechanism. Michael addition is a simple synthetic strategy for a variety of topologies, including linear, branched, and crosslinked polymers.[1]

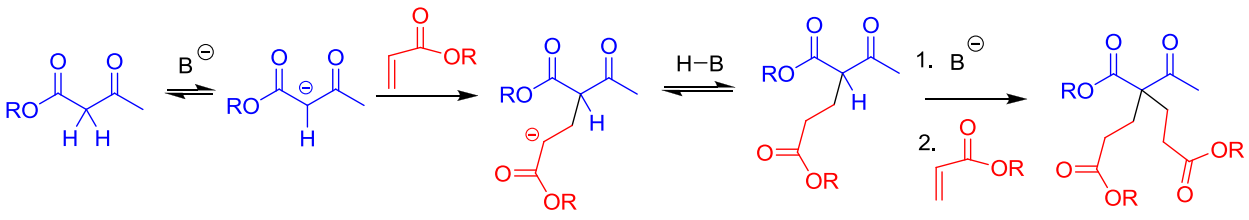

Figure 4.1. General carbon-Michael addition reaction

Abstraction of a proton from an acetoacetate methylene carbon generates a Michael donor that adds across Michael acceptors, which are often olefins with electron withdrawing groups (Figure 4.1).[8] Our research group has demonstrated the crosslinking of bisacetoacetate (bisacac) Michael donors with diacrylate Michael acceptors for biodegradable and biocompatible networks.[9-10] Previously, we investigated acid-cleavable, biocompatible networks synthesized from Michael addition crosslinking of telechelic PEG bis(acetoacetate) with dicumyl alcohol diacrylate (DCDA).[9] PEG, in general, facilitates biocompatibility and enhanced conductivity.[10-14] Base-catalyzed crosslinking reactions produced robust networks, and the ester linkages in the network degraded under acidic conditions to form soluble polymer with diene and carboxylic acid ends.[9] We also investigated biodegradable polycaprolactone (PCL)-based networks from PCL bisacac and neopentylglycol diacrylate.[10] PCL is well-known as a biodegradable polyester.[15-16] Furthermore, we examined the influence of supramolecular interactions in these networks through urethane-hydrogen bonding.[17] Bis(4-isocyanatocyclohexyl)methane was derivatized with hydroxyethyl acrylate and crosslinked with poly(propylene oxide) (PPG) bisacac. Incorporation of hydrogen-bonding groups produced higher tensile strengths and elongation at break as compared to similar networks without hydrogen bonding functionalities.[17]

In this thesis, we report the synthesis of ion-containing bisacac Michael donors and the influence of incorporating ionic-functional monomers on network structure-property relationships. Due to their reinforcing ionic aggregation, enhanced mechanical properties, and enhanced conductivity, ion-functional polymers perform as self-healing, conductive membranes for transducers or self-assembly. They act as transducer membranes to facilitate actuation and ionic liquid uptake. We recently reported ionic liquid swollen actuators from novel ion-containing polymers instead of the ubiquitous ionic Nafion®.[18] Ionic functionality allows for

enhanced ionic liquid uptake and subsequent conductivity, and our recent studies with zwitterionic-containing polymers showed that the ionic liquid prefers to localize in polymer ionic domains.[19] Ionic polymers also have application as antimicrobials.[20] The phosphonium and imidazolium functionalities show promise in antibacterial and antifungal coatings.[20-23]

Herein we describe the synthesis of three novel monomers, bisphosphonium-based, bisimidazolium-based, and non-ionic bisacacs, and their subsequent crosslinking with biocompatible PEG diacrylate. High crosslinking efficiency was demonstrated with both *in situ* FTIR spectroscopy and gel fraction analysis through Soxhlet extraction. Thermal and mechanical properties were investigated with DSC, DMA, and tensile testing. The networks were swollen with ionic liquid to compare their respective equilibrium ionic liquid uptake. We have previously reported electrospun zwitterionic polyacrylates as well as other functional polymers.[24-26] Electrospinning fibers results in a high surface to volume ratio, which may be advantageous for potential filtration and antimicrobial applications. We also report one of the first instances of both non-ionic and ionic electrospun fibers from Michael addition crosslinking reactions.

4.3 Experimental

4.3.1 Materials

Poly(ethylene oxide) (PEG) diacrylate (575 g/mol), tert-butylacetoacetate (98%), 1,8-diazabicyclo[5.4.0]undec-7-ene (DBU, 98%), 1,4-bis(diphenylphosphino)butane (98%), 1,4-dibromobutane, imidazole, sodium hydroxide, 1,4-butanediol, and 6-bromohexanol were purchased from Aldrich and used as received. HPLC-grade methylene chloride, dimethyl sulfoxide (DMSO), and toluene were purchased from Fisher Scientific and used as received. 1-

Ethyl-3-methylimidazolium ethylsulfate (EMIm ES) was purchased from Alfa Aesar, dried at 60 °C overnight, and stored over molecular sieves.

4.3.2 Synthesis of Butane-1,4-bis[(6-hydroxyhexyl)diphenylphosphonium] Bromide (or Bisphosphonium Diol)

A 1-neck, round-bottom flask with a Teflon® stir bar was flame-dried. 4-Bis(diphenylphosphino)butane (11.78 g, 27.6 mmol) was charged to the flask. The flask and contents were purged with argon for 30 min. Then, 6-bromohexanol (15.0 g, 82.8 mmol) in 3-fold excess was charged to the flask under argon, and 72.0 mL of dry chloroform was added. The reaction was purged with argon for an additional 30 min and then allowed to proceed at 70 °C under an argon blanket for 24 h. The reaction solution was diluted with 50 mL of chloroform, and a white powder was precipitated twice in ethyl ether and dried in a vacuum oven at 60 °C overnight. Typical yields exceeded 95%. FAB mass spectrometry m/z (+FAB, 100% M^+, exact mass, direct probe) provided 707.2764 g/mol for the exact mass with 707.2782 g/mol calculated. This ionic diol had a glass transition temperature of 52 ºC (DSC 20 ºC/min). A melting temperature was not observed below 200 ºC, below its degradation temperature. ^{1}H NMR (400 MHz, 25 ºC) in $CDCl_3$: δ (ppm) 1.47 (m, 16H), 1.91 (m, 4H), 3.13 (m, 4H). 3.13 (s, 2H, -OH), 3.58 (m, 8H), 7.56-7.92 (m, 20H, phenyl). ^{31}P NMR (162 MHz, 25 ºC, referenced to H_3PO_4 external standard) in $CDCl_3$: δ (ppm) 28.2. ^{13}C NMR (100 MHz, 25 ºC) in $CDCl_3$: δ (ppm) 134.69 (phenyl), 133.47 (phenyl), 130.39 (phenyl), 61.80 (2C, HO-CH_2-), 31.79 (4C, P^+-CH_2), 24.71 (2C, -CH_2-CH_2-OH), 22.32-19.69 (8C, -CH_2-).

4.3.3 Synthesis of 2,4,25,27-Tetraoxo-12,12,17,17-tetraphenyl-5,24-dioxa-12,17-diphosphoniaoctacosane Bromide (or Bisphosphonium Bisacac)

A 1-neck, round-bottom flask with a Teflon® stir bar was flame-dried. Bisphosphonium diol (2.00 g, 2.31 mmol) was charged to the flask. The flask and contents were purged with argon for 30 min. Then, *tert*-butylacetoacetate (4.03 g, 25.5 mmol) in over a 10-fold excess was charged to the flask, and 16.2 mL of dry chloroform was added. The reaction was purged with argon for an additional 30 min and then allowed to proceed at 70 °C under an argon blanket for 24 h. The reaction solution was diluted with 50 mL of chloroform and precipitated twice in ethyl ether. The ethyl ether was decanted each time from the precipitation vessel, and the product was dried in a vacuum oven at 60 °C for 48 h. The yield was 74%. FAB MS m/z (+FAB, 100% M^+, exact mass, direct probe) agreed with calculated values, 875.3183 g/mol (FAB MS) and 875.3205 g/mol (calculated). This bisacac monomer had a glass transition temperature of 51 ºC (DSC 20 ºC/min), and a melting point was not observed below its degradation temperature. The product existed as a waxy solid below 200 ºC. ^{1}H NMR (400 MHz, 25 ºC) in $CDCl_3$: δ (ppm) 1.33 (m, 4H), 1.52 (m, 12H), 1.93 (m, 4H). 2.23 (s, 6H), 3.18 (m, 4H), 3.44 (s, 4H), 3.61 (m, 4H), 4.06 (m, 4H), 7.62-7.79 (12H, phenyl), 7.89-8.02 (8H, phenyl). The enolate proton resonance appears at 4.94 ppm upon formation of the anion. ^{31}P NMR (162 MHz, 25 ºC, referenced to H_3PO_4 external standard) in $CDCl_3$: δ (ppm) 28.2. ^{13}C NMR (100 MHz, 25 ºC) in $CDCl_3$: δ (ppm) 201.02 (2C, carbonyl), 167.18 (2C, carbonyl), 135.09-129.97 (phenyl), 118.193 (phenyl), 117.347 (phenyl), 65.10 (2C, O-CH_2-), 50.12 (2C, CO-CH_2-CO), 30.525-20.061 (14C, -CH_2-).

4.3.4 Synthesis of 1,4-Di(1H-imidazol-1-yl)butane (or Bisimidazole)

Synthesis of the bisimidazole was accomplished following a literature procedure.[27] Imidazole (5.00 g, 73.4 mmol) and 5.88 g of an aqueous 50 wt % NaOH (73.4 mmol NaOH) solution were added to 40 mL of a mixture (50/50 w/w) of DMSO and toluene. The water was azeotropically distilled and collected with a Dean-Stark apparatus. The solution was cooled to 60 °C, and the lost volume was replaced with anhydrous DMSO. Then, 7.54 g of 1,4-dibromobutane (35.0 mmol) was added to the solution and stirred at 60 °C for 18 h, during which a white precipitate formed. Following the reaction, the DMSO and residual toluene were removed by distillation under vacuum leaving an oily powder to which water was added. White crystals formed overnight at 0 °C. The solution was filtered and washed with water and dried under vacuum at 40 °C. The glass transition temperature was -53 ºC, and the monomer displayed a T_c at 9 ºC and a T_m in the range of 63 to 67 ºC. ^{1}H NMR confirmed the structure.

4.3.5 Synthesis of 1,1'-(Butane-1,4-diyl)bis(3-(6-hydroxyhexyl)-1H-imidazol-3-ium) Bromide (or Bisimidazolium Diol)

Synthesis of the diimidazolium monomer. A 1-neck, round-bottom flask with a Teflon® stir bar was flame-dried. Bisimidazole with a butane spacer (2.15 g, 11.3 mmol) was charged to the flask. The flask and contents were purged with argon for 30 min. Then, 6-bromohexanol (4.66 mL, 34.0 mol) in 3-fold excess was charged to the flask under argon, and 18 mL of dry chloroform was added. The reaction was purged with argon for an additional 30 min and then allowed to proceed at 70 °C under an argon blanket for 24 h. The product was precipitated in ethyl ether as a viscous ionic liquid. The ether was decanted, and the product was dried in a vacuum oven at 60 °C overnight. Typical yields were 90%. FAB MS m/z (+FAB, 100% M^+,

exact mass, direct probe) agreed with calculated values, 471.2319 g/mol (FAB MS) and 471.2335 g/mol (calculated). This ionic liquid diol had a glass transition temperature of -30 ºC (DSC 20 ºC/min) and was a liquid at room temperature. A melting temperature was not observed. ^{1}H NMR (400 MHz, 25 ºC) in CD_3OD δ (ppm) 1.35-1.58 (m, 12H), 1.80-2.00 (m, 8H), 3.52 (m, 4H), 4.22 (m, 4H), 4.28 (m, 4H), 7.65 (d, 4H), 9.12 (m, 2H).

4.3.6 Synthesis of Mono(1,4-bis(3-(6-(3-oxobutanoyloxy)hexyl)-1H-imidazol-3-ium-1-yl)butan-1-ide) Dibromide (or Bisimidazolium Bisacac)

A 1-neck, round-bottom flask with a Teflon® stir bar was flame-dried. Bisimidazolium diol (1.27 g, 2.30 mmol) was charged to the flask. Then, *tert*-butylacetoacetate (3.46 g, 23.0 mmol) in 10-fold excess was charged to the flask, and 14.0 mL of chloroform was added. The reaction was purged with argon for an additional 30 minutes and then allowed to proceed at 70 °C under an argon blanket for 24 h. The reaction solution was purified with flash chromatography with 80/20 hexane/ethyl acetate, and the yield was 85%. The product was dried in a vacuum oven overnight at 60 °C. FAB MS m/z (+FAB, 100% M^+, exact mass, direct probe) agreed with calculated values, 639.2724 g/mol (FAB MS) and g/mol 639.2757 g/mol (calculated). This ionic liquid diol had a glass transition temperature of -27 ºC (DSC 20 ºC/min) and was a liquid at room temperature without an observable melting point. ^{1}H NMR (400 MHz, 25 ºC) in CD_3OD δ (ppm) 1.39-1.65 (m, 12H), 1.93 (m, 8H), 2.23 (s, 6H), 3.30 (s, 4H), 4.12-4.31 (m, 12H), 7.69 (m, 4H), 9.13 (m, 2H).

4.3.7 Synthesis of Butane-1,4-diyl Bis(3-oxobutanoate) (or Non-ionic Bisacac)

A 1-neck, round-bottom flask with a Teflon® stir bar was flame-dried. The 1.4-butanediol was dried overnight in a vacuum oven at 60 °C, and then the diol (1.03 g, 55.5 mmol) was charged to the flask. Then, *tert*-butylacetoacetate (17.8 g, 555 mmol) in 10-fold excess was charged to the flask. The reaction was purged with argon for an additional 30 min and then allowed to proceed at 70 °C under an argon blanket for 24 h. The reaction solution was purified with chromatography in an 80/20 hexane/ethyl acetate solution. The product was dried in a vacuum oven overnight at 60 °C. Yields exceeded 95%. FAB MS m/z (+FAB, 100% M^+, exact mass, direct probe) agreed with calculated values, 258.1116 g/mol (FAB MS) and 258.1103 g/mol (calculated). ^{1}H NMR (400 MHz, 25 ºC) in $CDCl_3$: δ (ppm) 1.70 (m, 4H), 2.24 (s, 6H), 3.44 (s, 4H), 4.14 (m, 4H). Enolate formation was observed with a downfield shift of the methylene hydrogens directly adjacent to the acac functionality at δ (ppm) 1.93 (m, 4H) and the enolate proton resonance at δ (ppm) 4.95 (s, 2H). ^{13}C NMR (100 MHz, 25 ºC) in $CDCl_3$: δ (ppm) 201.21 (2C, carbonyl), 167.37 (2C, carbonyl), 64.88 (2C, -CH_2-OAcac), 50.05 (2C, CO-CH_2-CO), 29.51 (2C, -CH_3), 26.47 (2C, -CH_2-).

4.3.8 Network Formation

A bisphosphonium bisacac (0.233 g, 0.236 mmol) was charged to a 20-mL scintillation vial, and 575 g/mol PEG diacrylate (0.190 g, 0.330 mmol) was subsequently added. A 1:1.4 molar ratio of bisacac:diacrylate was chosen based on previous optimization for these types of reactions in our research group to provide higher tensile strengths and gel fractions.[17] The reagents were dissolved in 800 µL of methylene chloride and stirred for 5 minutes or until fully dissolved. A catalytic amount of DBU (14.3 µL) was added to the vial, and the reagents were

vigorously stirred for 30 to 60 s before casting into Teflon® molds. Reactions were homogenous, and the viscosities increased dramatically as soon as DBU was added. The reaction proceeded in the molds for 24 h at room temperature, and films were dried in a vacuum oven overnight at room temperature. Soxhlet extraction and gel fraction calculations followed, and films were again dried overnight at reduced pressure and 60 ºC before subsequent analysis. All other networks were synthesized using this method with substitution of bisimidazolium or non-ionic bisacac monomers, maintaining the 1:1.4 molar ratio of bisacac:diacrylate.

4.3.9 Characterization

^{1}H NMR spectroscopy was conducted on a 400 MHz Varian UNITY NMR spectrometer at 23 ºC in $CDCl_3$ or CD_3OD. ^{31}P NMR was performed on this same spectrometer operating at 162 MHz in a magnetic field of 9.39 Tesla. Gel fractions were reported gravimetrically from initial over final mass values after Soxhlet extractions in methylene chloride for 10 h and subsequent drying in a vacuum oven under reduced pressure at 60 ºC overnight. FAB MS was performed on a JEOL JMS-HX-110 instrument in positive mode. A Perkin Elmer 7 with a heating rate of 10°C/min under nitrogen was used for TGA. DSC was instrumented with a Perkin Elmer Pyris 1 under nitrogen at 20 ºC/min. Values from the second heating cycle were reported. An ASI REACTIR 4000 was used for *in situ* FTIR spectroscopy at 25 ˚C with a resolution derived from 8 and 64 scans averaged every 30 s. Atomic Force Microscopy (AFM) was performed on a Veeco MultiMode AFM with an rms of 4.0 and setpoint amplitude of 3.3 mV. DMA was performed on a TA Instruments Q800 in tension mode with a frequency of 1H, oscillatory amplitude of 15 µm, and a static force of 0.01 N at 3 ºC/min from -100 to 120 ºC. Glass transition temperatures were determined from the peaks of the tan delta curve and onset of

the storage modulus damping. Tensile experiments produced stress-strain curves with an Instron 4411, crosshead speed of 2 mm/min, and ambient temperature. The reported values and standard deviations involved an average of three samples, and manual grips were used. Ionic liquid uptake experiments were completed according to a previous procedure in our research group.[19] Before starting the ionic liquid uptake experiments, all films were dried at 60 °C for 24 h under reduced pressure. EMIm ES was dried at 60 °C overnight, and placed in scintillation vials. Enough EMIm ES was added to fully immerse the films. One film was used per scintillation vial on EMIm ES. Once immersed, the vials were sealed, and Parafilm® was wrapped around the top. The scintillation vials were placed into a desiccator with low humidity. The films were removed for each measurement with tweezers and excess ionic liquid was lightly removed from the surface by blotting with a Kimwipe®. After each measurement, the ionic liquid uptake was calculated from the following equation: % ionic liquid uptake = $(X - X_0)/X_0$. X_0 is the initial weight of the film, and X is the weight after ionic liquid uptake at a specific time. Reaction solutions for electrospinning were prepared in a similar manner as casting networks in molds, except the solutions were quickly stirred and loaded into a 20-mL hypodermic syringe with an 18-gauge needle within seconds after base was added. The syringe was mounted in a syringe pump from KD Scientific, Inc. A high voltage power supply, a Spellman CZE1000R from Spellman High Voltage Electronics Corp., delivered 25 kV across the tip of a syringe needle that was connected with an alligator clip to the positive lead. There was a 20 cm tip-to-target distance, and the grounded metal target was a 304 stainless steel mesh screen that was ¼ inch x ¼ inch. The solution was pumped at 3 mL/h with a 25 kV constant voltage immediately after loading, and electrospinning continued until pumping was no longer possible due to gelation of the solution. Fibers were collected on the stainless steel mesh screen, and they were not Soxhlet

extracted due to their brittle nature. They were sputter-coated with an 8-nm layer mixture of platinum and gold to reduce electron charge effects in the microscope. Scanning electron microscopy was performed at 5 KV and 100 and 200 KX magnifications on a Leo 1550 field-emission scanning electron microscope (FESEM).

4.4 Results and Discussion

4.4.1 Synthesis of Networks from Carbon-Michael Addition Reactions

Carbon-Michael addition facilitated the synthesis of highly crosslinked ionic and non-ionic networks. The reaction involves abstraction of bisacac protons with base to generate carbanions, which add across activated olefins or diacrylates (Figure 1). The base should have a pK_a in the same range as the pK_a of the two acetoacetate methylene hydrogens, pK_a 12 and 13 respectively.[17,28] In our case, we selected the base 1,8-diazabicyclo[5.4.0]undec-7-ene (DBU) having a pK_a of 12. After abstraction of a proton with base and after addition across the olefin, the new carbanion generated can abstract a proton from the protonated base to form a neutral product. The catalytic base is thus regenerated. Bisacetoacetate (bisacac) precursors, having a functionality of four from their four abstractable methylene hydrogens are synthesized through a transesterification reaction of diols with *tert*-butylacetoacetate.[29] Thus, the synthesis of three novel bisacac monomers first included the synthesis of hydroxyl-functionalized precursors.

First, we synthesized a bisphosphonium bisacac monomer from 1,4-bis(diphenylphosphino)butane, 6-bromohexanol, and tert-butylacetoacetate. All reactions were purged thoroughly with argon for 30 minutes and kept under an argon blanket to prevent rapid oxidation of phosphine to phosphine oxide during the precursor and the monomer synthesis. Simple S_N2 reaction of the bisphosphine with a three molar excess of 6-bromohexanol in

chloroform at 70 ºC for 24 hours produced a bisphosphonium diol in excellent yield, > 95% (Figure 4.2).

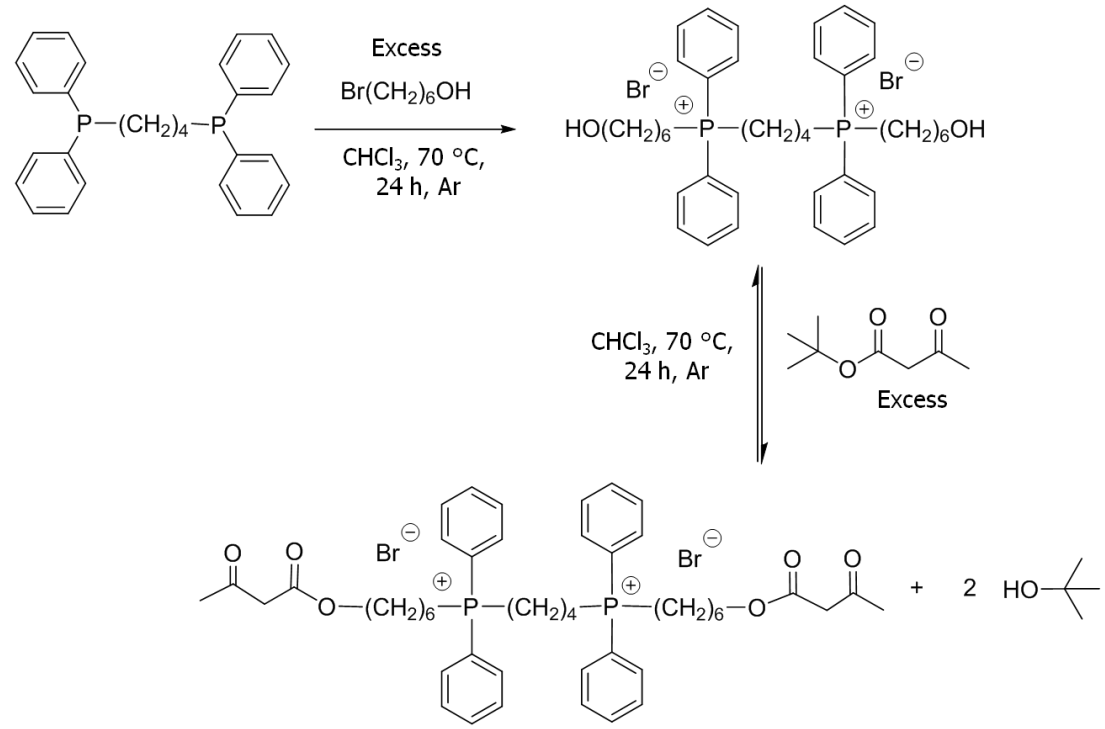

Figure 4.2. Bisphosphonium bisacac monomer synthesis

The ionic solid had a glass transition temperature of 52 ºC, and no melting point was observed below 200 ºC. However, a melting point could exist beyond its degradation point as it still remained a solid past the glass transition temperature.

Subsequently, this ionic diol was reacted with a 10-fold excess of *tert*-butylacetoacetate in chloroform at 70 ºC for 24 hours. The product was precipitated twice into ethyl ether to remove remaining *tert*-butylacetoacetate. Typical yields were 74%. ^{1}H NMR and ^{31}P NMR spectra also confirmed the structure (Figure 4.3).

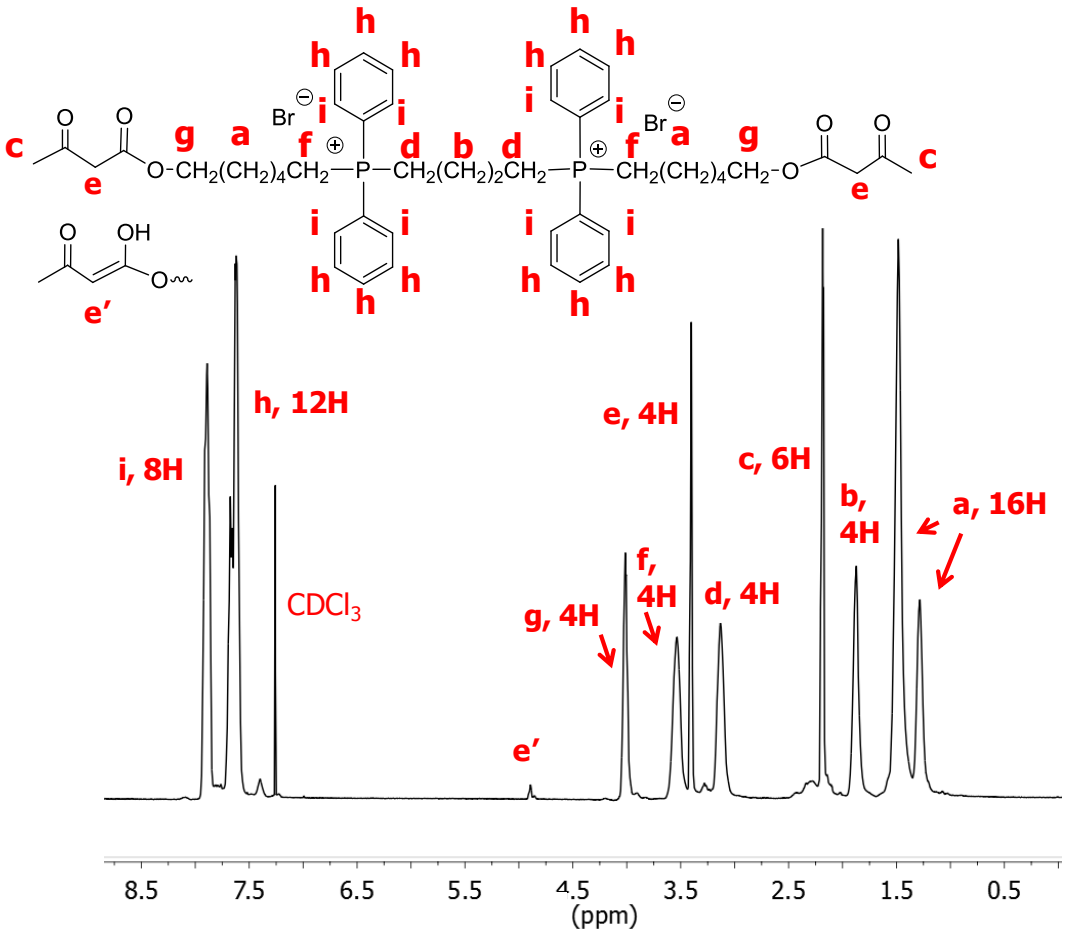

Figure 4.3. ^{1}H NMR spectrum of 2,4,25,27-tetraoxo-12,12,17,17-tetraphenyl-5,24-dioxa-12,17-diphosphoniaoctacosane bromide (or bisphosphonium bisacac); 400 MHz, $CDCl_3$

The glass transition temperature of the ionic solid was 51 ºC. No melting point was observed below 200 °C. The glass transition temperatures for the bisacac and diol bisphosphonium precursors were very similar, 51 and 52 ºC respectively. Functionalization with the *tert*-butylacetoacetate did not facilitate a large change in packing energies. If a melting point existed, the melting point could not be determined due to degradation above 200 ºC, although long alkyl chains improve melting points and crystalline packing efficiency for most phosphonium functionalities.[30]

A second ion-containing bisacac monomer was synthesized through a bisimidazole precursor (Figure 4.4).

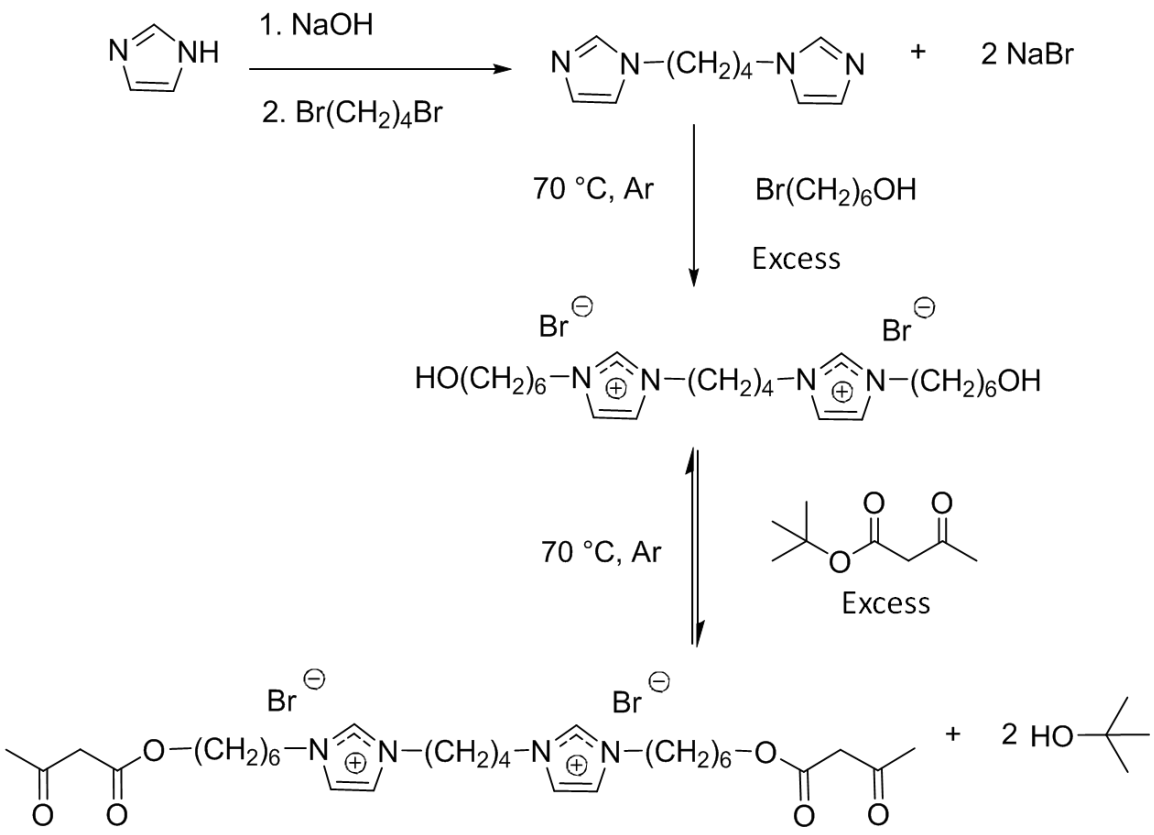

Figure 4.4. Bisimidazolium bisacac monomer synthesis

The synthesis of bisimidazole precursor followed a literature procedure.[27] Imidazole was deprotonated with sodium hydroxide for three to four hours, then 1,4-dibromobutane was added. Imidazole in excess capped the 1,4-dibromobutane through S_N2 reactions to produce the bisimidazole precursor, then reaction of the bisimidazole with a 3-fold excess of 6-bromohexanol

at 70 ºC for 24 hours produced a bisimidazolium diol. This ionic diol was a clear ionic liquid at room temperature with a glass transition temperature of -30 ºC and no observable melting point.

The diol was subsequently reacted with a 10-fold excess of *tert*-butylacetoacetate in chloroform at 70 ºC for 24 hours under argon to synthesize the bisacac monomer. ^{1}H NMR spectra confirmed the structure (Figure 4.5).

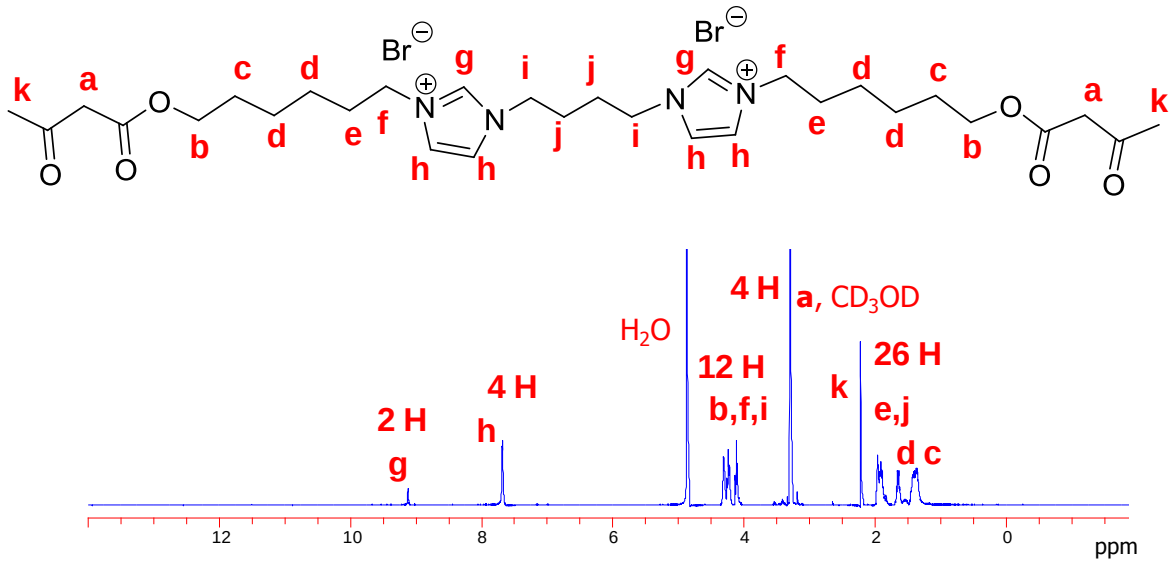

Figure 4.5. ^{1}H NMR spectrum of mono(1,4-bis(3-(6-(3-oxobutanoyloxy)hexyl)-1H-imidazol-3-ium-1-yl)butan-1-ide) dibromide (or bisimidazolium bisacac); 400 MHz, CD_3OD

The glass transition temperatures for the bisacac and bisimidazolium diol precursors were very similar, -27 and -30 ºC respectively. Functionalization with the *tert*-butylacetoacetate apparently did not result in a large decrease in the packing energy, similar to the bisphosphonium precursors. However, the bisimidazolium diol and the bisimidazolium bisacac did not have melting points, and they were room-temperature ionic liquids.

Reaction of 1,4-butanediol with *tert*-butylacetoacetate in chloroform at 70 ºC for 24 hours under argon facilitated the synthesis of a non-ionic bisacac monomer (Figure 4.6). The structure was confirmed with ^{1}H NMR spectra (Figure 4.7).

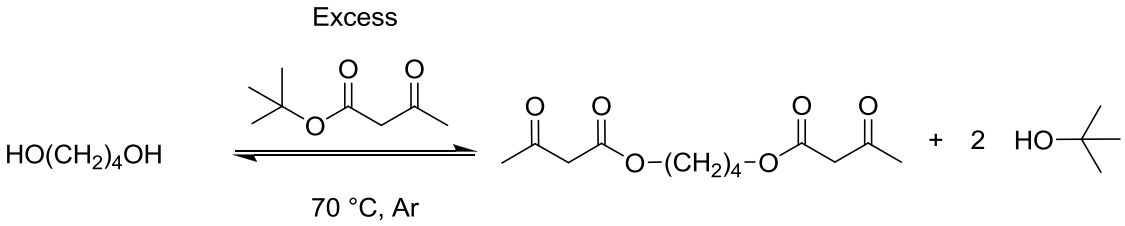

Figure 4.6. Non-ionic bisacac monomer synthesis

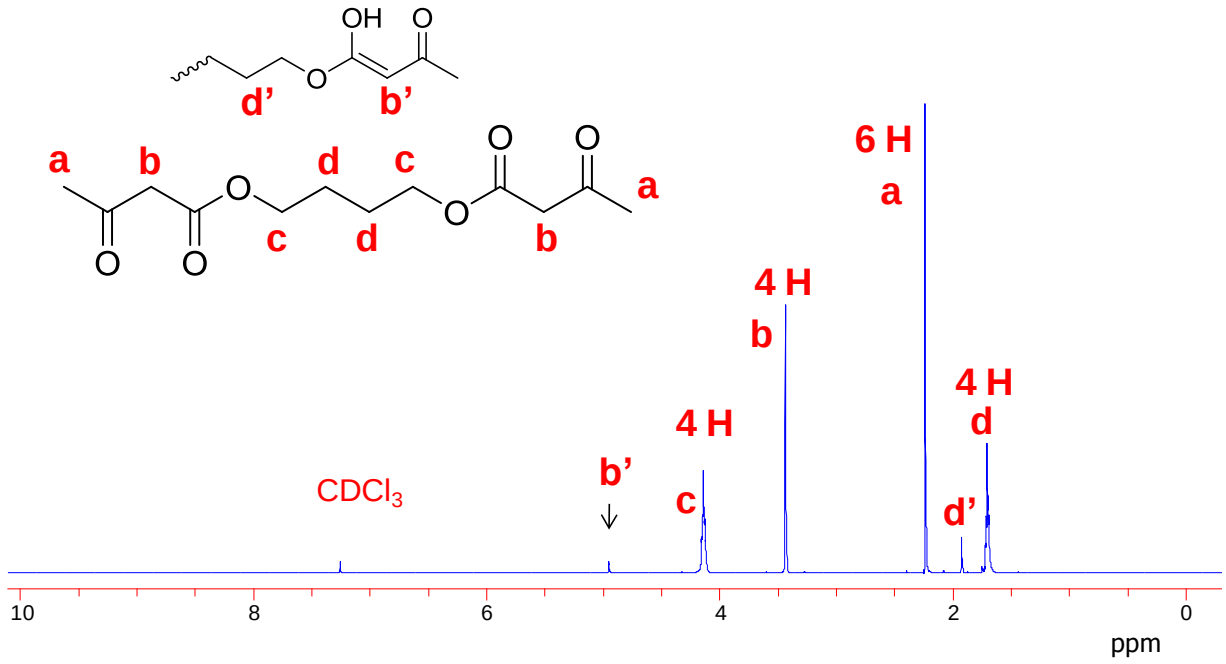

Figure 4.7. ^{1}H NMR spectrum of butane-1,4-diyl bis(3-oxobutanoate); 400 MHz, $CDCl_3$

These three novel bisacac monomers were separately crosslinked through Michael addition reactions with a biocompatible PEG diacrylate (Figure 4.8).

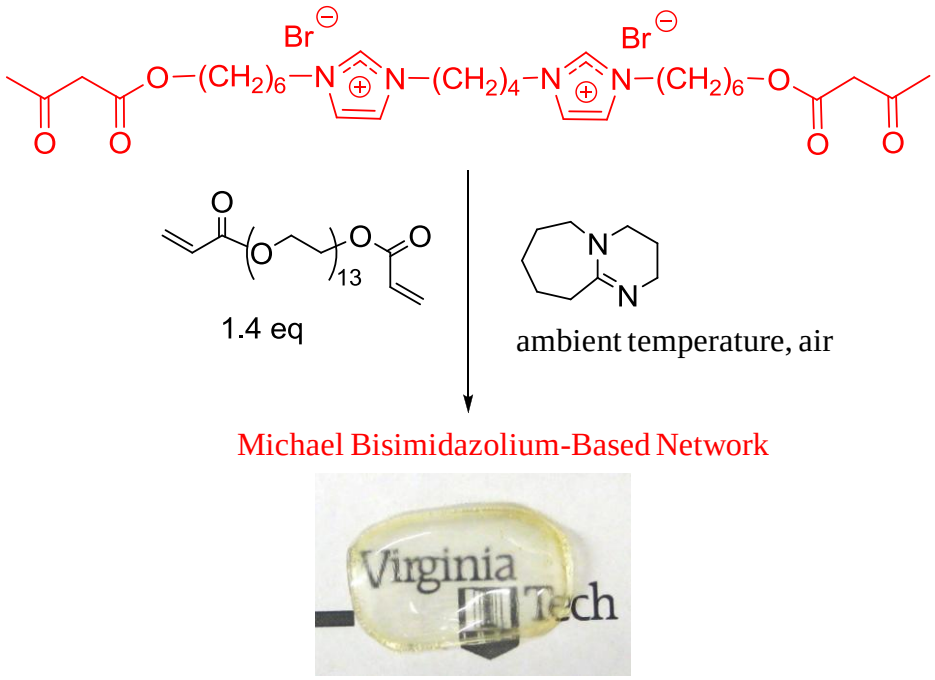

Figure 4.8. Synthesis and film formation of imidazolium-containing networks from Michael addition reactions

The low molecular weight PEG diacrylate (575 g/mol) has a functionality of 2, and the bisacac monomers each have a functionality of 4. A 1:1.4 ratio of bisacac to diacrylate facilitates complete reaction of acrylate functionalities in fast crosslinking reactions to prevent dangling acrylate ends that might be susceptible to further polymerization or degradation.[17] Previous results from crosslinking experiments in our research group showed that a 1:1.4 ratio produced networks with improved tensile properties and higher gel fractions compared to the stoichiometric 1:2 ratio of bisacac:diacrylate functionalities.[17]

Preparation of networks from Michael addition reactions involved combining the bisacac and diacrylate monomers in a 1:1.4 mole ratio in a scintillation vial. The reactants were then diluted with 800 µL of methylene chloride, and 14.5 µL of DBU was added. Once the DBU was added, the solutions immediately became viscous. The solution was stirred for one minute before

casting into Teflon® molds. After 24 hours at room temperature, the films were dried in a vacuum oven overnight. They were then Soxhlet extracted for 10 hours with methylene chloride and dried to produce transparent, free-standing films. The bisimidazolium-based, bisphosphonium-based, and non-ionic networks all had gel fractions (with an average of three samples) greater than 96 to 98 weight % with less than 7% error, so it was concluded that these materials were efficiently crosslinked (Table 4.1).

Table 4.1. Gel fractions

Bisacac Functionality	Gel Fraction (%, after Soxhlet extraction*)
Bisphosphonium	96 ± 6
Bisimidazolium	98 ± 4
Non-ionic	96 ± 7

*****10 hours, CH_2Cl_2

4.4.2 *In situ* FTIR Spectroscopy of Network Formation from Michael Addition Reactions

Monitoring the reactions with *in situ* FTIR on the surface showed complete conversion of diacrylate. The 800-820 cm^{-1} region involves out-of-plane bending of the hydrogens on the acrylate monomers. Over time, the absorption due to diacrylate-proton bending reduces to baseline, indicating complete conversion by disappearance of acrylate functionality (Figure 4.9).

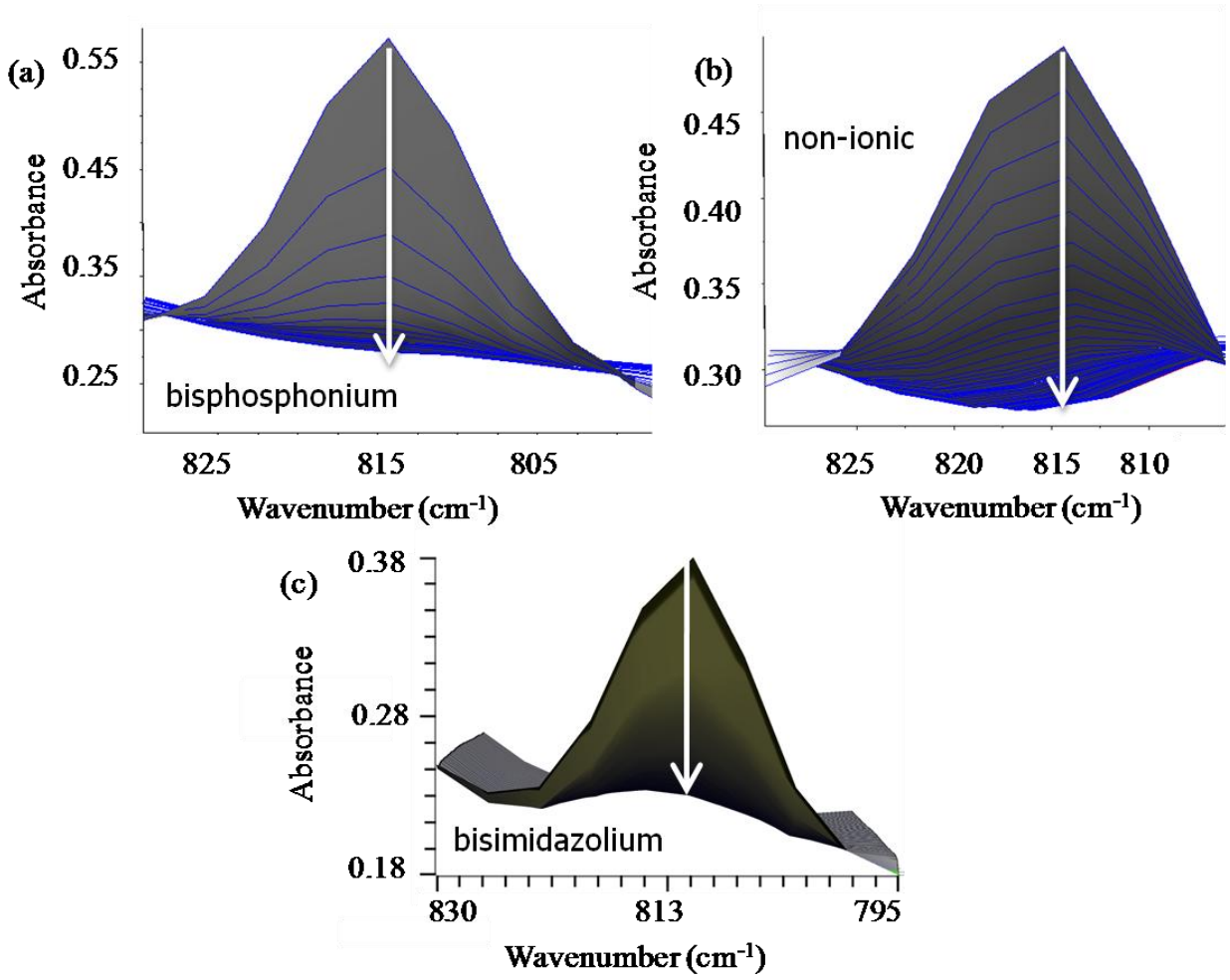

Figure 4.9. *In situ* FTIR spectra of out-of-plane bending of diacrylate protons over time in (a) bisphosphonium, (b) non-ionic, and (c) bisimidazolium Michael addition crosslinking reactions with PEG diacrylate; ASI REACTIR 4000, 25 ˚C, 64 scans averaged every 30 seconds

Viscosities of the crosslinking reactions increased essentially instantly, so comparing the reaction rates over time was difficult due to delays and mixing times before casting. However, all reactions were complete within the first 3-15 minutes.

Phosphines are known to add across activated olefins to catalyze carbon-Michael addition reactions through the synthesis of phosphonium ylides.[6] The ylide then deprotonates the

acetoacetate functionality. This carbanion then adds across additional activated olefins. The new carbanion produced from this addition abstracts a proton from the β-carbon, reforms the vinyl group, and eliminates phosphine. The phosphine catalyst is regenerated for subsequent reaction.[6] The formation of phosphonium ylides typically involves very strong bases such as alkyllithiums,[31] so the formation of phosphonium ylides in this reaction is expected to be extremely low. ^{31}P NMR spectra of a solution of bisphosphonium bisacac with excess DBU overnight in chloroform did not show any degradation to phosphine or phosphine oxides or other phosphorus centers (Figure 4.10).

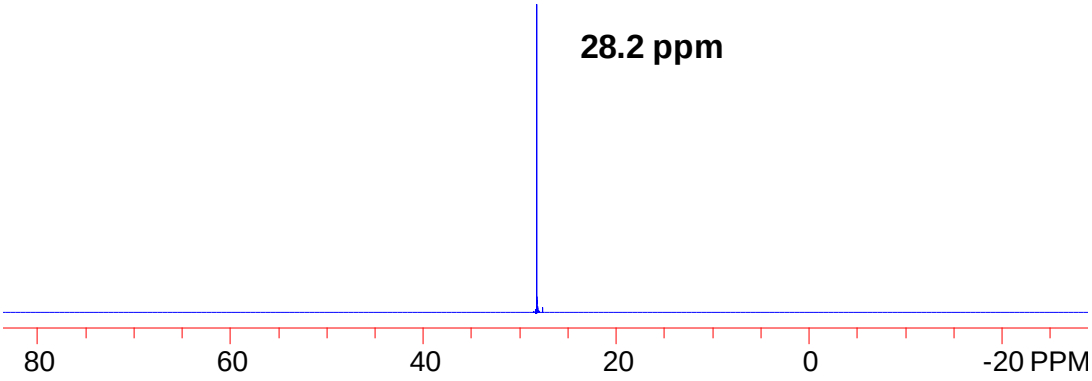

Figure 4.10. ^{31}P NMR spectrum of bisphosphonium bisacac monomer after 24 hours overnight in the presence of excess DBU; 162 MHz in a magnetic field of 9.39 Tesla, $CDCl_3$

Only one resonance at 28.2 ppm with the same shift as the bisphosphonium monomer resulted. However, even a trace amount of phosphine produced in the reaction through elimination would catalyze crosslinking. The bisphosphonium reaction proceeds to high gel fraction, greater than 96%, so the Hofmann elimination and production of phosphine during the reaction is considered minimal.

4.4.3 Thermal Properties of Networks Synthesized from Michael Addition Reactions

TGA indicated that the non-ionic networks were the most thermally stable. Therefore, including the ionic monomers decreased the thermal stability of the final crosslinked film, most likely because Hofmann elimination reactions can occur with these alkyl monomers. Although the imidazolium-containing networks appeared to be slightly less thermally stable than the phosphonium structures in these networks, both the phosphonium and imidazolium TGA curves were within experimental error (Figure 4.11). The 5 weight % loss for TGA under nitrogen of non-ionic, bisphosphonium, and bisimidazolium networks were determined resulting in temperature of 299, 249, and 248 ºC, respectively.

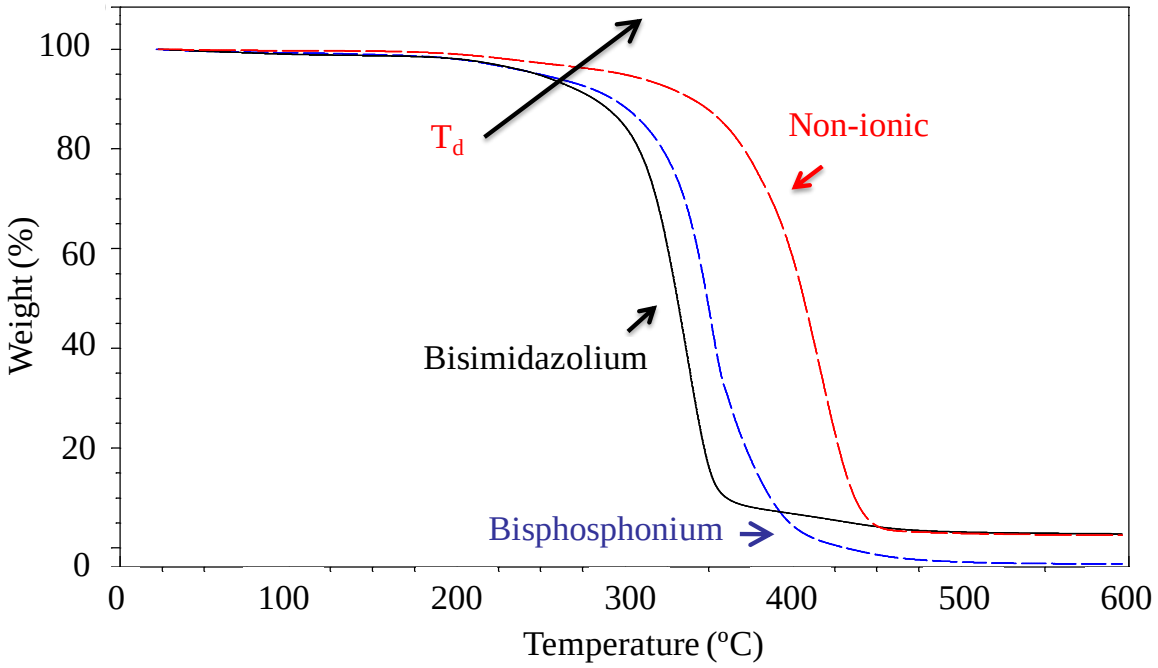

Figure 4.11. TGA curves indicating thermal stability of the ionic networks; 10 °C/minute, ramp 25 °C to 600 °C, N_2

Thermal analysis results using DMA and DSC showed increased glass transition temperatures and broadening of the glass transition temperature for the ionic versus non-ionic networks (Table 4.2). Ionic functionality and ionic aggregation in polymers is well-known to facilitate both increased and broadened transitions.[32-34]

Table 4.2. DSC and DMA results for bisphosphonium, bisimidazolium, and non-ionic networks

Type of Network	**DSC T_g[a] (°C)**	**DMA Onset T_g (°C)**	**DMA Tan Delta T_g[b] (°C)**
Bisphosphonium	-13	3	19
Bisimidazolium	-19	-11	3
Non-ionic	-33	-22	-12

[a]Midpoint T_g, 20 ºC/minute, -80 to 150 °C, N_2;
[b]Peak of Tan Delta, 3 ºC/minute, 1 Hz, -100 to 120 ºC, air

The bisphosphonium network had a higher temperature and broader transition than the bisimidazolium, and both ionic networks had higher temperature and broader transitions than the non-ionic network (Figure 4.12). DMA tan delta and storage moduli curves showed the same broadening trend in the glass transition temperature. The DMA tan delta glass transition from the bisphosphonium-containing network is 19 ºC, and the corresponding bisimidazolium-containing material showed the transition at 3 ºC. The non-ionic network had a glass transition of -12 ºC. The broadening is very apparent in the DMA tan delta curves (Figure 4.13).

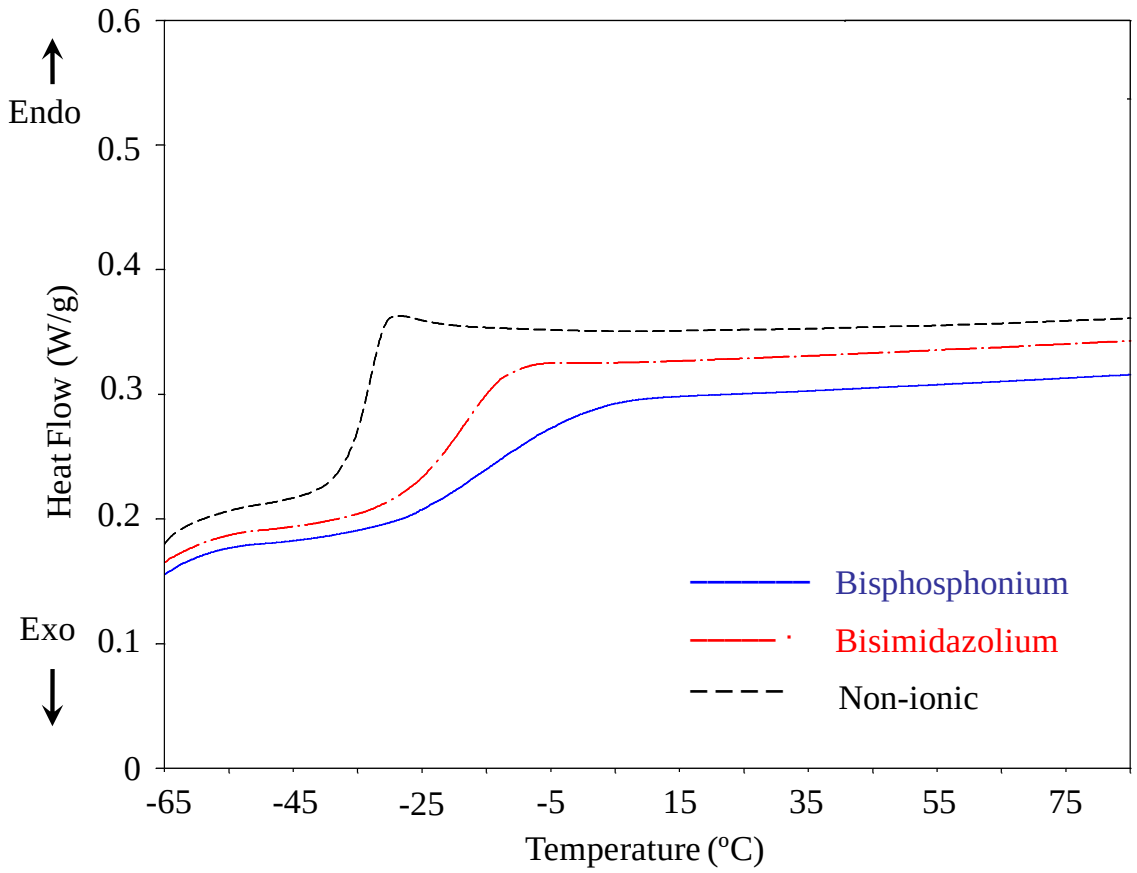

Figure 4.12. DSC thermograms of bisphosphonium, bisimidazolium, and non-ionic networks from Michael addition reactions; 20 ºC/minute, -80 to 150 °C, N_2

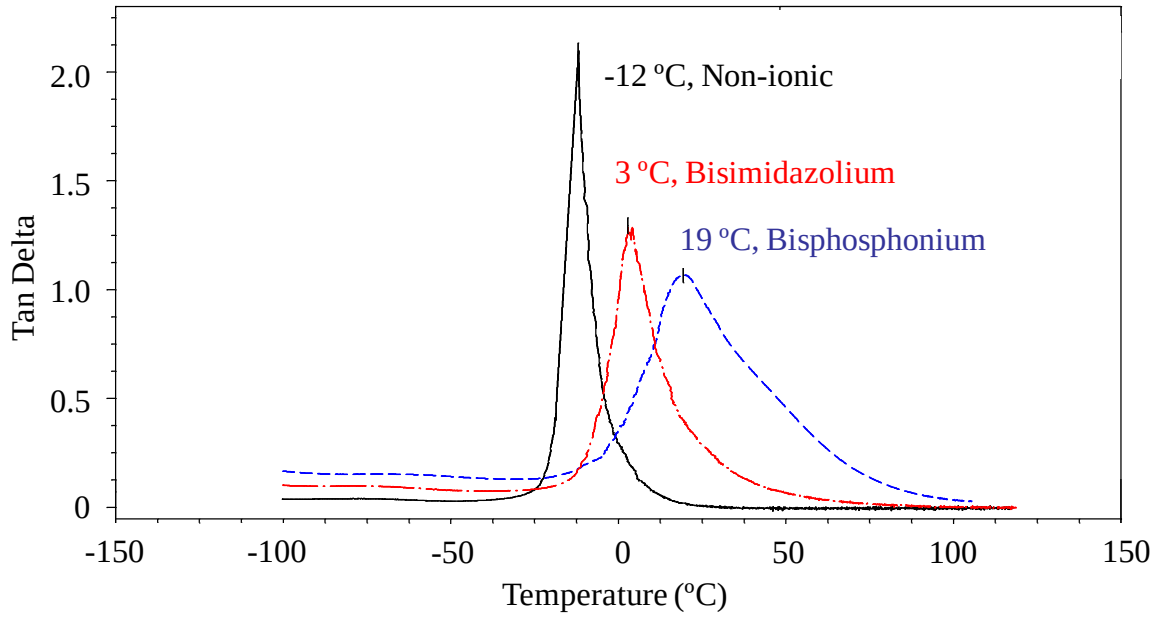

Figure 4.13. DMA tan δ curves of bisphosphonium, bisimidazolium, and non-ionic networks from Michael addition reactions; 3 ºC/minute, 1 Hz, -100 to 120 ºC, air

The DMA storage moduli profiles for each network showed the same broadening trends, and the glass transition increased with the use of an ionic crosslinker just as with the tan delta and DSC data. The DMA profiles, however, also showed similar plateau moduli for each type of network. Plateau moduli are related to crosslink density,[10, 35] and having similar plateau moduli suggests that the crosslink densities for all three non-ionic and ionic networks are similar. There is no flow or melting transition, so these polymers were successfully crosslinked to high conversion (Figure 4.14). The non-ionic networks had lower glass transitions, and these networks showed a slight increase in the plateau moduli due to clamping difficulties with such soft materials. However, *in situ* FTIR spectroscopy, high gel fractions greater than 96% gel, and no change in the DMA curves upon running multiple scans confirmed efficient crosslinking.

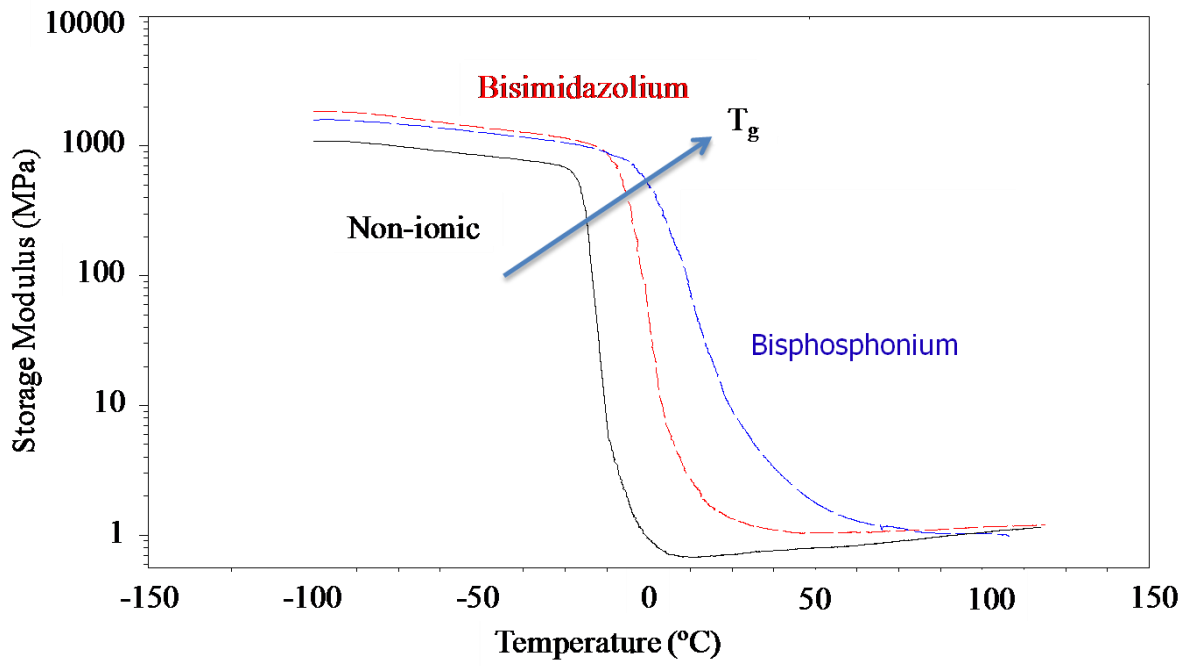

Figure 4.14. DMA curves of bisphosphonium, bisimidazolium, and non-ionic networks from Michael addition reactions; 3 ºC/minute, 1 Hz, -100 to 120 ºC, air

4.4.4 Tensile Experiments

In tensile experiments, bisphosphonium networks had higher strains at break and stresses at break than imidazolium or non-ionic networks (Table 4.3, Figure 4.15).

Table 4.3. Tensile properties of bisphosphonium, bisimidazolium, and non-ionic networks[a]

Type of Network	Tensile Stress at Break (MPa)	Tensile Strain at Break (%)	Young's Modulus (MPa)
Non-ionic	0.20 ± 0.07	10.6 ± 4.5	2.33 ± 0.03
Bisimidazolium	0.51 ± 0.08	32.6 ± 3.2	2.41 ± 0.62
Bisphosphonium	1.03 ± 0.16	65.5 ± 12.1	2.42 ± 0.31

[a] crosshead speed 2 mm/minute, 25 °C, average of three samples reported for each value

The strain at break followed the same trend with bisphosphonium networks having a greater value. The non-ionic network had lower stress at break and strain at break than both ionic networks. However, Young's modulus was approximately 2.3 to 2.4 MPa for all three ionic networks. One can use Young's modulus in tensile or the plateau modulus in DMA to calculate the crosslink density of the films. The equation related involves the following relationship:[10]

$$E = \rho RT/M_c$$

E is Young's modulus. Then ρ is the density. R is the gas constant, and T is the temperature of the experiment. M_c is the molecular weight between crosslinks. Having the same Young's moduli is another indication of similar crosslink densities for ionic and non-ionic networks.[10]

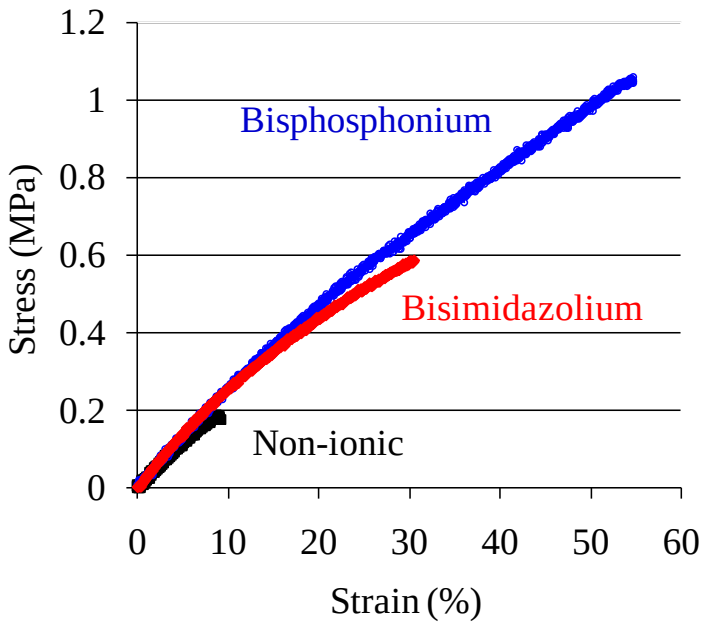

Figure 4.15. Tensile stress-strain curves of bisphosphonium, bisimidazolium, and non-ionic networks from Michael addition reactions; crosshead speed 2 mm/minute, 25 °C

Although the networks had comparable crosslink densities, stresses at break and strains at break in tensile experiments were enhanced through physical crosslinking (Figure 4.15). Ionic functionality is known to improve modulus and tensile properties in various polymers.[32-34] The ionic monomers were longer and larger, having both a butylene spacer and two hexyl groups on either side of the two ionic sites. These longer and larger monomers should have increased the distance between crosslink points, changing the crosslink densities. However, ionic and non-ionic films had similar plateau and Young's moduli, indicating that supramolecular interactions in the ionic films may have affected their crosslink densities. The bisphosphonium functionality involves large phosphorus cations that form weak physical crosslinking through electrostatic interactions. The phenyl rings on the phosphonium functionality provide rigidity as well as pi-pi stacking interactions. Supramolecular interactions make these particular networks dynamic. As a sample is stretched, crosslinking prevents chains from moving past one another or plastic deformation, but the sample chain segments are perturbed from their random coil state and aligned. The closeness of these chains allows dynamic electrostatic interactions to take place. In semicrystalline polymers, strain-induced crystallization provides hardening and elongation effects due to chain alignment.[36-38] In these amorphous ionomers, the energy stored and used to stretch the molecules causes slightly closer alignment of the ionic groups as the polymer chains are stretched. Electrostatic attraction between the ionic groups in closer proximity improves stress at break and strain at break.

The bisimidazolium ion appears to be less efficient at enhancing strain at break and stress at break compared to the bisphosphonium ion, and this may be at least partially attributable to the positive charge on each cation being delocalized over two nitrogens. Although the nitrogen atom is smaller than phosphorus, the two nitrogens in each imidazolium are confined in an

aromatic ring. This delocalization provides a monomer with weaker physical crosslinking and lower crystalline packing energies than the phosphonium cations. Therefore, these monomers typically have lower glass transition temperatures and melting points, and the bisimidazolium monomers are ionic liquids at ambient temperature whereas the bisphosphonium monomers are solids at room temperature. Ionic crosslinking and electrostatic interactions can account for the greater stress at break and strain at break for the ionic networks, and can also help to rationalize the large increase and broadening in the glass transition temperatures compared to the non-ionic networks. Coordination of PEG oxygens to the phosphonium and imidazolium cations may also contribute to physical crosslinking of the ionic materials.[39]

4.4.5 Atomic Force Microscopy of Ionic and Non-Ionic Networks

Atomic force microscopy (AFM) images indicated large, ~100-nm, ionic aggregates within the ionic networks, whereas the non-ionic networks did not show any surface features (Figure 4.16). The white or "hard" regions in these images possibly indicate large aggregates on the surface of the films. However, X-ray analysis is needed to conclude higher phosphorus content in the white or aggregate regions. TEM also is needed to investigate ionic aggregate formation in the bulk film, rather than just on the surface.

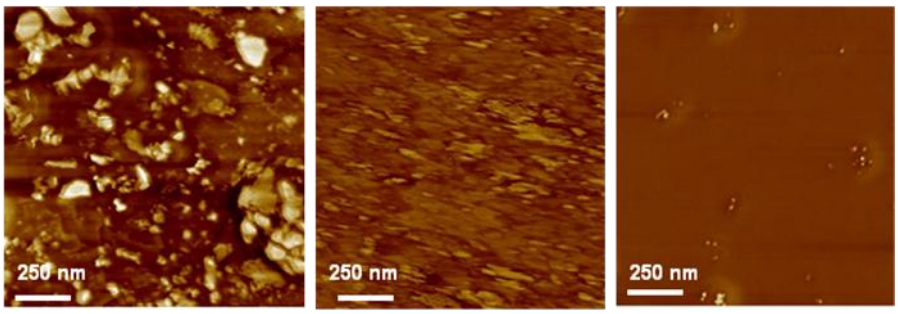

Figure 4.16. AFM of networks from Michael addition reactions: 1 x 1 μm images; rms 4.0 mV and amplitude setpoint 3.3 mV

4.4.6 Equilibrium Ionic Liquid Uptake of Ionic versus Non-Ionic Networks

One of the advantages of ion-containing polymers is their increased capacity to uptake ionic liquids since this could be important in potential electro-active polymer applications.[18-19, 40] The ionic liquid 1-ethyl-3-methylimidazolium ethylsulfate is commonly used in electro-active polymer and actuator applications. This ionic liquid has a melting point around -65 °C, and a conductivity of 3.82 mS/cm (25 °C).[19] Swelling the polymers to their equilibrium ionic liquid uptake over time provided evidence that the ionic networks uptake 2.5X as much ionic liquid as non-ionic ones (Table 4.4, Figure 4.17).

Table 4.4. Ionic liquid uptake over time

Type of Network	Equilibrium IL Uptake* (wt %)
Bisphosphonium	56.6 ± 3.4
Bisimidazolium	55.6 ± 3.4
Non-ionic	20.7 ± 5.2

***** thickness = 0.5 ± 0.1, average of 3 samples each film

Bisphosphonium and bisimidazolium networks had similar equilibrium ionic liquid uptake over time of 56.6 ± 3.4 % and 55.6 ± 3.4 % respectively (Figure 4.17). The mole % of ionic groups is the same for the bisphosphonium and the bisimidazolium networks. Therefore, there was no preference for the bisimidazolium network to uptake imidazolium ionic liquid over the bisphosphonium network. Both ionic polymers with the same mole % of ionic functionality resulted in the same ionic liquid uptake levels, despite having different types of functionality. Therefore, ionic liquid uptake depended more on the mole % of ionic groups than the type of ionic groups.

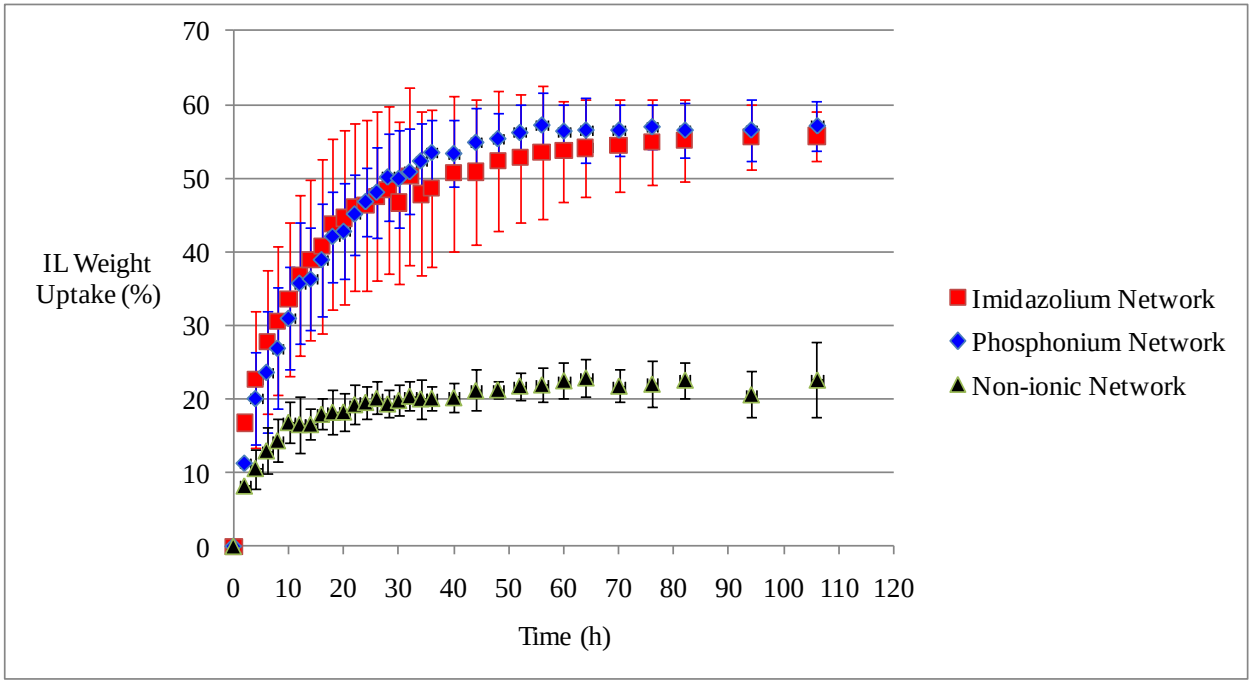

Figure 4.17. Ionic liquid uptake over time in networks from Michael addition reactions; 25 °C, 1-ethyl-3-methylimidazolium ethylsulfate, thickness = 0.5 ± 0.1, average of 3 samples each film

Non-ionic networks only had an uptake of 20.7 ± 5.2 % ionic liquid, compared to the nearly 56-57% uptake for the ionic polymers. A 2.5X increase in ionic liquid uptake resulted due to including ionic functionality.

4.4.7 DMA of Ionic and Non-ionic Networks with Varied Ionic Liquid Uptake

Absorption of ionic liquid in the networks from Michael addition reactions altered DMA behavior and produced changes in the thermal transitions. Long et al. previously investigated the effect of swelling polybetaines with EMIm ES.[19] The rubbery plateaus decreased dramatically with increased uptake of ionic liquid. However, the glass transition temperatures decreased slightly for polybetaines since ionic liquid absorbed mainly in the ionic domains of the polymers.[19]

In this thesis, we report unique DMA behavior of the networks from Michael addition reactions after swelling them with EMIm ES. Films of the bisphosphonium-based networks were swollen to 6 and 23 weight % EMIm ES. At 0, 6, and 23 weight % EMIm ES, the bisphosphonium-based films had volumes of 99 mm^3, 130 mm^3, and 141 mm^3 respectively. Increasing absorption of EMIm ES slightly sharpened the onset of the glass transition temperature and provided curves with one or two additional, broad thermal transitions (Figure 4.18, Figure 4.19).

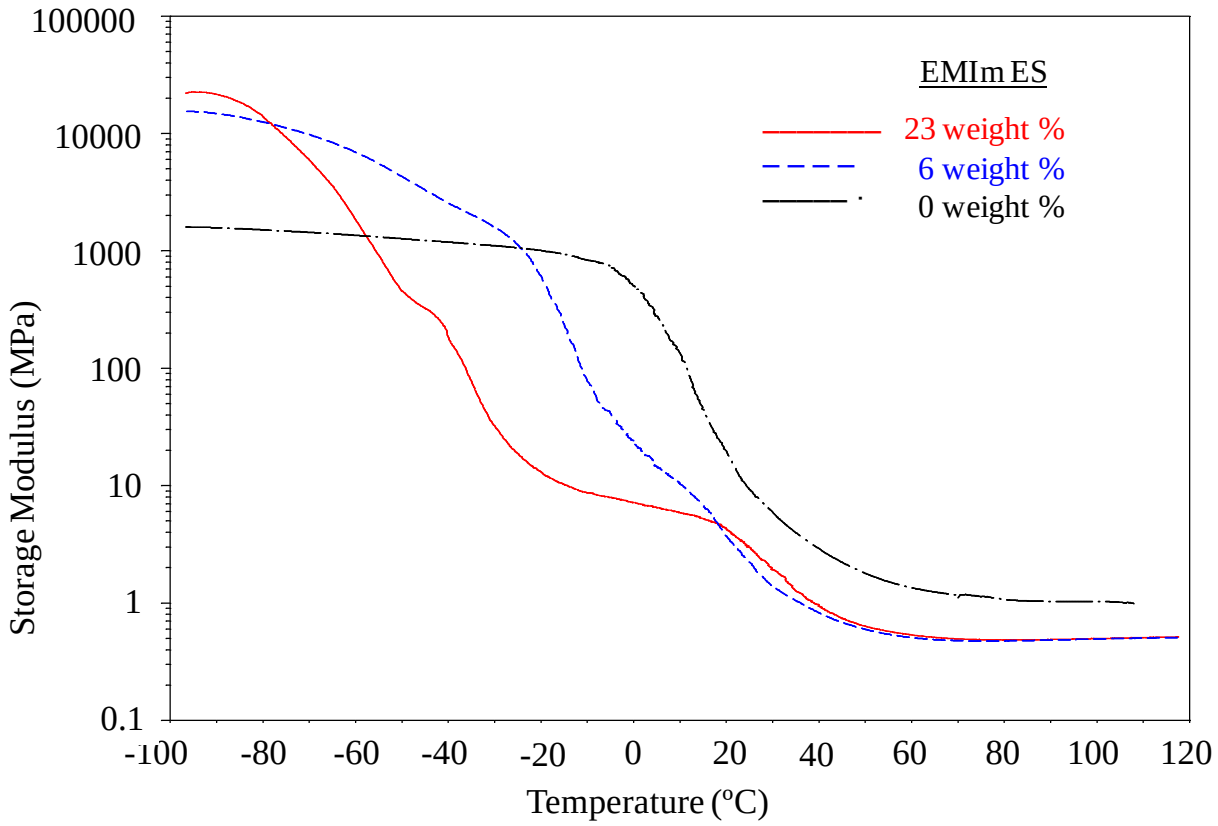

Figure 4.18. DMA curves of bisphosphonium networks from Michael addition reactions swollen with 0, 6, and 23 weight % EMIm ES ionic liquid; 3 ºC/minute, 1 Hz, -100 to 120 ºC, air

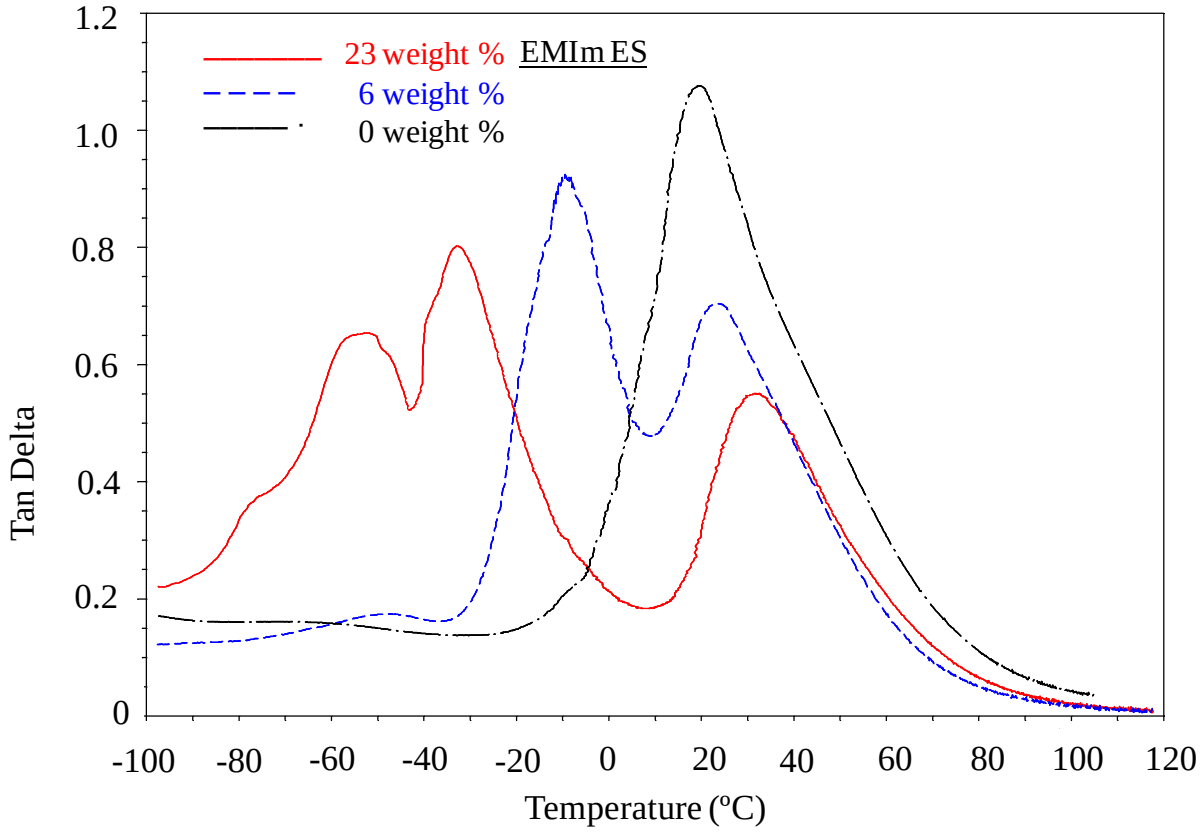

Figure 4.19. DMA tan δ curves of bisphosphonium networks from Michael addition reactions swollen with 0, 6, and 23 weight % EMIm ES ionic liquid; 3 ºC/minute, 1 Hz, -100 to 120 ºC, air

In previously-studied polybetaines, the ionic liquid preferred to locate in ionic domains of the polymer, and swelling with ionic liquid led to the disruption of ionic aggregates.[19] Swelling the bisphosphonium-based networks with EMIm ES possibly led to the disruption of phosphonium-based ionic aggregates in the films that were responsible for broadening of the ionic transition. The PEG oxygens can also coordinate cations, and addition of ionic liquid would also disrupt coordination of network cations with the PEG oxygens.[39]

Ionic sites can act as nucleating sites for crystal growth,[41-42] and EMIm ES can crystallize and has a melting point of -65 °C.[19] The additional thermal transitions in Figures 4.18 and 4.19 are most likely related to crystallization and melting of EMIm ES in the films. Below all transitions, the films swollen with 23 and 6 weight % EMIm ES had higher storage moduli than the films without any ionic liquid. Below its melting point, the ionic liquid acted as a filler. Above the melting temperature of EMIm ES crystallites, the ionic liquid acts as a diluent and lowers the plateau moduli. Therefore, the plateau moduli of the ionic liquid swollen films are slightly lower than those without or swollen with less ionic liquid. However, plateau moduli in crosslinked films are limited by the short distance between covalent crosslink points in the polymers.

Films of the non-ionic networks from Michael addition reactions were swollen to 14 weight % EMIm ES. Swelling the non-ionic networks produced very soft films that tore easily. The non-ionic films with 0 and 14 weight % EMIm ES had volumes of 54 mm^3 and 114 mm^3 respectively. Absorption of EMIm ES broadened and slightly decreased the glass transition temperature (Figure 4.20, Figure 4.21). Two additional, broad thermal transitions in the ionic liquid swollen film were observed, and the absorption of ionic liquid lowered the plateau moduli (Figure 4.20). These additional transitions may also be associated with crystallization and melting of EMIm ES.

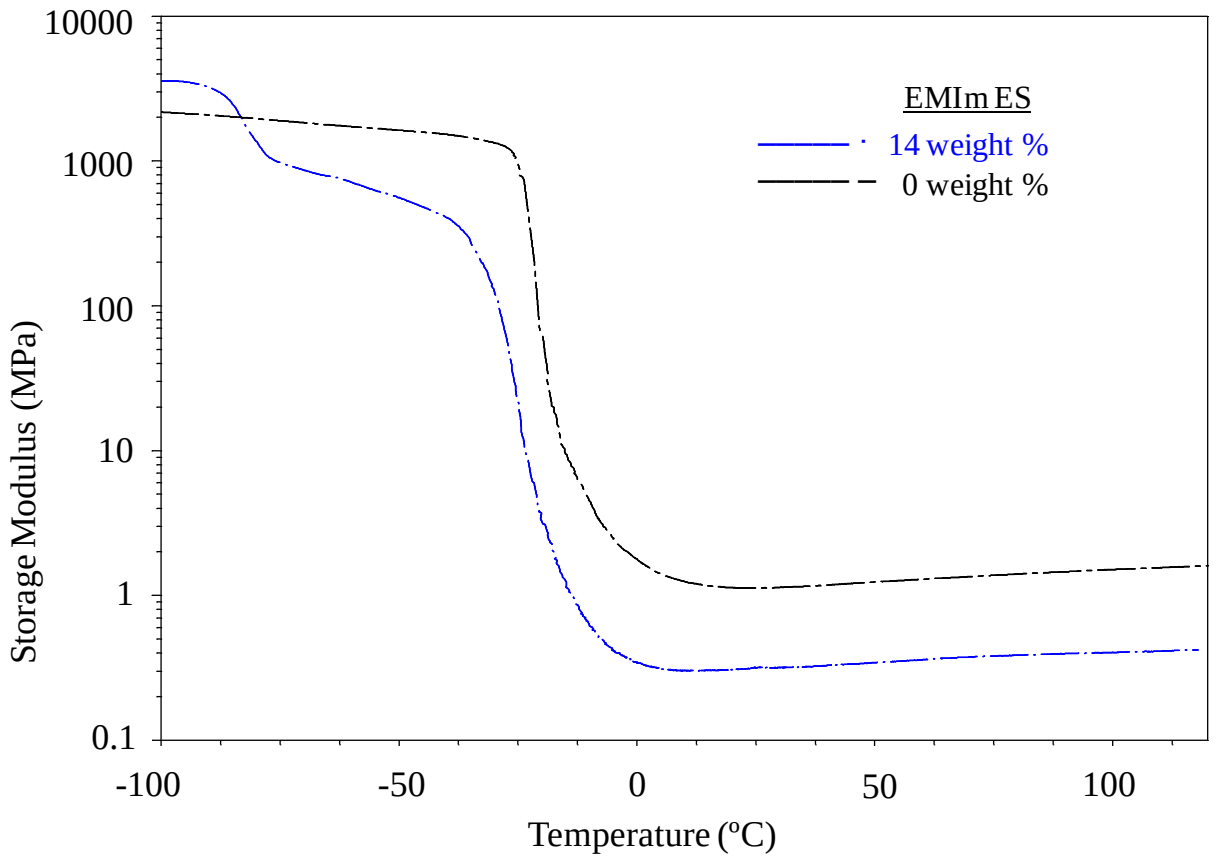

Figure 4.20. DMA curves of non-ionic networks from Michael addition reactions with 0 and 14 weight % EMIm ES ionic liquid; 3 ºC/minute, 1 Hz, -100 to 120 ºC, air

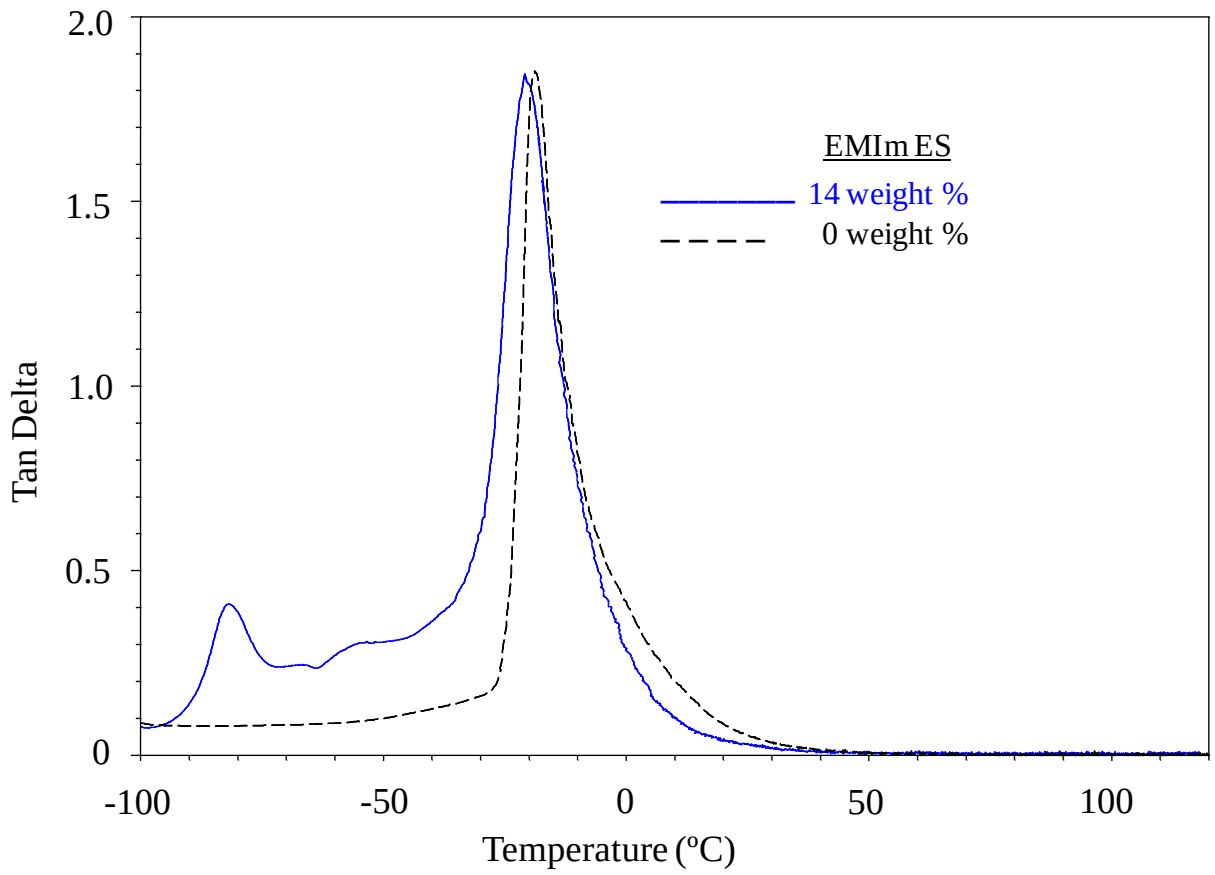

Figure 4.21. DMA tan δ curves of non-ionic networks from Michael addition reactions with 0 and 14 weight % EMIm ES ionic liquid; 3 ºC/minute, 1 Hz, -100 to 120 ºC, air

4.4.8 Electrospinning Ionic and Non-Ionic Networks from Michael Addition Reactions

One key issue relative to ionic networks for potential applications as electro-active polymers is to identify a means to process them efficiently into fibers. We report the formation of ionic and non-ionic electrospun fibers form Michael addition crosslinking reactions. Formation of fibers is also advantageous for numerous applications such as antimicrobial mats and filtration devices due to the resulting high surface to volume ratio, allowing large exposure to the polymer surface and active functionality.[24-26] Spinning fibers could also provide control

over morphology, porosity, pore size, and fiber diameter.[24-26] Electrospinning involves application of a voltage across a liquid drop at the end of a syringe and syringe pump. The applied voltage distorts the drop, and when enough voltage is applied to break the surface tension a jet erupts from the syringe tip and proceeds toward a grounded target in a whipping-like motion. This whipping provides thin, uniform fibers with few defects. The required equipment is relatively simple. In most cases, fiber diameter depends on solution concentration and viscosity.[24-26] For these materials that crosslink during the spinning operation, time and base concentration are also important factors. Solutions were prepared as described for film casting in Teflon® molds, except each reaction solution was added to a syringe. The viscosity changed over time as crosslinking began. Electrospinning produced free-standing fibers for all three polymers, non-ionic, bisimidazolium, and bisphosphonium networks (Figure 4.22). Future work will involve investigation and control of crosslinking and fiber formation through systematic variances in time and base concentration.

Scanning electron microscopy (SEM) of these fibers showed increased diameters for the non-ionic and imidazolium networks versus the phosphonium networks. The non-ionic networks had flat large fibers, while the phosphonium and imidazolium networks produce rounder fibers when spun from methylene chloride. We have demonstrated in recent experiments with zwitterionic polymers that ionic aggregation facilitates fiber formation even at low solution concentrations compared to non-ionic analogs.[24] The formation of cylindrical fibers in the phosphonium and imidazolium electrospinning process could also be at least partially attributable to electrostatic interactions during the spinning process.

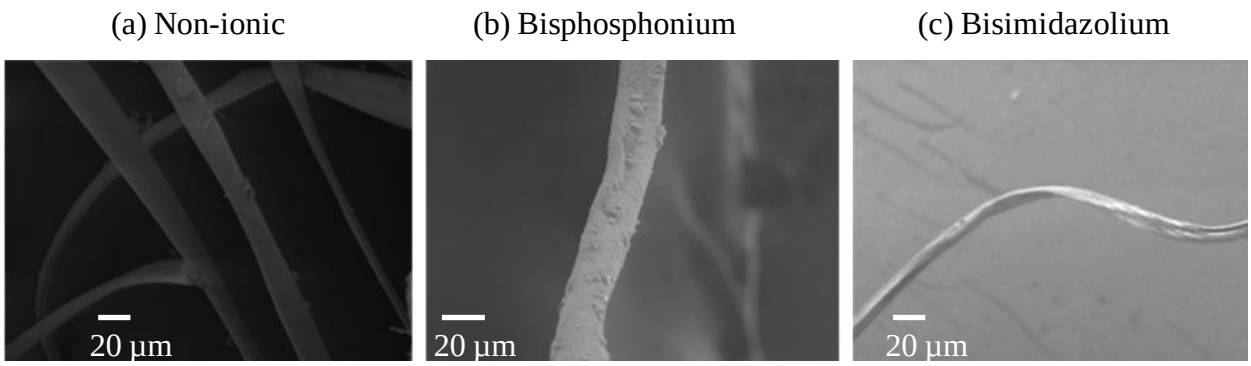

Figure 4.22. SEM images of electrospun fibers from Michael addition crosslinking reactions; 8 nm sputter-coated gold/platinum, 5 KV, 100 and 200 KX magnifications, Leo 1550 FESEM

4.5 Conclusions

We synthesized three novel monomers, bisphosphonium, bisimidazolium, and non-ionic bisacacs. This thesis conveys the first report of ionic networks from Michael addition reactions and their structure-property relationships. Synthesis of networks with a low molecular weight PEG diacrylate produced clear, transparent films with greater than 96% gel. *In situ* FTIR also provided evidence of fast, efficient crosslinking to high crosslink density. Young's moduli and plateau moduli were similar for all three networks with the same mole % of bisacac, and this supports the premise that all of the networks had similar crosslink densities. Use of the bisphosphonium functionality afforded broader and higher glass transition temperatures, increased stresses at break, and greater strains at break than either those of bisimidazolium or non-ionic networks. The non-ionic networks possessed lower and sharper glass transition values, strains at break and stresses at break than any of the ion-containing networks. Ionic functionality also afforded 2.5X the ionic liquid equilibrium uptake than uptake in the non-ionic analogs, and the bisphosphonium and bisimidazolium networks absorbed similar amounts. The bisphosphonium versus the bisimidazolium did not show any preference in rate or final

equilibrium uptake for absorbing imidazolium ionic liquid, 1-ethyl-3-methylethylimidazolium sulfate, and the ionic liquid uptake was dependent on mole % of ionic character and not the type of ionic functionality. We also described the first electrospun fibers from Michael addition crosslinking reactions, both ionic and non-ionic fibers. The small molecule reagents electrospun into insoluble and crosslinked fibers in one simple step. Future work should include electrospinning with various solution concentrations to study changes in fiber diameters, and rheology would help correlate gel time to solution concentration and viscosity.

4.6 Acknowledgements

Research was sponsored by the Army Research Laboratory and was accomplished under Cooperative Agreement Number W911NF-06-2-0014. The views and conclusions contained in this document are those of the authors and should not be interpreted as representing official policies, either expressed or implied, of the Army Research Laboratory or the U.S. Government. The U.S. Government is authorized to reproduce and distribute reprints for Government purposes notwithstanding any copyright notation hereon. The authors would also like to acknowledge Matthew T. Hunley for help with the electrospinning setup and help procuring SEM images. Steve M. June also aided in procuring AFM images of these polymers, and Matthew D. Green and Jenny B. England helped with the bisimidazole literature synthesis and general laboratory aid respectively.

4.7 References

1. Mather, B. D.; Viswanathan, K.; Miller, K. M.; Long, T. E. *Prog. Polym. Sci.* **2006**, *31*, 487–531.
2. Vernon, B.; Tirelli, N.; Bachi, T.; Haldimann, D.; Hubbell, J. *J. Biomed. Mater. Res.* **2003**, *64A*, 447–456.

3. Ferruti, P.; Bianchi, S.; Ranucci, E.; Chiellini, F.; Caruso, V. *Macromol. Biosci.* **2005**, *5*, 613–622.
4. Abbotto, A; Beverina, L; Chirico, G; Facchetti, A; Ferruti, P. G.; Gilberti, M. et al. *Macromol. Rapid Commun.* **2003**, *24*, 397–402.
5. Bergman, E. D.; Ginsburg, D.; Pappo, R. Org. React. **1959**, *10*, 179–556.
6. Gimbert, C.; Lumbierres, M.; Marchi, C.; Moreno-Manas, M.; Sebastian, R. M.; Vallribera, A. *Tetrahedron* **2005**, *61*, 8598–8605.
7. Rieger, J.; van Butsele, K.; Lecomte, P.; Detrembleur, C.; Jerome, R.; Jerome, C. *Chem. Commun.* **2005**, *2*, 274–276.
8. Little, R. D.; Masjedizadeh, M. R.; Wallquist, O.; McLoughlin, J. I. *Org. React.* **1995**, *47*, 315–552.
9. Mather, B. D.; Williams, S. R.; Long, T. E. *Macromol. Chem. Phys.* **2007**, *208*, 1949–1955.
10. Ozturk, G.; Long, T. E. *Journal of Polymer Science: Part A: Polymer Chemistry* **2009**, *47*, 5437–5447.
11. Yim, E. S.; Zhao, B.; Myung, D.; Kourtis, L. C.; Frank, C. W.; Carter, D.; Smith, R. L.; Goodman, S. B. *Journal of Biomedical Materials Research, Part A* **2009**, *91A(3)*, 894-902.
12. Rogero, S. O.; Malmonge, S. M.; Lugao, A. B.; Ikeda, T. I.; Miyamaru, L.; Cruz, A. S. *Artificial Organs* **2003**, *27(5)*, 424-427.
13. Wang, Y.-P.; Gao, X.-H.; Chen, J.-C.; Li, Z.-W.; Li, C.-L.; Zhang, S.-C. *Journal of Applied Polymer Science* **2009**, *113(4)*, 2492-2498.
14. Qi, L.; Lin, Y.; Wang, F. *European Polymer Journal* **1999**, *35(5)*, 789-793.
15. Lebourg, M.; Sabater Serra, R.; Mas Estelles, J.; Hernandez Sanchez, F.; Gomez Ribelles, J. L.; Suay Anton, J. *Journal of Materials Science: Materials in Medicine* **2008**, *19(5)*, 2047-2053.
16. Xu, X.-J.; Shastri, V. P. *Corrosion Engineering, Science and Technology* **2007**, *42(4)*, 293-299.
17. Williams, S. R.; Mather, B. D.; Miller, K. M.; Long, T. E. *Journal of Polymer Science: Part A: Polymer Chemistry* **2007**, *45*, 4118–4128.
18. Duncan, A. J. Barbar, J. A.; Long, T. E.; Leo, D. J. *Smart Mater. Struct*. **2009**, *18*, 104005 (11pp).
19. Brown, R. H.; Duncan, A. J.; Choi, J.-H.; Park, J. K.; Wu,T.; Leo, D. J.; Winey, K. I.; Moore, R. B.; Long, T. E. *Macromolecules* **2010**, *43*, 790–796.
20. Kanazawa, A.; Ikeda, T.; Endo, T., *Journal of Polymer Science: Part A: Polymer Chemistry* **1993,** *31*, 335-343.
21. Le Poul, N.; Campion, M.; Douziech, B.; Rondelez, Y.; Le Clainche, L.; Reinaud, O.; Le Mest, Y. *J. Am. Chem. Soc.* **2007**, *129*, 8801-8810.
22. De Luca, L. *Current Medicinal Chemistry* **2006**, *13*, 1-23.
23. Demberelnyamba, D.; Kim, K.-S.; Choi, S.; Park, S.-Y.; Lee, H.; Kim, C.-J.; Yoo, I.-D. *Bioorganic & Medicinal Chemistry* **2004**, *12*, 853-857.
24. Brown, R. H.; Hunley, M. T.; Allen, M. H.; Long, T. E. *Polymer* **2009**, *50*, 4781–4787.
25. McKee, M. G.; Layman, J. M.; Cashion, M. P.; Long, T. E. *Science* **2006**, *311(5759)*, 353-355.
26. McKee, M. G.; Wilkes, G. L.; Colby, R. H.; Long, T. E. *Macromolecules* **2004**, *37(5)*, 1760-1767.

27. So, Y. H. *Macromolecules* **1992**, *25(2),* 516-520.
28. Clemens, R. J.; Rector, F. D. *J. Coat. Technol.* **1989**, *61*, 83–91.
29. Jung, M. E. "Stabilized nucleophiles with electron deficient alkenes and alkynes," In: Trost BM, editor. *Comprehensive Organic Synthesis*. Oxford: Pergamon; 1991.
30. Abdallah, D. J.; Weiss, R. G., *Chem. Mater.* **2000,** 12, 406-413.
31. Xie, W.; Xie, R.; Pan, W.; Hunter, D.; Koene, B.; Tan, L.; Vaia, R., *Chem. Mater.* **2002,** *14*, 4837-4845.
32. Eisenberg, A.; Hird, B.; Moore, R. B., *Macromolecules* **1990,** *23*, 4098-4107.
33. Eisenberg, A.; King, M., *Ion-Containing Polymers*. Academic Press: New York, 1977.
34. Tant, M. R.; Mauritz, K. A.; Wilkes, G. L. eds. *Ionomers: Synthesis, Structure, Properties, and Applications.* Van Nostrand Reinhold Co., Inc. New York, NY, 1997.
35. Calvet, D.; Wong, J. Y.; Giasson, S. Macromolecules **2004**, *37*, 7762–7771.
36. Mulligan, J.; Cakmak, M. Macromolecules 2005, 38, 2333–2344.
37. Stoclet, G.; Seguela, R; Lefebvre, J. M.; Elkoun, S.; Vanmansart, C. *Macromolecules* **2010**, *43*, 1488–1498.
38. Marco, Y.; Chevalier, L. *Polymer Engineering and Science* **2008**, *48(3),* 530-542.
39. *Applications of Electroactive Polymers*. Bruno, S. ed. Chapman & Hall: New York, 1993, 75-113.
40. Duncan, A. J.; Leo, D. J.; Long, T. E. *Macromolecules* **2008**, *41(21),* 7765-7775.
41. *Modern Polyesters*. Scheirs, J.; Long, T. E. eds. John Wiley & Sons, Ltd.: West Sussex, England, 2003.
42. Tang, S.; Xin, Z. *Polymer* **2009**, *50*, 1054–1061.

Chapter 5: Examination of Thermal, Morphological, and Mechanical Properties of Bisphosphonium and Non-ionic and Ionic Networks from Michael Addition Reactions in the Presence of Multi-Walled Carbon Nanotubes

5.1 Abstract

Incorporation of carbon nanotubes into polymers enhances mechanical performance and conductivity. In particular, carbon nanotubes boost the Young's moduli and plateau moduli. Dispersion of these nanotubes into a polymer matrix imparts stiffness that can enhance the moduli of soft, hydrophilic polymers with low glass transition temperatures such as hydrophilic PEG-based networks from Michael addition crosslinking reactions. Carbon nanotube incorporation also provides decreased resistivity, or improved conductivity. In this thesis, ion-containing networks from Michael addition reactions were synthesized with a novel bisphosphonium bisacac and a novel non-ionic bisacac based on 1,4-butanediol. Clear, transparent films resulted after crosslinking. Bisphosphonium-containing and non-ionic PEG-based networks from Michael addition reactions in the presence of 1, 3, and 5 weight % unfunctionalized Baytubes®, pristine multi-walled carbon nanotubes (MWCNTs) from Bayer MaterialScience, were also prepared. Crosslinking in the presence of dispersed carbon nanotubes in the casting solution produced black, opaque films. Even with carbon nanotube incorporation, gel fractions were greater than 90 weight %. Soxhlet extractions resulted in no visible loss of the black carbon nanotubes from the films within over 10 hours. The Soxhlet thimbles were pristine after extraction, and the 10 weight % loss during Soxhlet extraction was assumed to result mostly

from the loss of uncrosslinked polymer. DMA and tensile experiments indicated that increasing MWCNT incorporation increased the plateau moduli and Young's moduli with little effect on the glass transition temperatures. For the non-ionic networks from Michael addition reactions, increasing nanotube content from 0 to 5 weight % decreased surface resistivity from 10^9 to 10^6 ohms/square, respectively. Ionic networks with 0 to 5 weight % MWCNTs showed a larger change in resistivity from 10^9 to 10^5 ohms/square. MWCNTs affected the surface conductivity in the ionic networks to a greater extent than in the non-ionic networks.

5.2 Introduction

Multi-walled carbon nanotube (MWCNT) composites are omnipresent in the literature and have exceptional purpose in electro-active and smart material applications.[1-2] They include several carbon-carbon bonded cylindrical nanotubes of various diameters from 1 nm (single-walled carbon nanotubes SWCNTs) to around 10 nm (MWCNTs) in diameter (Figure 5.1).[3] Lengths of the nanotubes are often a few μm.[4]

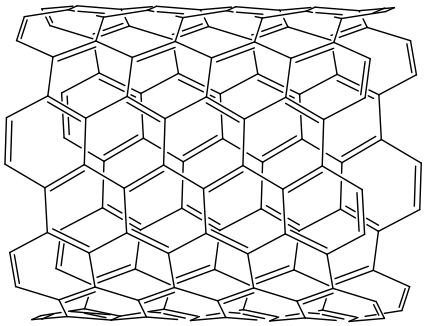

Figure 5.1. Structure of CNTs

Figure 5.1 is only a general representation of CNTs. MWCNTs come in many forms with various numbers of hollow, tubular walls inside each other, various diameters, and various

lengths. Several comprehensive reviews exist on the mechanical, morphological, thermal, conductive, and electro-active properties and potential applications of polymer composites with MWCNTs.[1-15] Inclusion of MWCNTs in a polymer matrix can improve thermal stability of the polymer,[16] alter or enhance morphology,[17] and increase conductivity.[1] Polymers reinforced with MWCNTs have application as separation media,[3] smart adhesives,[5] actuators,[2] biomarkers,[6] drug carriers,[6] and neural implants.[7] Singh et al. reviewed MWCNT composite materials for sensors, actuators, fuel cells, solar cells, and photovoltaics.[2] Additionally, Shi et al. investigated cell targeting and medical sensing of these polymers for drug delivery applications.[6] PEG is a biocompatible polymer often utilized in conductive polymer applications.[18-22] Rhee et al. dispersed MWCNTs in PEG to examine resultant tensile properties and crystallinity with varied nanotube content.[23] The nanotubes acted as nucleation sites for crystal growth. Dispersion of the nanotubes in the polymer matrix with a high-powered sonication probe proved beneficial for properties such as strain at break compared to other preparatory methods. With 2 weight % MWCNTs dispersed in the polymer matrix, the PEG crystallinity in the films increased 12.5-fold, because the nanotubes acted as nucleation agents for crystal growth. These PEG- and MWCNT-containing polymer composites also had up to 110 times the modulus of the neat PEG polymer.[23]

Several ways of preparing well-dispersed carbon nanotubes in PEG-based polymers exist, and these methods include using high-powered sonication, adding surfactants, and including the MWCNTs within the polymerization.[23] Utilizing fast Michael addition crosslinking reactions for network formation takes advantage of both high-power sonication and polymerization techniques to uniformly disperse MWCNTs in a PEG matrix. As previously described in chapter 4 of this dissertation, the Michael reaction involves abstraction of bisacac protons with base to generate

carbanions, which add across activated olefins or diacrylates.[24] The Michael reaction is ubiquitous in polymer chemistry,[24] and our research group has sound experience crosslinking bisacetoacetate (bisacac) Michael donors with diacrylate Michael acceptors.[24-27] Michael crosslinking produces robust films with mechanical integrity. In this thesis, we describe the *in situ* synthesis of MWCNT-PEG-based composites, their mechanical and tensile properties, and their surface resistivity. One unique feature of these films is capability to fully enclose the carbon nanotubes in the network through dispersing them and crosslinking around them. No visible loss of nanotubes is apparent with over 10 hours of Soxhlet extraction in methylene chloride. Ionomers and ionic-polymer composites are particularly attractive for electro-active polymer applications, and mobile ionic sites can enhance conductivity and lower resistivity.[28-29] Thus, we additionally investigate the effect of bisphosphonium cations on the mechanical and electrical properties of MWCNT composites compared to non-ionic analogs.

5. 3 Experimental

5.3.1 Materials

Poly(ethylene oxide) PEG diacrylate (575 g/mol), *tert*-butylacetoacetate (98%), 1,8-diazabicyclo[5.4.0]undec-7-ene (DBU, 98%), 1,4-bis(diphenylphosphino)butane (98%), 1,4-dibromobutane, imidazole, sodium hydroxide, 1,4-butanediol, and 6-bromohexanol were purchased from Aldrich and used as received. HPLC-grade methylene chloride, dimethyl sulfoxide (DMSO), and toluene were purchased from Fisher and used as received. Bayer MaterialsScience provided unfunctionalized, pristine Baytubes® CP 150 Batch Number A001AAA06 (multi-walled carbon nanotubes (MWCNTs)).

5.3.2 Synthesis of Carbon-Nanotube-Containing Non-Ionic Networks

First, the Baytubes® were sonicated with a sonication probe for 60 min in a 1 wt % solution in methylene chloride. A Hielscher Ultrasonics GmbH UP400S ultrasonic processor with sonotrode H3 was utilized with max amplitude of 210 um and acoustic power density of 460 W/cm^2. The probe was run at 70% of the amplitude and ultrasonic output. Butane-1,4-diyl bis(3-oxobutanoate) (non-ionic bisacac) was synthesized as described in 4.3.7 in chapter 4 of this thesis. The non-ionic bisacac (0.122 g, 2 eq) was charged to a 20-mL scintillation vial, and 575 g/mol PEG diacrylate (0.38 g, 1.4 eq) was subsequently added. These two reagents were dissolved in 200 µL of methylene chloride. Immediately after sonication of the nanotubes with the sonication probe, 5 wt % of the nanotube dispersion was added (2.64 mL). Methylene chloride was again added until the total solvent equaled 1600 µL. The solutions with the nanotubes were sonicated for an additional 30 minutes in a sonication bath. Then, a catalytic amount of DBU (28.6 µL) was added to the vial, and the reagents were vigorously stirred by hand by stirring the scintillation vial contents for 30 to 60 seconds before casting into Teflon® molds. The viscosities increased dramatically immediately following DBU addition. The reaction proceeded in the molds for 24 h at room temperature, and films were dried under reduced pressure in a vacuum oven overnight at room temperature. The materials were Soxhlet extracted for 10 h in methylene chloride, and gel fractions were measured to be around 90%. The films were dried overnight under reduced pressure and 60 ºC before subsequent analysis. No loss of black carbon nanotubes was visible during Soxhlet extractions, suggesting that most weight loss resulted from the extraction of uncrosslinked polymer. All other networks were synthesized using similar methods with varied compositions: 0, 1, 3, and 5 wt % MWCNTs.

5.3.3 Synthesis of Carbon-Nanotube-Containing Bisphosphonium-Based Networks

The bisphosphonium-based networks were synthesized using the method previously described in 5.3.2 for the non-ionic networks with 1:1.4 equivalents of diacrylate to bisacac monomers. Networks with 0, 1, 3, and 5 wt % of unfunctionalized Baytubes® MWCNTs were prepared. The only change to the procedure was the substitution of nonionic bisacac with bisphosphonium-containing bisacac monomer, 2,4,25,27-tetraoxo-12,12,17,17-tetraphenyl-5,24-dioxa-12,17-diphosphoniaoctacosane bromide. The bisphosphonium-containing bisacac monomer was synthesized according to sections 4.3.2 to 4.3.3 in chapter 4 of this thesis.

5.3.4 Preparation of Thin Films

Films cast in the Teflon® molds were not wide enough for surface resistivity measurements which required a width of 5 cm. Thin films for surface resistivity measurements were prepared from reaction solutions described in 5.3.2 and 5.3.3 drawn down with a 6-mil (0.03-mm) doctor blade over glass plates. The films made from the 6-mil doctor blade on glass plates were only used for surface resistivity measurements, and all other networks for tensile and DMA were synthesized in Teflon® molds instead of on glass plates. After addition of DBU, the solutions were poured into one end of the 6-mil doctor blade, and the reactant solutions were immediately drawn down across the glass plate. These films were allowed to dry at ambient temperature for 24 h and additionally in a vacuum oven under reduced pressure for 24 h. Resistivities were measured, and then the glass plates were rinsed with methylene chloride. Soxhlet extractions of these thin, 6-mil films were not possible due to the fragile nature of the films and since the films strongly adhered to the glass plates. The crosslinked films remained on the glass plates after washing with solvent. The films were dried in a vacuum oven at 60 °C for

12 h before surface resistivity measurements were again taken to ensure that any extraction of sol did not change these measurements and that efficient crosslinking had been achieved. Reported values are from fully rinsed and dried films.

5.3.5 Characterization

Gel fractions were reported gravimetrically from final over initial mass values after Soxhlet extractions in methylene chloride for 10 h and subsequent drying in a vacuum oven under reduced pressure at 60 ºC overnight. AFM was performed on a Veeco MultiMode AFM with an rms of 4.0 and amplitude setpoint of 3.3. DMA was performed on a TA Instruments Q800 in tension mode with a frequency of 1 Hz, oscillatory amplitude of 15 μm, and a static force of 0.01 N at 3 ºC/min from -100 to 150 ºC. Glass transition temperatures were determined from the peak of the tan delta curve and onset on the storage modulus damping. Tensile experiments were conducted with an Instron 4411 with a cross-head speed of 2 mm/min at ambient temperature utilizing manual grips. The reported values and standard deviations involve an average of three samples. Surface resistivities were measured with a Monroe Electronics meter model 291 on thin films produced with a 6-mil (0.03-mm) draw down blade on glass plates. The Monroe Electronics meter model 291 has the capability to measure 10^3 to 10^{12} ohms/square with an error of ±0.5 decades, applying 10 V for 10^3 to 10^5 ohms/square and 100 V for 10^6 to 10^{12} ohms/square. The meter dimensions are 6.5 x 13 x 3 cm with parallel bar electrodes approximately 5 cm apart. Multi-colored LEDs signified the power of ten values, conductive (green), dissipative (yellow), and insulative (red).

5.4 Results and Analysis

5.4.1 Preparation of MWCNT-Based Networks

Networks were synthesized using 2,4,25,27-tetraoxo-12,12,17,17-tetraphenyl-5,24-dioxa-12,17-diphosphoniaoctacosane bromide (bisphosphonium bisacac) or butane-1,4-diyl bis(3-oxobutanoate) (non-ionic bisacac) Michael donors (Figures 5.2 and 5.3). The synthesis of the monomers and the synthesis of their subsequent networks are described in chapter 4 of this thesis. A 575 g/mole PEG diacrylate served as the Michael acceptor. Each Michael acceptor had a functionality of 2 from the two acrylate groups. Each Michael donor had an assumed functionality of 4 with two deprotonatable hydrogens from each of two bisacac functional groups. The second deprotonatable hydrogen on each acac had a slightly higher pK_a of 13 compared to the first deprotonatable hydrogen with a pKa of 12.[30] Sterics are also involved with the second deprotonation.[30] Therefore, a functionality of 4 does not represent the "true" reactivity of the bisacac monomer.

When synthesizing crosslinked films, leaving dangling acrylate end groups is also unfavorable. These are reactive, can polymerize, and are not light stable. A stoichiometric ratio of 1 to 1.4, deficient in acrylate, ensured efficient crosslinking with no dangling acrylate end groups. Previous *in situ* FTIR studies described in chapter 4 and 90% gel fractions by Soxhlet extraction confirmed efficient crosslinking. Long et al. also indicated that a 1 to 1.4 ratio of bisacac to diacrylate improved tensile properties compared to a 1 to 2 ratio in Michael addition crosslinking reactions.[24] Reactant solutions with 0, 1, 3, and 5 weight % MWCNTs were prepared for both non-ionic and ionic networks and cast into Teflon® molds.

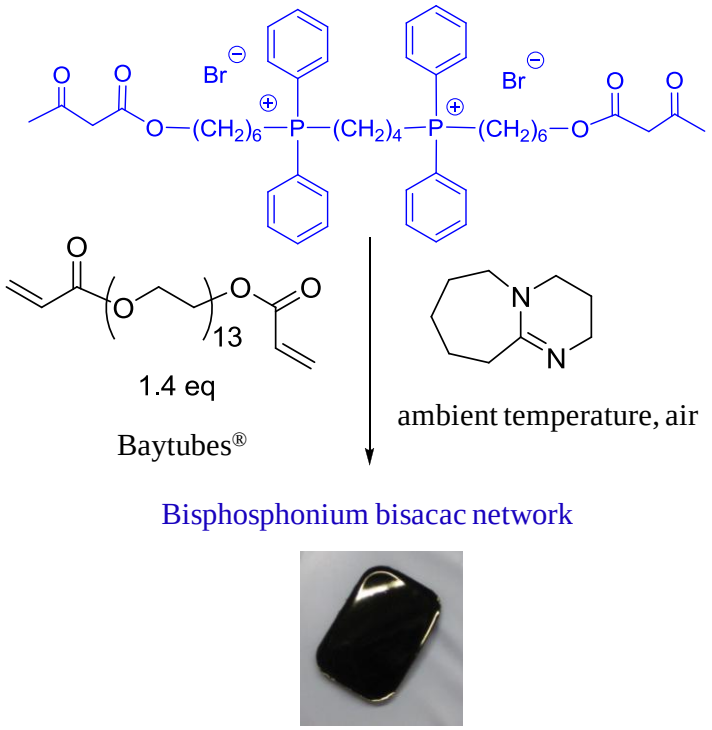

Figure 5.2. Synthesis of MWCNT-containing bisphosphonium-based networks

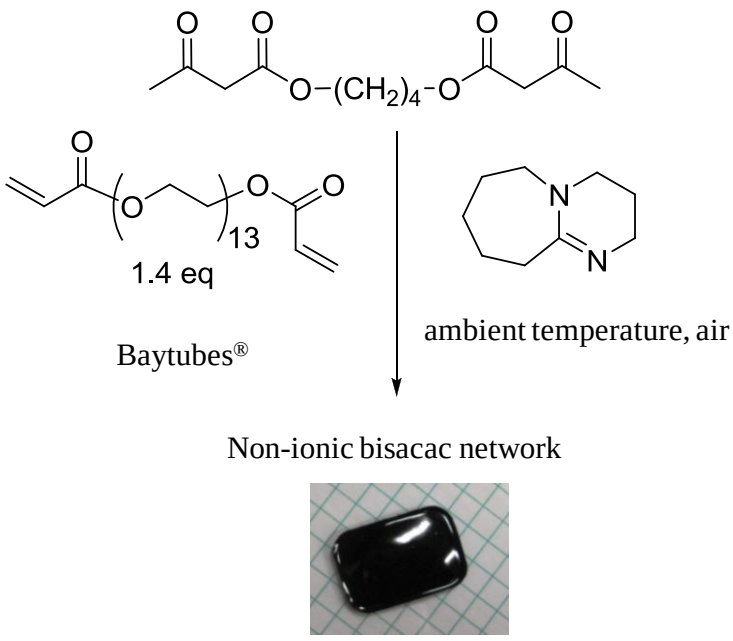

Figure 5.3. Synthesis of MWCNT-containing non-ionic networks

Synthesis of MWCNT-based networks involved including 0, 1, 3, and 5 weight % of probe-sonicated MWCNTs into reactant solutions before the addition of DBU catalyst. First, unfunctionalized Baytubes® were sonicated as 1 weight % solutions in methylene chloride. All other reagents were prepared in a scintillation vial with the exception of DBU, and 200 µL of methylene chloride was added. Baytubes® were added to 1, 3, or 5 weight % as necessary. Then, the methylene chloride was added until 1600 µL total was reached. DBU addition catalyzed crosslinking, and solutions were immediately cast into Teflon® molds once mixed. Both ionic and non-ionic networks with 0 to 5 weight % of MWCNTs had high gel fractions around 90%. No visible loss of the opaque MWCNTs occurred from the samples within over 10 hours of Soxhlet extraction with methylene chloride.

5.4.2 DMA of MWCNT-Containing Networks

Mechanical analysis of the networks was conducted after Soxhlet extraction. Non-ionic networks with 0, 1, 3, and 5 weight % of MWCNTs all displayed similar glass transition temperatures measured by DMA tan delta curves as expected (Figure 5.4). A slight increase in the glass transition was observed with an increase in carbon nanotube content, but the increase was within experimental error.

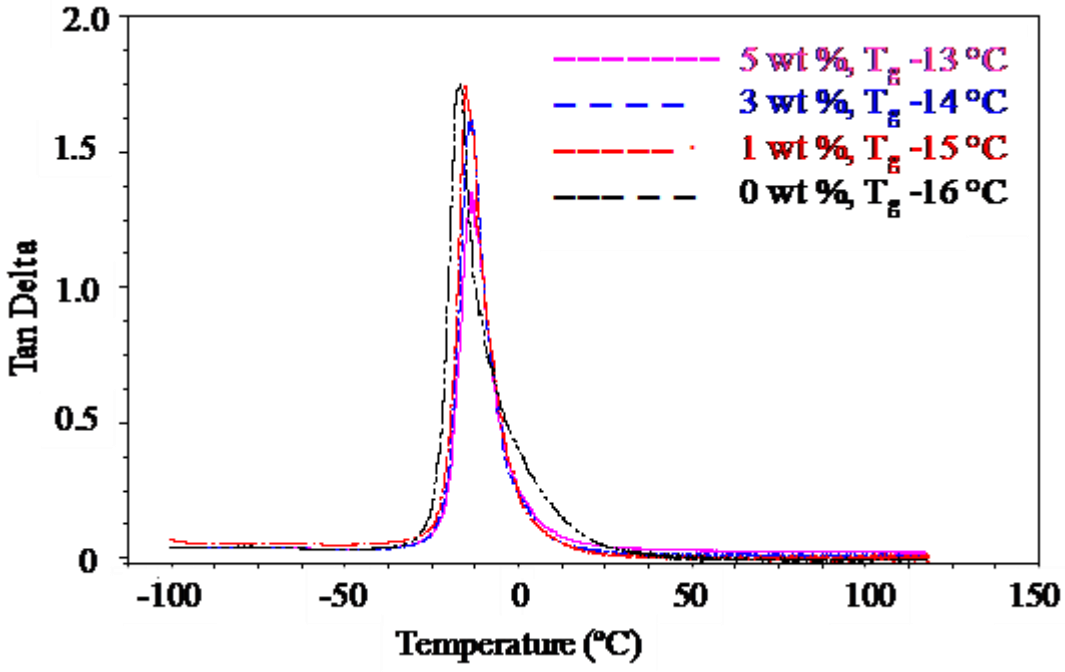

Figure 5.4. DMA tan delta curves of non-ionic bisacac crosslinked films with 0 to 5 weight % of MWCNTs; 3 ºC/minute, 1 Hz, -100 to 120 ºC, air

Additionally, non-ionic bisacac films with 0 to 5 weight % of MWCNTs showed increased plateau moduli going from 0 to 5 weight % respectively (Figure 5.5). The plateau modulus of the 0 weight % network around 1 MPa increased dramatically to around 10 MPa in the 5 weight % MWCNT-containing non-ionic network. Increasing the filler in the polymer correspondingly increased the storage modulus or stiffness of the polymer as in other polymer composites.[1,23]

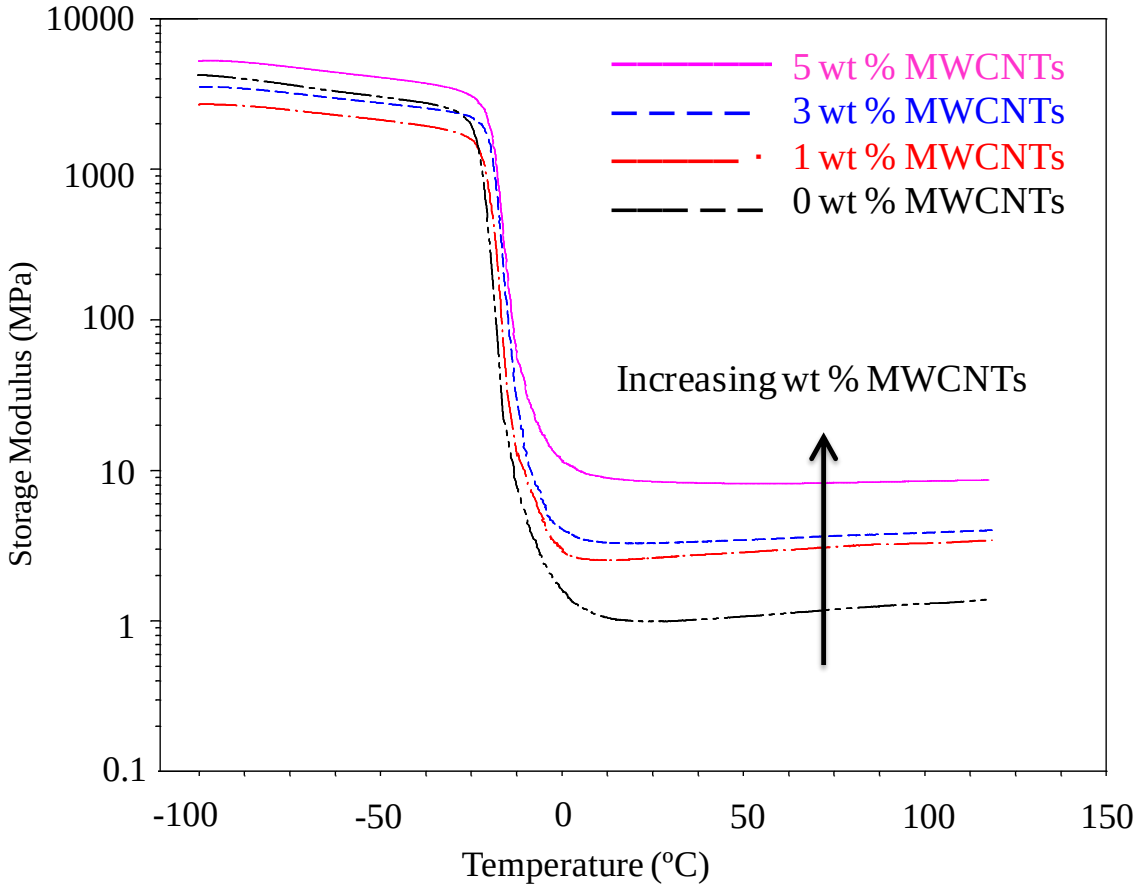

Figure 5.5. DMA storage moduli for non-ionic bisacac networks with 0 to 5 weight % MWCNTs; 3 ºC/minute, 1 Hz, -100 to 120 ºC, air

The bisphosphonium-based networks displayed the same trend. They all had similar glass transition temperatures within experimental error (Figure 5.6), and they also showed a large increase in plateau moduli with an increase in MWCNT loading (Figure 5.7). Adding a robust filler does not affect the glass transition temperature since it is not directly absorbed into the amorphous content of the polymer as a plasticizer or tackifier incorporates. The barrier to translational and rotational motions remains the same with MWCNT loading, but the plateau modulus where entanglements and crosslink density relate is increased with MWCNT content.

The nanotubes remain as large particulates dispersed within the polymer matrix, dramatically affecting the stiffness and softness of the material above its glass transition temperature since these they are trapped between the crosslinks points. Before the glass transition, the carbon nanotubes function as filler for networks with greater nanotube loading, so a slight increase in modulus is observed before the onset of the glass transition temperature. However, this increase is not comparable to the 10-fold greater plateau moduli that result from trapping of the carbon nanotubes between covalent crosslinks.

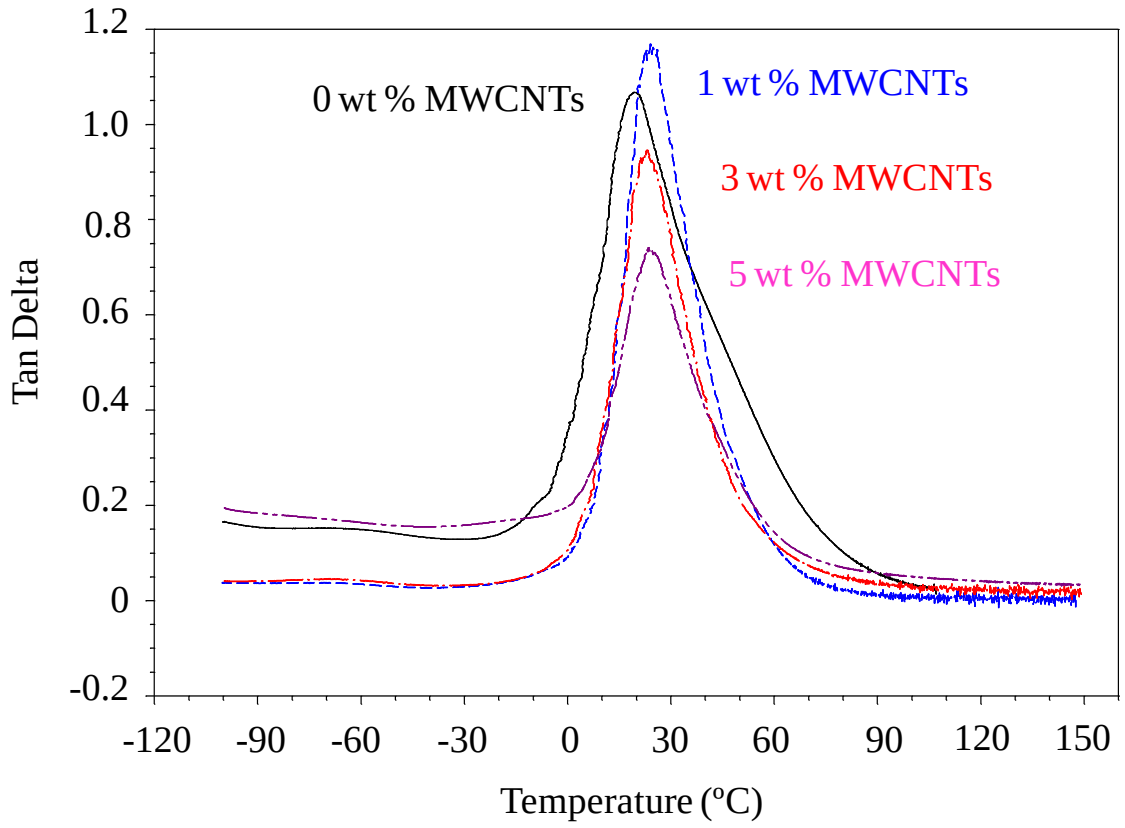

Figure 5.6. DMA tan delta curves for bisphosphonium-based networks with 0 to 5 weight % MWCNTs; 3 ºC/minute, 1 Hz, -100 to 150 ºC, air

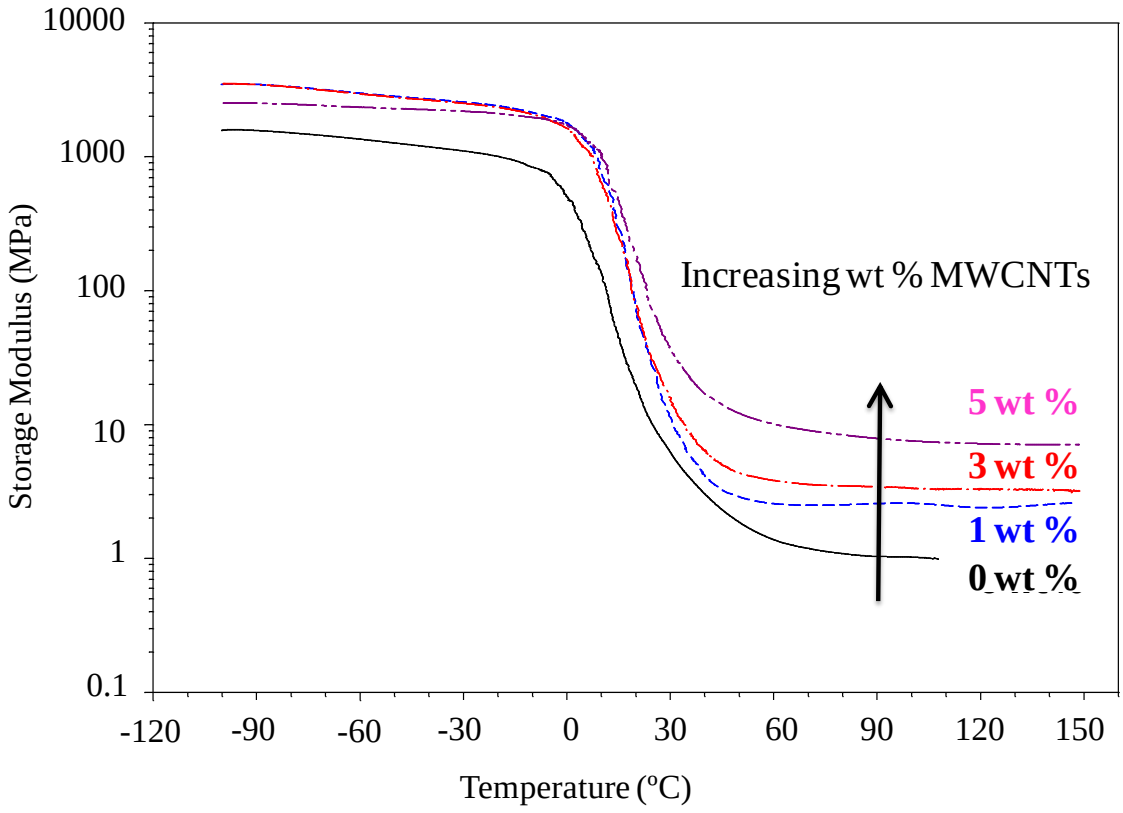

Figure 5.7. DMA storage moduli for bisphosphonium-based networks with 0 to 5 weight % MWCNTs; 3 ºC/minute, 1 Hz, -100 to 150 ºC, air

Both the ionic and non-ionic networks displayed increased plateau moduli from 1 to 10 MPa with 0 to 5 weight % MWCNTs. Plateau moduli relate to the crosslink density of the films as described in chapter 4 of this thesis.[31] Both the ionic and non-ionic networks have similar crosslink densities, and they both exhibit similar increases in plateau moduli with MWCNT loading. Thus, the ionic structure of the bisphosphonium-containing networks did not significantly enhance aggregation or deter distribution of the MWCNTs within the polymer, allowing both non-ionic and ionic DMA plateau moduli to increase proportionally with nanotube content.

5.4.3 Tensile of MWCNT-Containing Networks

In tensile experiments, bisphosphonium-containing networks produced much greater strains at break and stresses at break than non-ionic networks with similar MWCNT loadings (Table 5.1 and 5.2). The bisphosphonium-based networks exhibited enhanced stresses at break and strains at break compared to non-ionic analogs as discussed in chapter 4 of this dissertation. As also discussed in chapter 4, stress at break and strain at break are often enhanced through physical associations of the chains,[32-34] and ionic associations are increased as the polymer is stretched and chains compact. It is reasoned that the ionic groups can find each other in this more compact structure and that the ionic associations provide physical crosslinks that enhance both stress at break and strain at break. Pi-pi stacking interactions can occur in the bisphosphonium-containing monomer from phenyl rings attached to the phosphorus center. These pi-pi stacking interactions could partially be responsible for enhanced association. Also, the coordination of phosphonium cations to PEG oxygens could enhance the Young's moduli of the films over non-ionic analogs by providing physical crosslinking.[35]

Table 5.1. Tensile properties of non-ionic networks[a]

Wt % MWCNTs	Tensile Stress at Break (MPa)	Tensile Strain at Break (%)	Young's Modulus (MPa)
0	0.20 ± 0.07	10.63 ± 4.45	2.33 ± 0.03
1	0.27 ± 0.09	12.10 ± 2.69	4.52 ± 0.58
3	0.51 ± 0.06	12.25 ± 0.27	5.53 ± 0.61
5	1.17 ± 0.33	18.37 ± 2.72	7.41 ± 0.80

[a] crosshead speed 2 mm/minute, 25 °C, average of three samples reported for each value

Table 5.2. Tensile properties of bisphosphonium-containing networks[a]

Wt % MWCNTs	Tensile Stress at Break (MPa)	Tensile Strain at Break (%)	Young's Modulus (MPa)
0	0.51 ± 0.08	32.55 ± 3.16	2.41 ± 0.62
1	1.41 ± 0.17	61.79 ± 0.95	3.40 ± 0.56
3	4.86 ±0.80	102.76± 17.38	5.67 ± 0.78
5	3.58 ± 0.44	51.17 ± 0.91	10.02 ± 0.98

[a] crosshead speed 2 mm/minute, 25 °C, average of three samples reported for each value

The non-ionic networks exhibited similar strains at break and stresses at break with low standard deviations. Young's moduli increased from 2.33 to 7.41 MPa with an increase from 0 to 5 weight % MWCNTs. The 0, 1, 3, and 5 weight % loadings for all of the networks resulted in gradually increased Young's moduli. Stress at break and strain at break for the non-ionic polymers showed a slight increase with increased amount of MWCNTs. The stress-at-break and strain-at-break values increased for the bisphosphonium-containing networks from a 0 to 3 weight % MWCNT loading, but the 5 weight % MWCNT films had lower stress at break than the 3 weight % MWCNT films. Poor nanotube distribution can cause variances in mechanical properties.[23] Matrix distribution of MWCNTs may not have been as uniform for the ionic networks as for the non-ionic networks. Poor nanotube dispersion could be at least partially attributed to any ionic physical crosslinking. The hydrophobic carbon nanotubes may also disperse more appreciably in the non-ionic networks during solution casting due to their greater hydrophobicity than the ionic ones. The stress-strain curves for both non-ionic and ionic

networks with 0, 1, 3, and 5 weight % MWCNT loading are included below (Figure 5.8 and 5.9). They confirm the substantially higher stress at break and strain at break for the bisphosphonium-containing networks compared to non-ionic analogs as well as increased Young's moduli with increased loading.

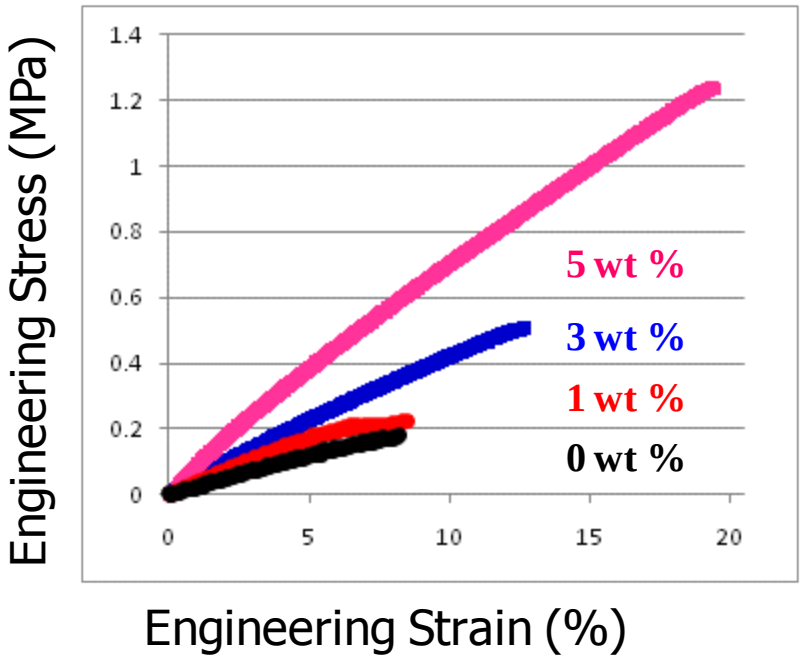

Figure 5.8. Stress-strain curves for non-ionic networks with MWCNTs incorporated; crosshead speed 2 mm/minute, 25 °C

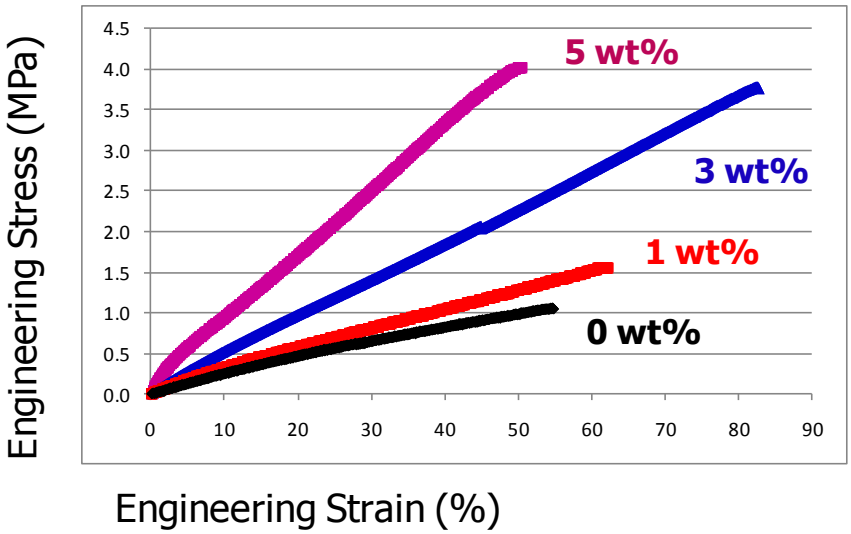

Figure 5.9. Stress-strain curves for bisphosphonium-containing networks with MWCNTs incorporated; crosshead speed 2 mm/minute, 25 °C

These stress-strain curves clearly indicate a large increase in stiffness with MWCNT loading for all polymers. With 5 weight % loading 10 MPa Young's moduli were achieved. A 50 MPa modulus is needed for most actuator or electro-active polymer applications.[28, 29] However, future work may achieve this using more rigid monomer structures.

5.4.4 Surface Resistivity of MWCNT-Containing Networks

Surface resistivities of the networks were measured on thin films with dimensions ≥ 6.5 x 13 x 3 cm. A draw down blade was used to make 6-mil (0.03-mm) crosslinked films on glass plates since at least a 5 x 5 cm film was required. A Monroe Electronics meter model 291 with parallel bar electrodes 5 cm apart and the capability to measure 10^3 to 10^{12} ohms/square with an error of ±0.5 decades was used. Surface resistivity is a measure of the resistance to flow of electrons over the surface of a square region of the material. The ASTM standard units of ohms/square reflect simply that the square geometry allows one to cancel the length and width of

the two-dimensional region being measured in the equation $\rho = RA$.[36-39] R is the resistance. A is the area, and ρ is the resistivity. The word "square" is a marker for this concept and is used to separate the surface resistivity values from ones of bulk or volume resistivity which have units of ohms-cm. Bulk or volume resistivity is highly dependent on the thickness of the cubic region or electrical resistivity through three dimensions.[38-39] PEG at 1000 g/mole has volume conductivity on the order of 10^{-7} S/cm.[38] Conductivity is approximately 1/resistivity.[40] Insulative polymers have surface resistivities > 10^{12} ohms/square.[37-39, 41] Static dissipative polymers have surface resistivities in the range of 10^5 to 10^{12} ohms/square, and finally conductive polymers have resistivities < 10^5 ohms/square.[37-39, 41]

Immediately after the addition of base to the MWCNT-containing reactant solutions, the solutions were drawn across a glass plate to form thin, 6-mil (0.03-mm) crosslinked films. The plates were allowed to dry at ambient temperature, washed with methylene chloride, and then dried again before surface resistivity measurements. Resistivity is inversely related to conductivity and measures the resistance to flow of electrons.[40] Therefore, lower resistivity correlates with higher conductivity. Surface resistivity is a measure of the resistance to flow of electrons on a coated surface and is not the total resistivity in the bulk film, but such measurements can provide some understanding of how ionic versus non-ionic networks generally affect the flow of electrons and how MWCNT loading increases electrical conductivity.

The bisphosphonium-containing networks had lower resistivities in almost all cases for equal loadings of MWCNTs compared to non-ionic analogs (Table 5.3). The bisphosphonium-containing and non-ionic networks with 0 weight % of carbon nanotubes both had resistivities on the order of 10^9 ohms/square. However, every other resistivity was an order of magnitude lower

for the bisphosphonium-based networks compared to the non-ionic networks with the same amount of MWCNTs. The bisphosphonium-containing network with 5 weight % loading, for example, had a resistivity of 10^5 ohms/square compared to the non-ionic analog with 10^6 ohms/square. Dispersion of MWCNTs in the ionic polymer matrix enhanced conductivity to a greater extent than in the non-ionic networks.

PEG-based polymers are commonly used to enhance ionic conductivity since lone pairs on oxygens in the main chain coordinate cations.[35] In this thesis, we examined electrical conductivity and not specifically ionic or electronic conductivity. The MWCNTs are electronic conductors due their unique, cylindrical honeycomb graphene-like structure with sp^2 bonds.[42] Carbon nanotubes are either conducting or semiconducting based on structure or how the nanotube is "rolled" due to the availability of momentum states along the length of the nanotube, or direction of conduction.[42] To the contrary, ionic polymers are potential ionic conductors. However, polyelectrolytes are ionic conductors when their ionic sites have mobility, but they are electrical insulators when their ionic sites cannot move towards opposite electrodes and carry charge.[35] Enhanced electrical conductivity results from movement of ions[35] or increased alignment of the carbon nanotubes in the polymer matrix compared to the non-ionic analogs.[43] These polyelectrolytes were crosslinked and contain immobile cations, and the ionic networks without MWCNTs had the same surface resistivity values as the non-ionic network without MWCNTs. It is hypothesized that alignment of the MWCNTs contributed to the conductivity. Dispersing hydrophobic MWCNTs in the hydrophilic, ionic networks may have resulted in enhanced alignment through van der Waals interactions between the MWCNTs during casting rather than just agglomeration of the nanotubes. However, the ionic networks could also have enhanced conductivity with MWCNTs compared to non-ionic ones with similar loadings due to

p-type doping. MWCNTs are slightly p-doped in water and electrolyte solutions.[50] The phosphonium ionic sites could possibly act as p-type dopants, and ionic sites' slight p-doping activity may be at least partially responsible for the lower resistivities for ionic MWCNT-based networks. Further studies are required to confirm that p-doping or alignment of the MWCNTs contributes to the enhanced electrical conductivity. All polymer films analyzed were not conductive and were still in the static dissipative range with surface resistivities $\geq 10^5$ ohms/square. Therefore, more work is needed to examine conductive composite formulations in these crosslinked films for different loadings of MWCNTs and possibly with increased alignment of the MWCNTs.

Table 5.3. Surface resistivity of ionic and non-ionic networks*

Wt % MWCNTs	Bisphosphonium-Containing Network Resistivity (ohms/square)	Non-ionic Network Resistivity (ohms/square)
0	10^9	10^9
1	10^7	10^8
3	10^6	10^8
5	10^5	10^6

*thickness 6-mil; dimensions ≥ 6.5 x 13 x 3 cm, 10 V and 100 V

5.4.5 Atomic Force Microscopy (AFM) of MWCNT-Containing Networks

Atomic force microscopy (AFM) of non-ionic networks allows us to examine the surface arrangement of carbon nanotubes within the soft polymer matrix. The AFM images of the

bisphosphonium-containing networks appear to contain aggregates as discussed in chapter 4. However, the non-ionic networks have a smooth, continuous surface. Imaging these non-ionic networks allows us to examine the placement of these nanotubes within the non-ionic polymer (Figure 5.10).

Aligning MWCNTs takes advantage of their high aspect ratios for improved composite electrical properties and strength.[43] Chan-Park et al. reviewed the multiple techniques used to align CNTs in a polymer matrix.[43] By TEM, Zhou et al. showed that solution casting polymers with CNTs in Teflon® molds and then simply stretching the materials achieves CNT alignment in the polymer.[44] Any shear or elongational flow during casting polymer solutions also aligns carbon nanotubes.[45] Applying surface acoustic waves,[46] melt-spinning the composites,[43, 47] or subjecting the casting solutions to magnetic forces[48] can improve alignment of the carbon nanotubes. Xin and Woolley even showed that flowing gas over the composite casting solution can induce alignment of the carbon nanotubes in the direction of the gas flow.[49]

AFM images of a non-ionic network from Michael addition reactions in the presence of 1 weight % MWCNTs indicates the possible alignment of the nanotubes in rows (the hard or white phases in Figure 5.10) throughout the network. The non-ionic network for AFM was prepared according to the procedure in 5.3.2 and solution cast in a Teflon® mold. The film was not made with the draw down blade, but it was cast in a Teflon® mold, covered with a Petri dish, and left to cure inside a chemical hood. Although the films were covered with a Petri dish, carbon nanotube alignment could be partially attributed to the air flow over the surface of the film inside the chemical hood. Crosslinking is very fast for these polymers, and alignment of the nanotubes must take place within a few minutes before cure. All films were Soxhlet extracted with methylene chloride for 10 hours in one direction over the film surface. However, diffusion of the

MWCNTs through the crosslinked matrix is assumed to not be appreciable enough for rearrangement. Due to Xin and Woolley's previous studies on gas flow inducing carbon nanotube alignment in solution, the chemical hood air flow may be at least partially responsible.[49] Additionally, hydrophobic interactions between the nanotubes cast in a hydrophilic solution may aid alignment, but further investigation with TEM is needed to determine if this alignment is reproducible in the bulk rather than just on the surface of the polymer. A study of MWCNT alignment in these PEG-based films with different film preparation methods would help confirm the method.

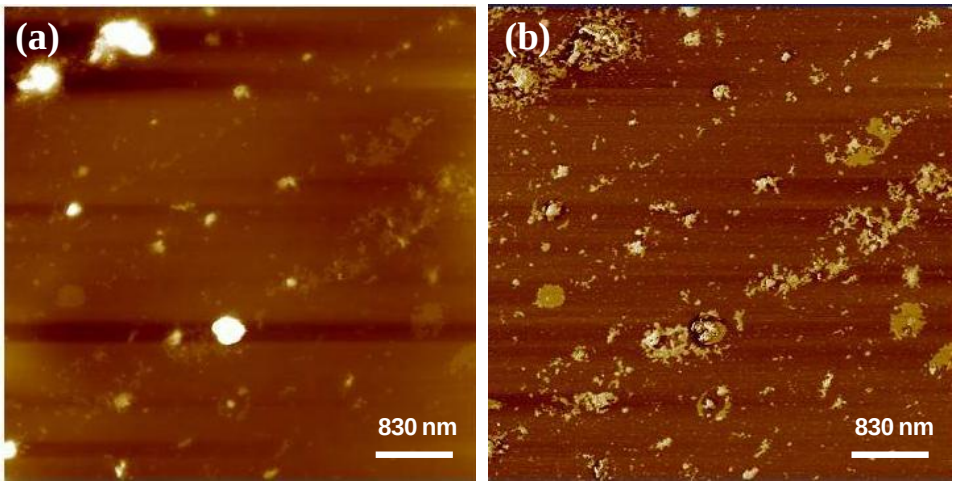

Figure 5.10. AFM of a 1 weight % MWCNT-containing non-ionic network; (a) height image, (b) phase image: 5 x 5 μm images; rms 4.0 mV and amplitude setpoint 3.3 mV

5.5 Conclusions

We examined the incorporation of unfunctionalized MWCNTs in networks from Michael addition reactions with both non-ionic and ionic bisacac crosslinkers and PEG diacrylate. Inclusion of MWCNTs improved Young's moduli and conductivity,[1-2] and our networks fully encapsulated the nanotubes and had gel fractions greater than 90%. The carbon nanotubes are

uniquely fixed in place in the network through dispersing them in the reagents and forming crosslinks around them that restrict their movement in the film, and even Soxhlet extraction for over 10 hours in methylene chloride did not visibly remove any carbon nanotubes from the films.

Incorporation of the MWCNTs did not significantly change the glass transition temperatures for networks with 0, 1, 3, or 5 weight % MWCNTs, but the plateau moduli increased dramatically with carbon nanotube loading for both ionic and non-ionic networks. Networks showed a 3-fold and a 4-fold increase in Young's moduli for the non-ionic and ionic networks with 5 weight % MWCNTs respectively. The stress at break and strain at break were similar for all the non-ionic networks with 0 to 5 weight % MWCNTs. These values varied in the bisphosphonium-containing networks possibly due to poorer distribution of the MWCNTs from ionic crosslinking in the polymers. Surface resistivity measurements for all bisphosphonium-containing versus non-ionic networks were an order of magnitude lower. Additionally, a non-ionic network showed MWCNT alignment in a 1 weight % nanotube-based film with AFM. TEM to investigate bulk film morphology is suggested future work.

5.6 Acknowledgements

Research was sponsored by the Army Research Laboratory and was accomplished under Cooperative Agreement Number W911NF-06-2-0014. The views and conclusions contained in this document are those of the authors and should not be interpreted as representing official policies, either expressed or implied, of the Army Research Laboratory or the U.S. Government. The U.S. Government is authorized to reproduce and distribute reprints for Government purposes notwithstanding any copyright notation hereon. We would also like to acknowledge Bayer MaterialScience for the carbon nanotubes samples, Baytubes® CP 150.

5.7 References

1. Chou, T.-W.; Gao, L.; Thostenson, E. T.; Zhang, Z.; Byrun, J. H. *Composites Science and Technology* **2010**, 70, 1-19.
2. Tiwari, I.; Singh, K. P.; Singh, M. *Russian Journal of General Chemistry* **2009**, *79(12)*, 2685-2694.
3. Ismail, A. F.; Goh, P. S.; Sanip, S. M.; Aziz, M. *Separation and Purification Technology* **2009**, *70*, 12–26.
4. Ra, E. J.; An, K. H.; Kim, K. K.; Jeong, S. Y.; Lee, Y. H. *Chemical Physics Letters* **2005**, *413*, 188–193.
5. Jeong, H. E.; Suh, K. Y. *Nano Today* **2009**, *4*, 335-346.
6. Shi, B. D. *Adv. Funct. Mater.* **2009**, *19*, 3356-3373.
7. Kotov, B. N. A.; Winter, J. O.; Clements, I. P.; Jan, E.; Timko, B. P.; Campidelli, S.; Pathak, S.; Mazzatenta, A.; Lieber, C. M.; Prato, M.; Bellamkonda, R. V.; Silva, G. A.Kam, N. W. S.; Patolsky, F.; Ballerini, L. *Adv. Mater.* **2009**, *21*, 3970-4004.
8. Li, B. T.; Hu, W.; Zhu, D. *Adv. Mater.* **2010**, *22*, 286-300.
9. Zhang, K.; Park, B.-J.; Fang, F.-F.; Choi, H.-J. *Molecules* **2009**, *14*, 2095-2110.
10. Hasan, B. T.; Sun, Z.; Wang, F.; Bonaccorso, F.; Tan, P. H.; Rozhin, A. G.; Ferrari, A. C. Adv. Mater. **2009**, *21*, 3874–3899.
11. Meng, Q.; Hu, J. *Composites: Part A* **2009**, *40*, 1661-1672.
12. Podsiadlo, P.; Shima, B. S.; Kotov, N. A. *Coordination Chemistry Reviews* **2009**, *253*, 2835–2851.
13. Cele, N.; Ray, S. S. *Macromol. Mater. Eng.* **2009**, *294*, 719-738.
14. Su, D. S. *ChemSusChem.* **2009**, *2*, 1009-1020.
15. Grodzka, E.; Pieta, P.; Dłuzewski, P.; Kutner, W.; Winkler, K. *Electrochimica Acta* **2009**, *54*, 5621–5628.
16. Huang, W.; Edenzon, K.; Fernandez, L.; Razmpour, S.; Woodburn, J.; Cebe, P. *Journal of Applied Polymer Science* **2010**, *115*, 3238-3248.
17. Zou, H.; Wang, K.; Zhang, Q.; Fu, Q. *Polymer* **2006**, *47*, 7821-7826.
18. Ozturk, G.; Long, T. E. *Journal of Polymer Science: Part A: Polymer Chemistry* **2009**, *47*, 5437–5447.
19. Yim, E. S.; Zhao, B.; Myung, D.; Kourtis, L. C.; Frank, C. W.; Carter, D.; Smith, R. L.; Goodman, S. B. *Journal of Biomedical Materials Research, Part A* **2009**, *91A(3)*, 894-902.
20. Rogero, S. O.; Malmonge, S. M.; Lugao, A. B.; Ikeda, T. I.; Miyamaru, L.; Cruz, A. S. *Artificial Organs* **2003**, *27(5)*, 424-427.
21. Wang, Y.-P.; Gao, X.-H.; Chen, J.-C.; Li, Z.-W.; Li, C.-L.; Zhang, S.-C. *Journal of Applied Polymer Science* **2009**, *113(4)*, 2492-2498.
22. Qi, L.; Lin, Y.; Wang, F. *European Polymer Journal* **1999**, *35(5)*, 789-793.
23. Narh, K. A.; Jallo, L.; Rhee, K. Y. *Polymer Composites* **2008**, 809-817.
24. Mather, B. D.; Viswanathan, K.; Miller, K. M.; Long, T. E. *Prog. Polym. Sci.* **2006**, *31*, 487–531.
25. Mather, B. D.; Williams, S. R.; Long, T. E. *Macromol. Chem. Phys.* **2007**, *208*, 1949–1955.
26. Williams, S. R.; Mather, B. D.; Miller, K. M.; Long, T. E. *Journal of Polymer Science: Part A: Polymer Chemistry* **2007**, *45*, 4118–4128.

27. Mather, B. D.; Miller, K. M.; Long, T. E. *Macromol. Chem. Phys.* **2006**, *207*, 1324–1333.
28. Duncan, A. J.; Leo, D. J.; Long, T. E. *Macromolecules* **2008**, *41(21)*, 7765-7775.
29. Duncan, A. J.; Akle, B. J.; Long, T. E.; Leo, D. J. *Smart Mater. Struct.* **2009**, *18*, 104005.
30. Clemens, R. J.; Rector, F. D. *J. Coat. Tech.* **1989**, *61*, 83-91.
31. Ozturk, G.; Long, T. E. *Journal of Polymer Science: Part A: Polymer Chemistry* **2009**, *47*, 5437–5447.
32. Eisenberg, A.; Hird, B.; Moore, R. B., *Macromolecules* **1990,** *23*, 4098-4107.
33. Eisenberg, A.; King, M., *Ion-Containing Polymers*. Academic Press: New York, 1977.
34. Tant, M. R.; Mauritz, K. A.; Wilkes, G. L. eds. *Ionomers: Synthesis, Structure, Properties, and Applications.* Van Nostrand Reinhold Co., Inc. New York, NY, 1997.
35. *Applications of Electroactive Polymers*. Bruno, S. ed. Chapman & Hall: New York, 1993, 75-113.
36. ASTM Standard D257, 1993, " Standard Method for DC Resistance of Conductance of Insulating Materials," Annual Book of ASTM Standards, American Society of Testing Materials , Vol.10.01, Philadelphia, PA, 1993, pp.103-119.
37. Schutte, C. L. Hutchins, R. O. *Polymer* **1993**, *34(3)*, 476-480.
38. Kathirgamanathan. P. *Polymer* **1993**, *34(7)*, 1549-1550.
39. Dangelmayer, G. T. *ESD Program Management, A Realistic Approach to Continuous Measureable Improvement in Static Control*, 2nd ed. Lucent Technologies, Kluwer Academic Publishers: Norwell, Massachusetts, 1999, 140.
40. Atkins, P.; de Paula J. *Physical Chemistry*, 7th ed. W. H. Freeman and Company: New York, 2002, 832-842.
41. Andrews, R.; Jacques, D.; Minot, M.; Rantell, T. *Macromol. Mater. Eng.* **2002**, *287*, 395.
42. Paul L. McEuen, P. L.; Fuhrer, M.; Park, H. *IEEE Transactions on Nanotechnolgy* **2002**, *1*, 78.
43. Yan, Y.; Chan-Park, M. B.; Zhang, Q. *Small* **2007**, *3(1)*, 24-42.
44. Jin, L.; Bower, C.; Zhou, O. *Appl. Phys. Lett.* **1998**, *73*, 1197.
45. Vigolo, B.; Penicaud, A.; Coulon, C.; Sauder, C.; Pailler, R.; Journet, C.; Bernier, P.; Poulin, P. *Science* **2000**, *290*, 1331.
46. Strobl, C. J.; Schaflein, C.; Beierlein, U.; Ebbecke, J.; Wixforth, A. *Appl. Phys. Lett.* **2004**, *85*, 1427.
47. Haggenmueller, R.; Gommans, H. H.; Rinzler, A. G.; Fisher, J. E.; Winey, K. I. *Chem. Phys. Lett.* **2000**, *330*, 219.
48. Garmestani, H.; Al-Haik, M. S.; Dahmen, K.; Tannenbaum, R.; Li, D. S.; Sablin, S. S.; Hussaini, M. Y. *Adv. Mater.* **2003**, *15*, 1918.
49. Xin, H. J.; Woolley, A. T. *Nano Lett.* **2004**, *4*, 1481.
50. Krüger, M.; Widmer, I.; Nussbaumer, T.; Buitelaar, M.; Schönenberger, C. *New J. Phys.* **2003**, *5(1)*, 138.

Chapter 6: Hydrophilic Polyurethane Ionomers with Varied Bisphosphonium Hard Segment Content

6.1 Abstract

Novel hydrophilic polyurethane ionomers containing a bisphosphonium chain extender were synthesized with 37.1, 46.0, and 67.1 weight % hard segment. For the first time, a series of phosphonium chain-extended polyurethanes with varied hard segment and ionic composition was synthesized. As the hard segment and ionic compositions were increased, melting points of the PEG soft segment of the polyurethane dropped from 30 to 14 °C. Ionic aggregation impeded PEG crystallization. Physical crosslinking from increased ionic composition broadened the glass transition temperatures and increased the plateau moduli in dynamic mechanical curves. The phosphonium-containing polyurethanes with varied hard segment showed unique film formation properties including memory of the Teflon® mold proportions during casting. Films cast in Teflon® molds shrank proportionally to the mold shape, resulting in films with ¾ of the mold width and length while increasing in the z direction, perpendicular to the mold. SAXS indicated increasing ionic content and increasing hard segment content resulted in shorter inter-aggregate spacing from 105 to 70 angstroms. All of the ionic polyurethanes exhibited an ionic aggregate peak in the SAXS profiles, and the non-ionic controls did not have this peak.

6.2 Introduction

Polyurethanes often contain microphase-separated, hard and soft segment domains, providing mechanical strength and elastomeric behavior.[1] Polyurethanes are used commercially

in biomedical implants[2-9] such as tissue scaffolds and catheters.[2-3] These polymers also have coating and adhesive applications,[10-14] and they are acoustic-damping foams.[15-18] In our research group, we have extensively examined branched and linear poly(urethane-urea)s[19-23] and poly(ester-urethane)s.[24] Our research group even illustrated electrospun fibers from branched poly(urethane-urea)s,[23] and we reported evidence of orientation of carbon nanotubes functionalized with hydrogen bonding groups into nanowires in electrospun polyurethane fibers.[25]

Ionic polyurethanes containing ionic sites either within or pendant to the backbone generally exhibit less hydrogen bonding, weaker phase separation, and higher water absorption than structurally similar non-ionic polyurethanes.[26] Kuo et al. chain-extended polyurethanes with sulfonic acid- or carboxylic acid-containing diols.[26] The ionic polyurethanes were synthesized through neutralization with 0.5 N sodium hydroxide in water/ methyl ethyl ketone solutions, and no discussion of the extent of neutralization was present. These anionic polyurethanes were compared to PTMO-based and 1,4-butanediol chain-extended polyurethanes. H-bonding weakened the C=O bond, making the FTIR peak shift from 1720 towards 1693 cm^{-1}. If ionic sites disrupt hydrogen bonding, the carbonyl region will shift to higher wavenumbers which indicate stronger C=O bonds. The C=O stretching region in FTIR was deconvoluted with a Gaussian fit to ratio the area of non-bonded urethane carbonyls to hydrogen-bonded urethane carbonyls. The ionic polymers contained greater amounts of non-bonded to hydrogen-bonded carbonyls compared to a non-ionic 1,4-butanediol chain-extended PTMO-based polyurethane.[26] Kuo et al. also suggested that ionic polyurethanes had weaker phase separation than non-ionic polyurethanes, and this weaker phase separation in ionic polyurethanes was indicated with DSC by the greater breadth in the endothermic region of the glass transition for the PTMO segment.[26]

The authors did not provide a concrete analysis that included DMA, which may have more definitely shown microphase separation through the indication of two melting points or multiple transitions. However, the ionic polymer absorbed 14-29% of their original weight in water compared to 2% absorption for the non-ionic polymer.[26] Cooper et al. also showed that pyridinium-containing, PTMO-based polyurethanes absorbed more water compared to non-ionic polyurethanes.[27]

Ionic sites in these polymers aggregate to provide physical crosslink points, and these aggregates possess a dissociation temperature. Changing the structure of the ionic group alters the size and structure of ionic aggregates and subsequently regulates polymer melt processability.[28-31] Buruiana et al. studied the micellization and aggregation of ionic polyurethanes through inclusion of fluorescent pyrene labels.[32] PEG-based polyurethanes were synthesized with a *N*-methyldiethanolamine chain extender. After polymerization, 4-chloromethylphenylcarbamoyl-1-oxymethylpyrene was used to quaternized the amines. Fluorescence spectra indicated a high excimer (or dimeric or heterodimeric molecule) to monomer intensity ratio.[32]

Polyurethanes containing ionic functionalities offer good antimicrobial activity,[27] biocompatibility,[5, 33-38] and conductivity,[33-38] providing polymers with high mechanical strength that could fight bacterial infection.[27] Cooper et al. synthesized ionic polymers through chain extending PTMO-based oligomers with *N*,*N*-bis(2-hydroxyethyl)isonicotinamide and through subsequent quaternization with various alkyl halides.[27] The extent of quaternization was not discussed, but a twenty percent molar excess of alkyl halide was used. The authors incorporated greater ionic character through varying the stoichiometric ratio of the polyol to the functionalized diol chain extender. Increasing the ionic content led to increased Young's moduli without large

changes in the ultimate stress. These pyridinium-containing polyurethanes possessed high antimicrobial activity towards *Staphylococcus aureus*.[27] Hung et al. investigated primary, secondary, and tertiary amine-containing polyurethanes which are quaternized at physiological pH.[5] These cationic polyurethanes had the capacity to bind with DNA in complexes, allowing DNA transfection. Also, the authors found that these cationic polymers exhibited lower toxicities than commonly used polyethylenimine (PEI) or poly(2-dimethylaminoethyl methacrylate) (PDMAEMA).[5] Wang et al. showed that PEG-based polyurethanes with sodiosulfonate side-chain grafts had moderate ionic conductivities from 10^{-6} to 10^{-7} S/cm at room temperature.[33] Using a PEG polyol also facilitates better biocompatibility and conductivity than PTMO-based polymers.[34-38] Biocompatible polyurethanes are already used in angioplasty,[39-41] and it is proposed that conductive, biocompatible polyurethane coatings may have future potential in many medical applications including sensing the extent of deployment of balloons for angioplasty.[42-43]

Although phosphonium chemistry is ubiquitous, investigation of phosphonium-containing polymers is a relativity unexplored field. The phosphonium functionality provides many advantages including flame retardancy, thermal stability, and self-assembly.[44-46] Phosphonium salts possess higher thermal stability[47] and greater antimicrobial activity[48] compared to structurally similar ammonium salts. Phosphonium functionalities are up to 70 to 80 °C more thermally stable by TGA at 2 °C/minute under nitrogen than similar ammonium molecules.[47] This thesis aims to elucidate the synthesis of hydrophilic polyurethanes chain-extended with a bisphosphonium diol. Previously, a PTMO-based polyurethane chain-extended with bisphosphonium salts was reported in our research group.[49] However, the hard segment and percent ionic hard segment was never varied, and this is the first series synthesized to investigate

the effect of phosphonium ionic aggregation on polymer properties. Also, PEG-based polyurethanes were used in this thesis due to their higher biocompatibility and higher conductivity than PTMO,[34-38] and PEG also had better solvation during polymerization at high ionic contents than PTMO-based ionic polyurethanes. Increasing hard segment and ionic contents in the polyurethanes changed polymer mechanical properties. This thesis expounds the interplay of crystallinity and ionic aggregation in several hydrophilic polyurethanes with varied composition.

6.3 Experimental

6.3.1 Materials

2-Bromoethanol (95%), dibutyltin dilaurate (DBTDL) (95%), 1,4-bis(diphenylphosphino)butane (98%), dimethyl sulfoxide (DMSO) (≥99.9%), chloroform-d (99.96 atom % D), acetic anhydride (≥99%), pyridine (≥99%), and 0.1 N potassium hydroxide in methanol were purchased from Aldrich and used as received. 1,4-Butanediol (≥99%) was purchased from Aldrich and distilled over calcium hydride under nitrogen. Bayer MaterialScience provided 4,4′-methylenebis(cyclohexyl isocyanate) (HMDI) (>99.5%) with an isomer mixture of 22% trans, trans, 54% trans, cis, and 24% cis, cis. HMDI was used as received. Poly(ethylene glycol) (PEG) diol with a M_n of 2180 g/mol was obtained from Aldrich. The PEG was dried overnight under reduced pressure in a vacuum oven at 60 °C before use. *N*,*N*-Dimethylformamide (DMF) (99%) from Aldrich was collected from an Innovative Technology, Inc., PureSolv-MD3 solvent purification system. Tetrahydrofuran (THF) (HPLC grade, ≥99%) from EMD Science was distilled under nitrogen from sodium benzophenone. A 1 wt % solution of DBTDL in dry THF was used as the catalyst solution. Chloroform (Optima

grade, ≥99.0%) was purchased from Fisher Scientific and distilled over calcium hydride under nitrogen. Anhydrous diethyl ether was purchased from VWR and used as received.

6.3.2 Synthesis of Butane-1,4-bis[(2-hydroxyethyl)diphenylphosphonium] Bromide Chain Extender

The synthesis of this chain extender was reported previously by our research group.[49] Bis(diphenylphosphino)butane (6.00 g, 14.1 mmol) was charged to a flame-dried, 100-mL flask with a Teflon® stir bar under argon. Three equivalents of 2-bromoethanol to one equivalent bis(diphenylphosphino)butane were used. The 2-bromoethanol (3.00 mL, 5.29 g, 42.3 mmol) was charged to the flask under argon. Then, 28.0 mL of dry chloroform was added, and the flask and contents were purged for 20 min with argon. The reaction continued at 65 ºC for 24 h under an argon blanket. Once cooled, 50 mL of chloroform was added to the product, and the bisphosphonium diol was precipitated in 900 mL of anhydrous diethyl ether and washed with an additional 50 mL of anhydrous diethyl ether. White crystals were collected and dried in a vacuum oven for 24 h at 60 ºC. FAB mass spectrometry m/z (+FAB, 100% M^+, exact mass, direct probe) provided 595.15 g/mol for the exact mass, and the melting point was 123-124 °C as reported earlier.[49] ^{1}H NMR (400 MHz, 25 ºC) in $CDCl_3$: δ (ppm) 2.026-2.206 (m, 4H), 3.129-3.269 (m, 4H), 3.413-3.630 (m, 4H), 3.913-4.122 (m, 4H), 5.431-5.573 (s, 2H, -OH), 7.601-7.863 (m, 20H, phenyl). ^{31}P NMR (162 MHz, 25 ºC, referenced to H_3PO_4 external standard) in $CDCl_3$: δ (ppm) 26.8.

6.3.3 Synthesis of Bisphosphonium Diol Chain-Extended, PEG-Based Polyurethane Ionomers

The synthesis of ionic polyurethanes closely followed the literature.[24, 28, 49] Both the PEG diol and the bisphosphonium diol were dried under reduced pressure in a vacuum oven at least 60 ºC overnight prior to reaction. All polymerizations utilized a flame-dried, 250-mL, 3-neck, round-bottom flask with attached addition funnel, condenser, and overhead stirrer. All polyurethanes were synthesized in two steps using the "prepolymer" method. Polymers with 37.1, 46.0, and 67.1 wt % hard segment were synthesized. Hard segment (HS) % was calculated using the following equation: % HS = 100 [(HMDI + chain extender)/(HMDI + chain extender + PEG)].[49] A characteristic synthesis of a 37.1 wt % hard segment ionic polyurethane is described. A 2180 g/mol PEG diol (2.00 g, 0.92 mmol) was charged to the 3-neck, round-bottom flask and purged with argon for 10 min. Bisphosphonium diol (0.643 g, 0.95 mmol) was dissolved under argon in 20.0 mL of dry DMF. The solution was cannulated into the addition funnel under argon. HMDI (0.5 mL, 0.538 g, 2.05 mmol) was charged to the flask, and five drops of a 1 wt % solution of DBTDL in dry THF were added. The first stage of the reaction of PEG diol with HMDI catalyzed by DBTDL was allowed to proceed in bulk at 75 ºC for 4 h. Completion of the first stage and significant conversion of hydroxyl groups to urethane groups were monitored with FTIR on samples taken during the reaction and additionally with *in situ* FTIR. After 4 h when the polyol was endcapped with isocyanate, the solution of bisphosphonium diol chain extender in DMF was added dropwise over 1 h to the reaction at 75 ºC under a nitrogen purge. After 24 h, the polyurethane solution in DMF was cast into a Teflon® mold. The cast films were dried at ambient temperature for 4 days, heated at approximately 40 ºC for 2 days, evacuated in the vacuum oven at ambient temperature for 3 h, and then dried in the vacuum

oven at 80-90 °C for 24 h to remove all residual DMF. The dried ionic polyurethane films were insoluble. ^{31}P NMR (400 MHz, 25 ºC, referenced to H_3PO_4 external standard) in $CDCl_3$: δ (ppm) 26.8.

6.3.4 Synthesis of 1,4-Butanediol Chain-Extended, PEG-Based Polyurethanes

Synthesis of the non-ionic polyurethane followed the same procedure as for the phosphonium-containing polyurethanes except 1,4-butanediol was added as the chain extender calculated to 37.1 wt % hard segment. These films were cast in the same manner, and they remained soluble in DMF and chloroform after drying.

6.3.5 Characterization

^{1}H NMR and ^{31}P NMR spectroscopic data were collected in $CDCl_3$ and CD_3OD on a Varian 400 MHz spectrometer operating at 400 and 162 MHz respectively. FAB MS was performed on a JEOL JMS-HX-110 instrument in positive mode. End group analysis on PEG diol was preformed prior to use. Approximately 2 grams of the PEG diol was dissolved in three flasks of 1:3 v:v acetic anhydride/pyridine solution. Three solutions without PEG diol were prepared as controls as well. The solutions were stirred for 48 h. Pyridine (10 mL) and HPLC grade water (10 mL) were added to each. All solutions were titrated with 0.1 N KOH solution and phenolphthalein indicator. Titration resulted in calculation of 2,180 g/mol for the PEG diol from the hydroxyl equivalent. An ASI REACTIR 1000 was used for *in situ* FTIR spectroscopy with a resolution derived from 8 and 64 scans averaged every 30 s. Dynamic light scattering (DLS) was conducted on a MALVERN CGS-3 at a 90° angle at ambient temperature. All solvents were filtered with a 200 nm filter prior to use, and all polymer solutions were filtered

with a 450 nm filter prior to analysis. A Perkin-Elmer TGA 7 under a nitrogen atmosphere at a heating rate of 10°C/min was used for TGA. A Perkin Elmer Pyris 1 under nitrogen at 5 ºC/min was used for DSC. Values from the second heating of a heat/cool/heat cycle were reported. DMA was conducted with a Seiko Instruments model DMS210 with a 3 ºC/min heating rate from -150 to 225 °C in tension mode with a frequency of 1 Hz, oscillatory amplitude of 15 µm, and a static force of 0.01 N. X-ray diffraction (XRD) was performed on a Nova diffractometer system from Oxford Diffraction with an Onyx CCD detector and a copper X-ray source. Small angle X-ray scattering (SAXS) profiles were collected with 60 second scans at the Station 4C1 PLS synchrotron radiation source (Pohang, Korea). AFM was instrumented with a Veeco MultiMode AFM with an rms of 4.0 and setpoint amplitude of 3.3 mV. A Philips EM 420 transmission electron microscope (TEM) equipped with a tungsten filament electron gun, 120 kV maximum accelerating voltage, and a CCD camera was used. Samples for TEM were prepared through cryomicrotoming 70 nm slices that were collected over DMSO/H_2O solutions. Surface resistivities were measured with a Monroe Electronics meter model 291. The Monroe Electronics meter model 291 has the capability to measure 10^3 to 10^{12} ohms/square with an error of ±0.5 decades, applying 10 V for 10^3 to 10^5 ohms/square and 100 V for 10^6 to 10^{12} ohms/square. The meter dimensions are 6.5 x 13 x 3 cm with parallel bar electrodes approximately 5 cm apart. Multi-colored LEDs signified the power of ten values, conductive (green), dissipative (yellow), and insulative (red).

6.4 Results and Discussion

6.4.1 Synthesis of Polyurethanes

The synthesis of the bisphosphonium-containing monomer proceeds through an S_N2 mechanism. A large excess of 2-bromoethanol was used to facilitate a fast, complete reaction with the aryl bisphosphine (Figure 6.1).

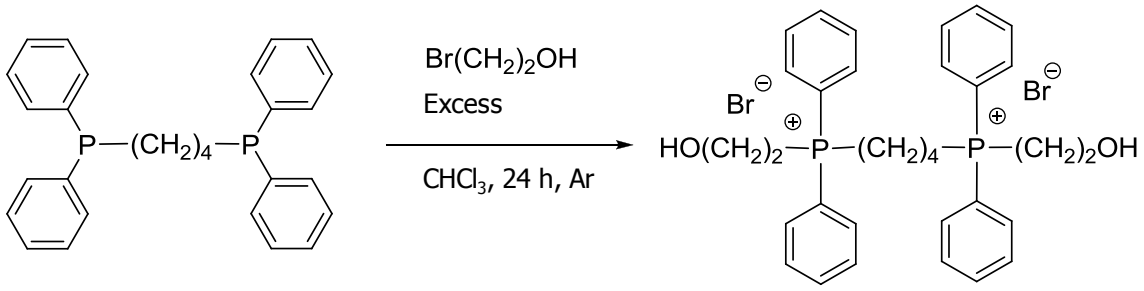

Figure 6.1. Synthesis of butane-1,4-bis[(2-hydroxyethyl)diphenylphosphonium] bromide chain extender

^{1}H NMR and ^{31}P NMR spectra confirmed the expected structure of the final product, and DSC thermograms indicated a melting point of 123-124 °C for this monomer.[49] An ionic liquid is designated as any ion-containing monomer that is a liquid at 100 °C or lower, so this monomer is not classically defined as an ionic liquid due to its high melting point being greater than 100 ºC.

PEG-based polyurethanes incorporating the bisphosphonium monomer were synthesized with typical, two-step conditions (Figure 6.2).[24, 28, 49]

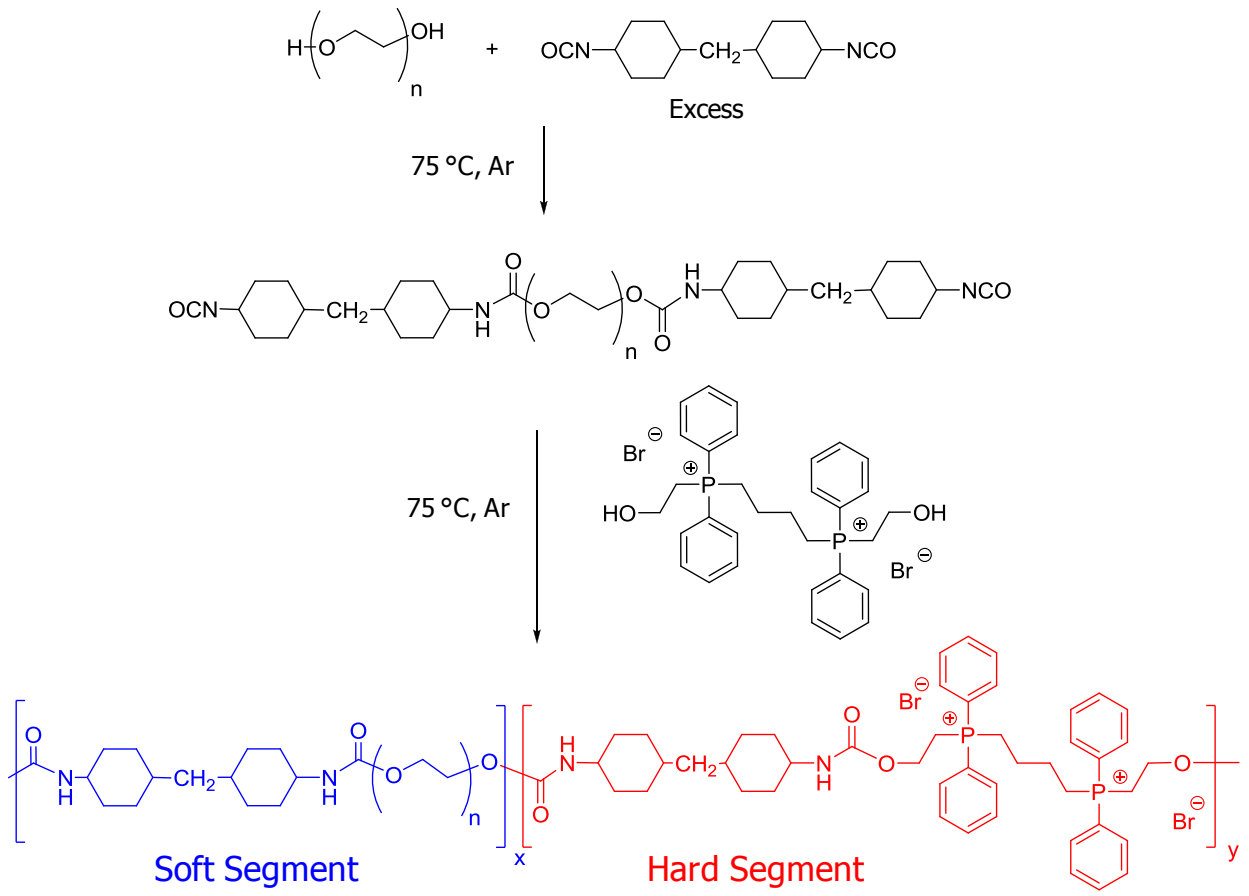

Figure 6.2. Synthesis of bisphosphonium-containing PEG-based polyurethanes

Polyol molecular weight was determined with acetic anhydride functionalization and subsequent titration with 0.1 N potassium hydroxide in methanol. Titration was completed before incorporation into polyurethane prepolymers to confirm a M_n of 2,180 g/mole. First, a PEG diol was reacted with excess 4,4′-methylenebis(cyclohexyl isocyanate) (HMDI) in bulk with mechanical stirring under an inert atmosphere and catalyzed with dibutyltin dilaurate (DBTDL). The ratio of diisocyanate to total diol was kept constant. Although the total moles of diol were kept constant, the mole ratio of PEG diol and bisphosphonium diol chain extender was varied to produce polyurethanes with 37.1, 46.0, and 67.1 weight % hard segment. *In situ* FTIR every 5 minutes of the first stage of the reaction as it proceeded and FTIR on samples drawn from the

reaction every hour were used to conclude that four hours was sufficient to terminate the 2,180 g/mole PEG diol with HMDI. After these four hours, the chain extender was dissolved in dry DMF and added dropwise under an inert atmosphere to the reaction. The reaction proceeded for 24 hours until no isocyanate peak remained in FTIR spectra, and films were cast directly into Teflon® molds. ^{31}P NMR spectra of the reaction solution confirmed that there was no significant degradation to any other type of phosphorus centers since the spectra exhibited only one resonance, the one for the phosphonium cation (Figure 6.3).

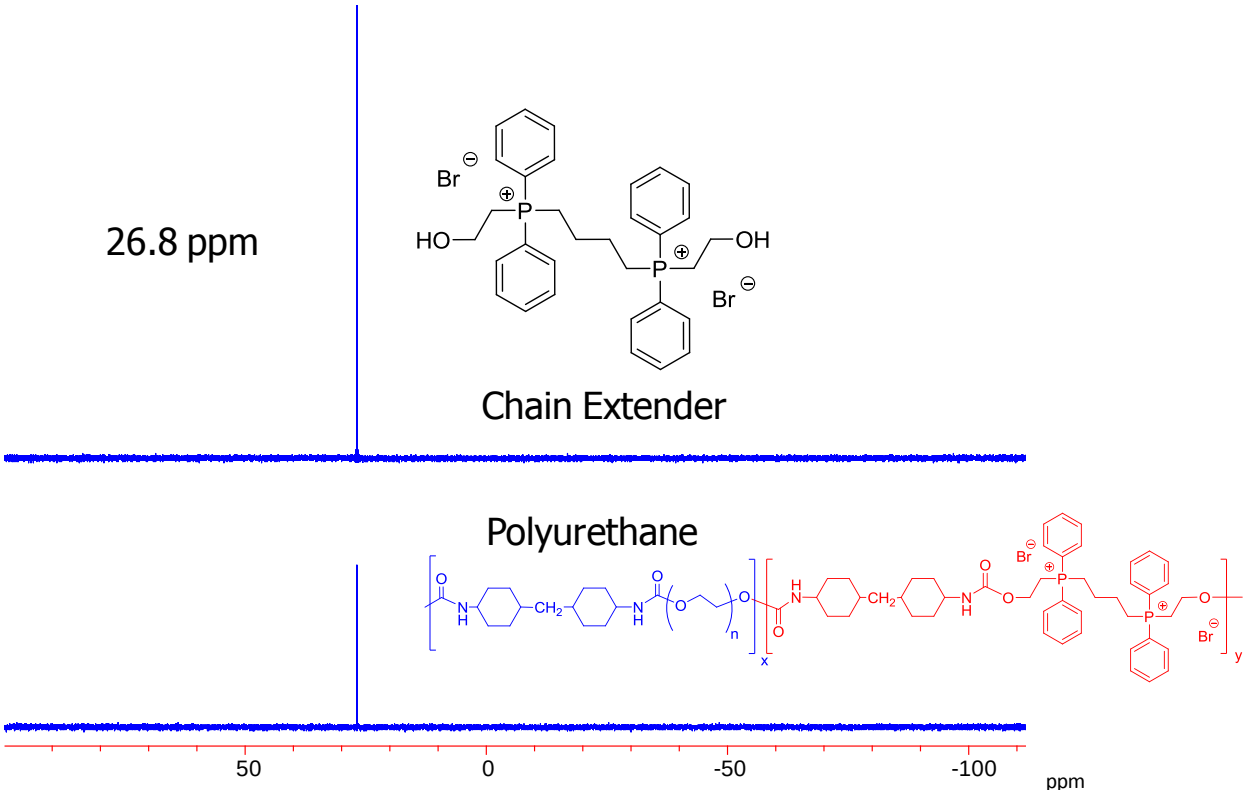

Figure 6.3. ^{31}P NMR spectra of phosphonium chain extender and phosphonium-based polyurethane; 162 MHz in a magnetic field of 9.39 Tesla, $CDCl_3$

6.4.2 Film Formation

We hypothesize that physical crosslinking through ionic aggregation and hydrophilicity resulted in rearrangement of the films during drying. Reaction solutions were cast directly into Teflon® molds. The cast films were dried at room temperature for four days, and shape change became evident. During solvent evaporation and film formation, the sides of the ionic films pulled away from the edges of the Teflon® molds, and the films shrank isotropically to ¾ the size of the mold in the x and y (or side) directions, parallel to the mold surface (Figure 6.4). Film dimensions increased in the z (or upward) direction perpendicular to the mold surface to account for changes in the x and y directions. Non-ionic analogs did not show this rearrangement, and casting the non-ionic polyurethanes led to films with the exact dimensions of the Teflon® molds used.

Teflon® has a large difference in intrinsic surface energy compared to the hydrophilic polyurethanes. Hydrophilic, ionic polyurethanes cast into hydrophilic glass petri dishes retained the shape of their molds; thus, it is hypothesized that hydrophobicity of the mold directly affected film shape, dimensions, and formation. The rearrangement of the ionic films was also attributed to the increased ionic aggregation taking place during solvent evaporation. Ionic aggregation in DMF solution of the ionic polyurethanes was also apparent with dynamic light scattering (DLS). DLS indicated intensity average diameters of approximately 200 nm for the aggregates as part of their size distribution in DMF at ambient temperature (Figure 6.5).

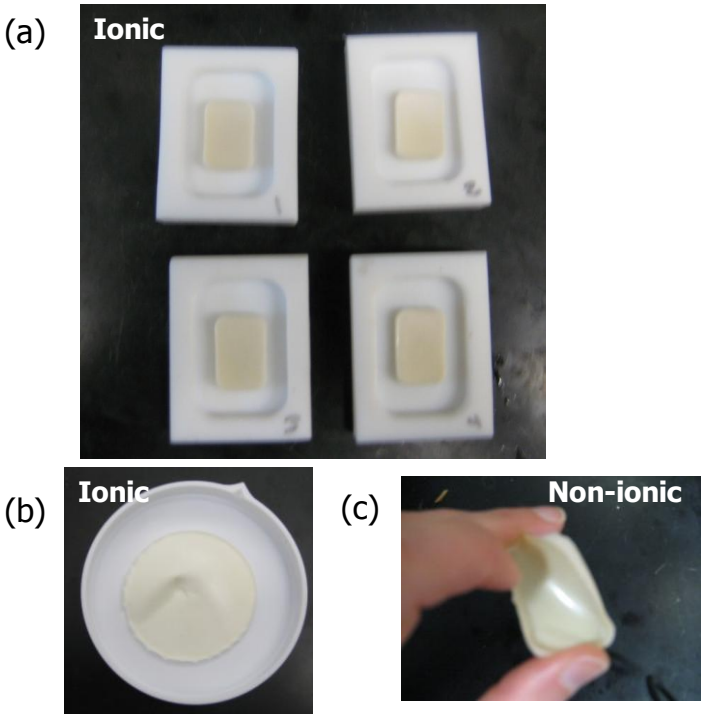

Figure 6.4. Shape change during film formation of (a, b) ionic and (c) non-ionic polyurethanes; ambient temperature

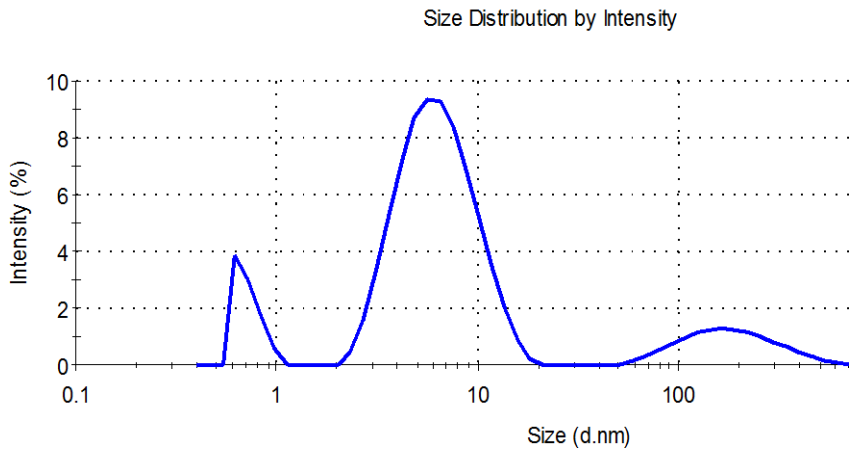

Figure 6.5. DLS profile of an ionic polyurethane with 37.1 weight % hard segment, indicating ionic aggregate formation in solution; MALVERN CGS-3, 90° angle, DMF, ambient temperature

After drying, the ionic polyurethane films were insoluble, but the dried 1,4-butanediol-chain-extended, non-ionic polyurethane films that did not contain bisphosphonium functionality were completely soluble. It is hypothesized that the insolubility of the ionic polyurethanes is partly due to ionic associations. However, hydrogen-bonding and rigidity of the ionic hard segment compared to 1,4-butanediol-based polymer may also contribute.

6.4.3 Thermal Properties

PEG-segment glass transitions for the polymers were within error of each other and did not significantly change with increasing phosphonium hard segment type or content (Table 6.1). Phase mixing would have resulted in increased PEG glass transition temperatures with increased bisphosphonium and hard segment (HS) content, so vast phase mixing is not evident although both soft and hard segments are hydrophilic.

Table 6.1. DSC and DMA of Phosphonium or BD PEG-based Polyurethanes

Soft segment (polyol)	Hard segment	HS (%)	T_g[a] (DMA, ˚C)	T_g[b] (DSC, ˚C)	T_m[b] (DSC, ˚C)
PEG	--	---	---	---	54
PEG	BD	37.1	-41	-35	35
PEG	P^+	37.1	-41	-30	30
PEG	P^+	46.0	-41	-33	26
PEG	P^+	67.1	-41	-33	14

[a]DMA, 3 ºC/minute, 1 Hz, -150 to 225 ºC, air [b]DSC Midpoint T_g, 5 ºC/minute, -80 to 220 °C, N_2

Although PEG soft segment (SS) glass transition temperatures did not drastically change with increased ionic HS, the PEG SS melting points decreased significantly as the phosphonium hard segment was increased, suggesting the disruption of PEG crystallinity. PEG diol had a melting point of 54 ºC, and the non-ionic 1,4-butanediol chain-extended PEG-based polyurethane had a lower melting point of 35 ºC. Incorporation of ionic HS had a drastic effect on the SS melting point compared to changes in SS glass transition.

Physical crosslinking in these ionic polymers through ionic interactions restricted crystallization, and the SS melting points decreased as HS was increased. MacNight et al. showed that increased ionic content led to decreased crystallinity in neutralized polyethylene-*co*-poly(methacrylic acid) copolymers,[50] and Long et al. and Colonna et al. also showed that ionic groups slow the crystallization rate in PET and PBT-based ionomers respectively.[51, 52] However, the disruption of hydrogen bonding with ionic incorporation is also reported in the polyurethane literature.[26] Hydrogen bonds have a typical strength of 20 kJ/mole, while electrostatic interactions have strengths around 200 kJ/mole.[40] The 10-fold increase in energy associated with electrostatic interactions compared to hydrogen bonding interactions leads to the disruption of urethane hydrogen-bonding in ionic polyurethanes.[26]

DMA data showed that the breadth of the glass transition temperatures in ionic polyurethanes increased with increasing ionic HS, and the 67.1 weight% HS polymer had the broadest transition (Figure 6.6).

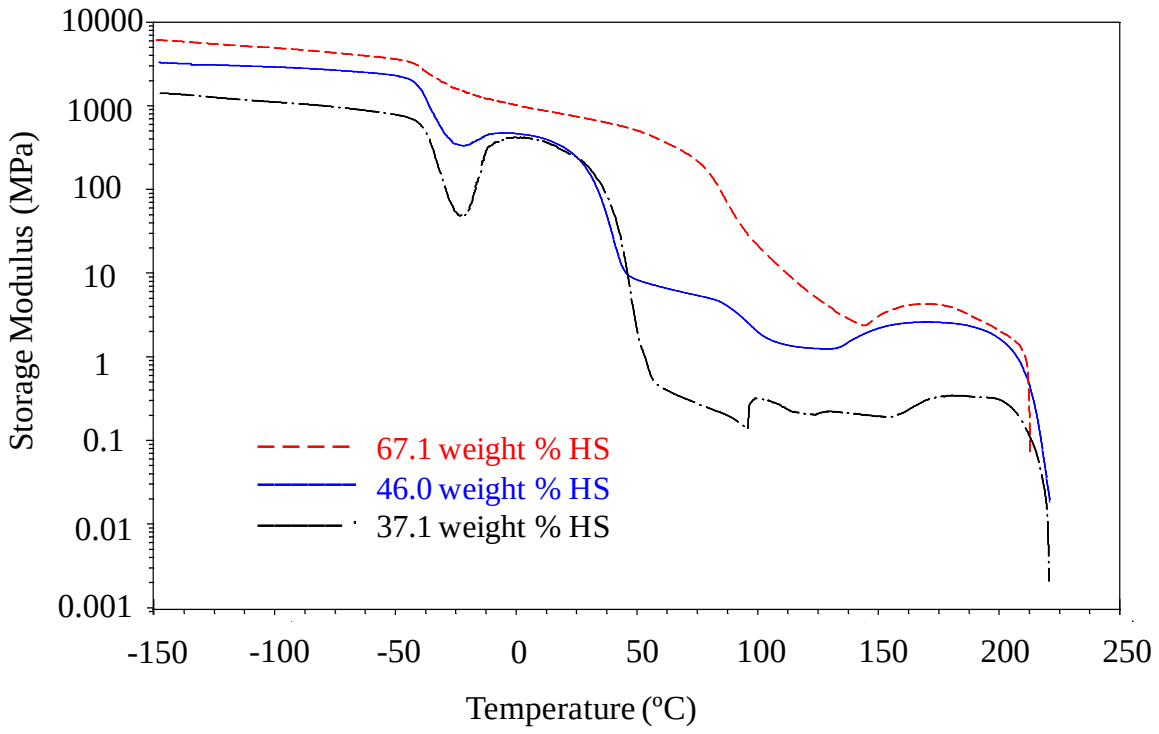

Figure 6.6. DMA storage moduli profiles for ionic polyurethanes with varied % HS; 3 ºC/minute, 1 Hz, -150 to 225 ºC, air

The second broadest transition occurred for the 46.0 weight % HS polyurethane, and the 37.1 weight % HS polymer had the sharpest glass transition temperature. All glass transition temperatures were around the same value of -41 ºC, and only their breadth drastically changed with hard segment content. It is hypothesized that ionic aggregation in these polymers subsisted above the glass transition temperature. Ionic aggregates that exist above the glass transition temperature of polymers are well-known to behave as physical crosslinks that broaden the glass transition.[29-30, 53]

PEG polyurethanes are known to crystallize during dynamic mechanical analysis, causing an increase in the storage modulus beyond the glass transition temperature and where the plateau modulus for most polymers begins.[54] Beyond the crystalline melting point for the PEG SS

around 50 ºC, the storage moduli scale with ionic hard segment content. The 67.1 weight % HS ionic polyurethane had a higher modulus than the 46.0 weight % HS polymer and subsequently the 37.1 weight % HS polyurethane. All ionic polymers started to crystallize above 100 ºC. Although the melting point of the PEG crystallites had been exceeded, the phosphonium hard segment may also crystallize. The melting point for phosphonium HS crystallites and all three ion-containing polymers occurred around 225 ºC according to DMA (Figure 6.6) where all three polymers started to flow. The onset temperature of flow is the same for all three polyurethanes with varied hard segment. Therefore, ionic aggregates as well as crystallites did not exist above 225 ºC for these polymers.

Semicrystalline polymers are opaque when the size of the crystallites are larger than the wavelength of light. According to DMA, all the PEG crystallites have melted when the temperature is above 70 °C during a 3 °C/minute temperature ramp. If only the PEG-segment of the polyurethane crystallized, then these films may start to show transparency above 70 °C. However, if the phosphonium hard segment also can crystallize, then the films may remain opaque. Films of a 37.1 weight % HS PEG-based ionic and non-ionic polyurethane were sandwiched between transparent microscope slides. Images were taken without and with a drop of silicon oil placed on each side of the microscope slides touching the polymer film. The silicon oil was used to counteract any light reflected due to surface roughness when investigating transparency. Ionic polymer films remained opaque above 87 °C under reduced pressure and even after equilibration for 60 minutes, but non-ionic films were transparent at 85 °C under reduced pressure (Figure 6.7). A 67.1 weight % HS ionic polymer also did not show transparency with heating up to 110 °C (Figure 6.8).

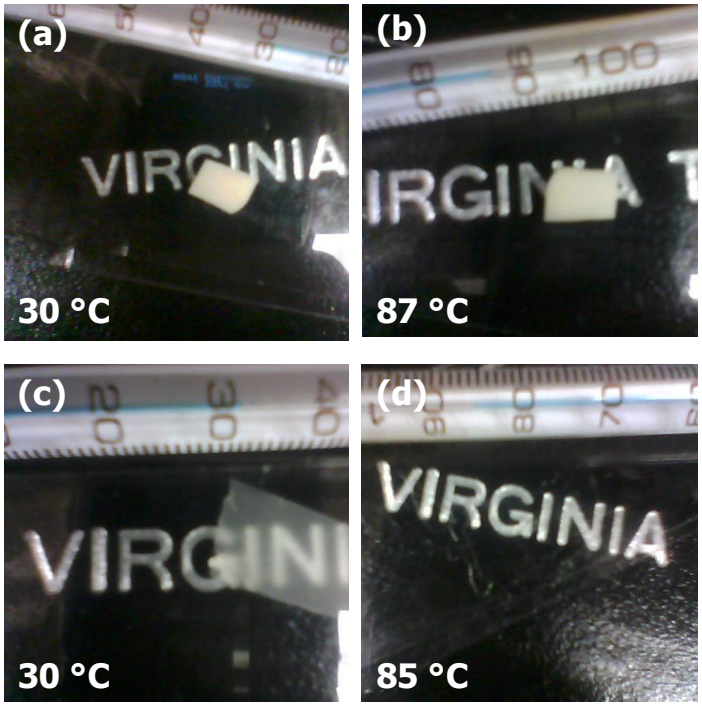

Figure 6.7. Images of 37.1 weight % HS ionic polymer films heated to (a) 30 °C and (b) 87 °C under reduced pressure; images of non-ionic 1,4-butanediol-based PEG polyurethanes heated to (c) 30 °C and (d) 85 °C under reduced pressure

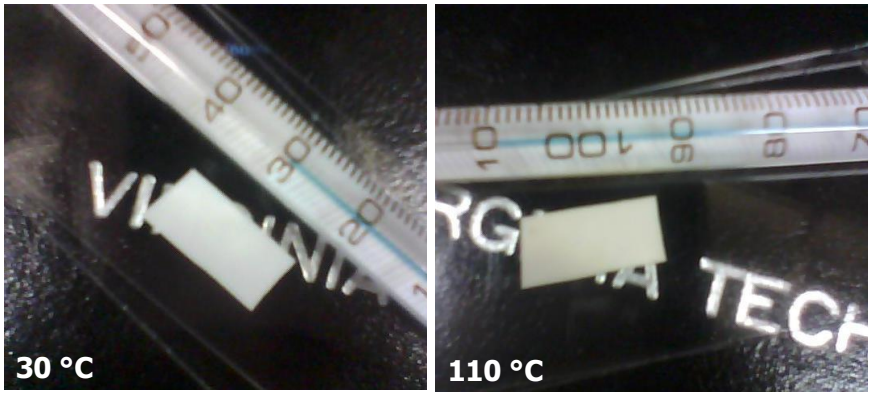

Figure 6.8. Images of ionic 67.1 weight % ionic polymer films heated to (a) 30 °C and (b) 110 °C

6.4.4 Analysis of X-ray Scattering

SAXS and X-ray diffraction (XRD) were performed to investigate long-range order with increased ionic hard segment content. Elastic scattering from X-rays was examined to probe crystalline and long-range order. Whereas SAXS measures larger distances in the nanometer to micrometer range, X-ray diffraction looks at smaller size dimensions with crystallites. XRD of these samples indicated increased order with increased bisphosphonium hard segment weight % (Figure 6.9).

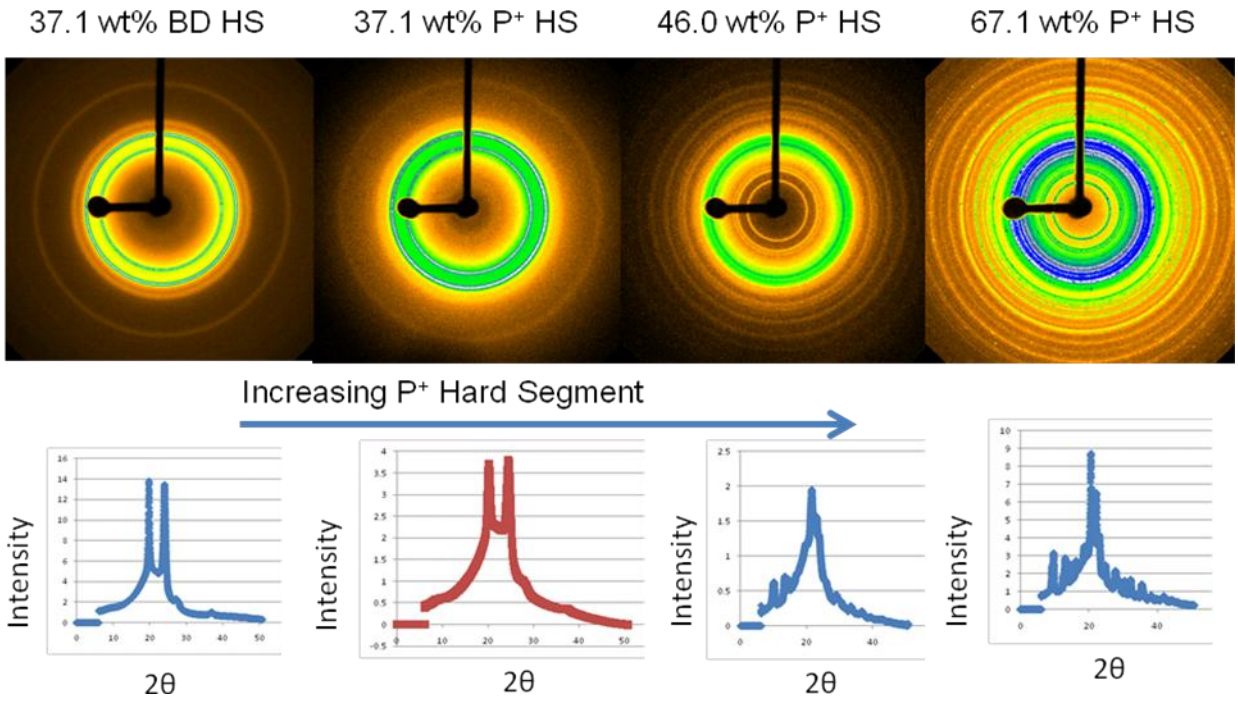

Figure 6.9. XRD profiles for polyurethanes with varied hard segment; Nova diffractometer system, Onyx CCD detector, copper X-ray source, ambient temperature

XRD scattering profiles showed an increased number of sharp peaks for the polymers with greater % HS. The value 2θ is related to q (the scattering vector) and d (the inter-particle scattering distance) through Bragg's law and the following equations:[29]

$n\lambda = 2d \cdot \sin(\theta)$

n = integer, λ = X-ray wavelength, d = inter-plane or inter-particle distance, θ = scattering angle

Equation 6.1. Bragg's law

$q_{max} = 2\pi/d$ d = Bragg scattering distance

Equation 6.2. Relationship of q (scattering vector) to d_{Bragg}

XRD scattering is usually attributed to small features below 5 nm such as crystallinity with smaller size dimensions than ionic aggregates (5-30 nm or 50-300 angstroms). Since the bisphosphonium-based polyurethanes had increasing order in XRD with increasing hard segment and with decreasing PEG SS content, this order may be partially attributed to crystallite formation in the bisphosphonium hard segment. This could also explain the rise in storage moduli for the ionic polyurethanes above 100 ºC and the melting point in DMA at 225 ºC (Figure 6.6).

Through the same equations and Bragg's law, we investigated X-ray scattering in the nanometer to micrometer range through SAXS. An ionic aggregate peak is well-known to occur in SAXS, attributed to the differences between elastic X-ray scattering in ionic aggregates versus the polymer matrix. The q_{max} for the ionic aggregate peak is inversely proportional to the inter-aggregate distance.[29] The breadth of the ionic aggregate peak also provides a profile of the breadth of ionic aggregate size distributions and inter-particle spacings. A wide range of sizes is known to occur in ionomers with a most populated distance at q_{max}.[29-30]

All of the ionic polyurethanes in our work displayed a SAXS ionic aggregate peak, and the non-ionic polyurethanes did not (Figure 6.10).

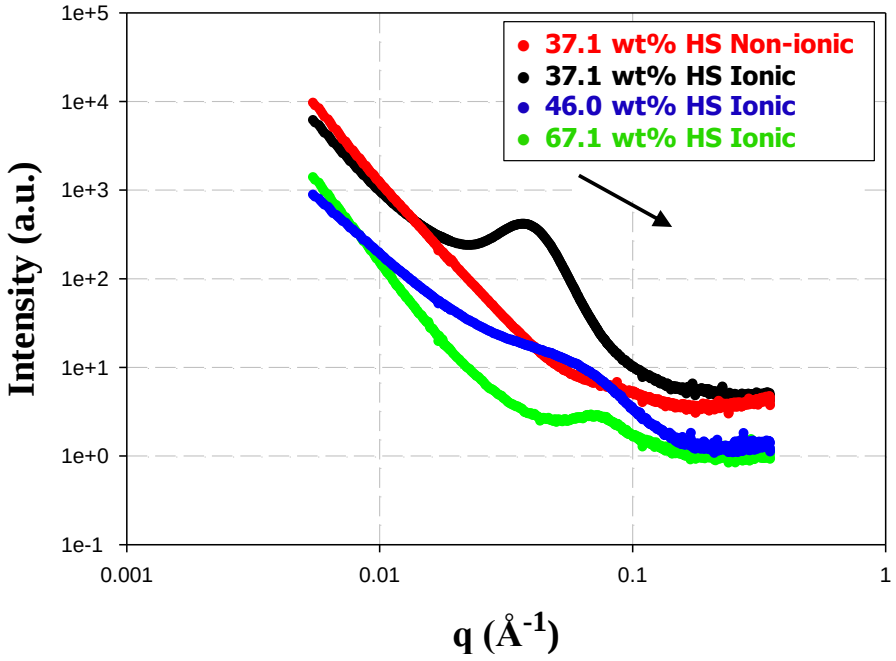

Figure 6.10. SAXS profiles of ionic polyurethanes with varied % HS; Station 4C1 PLS synchrotron radiation source (Pohang, Korea), ambient temperature, 60 second scans

A shift in q_{max} to higher values of q (lower values of d or shorter distances) is seen as the hard segment is increased from 37.1 to 46.0 to 67.1 weight %. Higher values of q correspond to shorter distances between these ionic aggregates, so increasing the amount of phosphonium salt in the polyurethanes also resulted in shorter spacing between ionic domains (Table 6.2).

Table 6.2. SAXS analysis of inter-aggregate spacing in polyurethanes with varied % HS

Type of HS	Wt % HS	q_{max} ($Å^{-1}$)	d (Å)
non-ionic	37.1	---	---
ionic	37.1	0.06	105
ionic	46.0	0.08	79
ionic	67.1	0.09	70

* Station 4C1 PLS synchrotron radiation source (Pohang, Korea), ambient temperature, 60 second scans

6.4.5 Atomic Force Microscopy of Ionic Polyurethanes

Microphase separation in these polyurethanes with hard and soft segments was investigated with AFM. AFM images may indicate some structural order in these polyurethane ionomers (Figure 6.11).

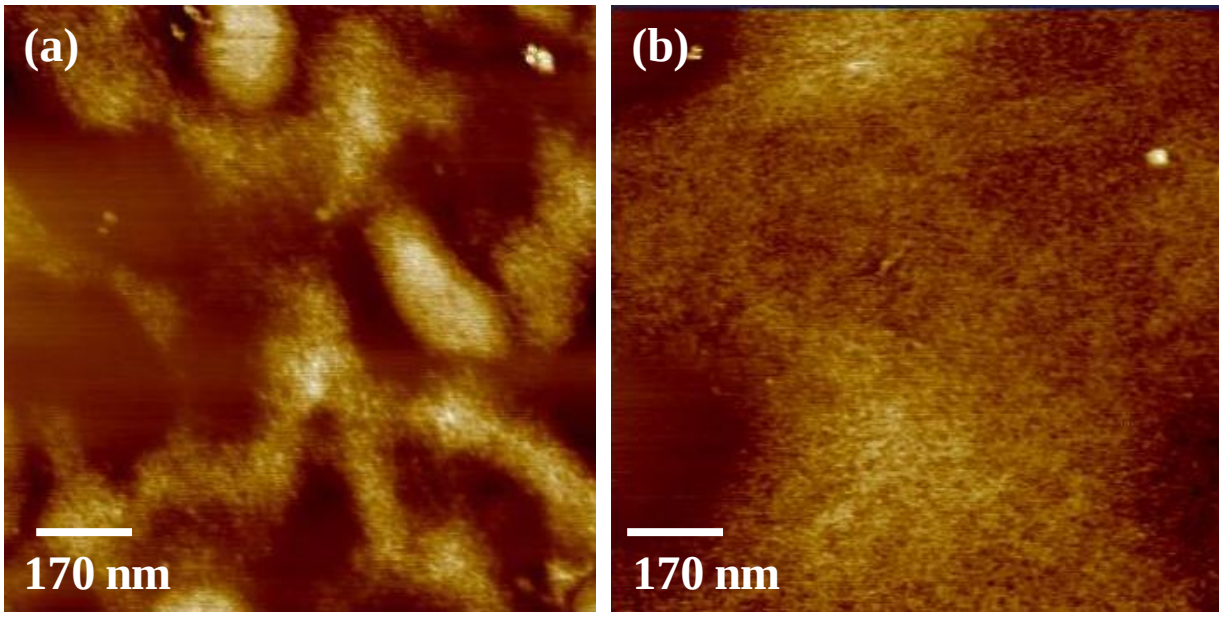

Figure 6.11. AFM images of ionic polyurethanes with varied % HS: (a) 37.1 weight % bisphosphonium HS and (b) 67.1 weight % bisphosphonium HS; 1 x 1 μm images; rms 4.0 mV and amplitude setpoint 3.3 mV

The soft segments (dark) containing polyol are separated from the hard segments (light) phases containing bisphosphonium salts. The AFM of these polymers displayed possible substructure in the 15-nm range, but these images are very clear compared to TEM images in the next section and represent only surface morphology rather than bulk polymer morphology.

6.4.6 Transmission Electron Microscopy of Ionic Polyurethanes

Transmission electron microscopy images indicated large, circular structures ~200 nm in diameter (Figure 6.12) in a 37.1 weight % HS phosphonium-based, PEG-containing polyurethane, similar to domain sizes observed by AFM for the same polyurethane (Figure 6.9). Long et al. previously showed that a more hydrophobic PTMO-based, phosphonium-containing polyurethane had 43 nm circular features in a scanning transmission electron microscopy (STEM) image.[49] In this thesis, the PEG-based ionic polyurethanes with greater ionic content and

hydrophilicity swelled significantly in DMSO/H_2O solutions, and good cryomicrotomed sections were difficult to collect. Although it is not expected that 70 nm films would retain a large amount of solution under reduced pressure in the TEM microscope, any residual DMSO/H_2O may have contributed to swelling of the films and larger domain sizes. The diameters of the circular structures in the TEM image appeared larger than the dimensions determined through SAXS, and the morphology may be attributed to ionic aggregation and/or phase separation. The SAXS data reflected both inter-particle and inter-aggregate spacing, and depended on the difference in the elastic scattering of X-rays between regions of hindered mobility, ionic content, and the amorphous regions of the polymer.[29-30] Analysis of SAXS data estimated inter-aggregate spacings of 7.0-10.5 nm for these polyurethane ionomers. The literature estimated 5-10 nm aggregates for 2.5-3.0 nm inter-aggregate spacings by SAXS.[30] Thus, the inter-aggregate spacing is often much less than the actual diameter of the aggregates, depending on ionic concentration and hydrophilicity of the polymer matrix.

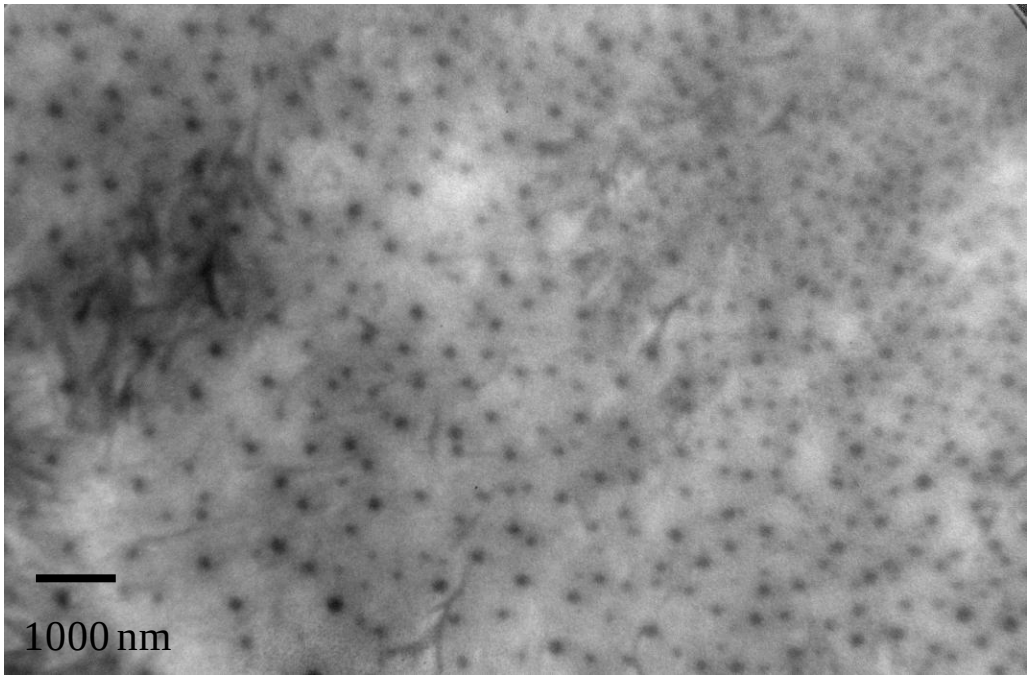

Figure 6.12. TEM image indicating circular structure in a 37.1 weight % HS phosphonium-based polyurethane; Philips EM 420 TEM, 100 KV, 70 nm sections collected over DMSO/H_2O solutions

6.4.7 Surface Resistivity Measurements

In chapter 5 of this thesis, we investigated surface resistivities of PEG-based networks from Michael addition reactions. Resistivity is inversely related to conductivity and measures the resistance to flow of electrons.[55] There are two main forms of conductivity, electronic and ionic. Ionic polymers are conductive when their anions and cations are able to move towards opposite electrodes, conducting electricity.[56] In chapter 5, the PEG-based phosphonium-containing network and the non-ionic PEG-based 1,4-butanediol-containing network (without MWCNTs) both had a surface resistivity of 10^9 ohms/square. It is proposed that the crosslinked structure in the films may have restricted mobility of the ionic sites and prevented these from vastly improving the conductivity.

In this chapter, we describe analysis of PEG-based polyurethanes with varied ionic content. The surface resistivities of the ionic and non-ionic polyurethanes were measured on films with dimensions ≥ 6.5 x 13 x 3 cm at ambient temperature. The films were approximately 0.60 ± 0.36 mm in thickness. The surface resistivities of the PEG-based, phosphonium-containing polyurethanes are compared to a non-ionic PEG-based, 1,4-butanediol-containing polyurethane (Table 6.3). The non-ionic polyurethane had the highest resistivity of 10^{12} ohms/square, a value indicating an insulative material.[57-60] The ionic polyurethane with a 37.1 weight % hard segment had a lower surface resistivity value of 10^{9} ohms/square, suggesting that the ionic sites did have a positive effect on conductivity compared to the non-ionic polymer. However, increasing the hard segment and ionic content in the polymers led to an increase in surface resistivity values, possibly due to restricted mobility of the ionic domains from enhanced ionic aggregation. Resistivity of PEG-based polymers is often increased with PEG crystallinity. However, the ionic polyurethane with the greatest amount of PEG SS and lowest amount of ionic HS had the lowest resistivity value. Enhanced ionic aggregation or phosphonium hard segment crystallinity with increased phosphonium hard segment may have contributed to restricted mobility of ionic sites and thus higher resistivities.

Table 6.3. Surface resistivity of ionic and non-ionic networks*

Hard Segment	Weight % Hard Segment	Resistivity (ohms/square)
BD	37.1	10^{12}
P^+	37.1	10^{9}
P^+	46.0	10^{10}
P^+	67.1	10^{10}

* 0.60 ± 0.36 mm thickness; dimensions ≥ 6.5 x 13 x 3 cm, 10 V and 100 V

6.5 Conclusions

We have prepared a new series of hydrophilic polyurethanes containing a cationic bisphosphonium chain extender. As the ionic content and hard segment content were simultaneously increased in the polymers, DSC and DMA data indicated PEG-segment glass transitions broadened and the plateau moduli increased. A high modulus is important for structural integrity in polyurethane-based biomedical devices such as tissue scaffolds and catheters.[2-3] Also, glass transition temperatures and moduli influence the hardness, abrasion resistance, adhesive properties, and applicability of polyurethane-based protective coatings.[29]

Conductivity is influenced by polymer morphology and ionic site mobility and is important in polyurethane-based sensing applications.[42-43, 56] In these polyurethanes, the PEG-segment melting point decreased with increased HS, indicating that the ionic hard segment impeded crystallization of the PEG segment. However, increasing ionic content in these polymers led to higher surface resistivity values. These higher surface resitivities were at least partially attributed to restricted mobility of the ionic sites due to enhanced ionic aggregation.

SAXS confirmed the presence of ionic aggregates in the polyurethanes, and increasing ionic content decreased the spacing between these ionic aggregates. TEM also indicated large, circular structures ~200 nm in diameter. Thus, including ionic character drastically changed the morphology of the polyurethanes.

Film forming properties are also important in adhesive and coating applications.[29] Films cast in Teflon® molds shrank to ¾ of the mold width and length, and this rearrangement was attributed to ionic aggregation and intrinsic surface energy differences between the hydrophilic polymers and Teflon®. Films of these materials were insoluble possibly due to their physical crosslinks, but solvent resistance after film formation is imperative for protective coatings.[29]

6.6 Acknowledgements

Research was sponsored by the Army Research Laboratory and was accomplished under Cooperative Agreement Number W911NF-06-2-0014. The views and conclusions contained in this document are those of the authors and should not be interpreted as representing official policies, either expressed or implied, of the Army Research Laboratory or the U.S. Government. The U.S. Government is authorized to reproduce and distribute reprints for Government purposes notwithstanding any copyright notation hereon. Jong Keun Park and Robert B. Moore are acknowledged for SAXS experiments and help with XRD experiments. Garth L. Wilkes is also acknowledged for insightful discussions.

6.7 References

1. Oertel G. Polyurethane handbook. 2nd ed. New York: Hanser Publishers; 1994, p. 629.
2. Boretos, J.W.; Pierce, W.S. *Science* **1967**,*158*,1481-1482.
3. Peppas, N. A.; Langer R. *Science* **1994**, *263(5154)*, 1715-1720.
4. Zdrahala, R. J.; Zdrahala, I. J. *J. Biomater. Appl.* **1999**,*14*, 67-90.

5. Hung, W. C.; Shau, M. D.; Kao, H. C.; Shih, M. F.; Cherng, J. Y. Journal of Controlled Release **2009**, 133, 68–76.
6. Guan, J.J.; Fujimoto, K.L.; Sacks, M.S.; Wagner, W.R. *Biomaterials* **2005**, *26*, 3961–3971.
7. Shau, M.D.; Tseng, S.J.; Yang, T.F.; Cherng, J.Y.; Chin, W.K. *J. Biomed. Mater. Res. Part A* **2006**, 736–746.
8. Tseng, S.J.; Tang, S.C.; Shau, M.D.; Zeng, Y.F.; Cherng, J.Y.; Shih, M.F. *Bioconjugate Chem.* **2005**, *16*, 1375–1381.
9. Yang, T.F.; Chin, W.K.; Cherng, J.Y.; Shau, M.D. *Biomacromolecules* **2004**, *5*, 1926–1932.
10. Czech, Z.; Pełech, R. *Progress in Organic Coatings* **2010**, *67(1)*, 72-75.
11. Chattopadhyay, D. K.; Raju, K.V.S.N. *Progress in Polymer Science* **2007**, *32(3)*, 352-418.
12. Zubielewicz, M.; Królikowska, A. *Progress in Organic Coatings* **2009**, *66(2)*, 129-136.
13. Deka, H.; Karak, N. *Progress in Organic Coatings* **2009**, *66(3)*, 192-198.
14. Malucelli, G.; Priola, A.; Ferrero, F.; Quaglia, A.; Frigione, M.; Carfagna C. *International Journal of Adhesion and Adhesives* **2005**, *25(1)*, 87-91.
15. Verdejo, R.; Stämpfli, R.; Alvarez-Lainez, M.; Mourad, S.; Rodriguez-Perez, M. A.; Brühwiler, P. A.; Shaffer, M. *Composites Science and Technology* **2009**, *69(10)*, 1564-1569.
16. Xu, J.; Buchholz, J. M.; Fricke, F. R. *Applied Acoustics* **2006**, *67(5)*, 476-485.
17. Bolton, J. S.; Gold, E. *Journal of Sound and Vibration* **1986**, *110(2)*, 179-202.
18. Wang, X.; Eisenbrey, J.; Zeitz, M.; Sun, J. Q. *Journal of Sound and Vibration* **2004**, *273(4-5)*,1109-1117.
19. Unal, S.; Yilgor, I.; Yilgor, E.; Sheth, J. P.; Wilkes, G. L.; Long, T. E. *Macromolecules* **2004**, *37*, 7081-7084.
20. Supriya, L.; Unal, S.; Long, T. E.; Claus, R. O. *Chem. Mater.* **2006,** *18*, 2506-2512.
21. Sheth, J. P.; Wilkes, G. L.; Fornof, A. R.; Long, T. E.; Yilgor, I. *Macromolecules* **2005,** *38*, 5681-5685.
22. Sheth, J. P.; Unal, S.; Yilgor, E.; Yilgor, I.; Beyer, F. L.; Long, T. E.; Wilkes, G. L. *Polymer* **2005**, *46*, 10180–10190.
23. McKee, M. G.; Park, T.; Unal, S.; Yilgor, I.; Long, T. E. *Polymer* **2005**, *46*, 2011–2015.
24. Unal, S.; Ozturk, G.; Sisson, K.; Long, T. E. *Journal of Polymer Science: Part A: Polymer Chemistry* **2008**,*46*, 6285–6295.
25. Hunley, M.T.; Pötschke, P.; Long, T.E. *Macromol. Rapid Commun.* **2009**, *30(24)*, 2102-2106.
26. Chen, K.-Y.; Kuo, J.-F.; Chen, C.-Y. *Biomaterials* **2000**, *21*, 161-171.
27. Grapski, J. A.; Cooper, S. L. *Biomaterials* **2001**, *22*, 2239-2246.
28. Unal, S. Synthesis and Characterization of Branched Macromolecules for High Performance Elastomers, Fibers, and Films. Ph.D. Thesis, Virginia Polytechnic and State University, Blacksburg, VA, 2005.
29. Tant, M. R.; Mauritz, M. R.; Wilkes, G. L., *Ionomers: Synthesis, Structure, Properties and Applications*. Blackie Academic & Professional: New York, 1997.
30. Eisenberg, A.; Kim, J. S. *Introduction to Ionomers*. Wiley: New York, 1998.
31. Mather, Brian D.; Baker, Margaux B.; Beyer, Frederick L.; Green, Matthew D.; Berg, Michael A. G.; Long, Timothy E. *Macromolecules* **2007**, *40(13)*, 4396-4398.

32. Buruiana, E. C.; Buruiana, T.; Strat, G.; Strat, M. *Journal of Polymer Science: Part A: Polymer Chemistry* **2005**, *43*, 3945–3956.
33. Wang, X.; Li, H.; Tang, X.; Chang, F.-C. *Journal of Polymer Science: Part B: Polymer Physics*, **1999**, *37*, 837–845.
34. Ozturk, G.; Long, T. E. *Journal of Polymer Science: Part A: Polymer Chemistry* **2009**, *47*, 5437–5447.
35. Yim, E. S.; Zhao, B.; Myung, D.; Kourtis, L. C.; Frank, C. W.; Carter, D.; Smith, R. L.; Goodman, S. B. *Journal of Biomedical Materials Research, Part A* **2009**, *91A(3)*, 894-902.
36. Rogero, S. O.; Malmonge, S. M.; Lugao, A. B.; Ikeda, T. I.; Miyamaru, L.; Cruz, A. S. *Artificial Organs* **2003**, *27(5)*, 424-427.
37. Wang, Y.-P.; Gao, X.-H.; Chen, J.-C.; Li, Z.-W.; Li, C.-L.; Zhang, S.-C. *Journal of Applied Polymer Science* **2009**, *113(4)*, 2492-2498.
38. Qi, L.; Lin, Y.; Wang, F. *European Polymer Journal* **1999**, *35(5)*, 789-793.
39. Aldenhoff, Y. B. J.; Blezer, R.; Lindhout, T.; Koole, L. H. *Biomaterials* **1997**, *18(2)*, 167-172.
40. Holmes, D. R.; Camrud, A. R.; Jorgenson, M. A.; Edwards, W. D.; Schwartz, R. S. *Journal of the American College of Cardiology* **1994**, *24(2)*, 525-531.
41. Ajili, S. H.; Ebrahimi, N. G.; Soleimani, M. *Acta Biomaterialia* **2009**, *5(5)*, 1519-1530.
42. Squire, J. C.; Rogers, C.; Edelman, E. R. Stent expansion and apposition sensing. U.S. Patent 6,179,858, January 30, 2001.
43. Squire, J. C.; Rogers, C.; Edelman, E. R. Stent Slip Sensing System and Method. U.S. Patent 6,091,980, July 18, 2000.
44. Hartley, F. R., John Wiley & Sons: 1994; Vol. 3, p 25-91.
45. Faroq, A. A., *Polymer Degradation and Stability* **1994**, *44*, 323-333.
46. Jin, R. ; Aoki, S. ; Shima, K. *Chem. Commun.* **1996**, 1939-1940.
47. Xie, W.; Xie, R.; Pan, W.; Hunter, D.; Koene, B.; Tan, L.; Vaia, R. *Chem. Mater.* **2002**, *14*, 4837- 4845.
48. Kanazawa, A.; Ikeda, T.; Endo, T., *Journal of Polymer Science: Part A: Polymer Chemistry* **1993**, *31*, 335-343.
49. Williams, R. S.; Wang, W.; Winey, K. I.; Long, T. E. *Macromolecules*, **2008**, 41 (23), 9072-9079.
50. Uemura, Y.; Stein, R. S.; MacKnight, W. J. *Macromolecules* **1971**, *4*, 490-494.
51. Kang, H.; Lin, Q.; Armentrout, R. S.; Long, T. E. *Macromolecules* **2002**, *35*, 8738-8744.
52. Berti, C.; Colonna, M.; Binassi, E.; Fiorini, M.; Karanam, S.; Brunelle, D. J. *Reactive and Functional Polymers* **2010**, *70(6)*, 366-375.
53. Gauthier, S.; Duchesne, D.; Eisenberg, A. *Macromolecules* **1987**, *20*, 753-759.
54. Silver, J. H. Myers, C. W.; Lim, F.; Cooper, F. L. *Biomaterials* **1994**, *15(9)*, 695-704.
55. Atkins, P.; de Paula J. *Physical Chemistry*, 7th ed. W. H. Freeman and Company: New York, 2002, 832-842.
56. *Applications of Electroactive Polymers*. Bruno, S. ed. Chapman & Hall: New York, 1993, 75-113.
57. Schutte, C. L. Hutchins, R. O. *Polymer* **1993**, *34(3)*, 476-480.
58. Kathirgamanathan. P. *Polymer* **1993**, *34(7)*, 1549-1550.

59. Dangelmayer, G. T. *ESD Program Management, A Realistic Approach to Continuous Measureable Improvement in Static Control*, 2nd ed. Lucent Technologies, Kluwer Academic Publishers: Norwell, Massachusetts, 1999, 140.
60. Andrews, R.; Jacques, D.; Minot, M.; Rantell, T. *Macromol. Mater. Eng.* **2002**, *287*, 395.

Chapter 7: Phosphonium-Containing Methacrylate Monomers and Diblock Copolymers

7.1 Abstract

Novel hydrogen-bonding, phosphonium ion-containing methacrylate monomers were synthesized with different alkylene spacers derived from ionic liquid precursors. (6-Hydroxyhexyl)trioctylphosphonium and (2-hydroxyethyl)trioctylphosphonium salts were synthesized by reaction of the respective bromoalkyl alcohols with trioctylphosphine. These ionic liquid precursors were then reacted with 2-isocyanatoethylmethacrylate to form hydrogen-bonding, phosphonium-containing methacrylate monomers. Block copolymerization using reversible addition fragmentation and chain transfer (RAFT) methods with polystyrene macroinitiators enabled predictable formation of phosphonium blocks while maintaining solubility throughout the reaction. ^{1}H and ^{31}P NMR spectra showed quantitative incorporation of the phosphonium functionality. AFM images indicated microphase separation in the block copolymers. SAXS profiles showed an ionic peak for the phosphonium-containing block copolymer with the longest alkylene spacer between the main chain and pendant phosphonium ion.

7.2 Introduction

Incorporation of ionic sites in polymers influences moduli, melt strengths, and glass transition temperatures.[1] Ionomers are defined as polymers with less than 15 mole % ionic groups, and these ionic aggregates govern properties in isolated areas of the polymer.[2-4]

Thermoreversible ionic interactions can provide self-healing capability. It is hypothesized that melting of ionic domains occurs when energy from the impacting substrate is transferred to the polymer upon impact.[5-6] The majority of energy associated with plastic deformation is dissipated as heat.[7-8] At high strain rates where the heating rate for the polymer is greater than the cooling rate, adiabatic conditions generate a temperature increase which is possible to measure during impact testing.[7,9] The mobility and reorganization of ionic sites into aggregates provides elastic recovery to repair defects.[5-6] In addition, the phosphonium cation offers a new avenue for self-assembly.[10] The majority of the present literature describes ionomers with anionic groups like carboxylate[3-4, 11-14] and sulfonate[15-17] anionic sites pendant to the polymer chain and mobile cations not tethered to the polymer. Ammonium-based ionic polymers are most cited among cationic polyelectrolytes and ionomers.[1, 11, 18-21] Phosphonium salts are particularly attractive due to greater thermal stability[22] and antimicrobial activity[23] compared to similar ammonium analogs. Vaia et al. indicated that phosphonium cations are approximately 70 to 80 °C more thermally stable than similar ammonium molecules by TGA under nitrogen at 2 °C/minute.[22]

Incorporation of ionic sites in polymers at varied concentration can considerably alter polymer properties.[1] Our research group has focused great attention on the synthesis of various ionic polymers for fiber applications[24] and DNA transfection.[25] We have shown that presence of a zwitterionic functionality benefits electrospinning of fibers at low concentrations through electrostatic interactions.[26] We also have shown that water-soluble, ammonium-based polymers bind with negatively-charged DNA to create polyplexes and transport polymer chains into cells.[25] The polyplex is intercalated into the nucleus, and DNA is transcribed.[25] Furthermore, we have extensively researched the relationship of hydrogen bonding at polymer termini[27] and in block copolymers with DNA purines including adenine.[28] A phosphonium-based uracil blended

with poly(9-vinlylbenzyladenine)-*block*-poly(*n*-butyl acrylate)-*block*-poly(9-vinylbenzyladenine) triblock copolymers provided enhanced plateau moduli for the polymer and greater solution viscosity in chloroform.[28] AFM indicated microphase separation, self-assembly, and morphology dependent on block copolymer structure and film preparation.[28]

To create block copolymers, "living" polymerization techniques are often employed.[16, 29-33] Ideal living polymerization involves three main concepts: simultaneous initiation of all growing polymer chains, all chains growing at the same rate, and no termination of chains.[29] Growth continues until all monomer is consumed and will continue once more monomer is added, providing a route to the formation of well-defined block copolymer structure.[29] Block copolymer structure can lead to microphase separation, creating various mesophases including lamellae.[16] We have explored several living free radical polymerization strategies to synthesize ionic block copolymers including anionic polymerization[16] and nitroxide mediated polymerization (NMP).[28] However, atom transfer radical polymerization (ATRP)[30] and reversible addition−fragmentation chain transfer (RAFT) polymerization[31-32] are also appropriate methods to synthesize ionic polymers.

Our research group recently investigated the living anionic synthesis of poly(methyl methacrylate)-*graft*-(poly(sulfonic acid styrene)-*block*-poly(*tert*-butylstyrene) and poly(methyl methacrylate)-*graft*-(poly(*tert*-butylstyrene)-*block*-poly(styrenesulfonic acid styrene).[16] The sodiosulfonate-based ionic sites were synthesized through neutralization with sodium hydroxide solutions. Pronounced aggregation resulted from including anionic sites pendant to the main chain as evidenced by the appearance of an ionic peak in the SAXS profiles. Increasing the connecting distance of the ionic sites from the main chain provided enhanced aggregation compared to having the pendant ionic sites tethered in close proximity to the main chain. Glass

transitions increased with increased ionic content, and higher glass transition temperatures resulted for the copolymers having pendant ionic sites far from the main chain. Lamellar morphologies also resulted due to microphase separation.[16]

Anionic polymerization provides limited functional group tolerance and demands more stringent methods compared to other pseudo-living techniques.[29, 31] Lowe et al. recently reviewed RAFT as an optimal process for cation-containing copolymers, hydrophilic copolymers, and methacrylates.[31] Methacrylates are deemed the "best-behaved" monomers for RAFT polymerizations, and various styrenic polymers also fair well with RAFT techniques.[31] Therefore, RAFT is a versatile process, useful for water soluble and organic soluble monomers and ideal for our phosphonium-containing block copolymers containing methacrylate functionalities, cationic moieties, and styrene comonomers.

Reversible addition of growing radicals and chain transfer to a RAFT reagent allow for the equilibration of growing and dormant chains to afford a linear relationship of molecular weight with conversion.[29, 31] This method controls the dispersity of polymer chains through a rapid and reversible addition and fragmentation mechanism. Thiocarbonylthio reagents provide fast chain transfer rates for monodisperse polymer growth, and the degree of polymerization is independent of the primary radicals and instead subject to monomer to RAFT reagent ratio.[29, 31] Farmer et al. outlined RAFT polymerization methods with *S*-(thiobenzoyl)thioglycolic acid.[33] Homopolymerization resulted in a dispersity of 1.38 for polystyrene.[33] This particular RAFT reagent is a commercially available one, requiring no additional syntheses.

Phosphonium-based polymers compose a small, relatively unexplored field.[34-45] McGrath et al. and Long et. al. synthesized some of the first phosphonium-based polymers through step-growth methods.[46-47] To date, RAFT techniques have achieved successful homopolymerization

of 4-vinylbenzyl(trimethylphosphonium) chloride and 4-vinylbenzyl(triphenylphosphonium) chloride monomers, but copolymerization was not reported.[32] Homopolymerization was conducted in aqueous media and resulted in low dispersities below 1.10 for various targeted molecular weights.[32] Therefore, choosing RAFT for the synthesis of our methacrylate-containing, phosphonium-based diblock copolymers was a logical next step.

In this thesis, the synthesis of two novel phosphonium-containing methacrylate monomers and copolymerization with styrene are reported. These two monomers have different alkylene lengths connecting the phosphonium ion to the backbone of their subsequent polymers. The thesis explores the fundamental synthesis and properties of these two novel monomers and their copolymers. The effect of altering alkyl lengths of substituents on the cationic monomer and the resulting effect of distance of the phosphonium functionality from the backbone of the polymer have been examined.

7.3 Experimental

7.3.1 Materials

2-Bromoethanol (95%), 6-bromohexanol (97%), trioctylphosphine (TOP) (≥90%), 2-isocyanatoethyl methacrylate (98%), styrene (99%), dibutyltin dilaurate (DBTDL, 95%), and *S*-(thiobenzoyl)thioglycolic acid (99%) were purchased from Aldrich and used as received. 2,2′-Azobis(2-methylpropionitrile) (AIBN, 98%) was purchased from Aldrich and recrystallized from methanol. *N*,*N*-Dimethylformamide (DMF, 99%) and hexanes (≥98.5%) were purchased from Aldrich. *N*,*N*-Dimethylformamide (DMF) (99%) and tetrahydrofuran (THF) (HPLC grade, ≥99%) from EMD Science were dried and collected from an Innovative Technology, Inc.,

PureSolv-MD3 solvent purification system. A 1 wt % solution of DBTDL in dry THF was used as a catalyst during monomer synthesis.

7.3.2 Synthesis of (2-Hydroxyethyl)trioctylphosphonium Bromide [(2-HE)TOPBr]

This procedure closely followed our previous work[4] and is also included in chapter 3 of this thesis. A 100-mL, double-neck, round-bottom flask with a Teflon® stir bar was flame dried, and a condenser and an addition funnel were attached. TOP (16.62 g, 44.8 mmol) was syringed into the flask and purged with argon for 30 min. Subsequently, 2-bromoethanol (5.66 g, 45.3 mmol) was syringed into the addition funnel under argon. A 1:1.01 molar ratio of phosphine to 2-bromoethanol was used. The 2-bromoethanol was added dropwise under argon to trioctylphosphine at 80 °C. The reaction proceeded at 80 °C for 3 h. The temperature was increased to 120 ºC for 3 h after addition complete addition of the 2-bromoethanol. Residual 2-bromoethanol was removed through vacuum distillation at 60 ºC and 0.3 mmHg. The isolated product was a clear, ionic liquid and was stored below 2 °C under an argon blanket. A 98% yield was achieved. ^{1}H NMR (400 MHz, 25 ºC) in $CDCl_3$: δ (ppm) 0.700 (t, 9H), 0.816-1.715 (36H), 2.205 (t, 6H), 2.506 (t, 2H), 3.87 (t, 2H), 4.473 (s, 1H). ^{31}P NMR (162 MHz, 25 ºC, referenced to H_3PO_4 external standard) in $CDCl_3$: δ (ppm) 32.8. m/z (+FAB, 100% M^+, Exact mass, Direct Probe) 415.4 g/mol as expected. DSC (20 °C/min, Ramp -90 to 30 °C) mp 4.8-5.4 °C.

7.3.3 Synthesis of (6-Hydroxyhexyl)trioctylphosphonium Bromide [(6-HH)TOPBr]

This procedure was also reported in chapter 3 of this thesis. A 100-mL, double-neck, round-bottom flask with a Teflon® stir bar was flame dried, and a condenser and an addition funnel were attached. TOP (12.0 g, 33.0 mmol) was syringed into the flask and purged with

argon for 30 min. 6-Bromohexanol (5.98 g, 33.0 mmol) was syringed into the addition funnel under argon, and was added dropwise over 3 h to TOP at 80 °C. The temperature was increased to 120 ºC for 5 h after complete addition of the 6-bromohexanol. Residual 6-bromohexanol was removed with vacuum distillation at 120 ºC and approximately 0.3 mmHg. The isolated product was a clear, ionic liquid and was stored below 2 °C under an argon blanket to prevent oxidation. A 98% yield was achieved. ^{1}H NMR (400 MHz, 25 ºC) in $CDCl_3$: δ (ppm) 0.834 (t, 9H), 1.151-1.885 (44H), 2.353 (t, 8H), 3.350 (t, 1H), 3.607 (t, 2H). ^{31}P NMR (162 MHz, 25 ºC, referenced to H_3PO_4 external standard) in $CDCl_3$: δ (ppm) 32.9. m/z (+FAB, 100% M^+, Exact mass, Direct Probe) 471.5 g/mol as expected. DSC (20 °C/min, Ramp -80 to 25 °C) mp 12.7-13.0 °C.

7.3.4 Synthesis of (2-(2-Oxycarbonyliminoethyl 2-methyl prop-2-enoate)ethyl) (trioctyl)phosphonium Bromide [(2-UME)TOPBr]

A flame-dried, 100-mL flask with a Teflon® stir bar was charged with 2.71 g (6.52 mmol) of (2-hydroxyethyl)trioctylphosphonium bromide. The flask and contents were dried overnight at 60 °C under reduced pressure in a vacuum oven. Once cooled to room temperature, the flask was charged with 1.01 g (6.52 mmol) of 2-isocyanatoethyl methacrylate (a 1:1 molar ratio of hydroxyl to isocyanate) and 8.0 mL (35 wt % solids) of THF under argon. One drop of a 1 wt % solution of DBTDL in dry THF was added. The reaction mixture was purged with argon for 10 min, and then the reaction was allowed to proceed at 50 °C for 4 h with stirring. THF was removed by rotavaporation at 25 °C, and the monomer was dried under reduced pressure in a vacuum oven overnight at room temperature. The final clear, ionic liquid monomer was stored below 2 °C under an argon blanket. ^{1}H NMR (400 MHz, 25 ºC) in $CDCl_3$: δ (ppm) 0.835 (t, 9H),

1.151-1.590 (44H), 1.930 (s, 3H), 2.424 (t, 6H), 2.626 (t, 2H), 2.919 (t, 2H), 3.442 (t, 2H), 4.201 (t, 2H), 5.601 (d, 1H)), 6.145 (d, 1H)), 6.465 (s, 1H). ^{31}P NMR (162 MHz, 25 ºC, referenced to H_3PO_4 external standard) in $CDCl_3$: δ (ppm) 32.0. m/z (+FAB, 100% M^+, Exact mass, Direct Probe) 571.3 g/mol as expected.

7.3.5 Synthesis of (6-(2-Oxycarbonyliminoethyl 2-methyl prop-2-enoate)hexyl) (trioctyl)phosphonium Bromide [(6-UMH)TOPBr]

The synthesis of this phosphonium-based methacrylate monomer followed the same procedure as described previously in section 7.3.4 except (6-hydroxyhexyl)trioctylphosphonium bromide was used as the hydroxyl-containing phosphonium salt. ^{1}H NMR (400 MHz, 25 ºC) in $CDCl_3$: δ (ppm) 0.825 (t, 9H), 1.131-1.708 (44H), 1.80 (s, 3H), 2.303 (t, 6H), 2.586 (t, 2H), 3.50 (t, 2H), 4.25 (t, 4H), 5.50 (d, 1H)), 6.10 (d, 1H), 6.70 (s, 1H). ^{31}P NMR (162 MHz, 25 ºC, referenced to H_3PO_4 external standard) in $CDCl_3$: δ (ppm) 32.9. m/z (+FAB, 100% M^+, Exact mass, Direct Probe) 626.5 g/mol as expected.

7.3.6 Synthesis of Phosphonium-Containing Homopolymers from (2-UME)TOPBr and (6-UMH)TOPBr

A flame-dried, 100-mL flask with Teflon® stir bar was charged with (2-UME)TOPBr (2.09 g, 3.21 mmol). AIBN (0.00527 g, 0.0321 mmol) was added to the flask. Dry DMF, (8.5 mL to make an ~20 wt % solids reaction mixture) was added. The mixture was purged with argon for 15 min, and then the reaction was allowed to proceed at 70 °C for 48 h under argon

with stirring. The mixture was cooled to room temperature, diluted with 7 mL chloroform, and precipitated into cold hexanes and dried overnight under reduced pressure at 50 °C. Isolated and dried products were insoluble in common organic solvents.

7.3.7 RAFT Polymerization of Styrene Precursor

An activated alumina column was used to remove the inhibitor from styrene. An example of the polystyrene block RAFT polymerization follows: Styrene (20 g, 0.192 mol), was charged into a clean, flame-dried, round-bottom flask. S-(Thiobenzoyl)thioglycolic acid (0.425 g, 0.0020 mol) and AIBN (0.0547 g, 0.00033 mol) were added to the flask. Then 90 mL of dry THF was added under nitrogen. The solution was purged for 30 min with nitrogen, placed under a nitrogen blanket, and submerged in an oil bath at 70 °C for 24 h. Each of the polymers was precipitated in 400 mL of methanol. The RAFT chain-end functionalized polymer adhered to the bottom of the precipitation flask. The methanol was decanted, and then 400 mL of methanol was added. This process was repeated three times to wash the polymer, and then the product was rotaevaporated and dried under reduced pressure at 40 °C overnight. M_n (SEC) equaled 12,000 g/mol. M_w equaled 16,000 g/mol with a PDI of 1.35. ^{1}H NMR (400 MHz, 25 ºC) in $CDCl_3$: δ (ppm) 0.854-2.510 (m, 3H), 6.236-7.440 (m, 5H).

7.3.8 Synthesis of (2-UME)TOPBr Copolymers with Polystyrene Macroinitiators

A similar procedure to the one in section 7.3.7 was used to prepare block copolymers from the polystyrene macroinitiator. The addition of 24 units was targeted. Polystyrene

macroinitiator (2.11 g, 0.176 mmol) and (2-UME)TOPBr (2.10 g, 4.24 mmol) were added to a flame-dried 1-neck flask with a Teflon® stir bar. AIBN (0.00345 g, 0.0210 mmol) was added. The flask was septa-sealed and purged with argon for 30 min. Then dry THF (18.5 mL) was added under argon, and the solution was purged for 30 min. The temperature was increased to 60 °C for 48 h. The polymer was precipitated in hexanes (~400 mL). ^{1}H NMR (400 MHz, 25 ºC) in $CDCl_3$: δ (ppm). The resultant number of units added to the polystyrene block equaled 22 with ^{1}H NMR, or 19.0 mole %. ^{1}H NMR (400 MHz, 25 ºC) in $CDCl_3$: δ (ppm) 0.676-0.999, 1.035-1.672, 1.663-2.138, 2.273-2.407, 2.533-2.677, 3.708-4.229, 6.248-6.876, 6.248-7.387. ^{31}P NMR (162 MHz, 25 ºC, referenced to H_3PO_4 external standard) in $CDCl_3$: δ (ppm) 33.4. M_n (NMR) equaled 14,300 g/mol.

7.3.9 Synthesis of (6-UMH)TOPBr Copolymers with Polystyrene Macroinitiators

The same procedure in section 7.3.8 was used to prepare block copolymers with the polystyrene macroinitiator, except the phosphonium-containing methacrylate monomer was (6-UMH)TOPBr. The addition of 20 units was targeted. ^{1}H NMR spectra showed a 14.8 mole % incorporation of phosphonium monomer and 20-unit addition to the block copolymer. ^{1}H NMR (400 MHz, 25 ºC) in $CDCl_3$: δ (ppm) 0.791-0.998, 1.197-1.718, 1.709-2.205, 2.255-2.703, 3.289-4.455, 6.274-6.853, 6.877-7.241. M_n (NMR) equaled 26,000 g/mol. M_n (SEC) equaled 26,000 g/mol. M_w equaled 36,000 g/mol with a PDI of 1.40. ^{31}P NMR (162 MHz, 25 ºC, referenced to H_3PO_4 external standard) in $CDCl_3$: δ (ppm) 32.7.

7.3.10 Characterization

^{1}H and ^{31}P NMR spectra were collected in $CDCl_3$ and CD_3OD on a Varian 400 MHz spectrometer operating at 400 and 162 MHz respectively. Fast atom bombardment mass spectrometry (FAB MS) was performed on a JEOL JMS-HX-110 instrument in positive mode. DSC was conducted under nitrogen with a Perkin Elmer Pyris 1 instrument at 20 ºC/min. Values from the second heating of heat/cool/heat cycles are reported. TGA was instrumented under nitrogen with a Perkin-Elmer TGA 7 instrument and a heating rate of 10 °C/min. An ASI REACTIR 4000 instrument was used for *in situ* FTIR spectroscopy with a resolution derived from 8 scans averaged every 30 s. AFM was performed on a Veeco MultiMode AFM with a rms of 4.0 and setpoint amplitude of 3.3. Rheology was conducted on an AR 2000 with Peltier plate geometry with 45 mm plates at 25 °C. A Philips EM 420 transmission electron microscope (TEM) with a 120 kV maximum accelerating voltage and a CCD camera was used. Samples for TEM were placed in epoxy and microtomed into 70 nm slices that were collected over DMSO/H_2O solutions. SAXS profiles were collected at the Army Research Laboratories (ARL) with a pinhole-collimated 3 m camera. An Ultrax18 rotating copper anode generator operated at 45 kV and 100 mA generated the X-rays. Data analysis was completed with Igor Pro v5.04B from Wavemetrics, Inc.

7.4 Results and Discussion

7.4.1 Synthesis and Characterization of Phosphonium-Based Monomers

Quaternization reactions on polymer precursors have been used to synthesize phosphonium-based methacrylates. However, this method often does not provide 100%

conversion as electrostatic repulsion of ionic units and steric hindrance can prevent the quaternization of all precursor units in the polymer.[48] Unquaternized units produced from this electrostatic repulsion during chemical modification are randomly spaced along the main chain,[48] and direct synthesis of polymers by using a methacrylate-based phosphonium-containing monomer eliminates these problems. It was anticipated that controlling the charge concentration and distribution along the polymer backbone would be important for understanding structure-property relationships related to thermal,[49-51] mechanical,[52-53] and antimicrobial evaluation.[54]

For this study, synthesis of hydroxyl-containing ionic liquid precursors and reaction with isocyanate-containing methacrylates provided a unique route to hydrogen bonding monomers with phosphonium ions. The quaternization of trioctylphosphine with bromoalcohols to form phosphonium ionic liquids proceeded through an S_N2 mechanism (Figure 7.1).

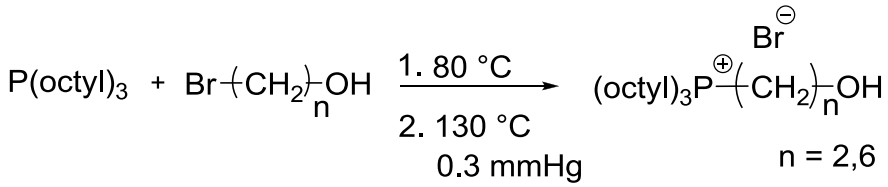

Figure 7.1. Synthesis of hydroxyl-containing phosphonium ionic liquids, (a) (2-HE)TOPBr and (b) (6-HH)TOPBr

Slow addition of 2-bromoethanol helped to prevent elimination of the hydroxyl group to form water and a vinyl phosphonium salt. Above 150 ˚C elimination of water to form vinyl trioctylphosphonium bromide occurs (chapter 3, Figure 3.5).[2, 55] The reaction temperature must be kept under 150 ˚C to prevent elimination.[2, 55] Synthesis of (6-UMH)TOPBr proceeded

similarly. The phosphonium ionic liquid precursors were liquids at room temperature as seen in Figure 7.2 and analyzed with DSC.

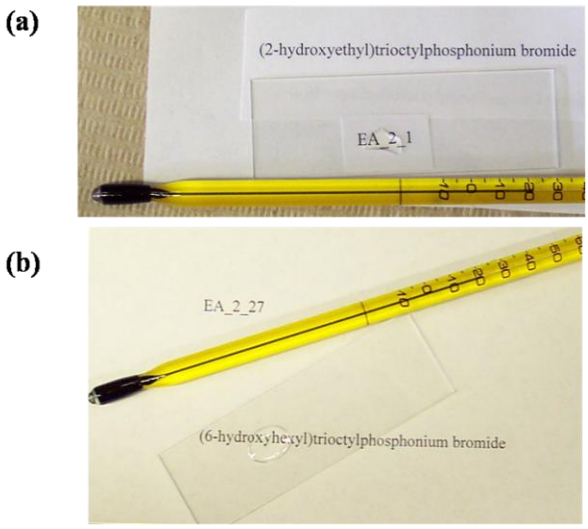

Figure 7.2. Images of room-temperature, hydroxyl-containing phosphonium ionic liquids, (a) (2-HE)TOPBr and (b) (6-HH)TOPBr

DSC thermograms of (2-HE)TOPBr indicated a melting point of 4.8-5.4 °C, and DSC traces of (6-HH)TOPBr indicated a melting point of 12.7-13.0 °C. This trend of increasing melting point with increasing alkyl chain length was expected and has been reported previously for phosphonium salts.[56] The viscosity of the (6-HH)TOPBr is also higher than that of (2-HE)TOPBr. The longer chain of the hexyl-containing phosphonium ionic liquid aided in packing of the salt into a crystalline lattice to increase the melting point. Also, hydroxyl hydrogen bonding is more readily facilitated between phosphonium molecules with a longer spacer. With the ethyl spacer, the hydroxyl is closer to the phosphorus center and in closer proximity to the three, long, octyl chains. Linear fits of rheological curves of the hydroxyl-containing precursors in the linear viscoelastic region and measured with parallel-plate geometry indicated a complex viscosity of 7.5 Pa*s for (6-HH)TOPBr and 4.5 Pa*s for (2-HE)TOPBr (Figure 7.3).

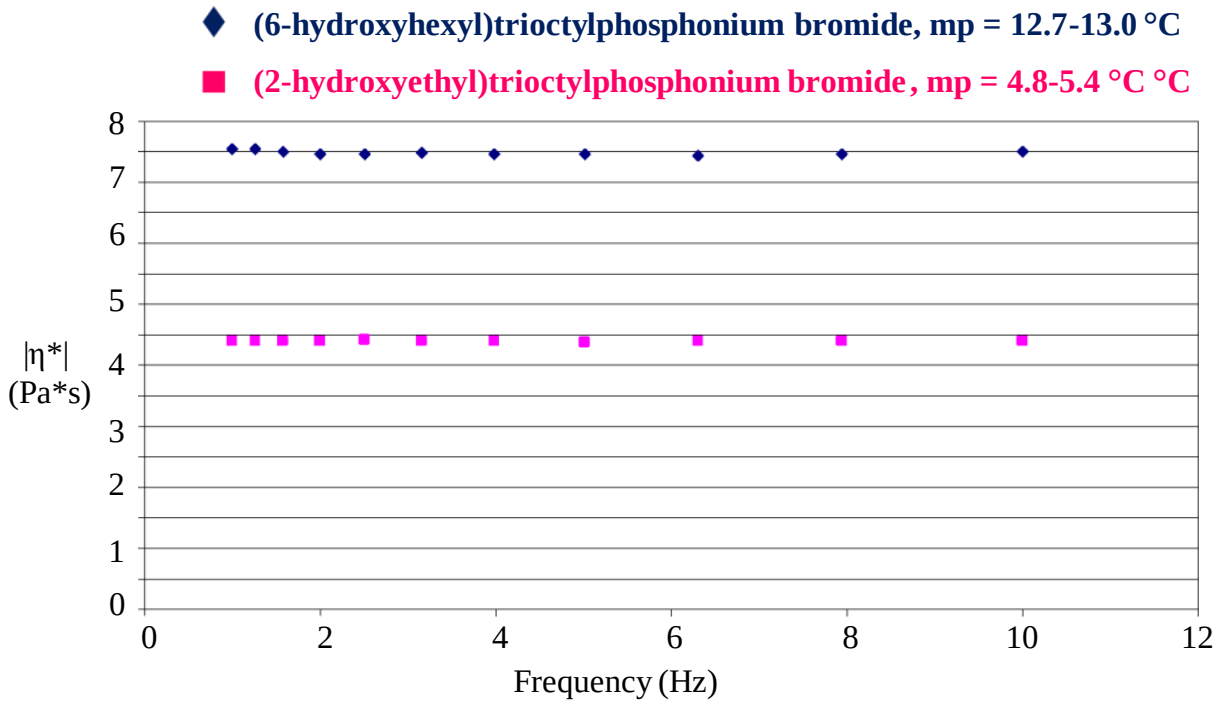

Figure 7.3. Rheology of hydroxyl-containing phosphonium ionic liquids; Rheology: 45 mm plate, Peltier Plate, 25 °C, DSC: 20 °C/minute, Ramp – 90 or -80 to 25 or 30 °C

Synthesis of phosphonium-based methacrylate monomers was achieved through reaction of hydroxyl-containing salts with 2-isocyanatoethyl methacrylate (Figure 7.4). *In situ* FTIR spectroscopy was used to evaluate completion of the reaction in THF at 50 ˚C (Figure 7.5). Disappearance of the isocyanate group at 2300 to 2175 cm^{-1} and appearance of the urethane carbonyl from 1750 to 1700 cm^{-1} were monitored over time. In 4 hours, reaction was complete.

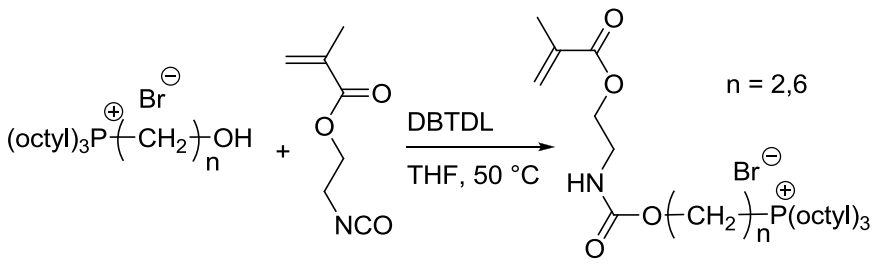

Figure 7.4. Synthesis of methacrylate-based phosphonium monomers, (a) (2-UME)TOPBr and (b) (6-UMH)TOPBr

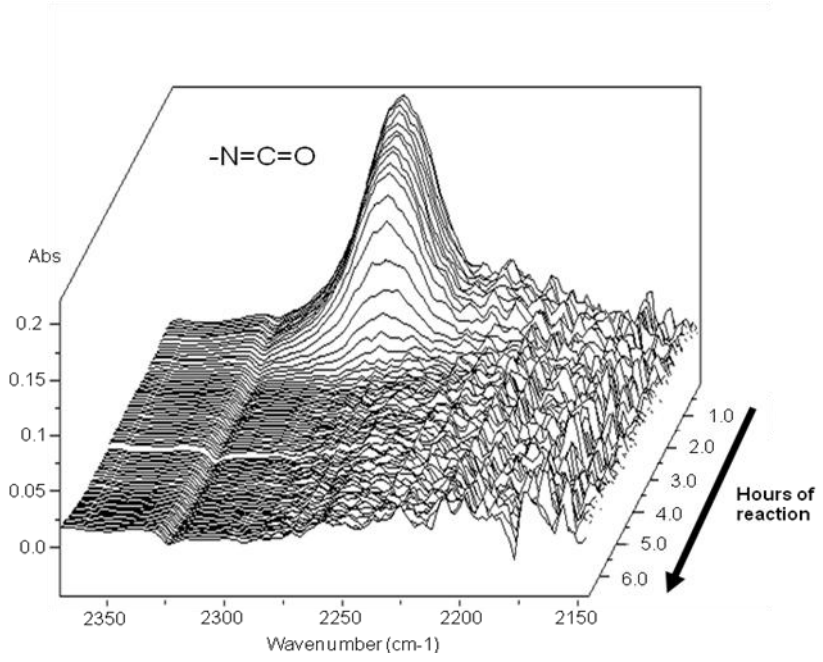

(a)

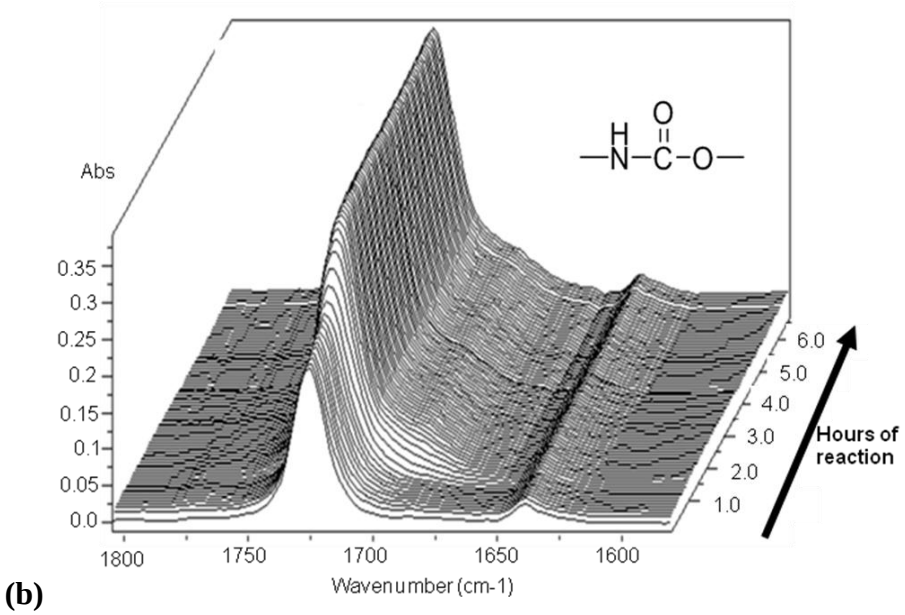

(b)

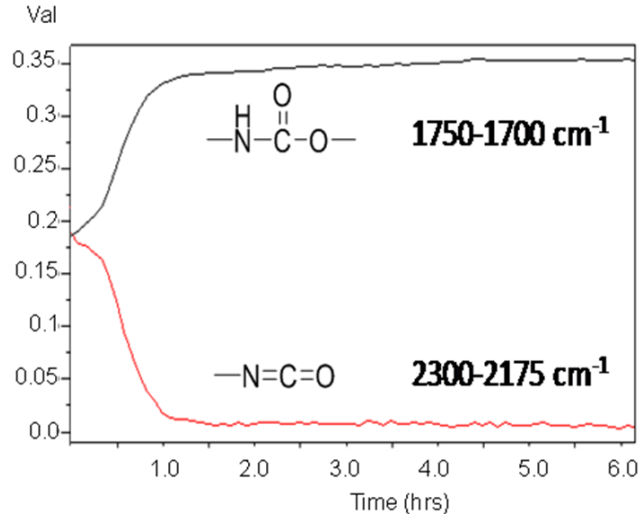

(c)

Figure 7.5. *In situ* FTIR of the formation of ionic liquid methacrylate-containing phosphonium monomer (6-UMH)TOPBr: (a) disappearance of the isocyanate group, (b) appearance of the urethane carbonyl, (c) absorbance versus time; ASI REACTIR 4000, 8 scans averaged every 30 seconds

7.4.2 Synthesis of Phosphonium-Containing Methacrylate Polymers

Homopolymers of both phosphonium-based methacrylate monomers precipitated from solution during the reaction. A copolymer approach was selected to investigate the effect of an ionic block on properties of polystyrene. First, a polystyrene block was synthesized via RAFT polymerization utilizing published procedures (Figure 7.6).[33] A ratio of 1 to 6 moles of AIBN relative to the RAFT agent was used to achieve narrow polydispersities. The polydispersity of polystyrene using this particular RAFT agent was slightly high at 1.35, but the reasons for selecting this RAFT agent were its commercial availability and solubility. The polystyrene macroinitiator utilized to synthesize the copolymers had a number-average molecular weight of 12,000 g/mole and a weight-average molecular weight of 16,000 g/mole as determined through SEC. Synthesizing the polystyrene block first facilitated solubility as the second block formed. The relative hydrophobicity of the polystyrene block compared to the more hydrophilic phosphonium-containing methacrylate block and diblock copolymer structure aided in microphase separation. Polystyrene is a relatively brittle polymer. Both the polystyrene and diblock copolymers resulted in brittle films.

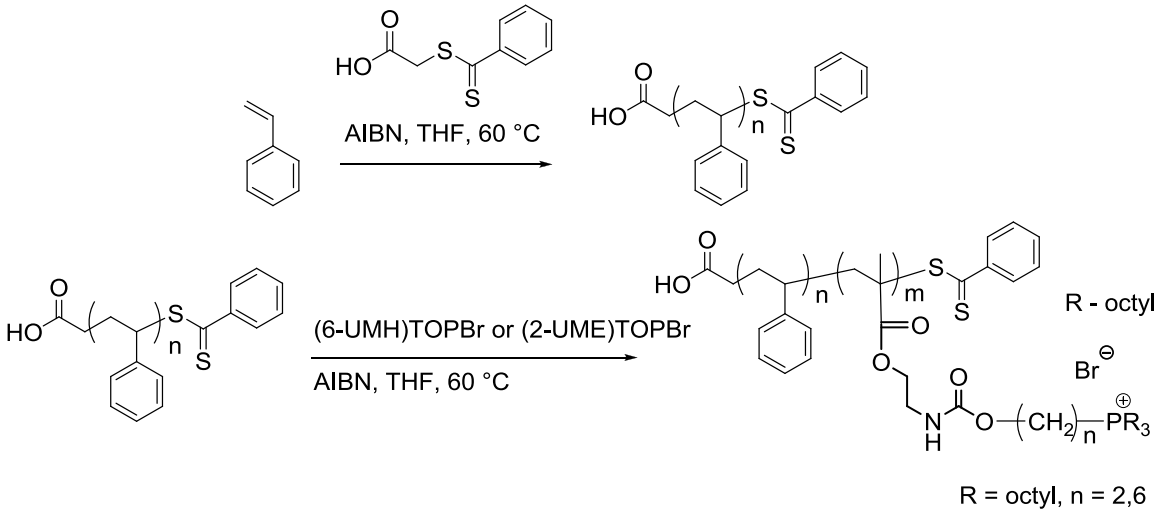

Figure 7.6. Synthesis of (6-UMH)TOPBr-containing RAFT copolymers with polystyrene precursors

Reactions to synthesize the diblock copolymers from the polystyrene macroinitiator proceeded with addition of either the (2-UME)TOPBr or (6-UMH)TOPBr phosphonium monomer in THF (Figure 7.6). For the (6-UMH)TOPBr copolymer, the polystyrene macroinitiator used had a 12,000 g/mole number-average molecular weight and a polydispersity index of 1.35. The copolymer had a 26,000 g/mole number-average molecular weight from ^{1}H NMR and SEC, and this copolymer had a PDI of 1.40 from SEC. The targeted amount of phosphonium monomer in the block copolymer was 15 mole %. ^{1}H NMR spectra confirmed a 14.8 mole % incorporation of phosphonium monomer units in the diblock copolymer structure. This composition remained soluble throughout the reaction, and the product was soluble in tetrahydrofuran and chloroform. The SEC traces showed monomodal peaks for both the polystyrene precursor and the final block copolymer (Figure 7.7).

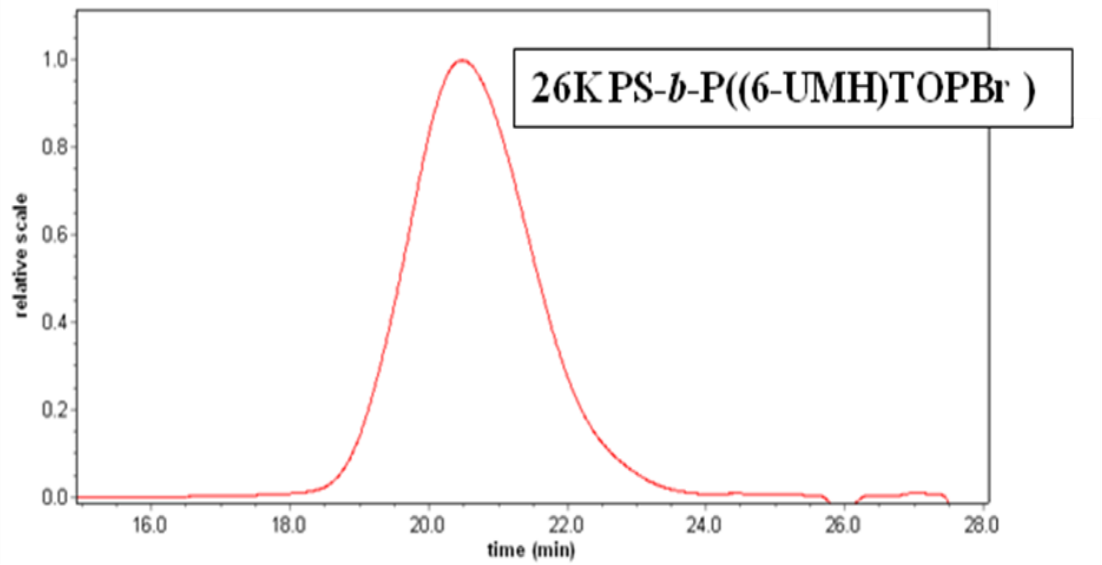

Figure 7.7. Refractive index chromatogram for the PS-*b*-P((6-UMH)TOPBr) copolymer, referenced to polystyrene standards, THF, 40 °C, 1.0 mL/minute

Shortening the alkylene spacer of the phosphonium functionality from hexyl to ethyl in the methacrylate monomer shortened the distance of the phosphonium group from both the main chain of the polymer and from the hydrogen-bonding urethane linkage. For the (2-UME)TOPBr copolymer, the polymer remained soluble in THF throughout the reaction, and a 24-unit addition was also targeted with a 22-unit addition confirmed with ^{1}H NMR spectra. ^{31}P NMR spectra did show only one type of phosphorus center in the polymer, the phosphonium cation. After precipitation and drying, the polymer was insoluble in water, THF, and DMF. The phosphonium-based polyurethanes in chapter 6 were also insoluble in their reaction solvent after drying. It is hypothesized that their insolubility after precipitation and drying was partly attributed to electrostatic association of the phosphonium ions in the bulk polymer films. The percent ionic

character of a polymer can drastically change its solubility in organic solvents and even lead to physical gelation at high ionic contents.[11, 57-58]

7.4.3 Morphological Examination of Phosphonium-Containing Copolymers

AFM images (Figures 7.8 and 7.9) showed microphase separation. Figure 7.8 depicts 1 and 3 μm AFM images of PS-*b*-poly((2-UME)TOPBr) with a 100-unit polystyrene block attached to a 22-unit phosphonium-containing methacrylate block. Strong microphase separation existed producing soft channels (dark phase) of 15-20 nm and hard channels (light phase) of 25-50 nm. It is hypothesized that the soft (or dark) phase is the hydrophilic phosphonium block, and the hard (or light) phase is the polystyrene block. Figure 7.9 depicts 1 and 3 μm AFM images of PS-*b*-poly((6-UMH)TOPBr) with a 100-unit polystyrene block attached to a 20-unit phosphonium-containing methacrylate block. The soft (dark) and hard (light) phases are again 20-50 nm, but resolution of the channels is much less clear. It is hypothesized that increasing the distance of the phosphonium functionality from the backbone of the polymer by increasing the spacer length from ethyl to hexyl resulted in more hydrophobic character, less-clear microphase separation, and greater phase mixing of the polystyrene and phosphonium blocks.

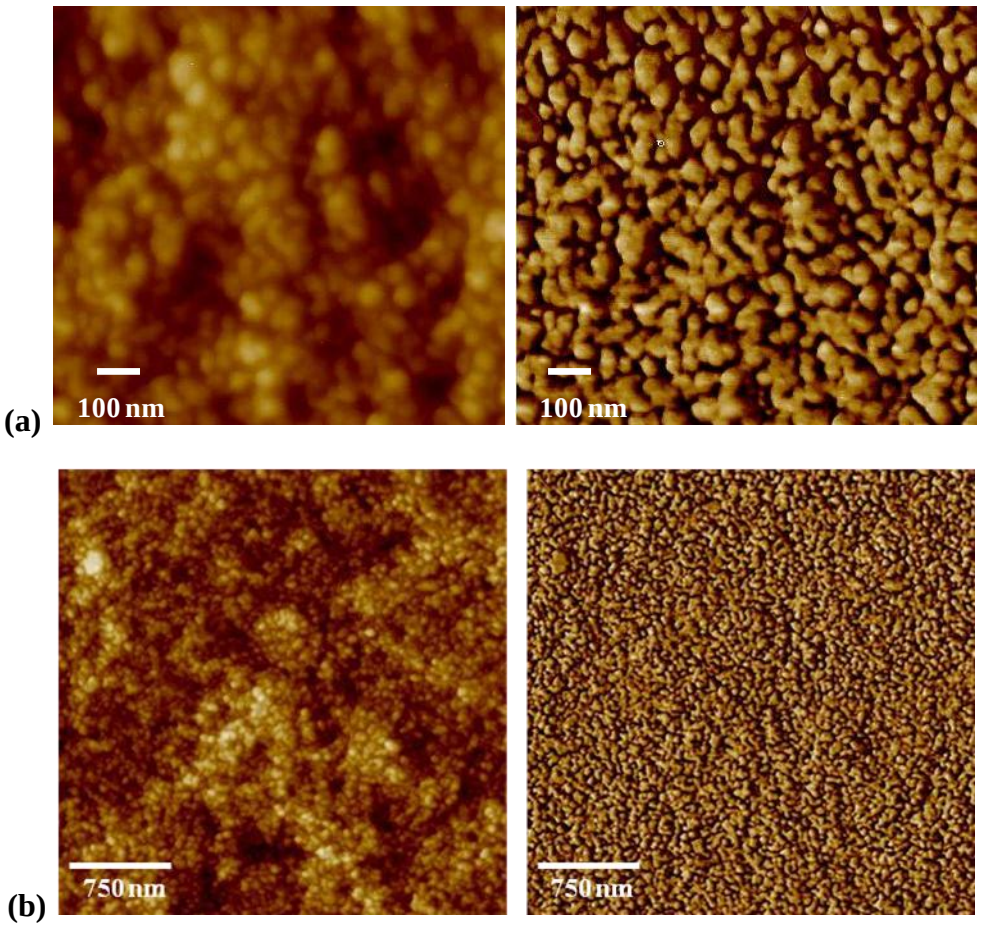

Figure 7.8. AFM images of PS-*b*-poly((2-UME)TOPBr) showing strong microphase separation in a (a) 1 μm image and a (b) 3 μm image; rms 4.0 mV and amplitude setpoint 3.3 mV

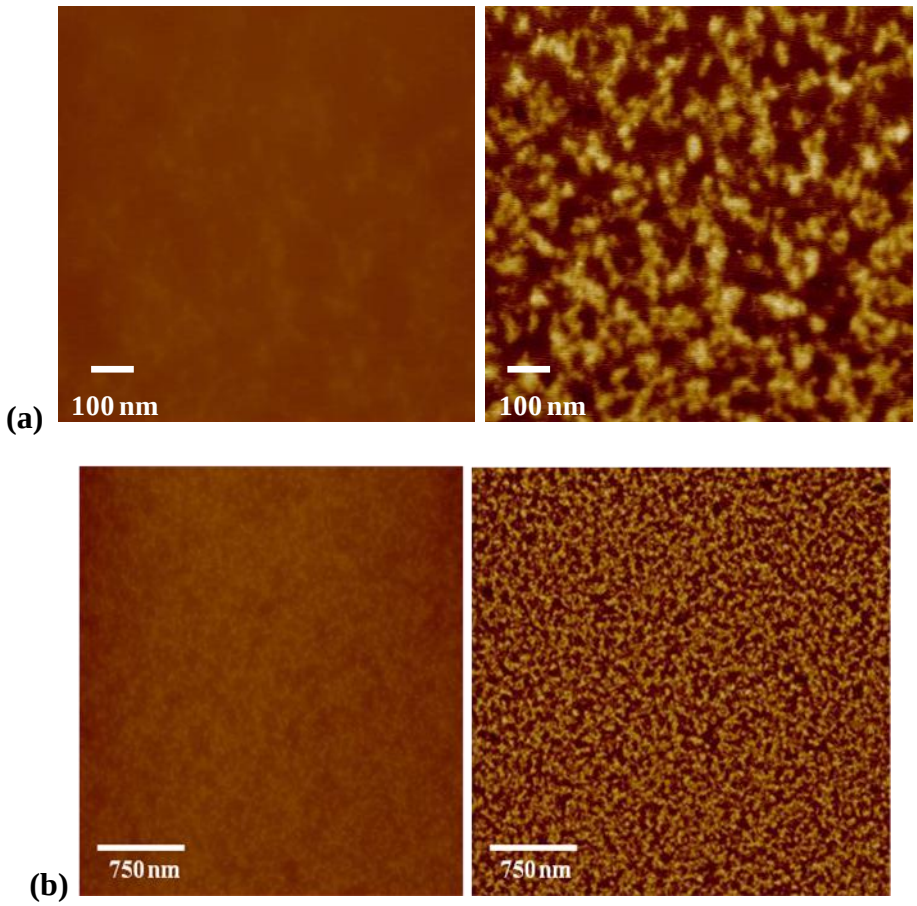

Figure 7.9. AFM images of PS-*b*-poly((6-UMH)TOPBr) showing microphase separation but some phase mixing in a (a) 1 μm image and a (b) 3 μm image; rms 4.0 mV and amplitude setpoint 3.3 mV

TEM images of both polymers also showed features that were 40-50 nm in diameter, approximately the same size features as those in the AFM images. Additional substructure with a diameter of only a few nanometers was also apparent in some images (Figure 7.10).

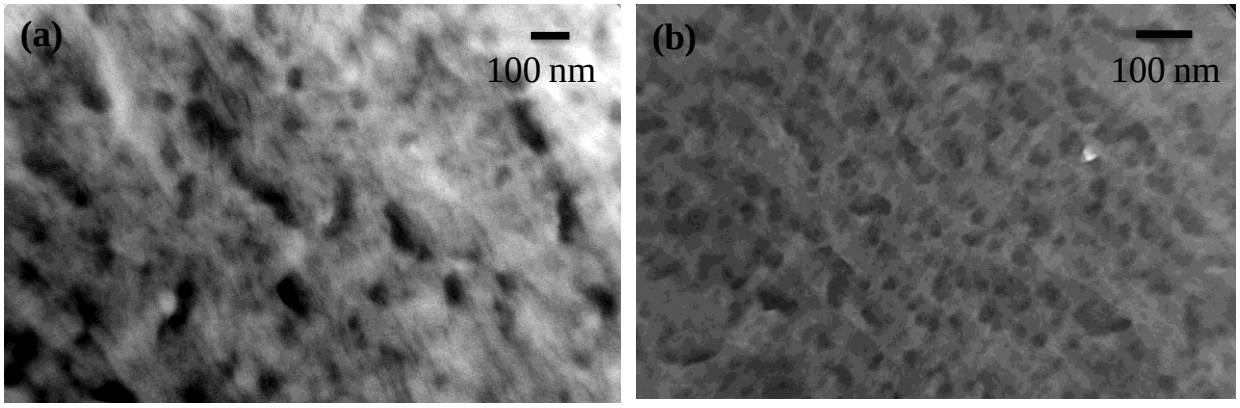

Figure 7.10. TEM images of (a) PS-*b*-poly((2-UME)TOPBr) and (b) PS-*b*-poly((6-UMH)TOPBr); Philips EM 420 TEM, 100 KV, 70 nm sections collected over DMSO/H_2O solutions

SAXS profiles indicated a potential ionic peak in PS-*b*-poly((6-UMH)TOPBr) having a diameter of approximately 3.22 nm (Figure 7.11) calculated from the relationship of $q_{max} = 2pi/d$ where d equals Bragg scattering distance.[11] Long et al. previously indicated that ionic peaks were more pronounced in SAXS profiles of sodiosulfonate-containing ionomers with ionic groups far away from the main chain rather than close to the main chain.[16] The authors suggested that the formation of ionic aggregates was more facile when ionic sites were farther from the main polymer chain.[16]

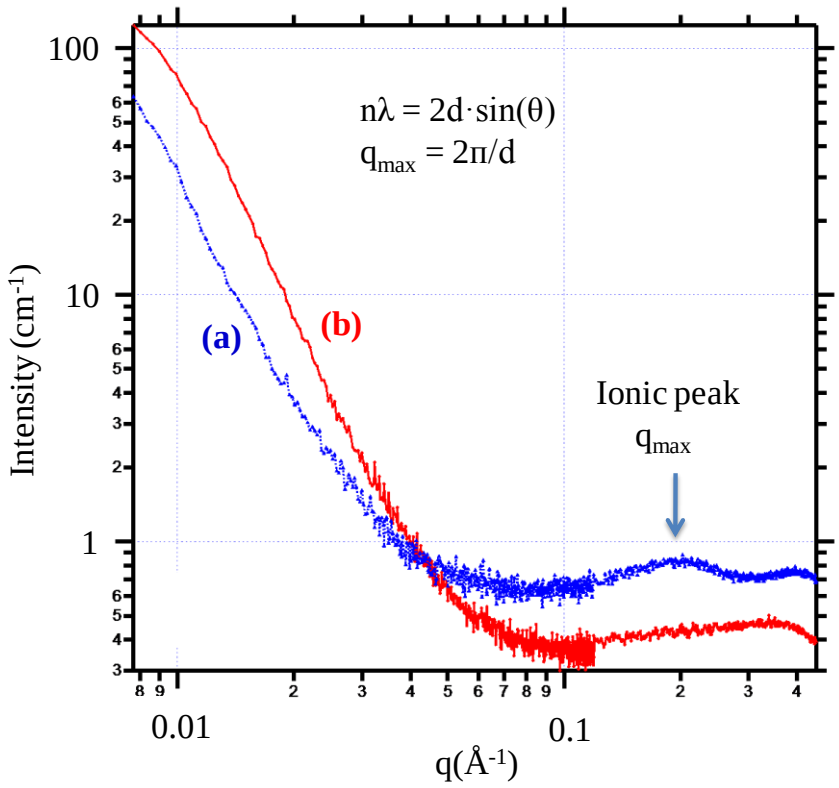

Figure 7.11. SAXS profiles of (a) PS-*b*-poly((6-UMH)TOPBr) and (b) PS-*b*-poly((2-UME)TOPBr); 3 m camera, copper X-ray source, Igor Pro v5.04B

7.4.4 Thermal Properties

DSC thermograms confirmed a glass transition of 99 ˚C for the 12,000 number-average g/mole polystyrene macroinitiator (Table 7.1). The PS-*b*-poly((2-UME)TOPBr) block copolymer had two glass transition temperatures, 40 and 98 ˚C. The PS-*b*-poly((6-UMH)TOPBr) had two glass transition temperatures as well; however, these temperatures were much closer together, 68 and 98 °C. Having two glass transition temperatures indicated microphase separation as observed in the AFM images (Figure 7.8 and 7.9). Lengthening the side-chain length in non-ionic acrylic polymers caused the glass transition temperature to decrease.[29-30] However, we have shown in

our own research that higher glass transition temperatures result from placement of the ionic groups at the terminus of side-chains due to more easily formed ionic aggregates.[16] Sulfonated block copolymers exhibited greater ionic aggregation when the ionic group remained farther from the backbone of the polymer. These ionic groups had greater mobility and could easily aggregate.[16]

Table 7.1. DSC data of PS-*b*-poly((6-UMH)TOPBr and PS-*b*-poly((2-UMH)TOPBr

Polymer Type	P^+ units (NMR)	P^+ mole % (NMR)	M_n (SEC)	DSC T_g (°C)
PS	0	---	12,000	99
PS-*b*-P((2-UME)TOPBr	22	19.0	26,000	40, 98
PS-*b*-P((6-UMH)TOPBr	20	14.8	---	68, 98

*DSC Midpoint T_g, 20 ºC/minute, -80 to 220 °C, N_2

7.5 Conclusions

Two monohydroxyl-containing phosphonium ionic liquids with different alkylene spacers were synthesized, (2-HE)TOPBr and (6-HH)TOPBr. Rheology indicated that the hydroxyhexyl-containing phosphonium salt had a higher viscosity than the hydroxyethyl-containing one, and DSC showed a higher melting point as well. Lengthening the alkylene spacer facilitated better crystalline packing. Two novel, phosphonium-containing methacrylate-based monomers, (6-UMH)TOPBr and (2-UMH)TOPBr, were successfully synthesized from these hydroxyl-containing ionic liquid precursors through reaction with 2-isocyanatoethyl methacrylate. The reactions were monitored with *in situ* FTIR for appearance of the urethane carbonyl and disappearance of the isocyanate group. Reactions were complete within 4 hours, and products were then used to make block copolymers with styrene.

Homopolymers of the phosphonium monomers were insoluble and precipitated from solution as the polymerizations proceeded. Polystyrene macroinitiators were used to make block copolymers through RAFT polymerization. Addition of the hydrophilic phosphonium monomer units resulted in microphase separated block copolymers as indicated with AFM images. DSC glass transition temperatures of the hydrophilic blocks were 40 and 68 ˚C for the ethyl and hexyl spaced units respectively. The polystyrene block exhibited a glass transition of 98 to 99 ˚C for all diblock copolymers. Lengthening the spacer of the phosphonium functionality off the backbone increased the methacrylate phosphonium block glass transition temperature. Increasing hydrophobicity also decreased the microphase separation and enhanced phase mixing between the polystyrene and polyphosphonium blocks. AFM images indicated microphase separation in all diblock copolymers with soft phases from 15-20 nm and hard phases from 20-50 nm.

7.6 Acknowledgements

Research was sponsored by the Army Research Laboratory and was accomplished under Cooperative Agreement Number W911NF-06-2-0014. The views and conclusions contained in this document are those of the authors and should not be interpreted as representing official policies, either expressed or implied, of the Army Research Laboratory or the U.S. Government. The U.S. Government is authorized to reproduce and distribute reprints for Government purposes notwithstanding any copyright notation hereon. The authors would like to acknowledge Dr. Fredrick Beyer for SAXS and Tom Glass for ^{31}P NMR spectrometry. The authors would also like to thank Steve June for help with collecting AFM images.

7.7 References

1. Eisenberg, A.; Kim, J. S. *Introduction to Ionomers*. Wiley: New York, 1998.
2. Unal, S. Synthesis and Characterization of Branched Macromolecules for High Performance Elastomers, Fibers, and Films. Ph.D. Thesis, Virginia Polytechnic and State University, Blacksburg, VA, 2005.
3. Eisenberg, A.; King, M., *Ion-Containing Polymers*. Academic Press: New York, 1977; p 15.
4. Eisenberg, A.; Hird, B.; Moore, R. B. *Macromolecules* **1990**, *23*, 4098-4107.
5. Kalista, S. J.; Ward, T. C.; Oyetunji, Z. *Mechanics of Advanced Materials and Structures* **2007**, *14*, 391–397.
6. R. Fall, Puncture Reversal of Ethylene Ionomers—Mechanistic Studies, M.S. Thesis, Virginia Tech, Blacksburg, Virginia, 2001.
7. Craig, S. J.; Gaskell, D. R.; Rockett, P.; Ruiz, C. *Journal de Physique IV* **1994**, *4(C8)*, 41-46.
8. Taylor, G.I.; Quinney, M.A. *Proc. Royal Soc. A* **1934**, *143***,** 307 – 326.
9. Marchand, A.; Duffy, J. J. *Mech. Phys. Solids* **1988**, *36*, 251 – 283.
10. Jin, R. ; Aoki, S. ; Shima, K. *Chem. Commun.* **1996**, 1939-1940.
11. Tant, M. R.; Mauritz, M. R.; Wilkes, G. L., *Ionomers: Synthesis, Structure, Properties and Applications*. Blackie Academic & Professional: New York, 1997.
12. Buruiana, T.; Buruiana, E. C. *Journal of Applied Polymer Science* **2005**, *96*, 577–582.
13. Lahor, A.; Nithitanakul, M.; Grady, B. P. *European Polymer Journal* **2004**, *40*, 2409–2420.
14. Ibarra, L.; Alzorriz, M. *Journal of Applied Polymer Science* **2003**, *87(5)*, 805-813.
15. Kang, H.; Lin, Q.; Armentrout, R. S.; Long, T. E. *Macromolecules* **2002**, *35*, 8738-8744

16. Saito, T., Mather, B. D.; Costanzo, P. J.; Beyer, F. L.; Long, T. E. *Macromolecules* **2008**, *41*, 3503-3512.
17. Paddison ,S. J. *Annual Review of Materials Research* **2003**, 33, 289-319.
18. Buruiana, E.C.; Buruiana, T.; Melinte, V. *Reactive & Functional Polymers* **2006**, *66(10)*, 1132-1140.
19. Pazhanisamy, P., Ariff, M.; Anwaruddin, Q. *Journal of Applied Polymer Science* **2005**, *98(3)*, 1100-1105.
20. Tsou, A. H.; Duvdevani, I.; Agarwal, P. K. **2004**, 45(10), 3163-3173.
21. van de Wetering, P.; Cherng, J.-Y.; Talsma, H.; Hennick, W. E., *J. Cont. Rel.* **1997,** 49, 59. van de Wetering, P.; Cherng, J.-Y.; Talsma, H.; Crommelin, D. J. A.; Hennick, W. E., *J. Cont. Rel.* **1998,** 53, 145.
22. Xie, W.; Xie, R.; Pan, W.; Hunter, D.; Koene, B.; Tan, L.; Vaia, R. *Chem. Mater.* **2002**, *14*, 4837-4845.
23. Kanazawa, A.; Ikeda, T.; Endo, T., *Journal of Polymer Science: Part A: Polymer Chemistry* **1993**, *31*, 335-343.
24. McKee, M. G.; Hunley, M. T.; Layman, J. M.; Long, T. E. *Macromolecules* **2006**, *39*, 575-583.
25. Layman, J. L.; Ramirez, S. M.; Green, M. D.; Long, T. E. *Biomacromolecules* **2009**, *10*, 1244–1252.
26. Brown, R. H.; Hunley, M. T.; Allen, M. H.; Long, T. E. *Polymer* **2009**, *50*, 4781–4787.
27. Mather, B. D.; Lizotte, J. R.; Long, T. E. *Macromolecules* **2004**, *37*, 9331-9337.
28. Mather, B. D.; Baker, M. B.; Beyer, F. L.; Green, M. D.; Berg, M. A. G.; Long, T. E. Macromolecules **2007**, *40*, 4396-4398.
29. Moad, G.; Rizzardo, E.; Thang, S. H. *Aust. J. Chem.* **2005**, *58*, 379-410.
30. Li, Y.; Armes, S. P.; Jin, X.; Zhu, S. *Macromolecules* **2003**, *36*, 8268-8275.
31. Lowe, A. B.; McCormick, C. L. *Prog. Polym. Sci.* **2007**, *32*, 283–351.
32. Wang, R.; Lowe, A. B. *Journal of Polymer Science: Part A: Polymer Chemistry* **2007**, *45*, 2468–2483.
33. Farmer, S. C.; Patten, T. E. *Journal of Polymer Science: Part A: Polymer Chemistry* **2002**, *40*, 555–563.
34. Parent, J. S.; Penciu, A.; Guillen-Castellanos, S. A.; Liskova, A.; Whitney, R. A. *Macromolecules* **2004**, *37*, 7477-7483.
35. Zhou, P.; Blumstein, A. *Polymer* **1997**, *38(3)*, 595-604.
36. Jenkins, I. H.; Kar, A. K.; Lindsell, W. E.; Murray, C.; Preston, P. N.; Wang, C.; Wherrett, B. S. *Macromolecules* **1996**, *29(20)*, 6365-6370.
37. Seyferth, D.; Masterman, T. C. *Macromolecules* **1995**, *28*, 3055-3066.
38. Lindsell, W. E.; Radha, K.; Soutar, I.; Stewart, M. J. *Polymer* **1990**, *31*, 1374-1378.
39. Atmaca, L.; Kayihan, I.; Yagci, Y. *Polymer* **2000**, *41*, 6035-6041.
40. Kanazawa, A.; Ikeda, T. *Coordination Chemistry Reviews* **2000**, *198*, 117-131.
41. Nishikubo, T.; Koichi, A.; Uchida, J. *Makromol. Chem.* **1989**, *190*, 1471-1482.
42. Nishikubo, T.; Uchida, J.; Matsui, K.; Iizawa, T. *Macromolecules* **1988**, *21*, 1583-1589.
43. Tomoi, M.; Kori, N.; Kakiuchi, H. *Makromol. Chem.* **1986**, *187*, 2753-2761.
44. Kenawy, E.; Abdel-Hay, F. I.; El-Shanshoury, E. R.; El-Newehy, M. H. *Journal of Polymer Science: Part A: Polymer Chemistry* **2002**, *40*, 2384-2393.
45. Parent, J. S.; Liskova, A.; Resendes, R. *Polymer* **2004**, *45*, 8091-8096.

46. Ghassemi, H.; Riley, D. J.; Curtis, M. Bonaplata, E.; McGrath, J. E. *Appl. Organometal. Chem.* **1998**, *12*, 781–785.
47. Williams, S. R.; Wang, W.; Winey, K. I.; Long, T. E. *Macromolecules* **2008**, *41(23)*, 9072-9079.
48. Marechal, E., *Comprehensive Polymer Science The Synthesis, Characterization, Reactions & Applications of Polymers*. Pergamon Press: 1989; Vol. 6.
49. Li, S.-D.; Zhang, C.-H.; Dong, J.-J.; Ou, C.-Y.; Quan, W.-Y.; Yang, L.; She, X.-D. *Carbohydrate Polymers* **2010**, *81(2)*, 2182-2187.
50. Zhang, B.-Q.; Chen, G.-D.; Pan, C.-Y.; Luan, B.; Hong, C.-Y. *Journal of Applied Polymer Science* **2006**, *102(2)*, 1950-1958.
51. Avci, D. *Polymer Bulletin* **2000**, *44(5-6)*, 1436-2449.
52. Huang, Y.; Xiao, C. Polymer **2007**, *48(1)*, 371-381.
53. Charlier, P.; Jerome, R.; Teyssie, P.; Utracki, L. A. *Macromolecules* **1992**, *25*(2), 617–624.
54. Song, Y.; Zhang, J.; Gan, W.; Zhou, J.; Zhang, L. *Ind. Eng. Chem. Res.* **2010**, *49*(3), 1242–1246.
55. Hartley, F. R., John Wiley & Sons: 1994; Vol. 3, p 25-91.
56. Abdallah, D. J.; Weiss, R. G., *Chem. Mater.* **2000,** 12, 406-413.
57. Weiss, R. A.; Turner, S. R.; Lundberg. R. D. *Journal of Polymer Science: Polymer Chemistry Edition* **2003**, *23(2)*, 525 – 533.
58. Ariza, M. J.; Jones, D. J.; Rozière, J. *Desalination* **2002**, *147(1-3)*, 183-189.

Chapter 8. Synthesis and Degradation of Bisphenol Phosphonium-Based Monomers

8.1 Abstract

Two novel bisphenol phosphonium monomers with or without alkylene spacers are described, and their potential use in high-temperature, base-catalyzed polysulfone reactions was analyzed. These salts have phenolic sites that make them suitable monomers in the synthesis of polysulfones, interfacial polyesters, or polyurethanes. The phenolic functionality is an antioxidant, and the phosphonium cation operates as a biocide. Alkyl phosphonium salts are especially known to degrade through β-H elimination, or Hofmann elimination. Under basic conditions, long reaction times, and high temperatures, the Hofmann elimination prevented bisphosphonium salts with alkylene spacers from surviving over 12 hours in base-catalyzed polysulfone reactions at 150 ºC. However, elimination occurred on the periphery of the monomer, preferentially forming vinyl-containing phenolic groups. Removing any external alkylene spacers between the phosphonium ions and phenolic groups subsequently prevented degradation under typical polysulfone reaction conditions. Thus, the short alkylene spacer between the phosphonium functionalities in the monomer was unharmed under harsh conditions possibly due to steric hindrance and instability of the elimination products. However, reactivity of this rigid bisphosphonium monomer was extremely low, and incorporation of the monomer into the final polysulfone was limited and often undetectable in over 12 hours of reaction at 150 ºC. Model reactions and ^{31}P NMR spectra of solutions post-reaction indicated no degradation of the phosphonium centers once these external alkylene spacers were removed from the monomer.

8.2 Introduction

The inclusion of ionic sites in polysulfones and other high performance polymers is increasingly popular, including use of ionic liquids and dopants, for fuel cell, electrochemical, and transducer applications.[1-4] For example, Bjerrum et al. examined ionic, sulfonated polysulfone for fuel cell and ion exchange applications, and these polyelectrolytes exhibited improved conductivity.[1] Polysulfone ionomers with pendant sulfonate groups are attractive for use as fuel cell membranes due to their chemical and thermal stability at temperatures even above 100 °C at high relative humidity and in corrosive environments.[5] Commercial polysulfones like UDEL® have excellent hydrolytic stability,[6] and Dickinson has even reviewed the use of UDEL in medical applications.[7] Lojoiu and Sanchez, however, recently wrote a review on sulfonated polysulfone ionomers for fuel cell applications.[8] In our research group, we have also examined sulfonated polysulfones for use in actuators and sensors. Sulfonation resulted in improved ionic liquid uptake and conductivity.[2-3]

Cost of precious metals like platinum used in hydrogen proton exchange membrane fuel cell electrodes for conductivity of ions has limited the commercial viability of this type of fuel cell.[9-10] However, alternative cationic membranes with mobile hydroxide anions for hydroxide exchange membrane fuel cells are attractive since non-precious metals in the electrodes can be used instead to achieve high power density.[10] Phosphonium salts are particularly desirable for their excellent thermal stability compared to ammonium cations,[11] and most fuel cells are operated at temperatures from 60 to 130 °C.[12] Polymers with phosphonium-based hydroxides have been synthesized for fuel cell applications, but most of these phosphonium-based polymers suffered from chemical instability in corrosive environments.[10, 13-14] However, Yan et al. recently synthesized polysulfone ionomers with pendant tris(2,4,6-trimethoxyphenyl)phosphonium ions,

and these ionomers showed excellent chemical, thermal, and hydrolytic stability even in the presence of potassium hydroxide solutions.[10]

Ionic polysulfones are also attractive for their antimicrobial activity.[15] Ioan et al. synthesized ionic polysulfones to study their morphology and antimicrobial activity against *Escherichia coli* and *Staphylococcus aureus* strains, and increasing ionic content increased the antimicrobial action against both types of bacteria.[15] However, polymers with different charge density displayed different morphologies, and the thermal history and morphology of the membranes were important for bacterial adhesion to the surface. They examined the hydrophilic/hydrophobic properties of the polymers through increasing charge concentration. The hydrophilic, ionic polymers exhibited enhanced adhesion of hydrophilic *E. coli* compared to hydrophobic *S. aureus*. Thus, ionic content in the polymer is not only important for electro-active applications, but it also facilitates adhesion and antimicrobial action.[15] Phosphonium-based polymers are also desirable for their enhanced antimicrobial activity compared to ammonium-based analogs,[16] and it is hypothesized that phosphonium-based polysulfones may also possess enhanced antimicrobial activity.

In this thesis, we report preliminary results on the synthesis of phosphonium-based bisphenols for inclusion in polysulfone reactions. We explain the synthesis of two novel bisphosphonium bisphenols, and we also indicate the difficulties encountered with including these bisphenols in polysulfone reactions. The results described in this chapter should encourage future work with these monomers in polysulfone, polyurethane, and polyester reactions. Tailoring monomer structure for specific degradation patterns may lead to reversible, easily degradable polymers. Two phosphonium-based bisphenol monomers are described. One degrades in basic conditions, and at high temperatures β-H elimination was observed. We also

describe one novel ionic bisphenol which does not degrade under these conditions. High performance polymers such as polyesters, polysulfones and polyurethanes, often possess low solubility, require high-temperature melt processing, and are not easily degradable when disposed.[17-18] Using these monomers in future polyurethane or polyester reactions, for example, may lead to an interesting comparison in terms of both thermal and base stability for application as degradable polymers.

8.3 Experimental

8.3.1 Materials

4-Hydroxyphenethyl bromide (96%) was purchased from Aldrich and recrystallized from chloroform/hexane. 1,4-Bis(diphenylphosphino)butane (98%), (4-hydroxyphenyl)diphenylphosphine (98%), 1,4-dibromobutane (99%), *N*,*N'*-dimethylacetamide (DMAc, 97%), and toluene were purchased from Aldrich and used as received. Potassium carbonate (99%), bisphenol A (BPA, ≥99%), and bis(4-fluorophenyl) sulfone (99%) were purchased from Aldrich and dried in a vacuum oven overnight at 60 °C before use. Anhydrous diethyl ether was purchased from VWR and used as received. Methanol was purchased from EMD Science. *N*,*N*-Dimethylformamide (DMF) (99%) from Aldrich was collected from a PureSolv-MD3 solvent purification system from Innovative Technology, Inc. Chloroform was purchased from Fisher Scientific and distilled from calcium hydride under nitrogen.

8.3.2 Synthesis of a Phosphonium-Based Bisphenol Containing External Alkylene Spacers (BPP1)

Bis(diphenylphosphino)butane (0.35 g, 0.829 mmol) was charged into a flame-dried, 100-mL, 1-neck, round-bottom flask with a Teflon® stir bar under argon. Three equivalents of 4-hydroxyphenethyl bromide to one equivalent of bis(diphenylphosphino)butane were used. The 4-hydroxyphenethyl bromide (0.5 g, 2.49 mmol) was charged into the flask under argon. Then 4.6 mL of dry chloroform was added, and the flask and contents were purged for 20 min with argon. The reaction continued at 65 ºC for 24 h under an argon blanket. Once cooled, 50 mL of methanol were added to the product, and the bisphosphonium diol was precipitated in 900 mL of diethyl ether and washed with an additional 50 mL of diethyl ether. White crystals were collected and dried in a vacuum oven for 24 h at 60 ºC. One ^{31}P NMR peak was seen at 26.7 ppm in CD_3OD, confirming that only one type of phosphorus center existed in the product. ^{1}H NMR (400 MHz, 25 ºC) in CD_3OD δ (ppm) 1.488-1.621 (m, 4H), 2.683-2.799 (m, 4H), 2.837-2.955 (m, 4H), 3.217-3.346 (m, 4H), 6.618-6.679 (m, 4H), 6.955-7.022 (m, 4H), 7.644-7.862 (m, 20H), 7.871 (s, 2H, Ph-OH). DSC (20 °C/min, Ramp -10 to 200 °C) mp 120-123 °C.

8.3.3 Synthesis of a Phosphonium-Based Bisphenol Without External Alkylene Spacers (BPP2)

(4-Hydroxyphenyl)diphenylphosphine butane (1.09 g, 3.92 mmol) was charged into a flame-dried, 100-mL, 3-neck round-bottom flask with a Teflon® stir bar and with an attached condenser under argon. Three equivalents of (4-hydroxyphenyl)diphenylphosphine to one equivalent of 1,4-dibromobutane were used. The 1,4-dibromobutane (0.16 mL, 0.283 g, 1.31 mmol) was charged into the flask under argon. Then dry DMF (9.3 mL) was added, and the flask

and contents were purged for 20 min with argon. The reaction continued at 65 ºC for 24 h under an argon blanket. Once cooled, 50 mL of methanol was added to the product, and the bisphosphonium diol was precipitated in 900 mL of diethyl ether and washed with an additional 50 mL of diethyl ether. White crystals were collected and dried in a vacuum oven under reduced pressure for 24 h at 60 ºC. One ^{31}P NMR peak in CD_3OD was observed at 26.6 ppm, confirming that only one type of phosphorus center existed in the product. ^{1}H NMR (400 MHz, 25 ºC) in CD_3OD δ (ppm) 1.801-1.954 (m, 4H), 3.311-3.489 (m, 4H), 7.024-7.104 (m, 4H), 7.493-7.861 (m, 24H). DSC (20 °C/min, Ramp -10 to 200 °C) mp 215-216 °C.

8.3.4 Synthesis of Polysulfone Copolymers with BPA

All polymerizations utilized a flame-dried, 250-mL, 3-neck, round-bottom flask with an attached Dean-Stark trap, condenser, and overhead stirrer. All polysulfones were synthesized using a drying step with toluene for 4 to 12 h. Toluene and water were removed after this time, and the reaction temperature was increased. A characteristic synthesis of a 50/50 mole % BPA to phosphonium bisphenol ionic polysulfone is described. BPP1 (1.62 g, 1.96 mmol), bis(4-fluorophenyl) sulfone (1.01 g, 3.93 mmol), potassium carbonate (0.682 g, 4.92 mmol), BPA (0.4918 g, 1.97 mmol), and DMAc (13.1 mL) were charged to the 3-neck, round-bottom flask. Toluene (50 mL) was added. The reaction was purged with argon for 1 h. Then water was removed by azeotropic distillation at 135 °C for 12 h under argon. The toluene was removed, and the reaction temperature was increased to 155 °C for 12 h. ^{1}H and ^{31}P NMR spectra were taken before and after precipitation and drying of the product. The product was allowed to cool to room temperature and precipitated in ethyl ether/methanol solutions. The product was dried overnight in a vacuum oven under reduced pressure at 60 °C to remove ethyl ether.

8.3.5 Characterization

^{1}H and ^{31}P NMR spectra were collected in $CDCl_3$ and CD_3OD on a Varian 400 MHz spectrometer operating at 400 and 162 MHz respectively. FAB MS was performed on a JEOL JMS-HX-110 instrument in positive mode. DSC was carried out with a Perkin Elmer Pyris 1 under nitrogen at 5 or 20 ºC/min. Values from the second heating scan were reported. A Perkin-Elmer TGA 7 was used for TGA under nitrogen at a heating rate of 10 °C/min.

8.4 Results and Discussion

8.4.1 Synthesis of Phosphonium-Based Bisphenol Monomers and Their Thermal Properties

Synthesis of the bisphosphonium-containing monomer (BPP1) proceeded through an S_N2 mechanism with 4-hydroxyphenethyl bromide and 1,4-bis(diphenylphosphino)butane. An excess of phenol was used (Figure 8.1).

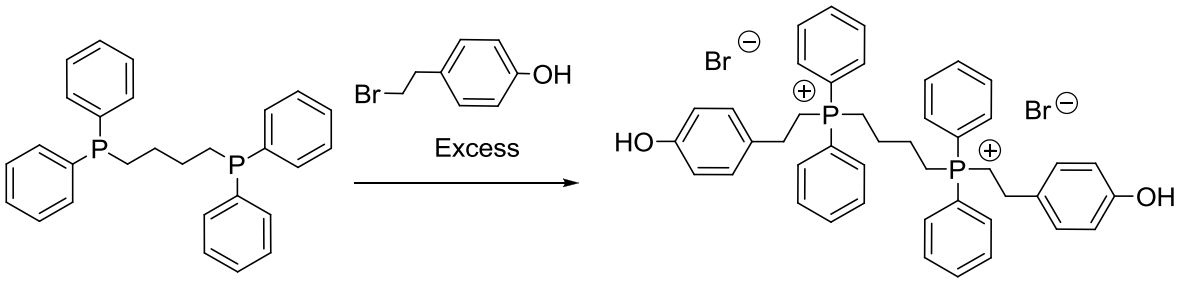

Figure 8.1. Synthesis of BPP1

The bisphenol product precipitated out during the reaction in chloroform, and only the bisphenol and not the mono-phenol precipitated. The product was isolated by dissolving it in methanol and

precipitating in ethyl ether. ^{1}H and ^{31}P NMR spectra confirmed the structure of the final product (Figure 8.2).

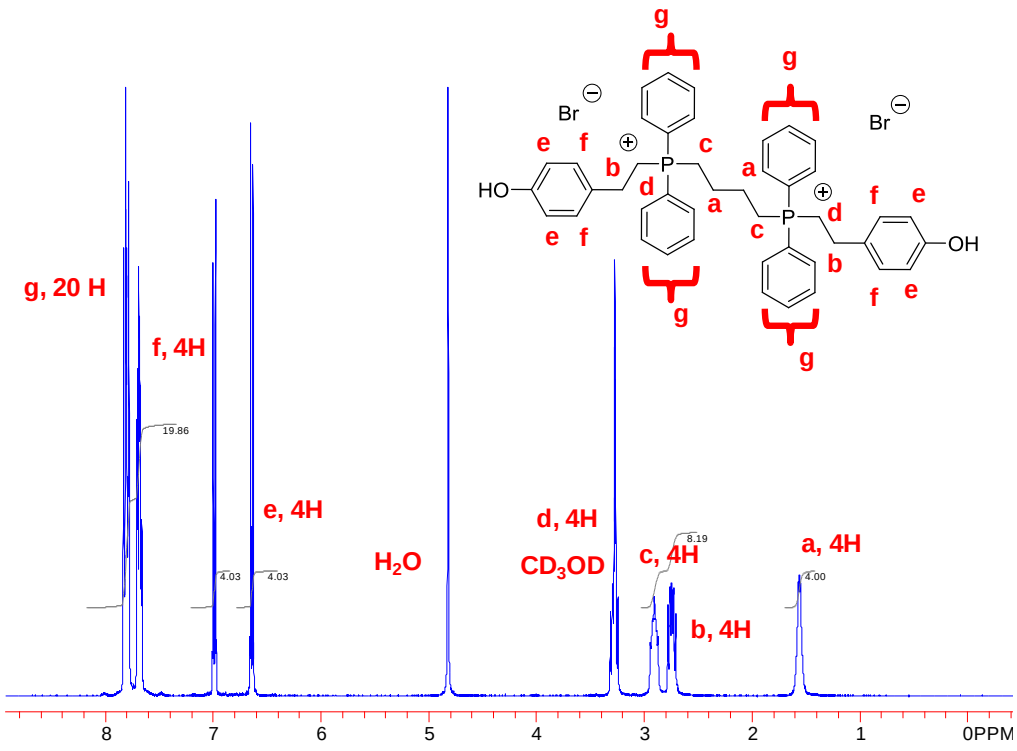

Figure 8.2. ^{1}H NMR spectrum of BPP1; 400 MHz, CD_3OD, ambient temperature

DSC thermograms showed a melting point of 117 °C for this monomer (DSC: 20 °C/minute, Ramp 40-240 °C). In bulk, the monomer degrades in one-step as measured by TGA (Figure 8.3).

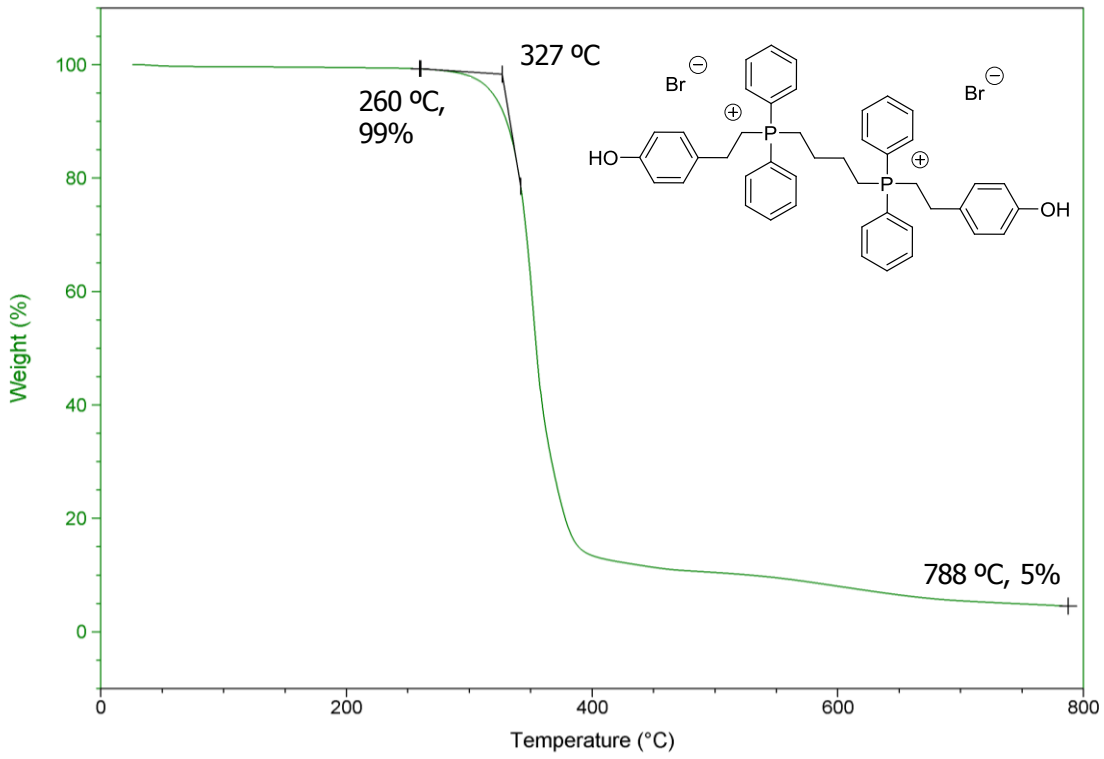

Figure 8.3. Thermal degradation by TGA of BPP1; 10 °C/minute under nitrogen

Synthesis of phosphonium-containing polysulfones and copolymers with BPA followed similar procedures (Figure 8.4).

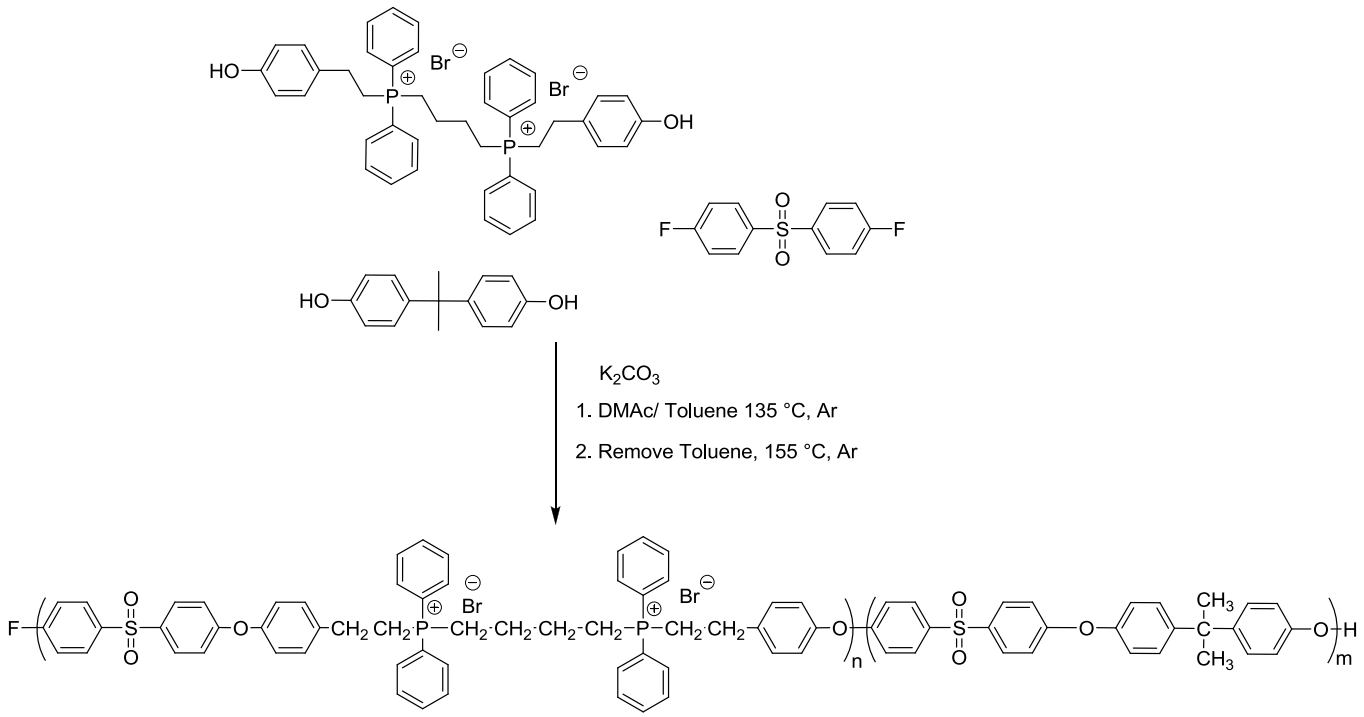

Figure 8.4. Synthesis of polysulfone copolymers with BPP1

Homopolymers of the bisphenol phosphonium monomer and copolymers with BPA showed that the phosphonium cation degraded under the polymerization conditions. The ^{1}H NMR spectra showed degradation of the bisphenol phosphonium cation to form styrenic ends (Figure 8.5).

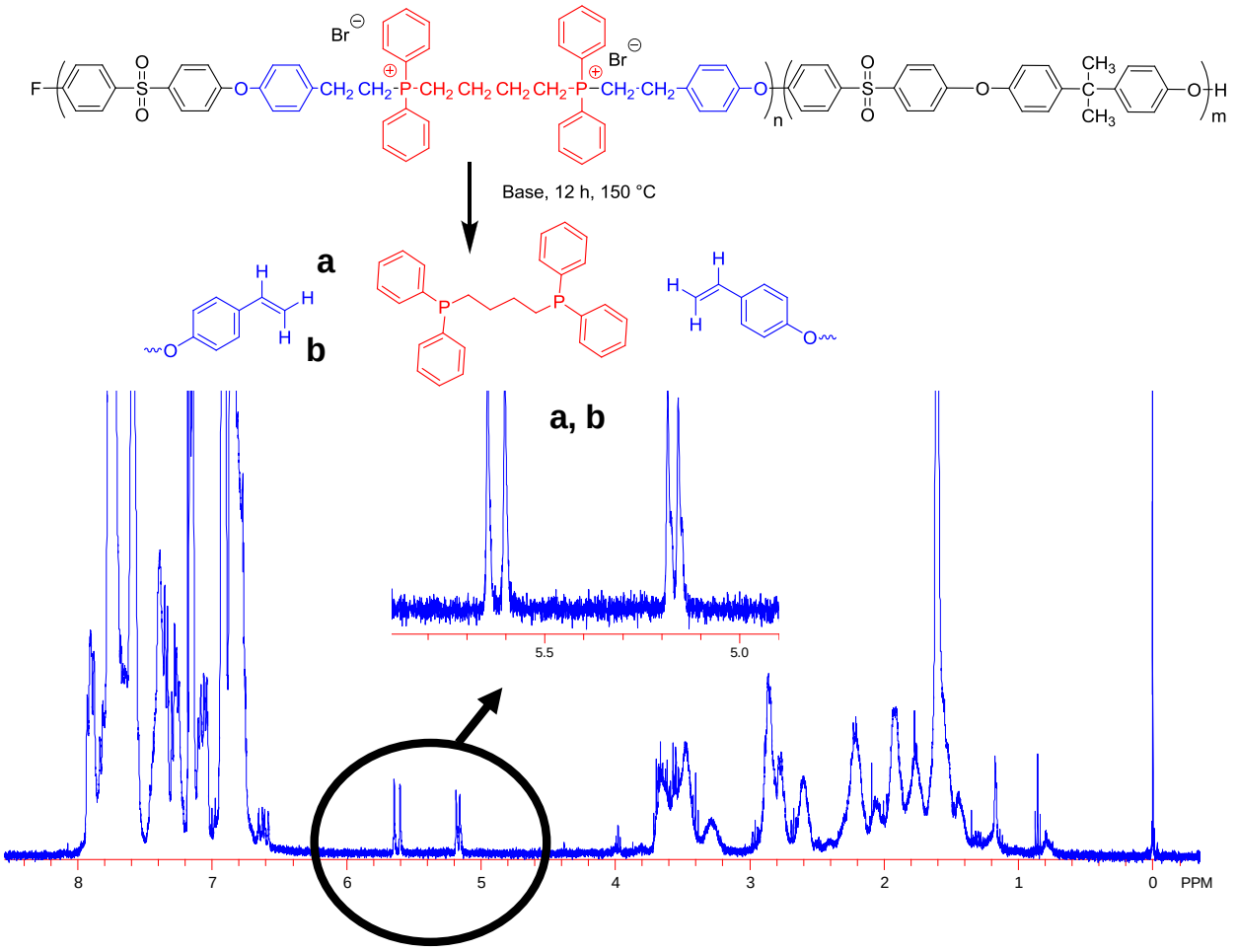

Figure 8.5. Degradation through β-H elimination as observed with a ^{1}H NMR spectrum; 400 MHz, $CDCl_3$, ambient temperature

The suggested mechanism of degradation is β-H elimination on the outsides of the phosphonium cationic unit (Figure 8.6). Eliminating internally by the four-carbon alkylene spacer was not apparent with ^{1}H NMR spectra. A study of the thoroughly-dried phosphonium-based bisphenol monomer in anhydrous DMAc under nitrogen for 12 hours at 155 °C revealed no decomposition and only one ^{31}P NMR peak. Multiple isothermal TGA studies showed no degradation of the phosphonium bisphenol at 155 °C under an inert atmosphere. However, the base used in the polysulfone reactions, potassium carbonate, is expected to facilitate degradation of the salt. ^{1}H

NMR spectra showed degradation of the phosphonium salt when base was added during the reactions, in isothermal TGA scans and in model studies. ^{1}H NMR spectra indicated that elimination occurred primarily through β-H elimination and formation of a styrenic group (Figure 8.6).

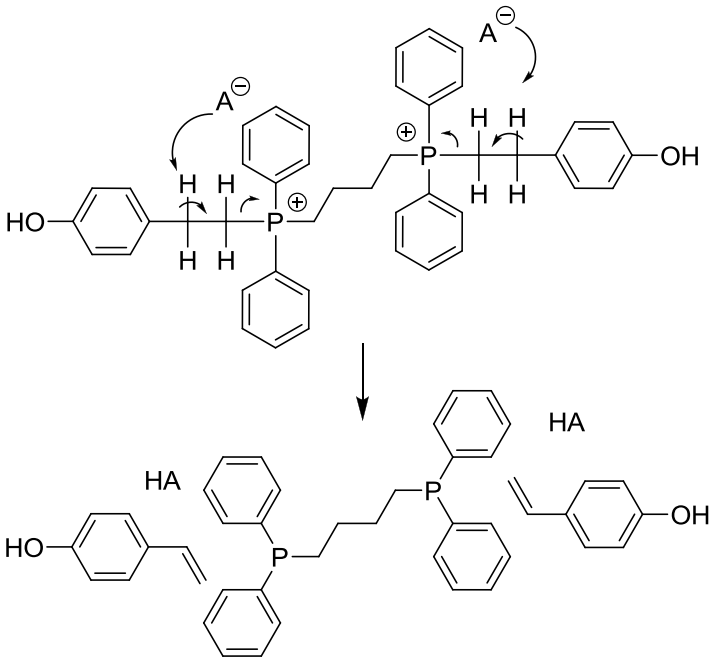

Figure 8.6. β-H elimination mechanism occurring during the polysulfone reaction with BPP1

Targeting 0, 5.4, and 50 mole % phosphonium monomer incorporation produced copolymers with decreasing glass transitions with increasing mole % of phosphonium salt (Figure 8.7). The molecular weights were lower and PDI values were lower for polymer reactions containing more phosphonium functionality (Table 8.1). Solubility of the polymer also changed with an increase in polymer ionic content.

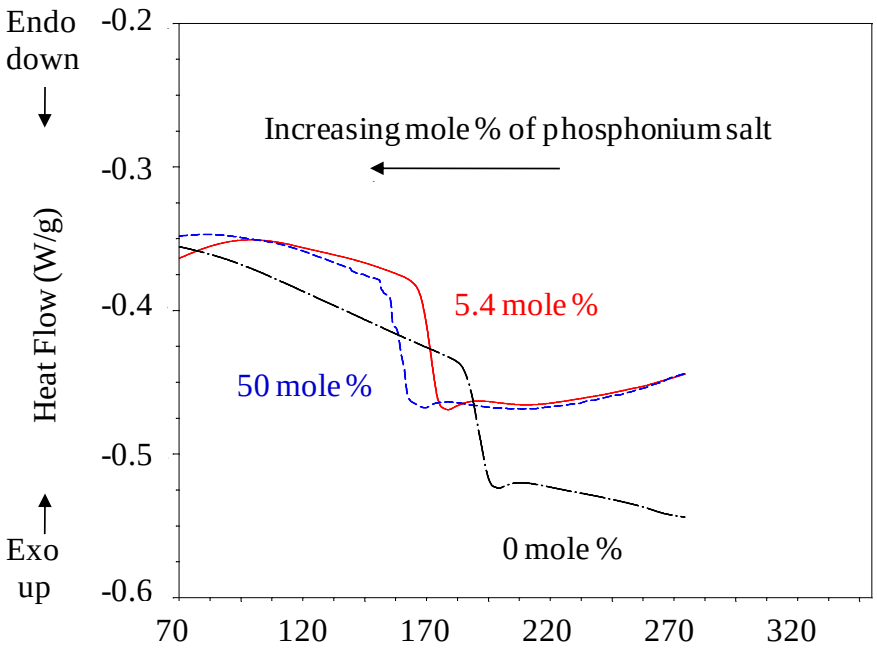

Figure 8.7. DSC thermograms of ionic polysulfones with BPP1; 5 ºC/minute under nitrogen

Table 8.1. Solubility and size-exclusion chromatography of polysulfones with BPP1

P^+ (mole %)	SEC M_n[a] (g/mole)	SEC M_w[a] (g/mole)	PDI[a]	T_g[b] (°C)	MeOH Soluble	THF Soluble	$CHCl_3$ Soluble
50%	---	---	---	156	Yes	No	Yes
5.4%	17,200	25,000	1.46	175	No	Yes	Yes
0%	20,400	45,200	2.21	190	No	Yes	Yes

[a]SEC: THF, 40 °C, 1 mL/minute [b]DSC 5 °C/minute

Yan et al. showed that steric hindrance around the alkylene groups connected to phosphonium cations was important to avoid basic instability in phosphonium-based polysulfones.[10] In this thesis, we also indicate that the elimination of accessible alkylene

functionalities is of key importance to the chemical stability of polysulfone ionomers. To avoid β-H elimination and the formation of a styrenic group, a new phosphonium bisphenol monomer (BPP2) was pursued from the commercially available (4-hydroxyphenyl)diphenylphosphine and 1,4-dibromobutane (Figure 8.8).

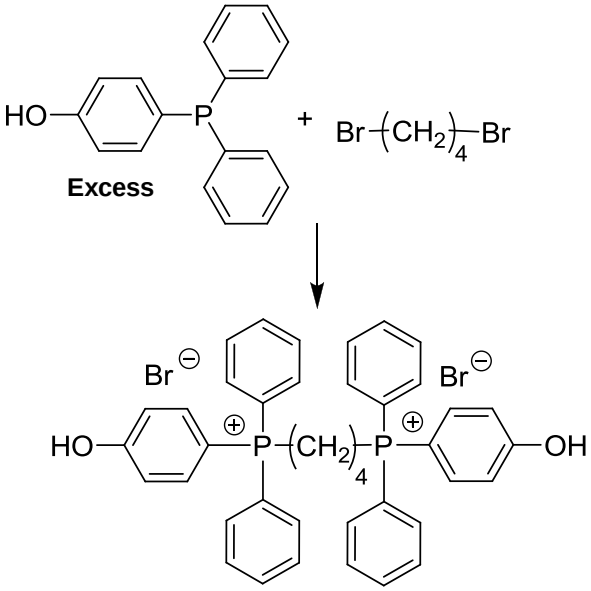

Figure 8.8. Synthesis of BPP2

The reaction was conducted at 80 °C under nitrogen with mechanical stirring. Excess phosphine was used to facilitate the reaction, and the product was precipitated into ethyl ether with greater than 98% yield. The resultant monomer was thermally stable up to 323 °C under nitrogen (by TGA) and lost less than 3% weight over 12 hours under nitrogen at 155 °C (in an isothermal TGA study). ^{1}H and ^{31}P NMR spectra confirmed the structure (Figure 8.9).

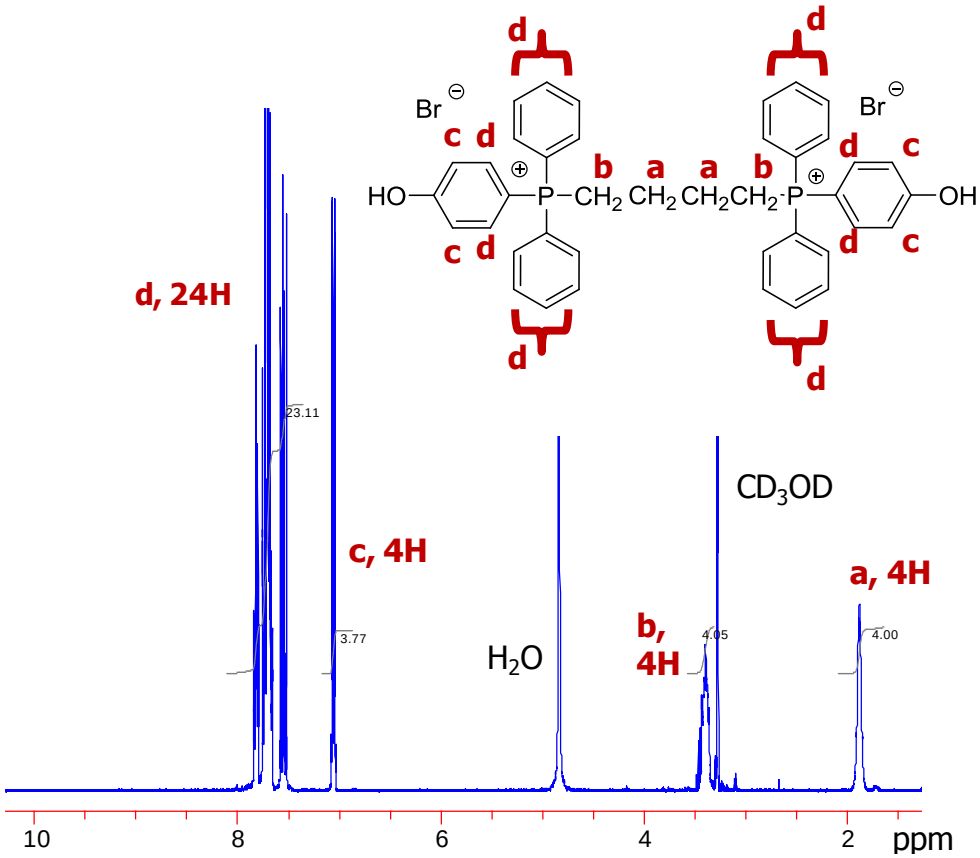

Figure 8.9. ^{1}H NMR spectrum of BPP2; 400 MHz, CD_3OD, ambient temperature

This novel bisphenol survived a model polysulfone polycondensation reaction with no degradation to any other types of phosphorus centers, and this new monomer was used to make BPA copolymers. Removal of the external alkylene group removed the possibility for β-H elimination on the outside of the phosphonium salts. Then 50/50 phosphonium-containing bisphenol to BPA copolymers were prepared. No degradation of the phosphonium functionalities through β-H elimination to vinyl compounds was observed from analysis of the post-reaction solution (Figure 8.10).

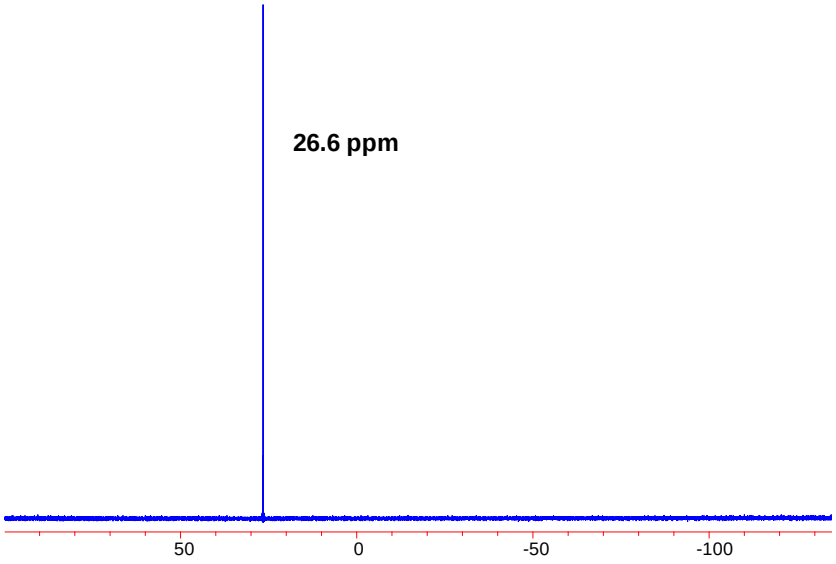

Figure 8.10. ^{31}P NMR after reaction, indicating no degradation to any other phosphorus centers; 162 MHz, CD_3OD, ambient temperature

However, after isolation of the polymer product, phosphonium incorporation was minimal by ^{1}H NMR, and phosphorus was often not detectable with ^{31}P NMR after precipitation of the polymer. Large quantities of unreacted phosphonium-based monomer were isolated from the product. It is hypothesized that ionic aggregation in the reaction solution prevented the accessibility of the BPP2 phenolic groups for reaction. The alkylene spacers in BPP1 helped improve accessibility of the phenolic sites for reaction and incorporation of the phosphonium-based BPP1 monomer into polysulfones, but these alkylene spacers also led to facile degradation through β-H elimination. Future work should include screening BPP2-containing reaction solutions with DLS for ionic aggregation and attempting the reaction under more dilute concentrations in solution.

8.5 Conclusions and Future Directions

Two different phosphonium-containing bisphenol monomers were synthesized, BPP1 and BPP2. Polysulfones containing these phosphonium bisphenol monomers were pursued. BPP1 degraded in the polysulfone reaction through β-H elimination. BPP2 was synthesized to remove the external alkylene groups contributing to the facile elimination, and BPP2 did not show any degradation to vinyl compounds in the polysulfone synthesis. However, low incorporation of the phosphonium monomer resulted. It is hypothesized that ionic association may have prevented the accessibility of the phenolic groups in the phosphonium-based bisphenol monomer in solution. However, the results reported are only preliminary. Future directions should include screening reactant solutions with DLS and using dilute reactant solutions. In pursuit of synthesizing phosphonium-containing polysulfones, it is necessary to study the reactivity of the phosphonium-based bisphenol versus its state of aggregation. Future work should also include examination of longer reactions times, provided this monomer maintains isothermal stability under basic conditions at 150 ºC for longer times, 24 to 48 hours. However, these bisphosphonium-based bisphenols may also serve as excellent monomers for polyurethanes and interfacial polyesters where alkaline conditions and high temperatures are not required for polymer synthesis.

8.6 Acknowledgements

Research was sponsored by the Army Research Laboratory and was accomplished under Cooperative Agreement Number W911NF-06-2-0014. The views and conclusions contained in this document are those of the authors and should not be interpreted as representing official policies, either expressed or implied, of the Army Research Laboratory or the U.S. Government.

8.7 References

1. Hasiotis, C.; Qingfeng, L.; Deimede, V.; Kallitsis, J. K.; Kontoyannis, C. G.; Bjerrumb, N. J. *Journal of The Electrochemical Society* **2001**, *148*, A513-A519.
2. Duncan, A. J. Barbar, J. A.; Long, T. E.; Leo, D. J. *Smart Mater. Struct*. **2009**, *18*, 104005.
3. Duncan, A. J.; Leo, D. J.; Long, T. E. *Macromolecules* **2008**, *41(21)*, 7765-7775.
4. Hasiotis, C.; Deimede, V.; Kontoyannis, C. *Electrochimica Acta* **2001**, *46*, 2401–2406.
5. Karlsson, L. E.; Jannasch, P. *Electrochemica Acta* **2005**, *50(9)*, 1939-1946.
6. Harper, C. A. *Handbook of Plastics, Elastomers, & Composites, 4th ed.* McGraw-Hill Companies, Inc.: New York, 2002, p. 61.
7. Dickinson, B. L. *J. Biomater. Appl.* **1988** , *3(4)*, 605-634.
8. Lojoiu, C.; Sanchez, J.-Y. *High Performance Polymers* **2009**, *21(5)*, 673-692.
9. Borup, R.; Meyers, J.; Pivovar, B.; Kim, Y. S.; Mukundan, R.; Garland, N.; Myers, D.; Wilson, M.; Garzon, F.; Wood, D.; Zelenay, P.; More, K.; Stroh, K.; Zawodzinski, T.; Boncella, J.; McGrath, J. E.; Inaba, M.; Miyatake, K.; Hori, M.; Ota, K.; Ogumi, Z.; Miyata, S.; Nishikata, A.; Siroma, Z.; Uchimoto, Y.; Yasuda, K.; Kimijima, K. I.; Iwashita, N. *Chem. Rev.* **2007**, *107*, 3904 – 3951.
10. Gu, S.; Cai, R.; Luo, T.; Chen, Z.; Sun, M.; Liu, Y.; He, G.; Yan, Y. *Angew. Chem. Int. Ed.* **2009**, *48*, 1–5.
11. Xie, W.; Xie, R.; Pan, W.; Hunter, D.; Koene, B.; Tan, L.; Vaia, R. *Chem. Mater.* **2002**, *14*, 4837- 4845.
12. Adjemian, K.T.; Srinivasan. S.; Benziger, J.; Bocarsly, A.B. *Journal of Power Sources* **2002**, *109*, 356.
13. Fenton, G. W.; Ingold, C. K. *J. Am. Chem. Soc.* **1929**, 2342 – 2357.
14. Zanger, M.; Vanderwerf, C. A.; McEwen, W. E. *J. Am. Chem. Soc.* **1959**, *81*, 3806 – 3807.
15. Filimon, A.; Avram, E.; Dunca, S.; Stoica, I.; Ioan, S. *Journal of Applied Polymer Science* **2009**, *112*, 1808–1816.
16. Kanazawa, A.; Ikeda, T.; Endo, T., *Journal of Polymer Science: Part A: Polymer Chemistry* **1993**, *31*, 335-343.
17. Bjorksten Research Laboratories, Inc. *Polyesters and Their Applications*. Reinhold Publishing Corporation: New York, 1956.
18. *Modern Polyesters*. Scheirs, J.; Long, T. E. eds. John Wiley & Sons, Ltd.: West Sussex, England, 2003.

Chapter 9: Imidazole- and Imidazolium-Containing Polymers for Biology and Material Science Applications

Reprinted from *Polymer*, 51, E. B. Anderson, T. E. Long, Imidazole- and Imidazolium-Containing Polymers for Biology and Material Science Applications, 2447-2454, Copyright 2010, with permission from Elsevier

9.1 Abstract

The imidazole ring is ubiquitous in nature, and imidazole functionality plays a critical role in many structures within the human body, notably as histamine and histadine. Imidazoles offer many biophysical interactions including their ability to hydrogen bond with drugs and proteins. In contrast, imidazolium salts have lost their strong hydrogen-bonding ability through alkylation of both nitrogens, but they are able to aggregate electrostatically. Imidazolium salts are used to extract metal ions from aqueous solutions, dissolve carbohydrates, create polyelectrolyte brushes on surfaces, coat metal nanoparticles, provide antimicrobial action, and create oriented liquid crystals. Bioactive applications include imidazolium hydrogels, antiarrhythmics, and anti-metastic agents. This review will describe the synthesis and design of imidazole derivatives and imidazolium-containing polymers as bioactive materials. Imidazole-based polymers readily associate with biological molecules through hydrogen-bonding, and imidazolium analogs offer electrostatic interactions, aggregation, and self-assembly. Design of novel imidazole- and imidazolium-based macromolecules remains as an exciting and emerging field.

9.2 Introduction to Imidazole and Imidazolium Salts: Application

From clicking drugs onto the backbones of delivery vectors[1] to synthesizing N-heterocyclic carbene ligands for antitumor compounds,[2] nitrogen heterocycles have a long history in biomedical research and remain a front-runner for bioactive applications. Imidazoles and their salts in particular comprise a boundless and emerging field. The polar imidazole ring, which contains two nitrogens separated with a methylene, hydrogen bonds through the amino hydrogen as the donor and the imino nitrogen as the acceptor (Figure 9.1).[3-4]

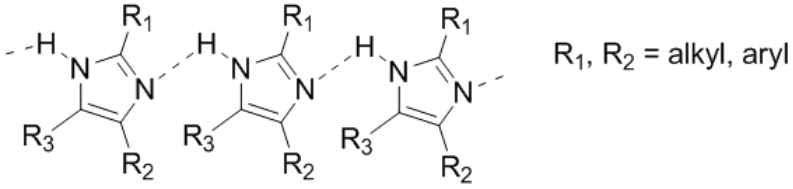

Figure 9.1. General imidazole structure with self-complementary hydrogen bonding;[3,12] Adapted with permission from Brédas, J. L.; Poskin, M. P.; Delhalle, J.; André, J. M.; Chojnacki, H. *J. Phys. Chem.* **1984**, *88*, 5882-5887. Copyright 1984 American Chemical Society

Many uses of the imidazole ring as a bioagent revolve around its ability to bond to metals as a ligand[5-9] and its ability to hydrogen bond with drugs and proteins. This aptitude has resulted in the use of polyimidazoles as oxygen transport membranes.[8] Furthermore, chemical modification of the imidazole functionality has led to desired covalent or physical crosslinking and the production of functional or multifunctional polymers.[10] The imidazole ring's biocompatibility provides a scaffold for biomimetic applications,[9] including the use of imidazoles as DNA sequence targets for alkylating DNA and suppressing gene expression.[11] Not only are imidazoles biocompatible, but they also are antimicrobial. The 1-alkyl imidazoles offer

antibacterial activity,[12] and imidazoles inhibit enzymes and kill fungal pathogens.[12] Imidazoles also play a role in inhibition of post-translational farnesylation, which is a key step for Ras proteins that influence cancer proliferation.[12] The amino acid histamine, a naturally occurring imidazole in the body, is involved with everyday functions: sleeping, eating, drinking, and cognitive processes.[12] Imidazole-based antagonists for histamine may provide treatments for Alzheimer's disease and depression.[4,12] Vitamin B_{12}, DNA purines, and biotin all involve imidazole residues.[4,12-13] Imidazoles are also anti-inflamatory agents and regulate blood pressure.[13] They offer high thermal stability and are often used in high temperature polymeric products.[4,14] The imidazole ring offers high chemical stability, stability to harsh acids and bases, and resistance to hydrogenation. However, it undergoes several typical aromatic substitution reactions to provide functional derivatives.[4,14]

Despite the loss of directed, self-complementary hydrogen bonding through alkylation of the imidazole ring, electrostatic aggregation of imidazolium salts is a tunable, self-assembly process, which is instrumental to several applications. Imidazolium salts are used to extract metal ions from aqueous solutions and coat metal nanoparticles,[15] dissolve carbohydrates,[16] and create polyelectrolyte brushes on surfaces.[17] For example, atom transfer radical polymerization (ATRP) was used to graft poly(1-ethyl-3-(2-methacryloyloxy ethyl)imidazolium chloride) brushes onto gold surfaces.[17] One of the imidazolium salt's most promising attributes is its antimicrobial action[12,18] and molecular self-assembly into liquid crystals.[19-20] 1-Alkyl-3-methylimidazolium chlorides and bromides, 1-alkyl-2-methyl-3-hydroxyethylimidazolium chlorides, and *N*-alkyl-*N*-hydroxyethylpyrrolidinonium, for example, all exhibit strong biocidal activity.[18] Hydrogels form from polymerized methylimidazolium-based ionic liquids with acryloyl groups; the polymer self-assembles into organized lamellae with unique swelling properties, leading to bioactive

applications.[19] Other bioactive applications for imidazolium salts include antiarrhythmics,[21] anti-metastic agents,[22-23] and imidazolium-based steroids.[24] Separation applications include efficient absorption of CO_2.[25] Imidazolium salts enhance vesicle formation as imidazolium surfactants,[26] and they also find application in polymeric actuators.[27]

The imidazole ring and its salts afford a wealth of biophysical-related applications, and attachment of imidazole derivatives to polymers represents a new and relatively unexplored field. The supramolecular association of novel imidazolium-containing biopolymers for antimicrobial and antimycotic drug applications receives significant attention. Weak ionic interactions may facilitate bioactivity and selectivity.

9.3 Imidazole Ring: Biology and Physical Attributes

De Luca provided a focused earlier view of imidazoles with concentration on their current use as bioactive compounds,[12] and she outlined the roles of imidazoles in antibiotics to anti-inflammatory agents. Several imidazole structures exist in nature. Histamine is one of the most important and has potent physiological effects (Figure 9.2).[12,28]

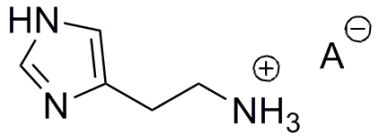

Figure 9.2. Histamine at physiological pH, A is the counter anion and has numerous possibilities, including chloride and heparin;[28] Adapted with permission from Durant, G. J.; Ganellin, C. R.; Parsons, M. E. *J. Med. Chem.* **1975**, *18(9)*, 905-909. Copyright 1975 American Chemical Society

Imidazolium ionic liquids offer templates for synthesis of functionalized carbohydrates.[16,29] Carbohydrates bind to proteins and control synthon transfer between cells.[16,29] Imidazolium-based steroids were reported,[24] and imidazolium salts serve as antiarrhythmics[21] and anti-metastic agents.[2,22-23] Lee et al. investigated the antimicrobial and antifungal properties of several imidazolium salts that inhibited growth of gram-negative bacteria, gram-positive bacteria, and fungi.[18]

Cytotoxicity and *in vitro* behavior of imidazolium-based polymers are relatively unexplored. Toxicity of imidazolium ionic liquids and other small molecules show the general trend that cytotoxicity is highly dependent on the counter anion and the length of any alkyl chains on the nitrogens of the imidazole ring. Longer alkyl chains increase the cytotoxicity.[30] Imidazolium salts were found to have anti-fibrotic properties in mouse hepatic stellate cells. This finding indicates that these imidazolium salts prevent liver fibrosis.[31] These salts also possess anti-metastic properties.[32] However, imidazolium-based polymer *in vitro* studies offer a huge area for future research.

Dupont and Suarez recently reviewed the physical properties of imidazolium salts, specifically imidazolium ionic liquids.[33] The desirable chemical and thermal stability of the imidazolium ring was noted, as well as interesting solubility and conductivity. Large cations hinder allocation into a lattice, and, therefore, ionic compounds with low lattice energies exist as ionic liquids at temperatures below 100 °C.[33-37] Room temperature ionic liquids are particularly attractive. The low melting point of imidazolium salts derives from large cations requiring lower energy to break electrostatic interactions. Adding long alkyl chains to these salts decreases both packing ability and lattice energy to depress the melting point. Asymmetry also negatively influences ordering and promotes low melting salts. Long-range Coulomb interactions in ionic

liquids promote longer spatial correlations than van der Waals forces.[33-38] The 1,3-dialkylimidazolium cations form cationic and anionic channels where three anions flank each cation and vice versa.[33] The fluid structure is considered self-assembled and supramolecular. Imidazolium ionic liquids also have high thermal stability.[33,39] Dupont and Suarez outlined how decomposition of imidazolium salts follows several pathways, including 2-position deprotonation to form carbenes (pk_a 21-23)[33,40-45] and Hoffman elimination.[33,46-47]

Imidazolium salts enable many emerging applications including nanocomposites,[33,48-58] reaction solvents,[33] and CO_2 absorbents.[25] These salts form self-assembled monolayers,[15] create one-dimensional ion conduction for columnar, uniaxially-oriented liquid crystals, and enhance vesicle formation.[26] Some imidazolium salts are liquid crystals and possess ion conductivity.[33,59,60] Most imidazolium salts show relatively higher solubility of CO_2 compared to O_2 and other gases, which derives from weak Lewis acid-base interactions with anions.[25,61] Electron-rich metals or even metals in nanoparticles cause carbene formation of 4- and 5-imidazole ring positions due to their lower acidity than the 2 position.[33,62-64] Imidazolium coated and functionalized nanoparticles exist,[15] and stabilization of nanoparticles in imidazolium ionic liquids occurs through surfactant-like interactions.[65-66]

9.4 Imidazole and Imidazolium-Based Polymers

Although the scope of published reactions involving imidazole ring formation is too large to review in this document, Grimmett outlined key approaches to various substituted imidazoles.[14] The Weidenhagen synthesis, for example, involves α-hydroxyketones that are oxidized to dicarbonyls with cupric acetates.[4] A hydroxyketone is converted to a ketoaldehyde or diketone, and a cuprous ion is created. The aldehyde, dicarbonyl-containing compound, and

ammonia react to form an imidazole cuprous complex. Hydrogen sulfide is commonly used to form free imidazole from its metal salt form.[4]

Alkylation of imidazoles and imidazolium synthesis is simple compared to their heterocylic ring formation. Alkylation of the secondary amine simply proceeds through deprotonation of the amino hydrogen with a base followed with attack of halogenated alkyls. The second nitrogen is subsequently alkylated in a second reaction with haloalkyls.[16] Figure 9.3 exemplifies this strategy for the synthesis of a hydroxyl-containing imidazolium salt.

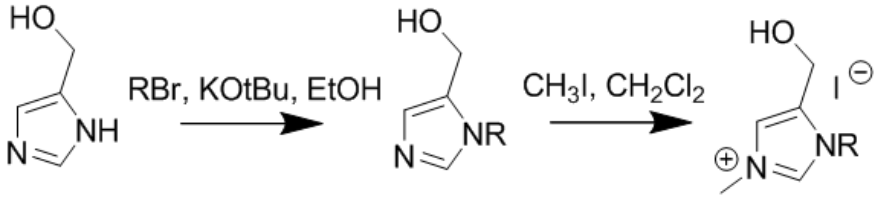

Figure 9.3. Koschella et al. present a classic example of the synthesis of imidazolium salts from imidazoles;[16] Adapted with permission from El Seoud, O. A.; Koschella, A.; Fidale, L. C.; Dorn, S.; Heinze, T. *Biomacromolecules* **2007**, *8(9)*, 2629-2647. Copyright 2007 American Chemical Society

Many imidazole- and imidazolium-based polymers exist. The vast majority of literature focuses on olefin-containing imidazole monomers. Ferruti et al. synthesized novel alkyl methacrylate-based imidazoles as precursors for various functional polymers using poly(hydroxyethyl acrylate) (HEMA) and *N,N'*-carbonyldiimidazole (CDI) in chloroform at room temperature without a catalyst (Figure 9.4).[10]

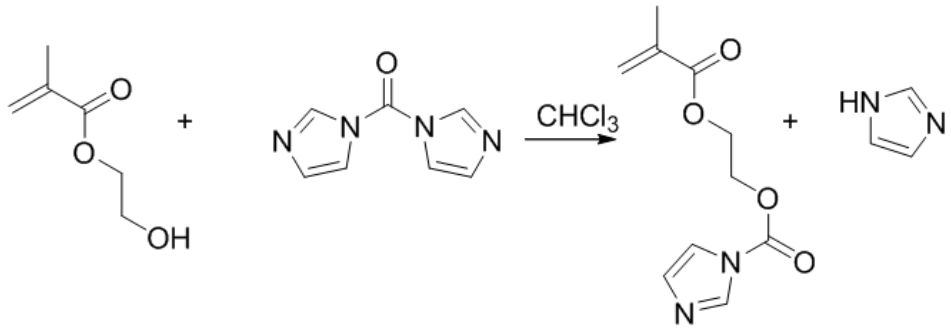

Figure 9.4. Synthesis of imidazole vinyl monomer;[10] Elisabetta Ranucci, Gloria Spagnoli, Paolo Ferruti: 2-[(1-Imidazolyl)formyloxy]ethyl methacrylate as a new chemical precursor of functional polymer. *Macromolecular Rapid Communications*. 1999. Volume 20. Pages 4-5. Copyright Wiley-VCH Verlag GmbH & Co. KGaA. Adapted with permission

Liu et al. synthesized novel polyelectrolyte gels for solid-state electrochemical devices as the dye-sensitized solar cell.[67] Their polyelectrolyte gel was based on 1-ethyl-3-(2-methacryloyloxyethyl)imidazolium iodide (PEMEImI). PEMEImI upon addition of I_2 and polyacrylonitrile plasticizers formed a gel with ionic conductivity of 1 x 10^{-3} S/cm at room temperature.[67] Having both free anions and cations causes polarization through migration of these charges to opposite electrodes. Immobilizing one of the ions in a polymer reduces resistivity and polarization.[67] Nishide et al. used poly(1-vinylimidazole)s to coordinate to cobalt oxygen carriers to form reversible oxygen-binding polymer membranes for facilitated oxygen transport (Figure 9.5).[8,68]

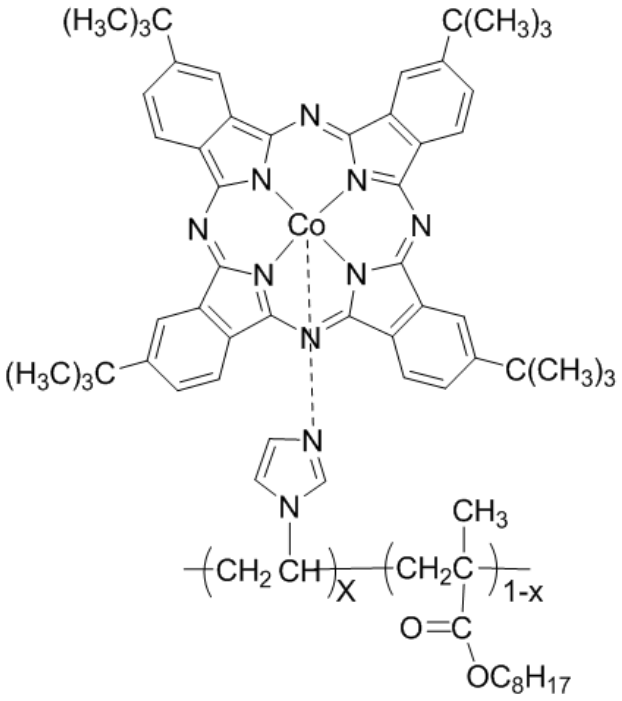

Figure 9.5. Poly(1-vinylimidazole) coordinated to cobalt oxygen carriers;[8] Adapted from *Reactive and Functional Polymers*, 66/8, Nalinakumari Preethi, Hiromi Shinohara, Hiroyuki Nishide, Reversible oxygen-binding and facilitated oxygen transport in membranes of polyvinylimidazole complexed with cobalt-phthalocyanine, 851-855, Copyright (2006), with permission from Elsevier

Firestone et al. studied cation structure as related to the lyotropic mesophase behavior of self-assembled imidazolium ionic liquids and their polymers.[20] Both the effects of alkyl chain length and introducing an acryloyl group for polymerization onto the end of the alkyl were investigated with small angle X-ray scattering (SAXS). Small angle X-ray scattering provides a measure of the distances between phases and ionic aggregates in polymers through X-ray scattering in these regions. This technique is used commonly to measure the inter-particle distance between ionic aggregates in ionomers and polyelectrolytes.[20,69-72] Some ionic liquids

self-assemble into strong physical gels upon water addition. Acryloyl groups add photopolymerizable sites to increase the mechanical integrity of these gels. Using an eight-carbon alkyl produced weakly-ordered, lyotropic mesophase, and lamellar structure biomembranes with water channels. The structure was maintained after polymerization. A longer, decyl chain increased order and formed tetragonal perforated structures. Once polymerized, cubic structures were obtained.[20] Firestone et al. also investigated hydrogels, including self-assembly of ionic liquids and subsequent polymerization for biomimetic applications.[19] Polymerization of acryloyl-based imidazolium salts formed hydrogels with a lamellar structure. The gels swelled nearly 200 times their volume, forming disordered lamellae. A physically crosslinked gel that swells to a pre-determined dimension is considered a responsive polymer.[19,73] These types of responsive polymers and hydrogels enabled drug release applications, sensors, and artificial muscles.[19]

Many other bio-related, imidazole-containing polymers exist. For example, Sugiyama and Bando synthesized *N*-methylimidazole-containing polyamides for sequence-specific DNA alkylation.[11] They coupled imidazole or pyrrole groups with carboxylic acids to synthesize these polyamides through classical solid-phase peptide synthesis (Figure 9.6).[74]

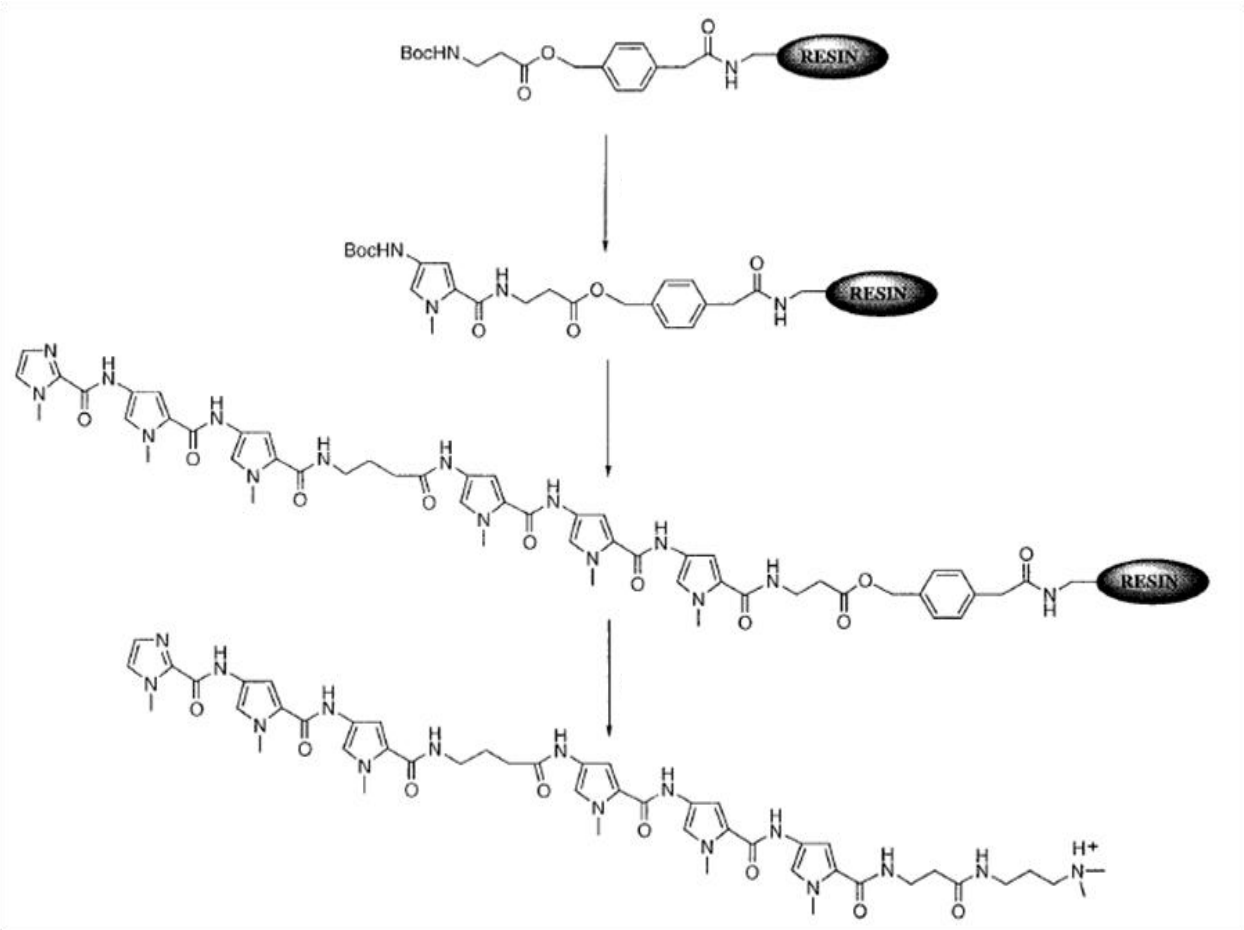

Figure 9.6. An example of solid-phase synthesis of a polyamide on a solid support;[74] Reprinted with permission from Baird, E. E.; Dervan, P. B. *J. Am. Chem. Soc.* **1996**, *118*, 6141-6146. Copyright 1996 American Chemical Society

Blocking specific DNA sequences suppresses expression of corresponding genes. Deemed "knowledge-based therapy," regulating gene expression could in turn silence cancer cell proliferation. These polyamides selectively bound sequences in the minor groove of the DNA double helix, allowing alkylating agents to target one sequence (Figure 9.7).[11]

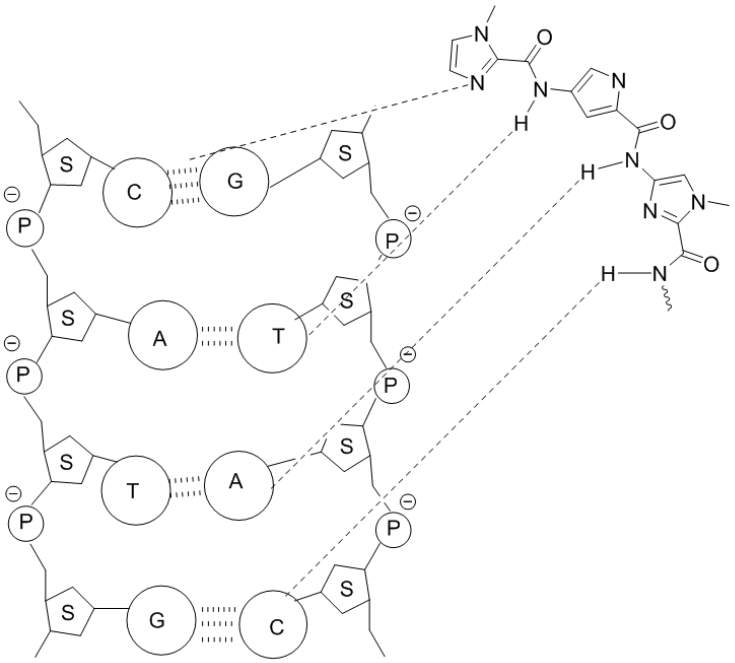

Figure 9.7. H-bonding of *N*-methylimidazole-containing polyamides with DNA for sequence-specific DNA alkylation; G = guanine, C= cytosine, A = adenine, T = thymine, P = phosphate, S = deoxyribose sugar;[11] Adapted with permission from Bando, T.; Sugiyama, H. *Acc. Chem. Res.* **2006**, *39*, 935-944. Copyright 2006 American Chemical Society

The imidazolium salt was selective for G-C base pairs, and gene-silencing did result. These polymers represent a step closer to tailor-made anticancer agents and offer advantages including their automated solid-phase synthesis and flexibility.[11] Besides novel vinyl imidazoles and imidazolium-based polymers, novel imidazolium ionenes,[75-78] main-chain metal-coordinated polymers,[6] and pseudorotaxanes exist.[79]

Ohno et al. synthesized imidazolium salts in the backbone of the polymer, or ionenes, via hydroboration reactions (Figure 9.8).[75]

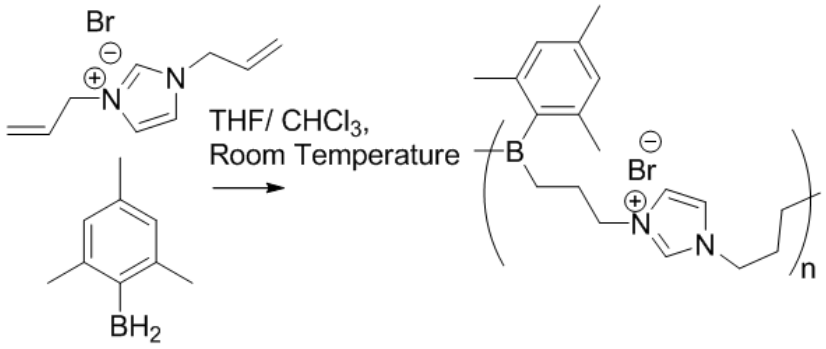

Figure 9.8. Imidazolium ionenes formed from hydroboration reactions;[75] Adapted with permission from Matsumi, N.; Sugai, K.; Miyake, M.; Ohno, H. *Macromolecules* **2006**, *39*, 6924-6927. Copyright 2006 American Chemical Society

Conductive polyelectrolytes were formed from 1,3-diallylimidazolium bromide. An anion exchange provided lithium bis(trifluoromethylsulfonyl)imide based organoboron polymers. An ionic conductivity of 3.74 x 10^{-5} to 1.93 x 10^{-5} S/cm at 50 °C resulted.[80] Anion trapping of organoboron was successful.

In two studies, Ohno and co-workers studied a multitude of different imidazolium-containing polymers and composites where various counterions and structures affected conductivity. They synthesized polyelectrolytes through both the functionalization of imidazolium salts with acrylic groups through DCC coupling reactions with hydroxyl-containing imidazolium salts[80] and reactions between lithium 9-borabicyclo[3,3,1]nonane hydride and 1,3-dihydroxyethyl imidazolium bromide.[81] Anion exchange to bis(trifluoromethylsulfonyl)imide for the later polymers led to high ionic conductivity of 3.4 x 10^{-6} S/cm at 50 °C. The glass transition temperature of -6 °C provided promising mechanical properties and high conductivity. Ohno and co-workers also studied nitrile rubber composites imidazolium zwitterions.[82] Addition of imidazolium at 9.2 weight % provided an 8-fold increase in ionic conductivity through

decreasing the interaction of nitrile rubber with lithium cations. Microphase separation also was observed.[82]

Long recently described a facile ionene synthesis from an easily accessible bisimidazole as illustrated in Figure 9.9.[76-78] This synthesis is facilitated through S_N2 reactions coupling dibromides and bisimidazoles and is another rare example in the literature of step-growth methods to imidazolium-containing polymers.

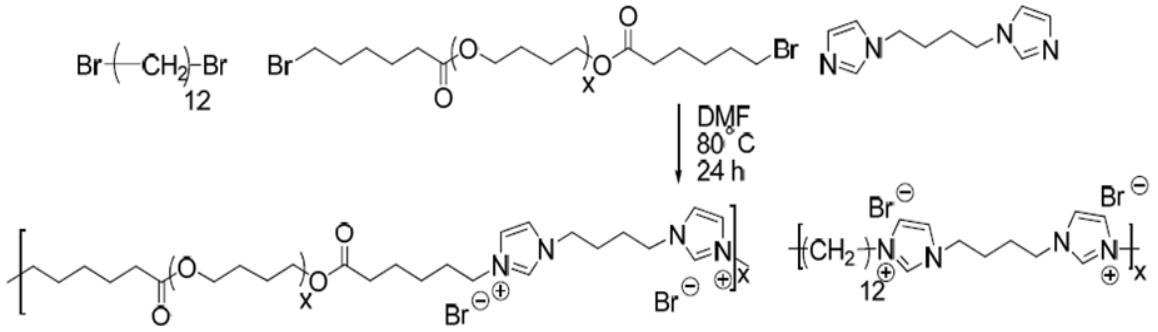

Figure 9.9. Synthesis of segmented imidazolium-based ionenes with PTMO soft segments;[76] Adapted from *Polymer*, 51/6, S. R. Williams; D. S. Cruz; K. I. Winey, T. E. Long, Ionene segmented block copolymers containing imidazolium cations: structure-property relationships as a function of hard segment content. Copyright (2010), with permission from Elsevier

Catalano et al. synthesized silver, gold, and palladium-based imidazole-containing complexes that formed luminescent polymers with in-chain metal coordination.[6] Ghosh et al. used silver imidazole-containing complexes as initiators for ring-opening polymerization of L-lactides in bulk.[7] Ring-opening polymerization of lactide monomers and homogeneous catalysis was achieved. Bielawski et al. also used step-growth polymerization of bis(*N*-heterocyclic carbene)s to synthesize poly(enetetramine)s as conjugated polyelectrolytes for biological sensing

and electronic applications (Figure 9.10).[83-84] This approach is a novel method to step-growth based imidazolium-containing polymers, but oxidatively unstable polymers were obtained. Polymerization of these monomers provided tailored spectroscopic and electronic properties.

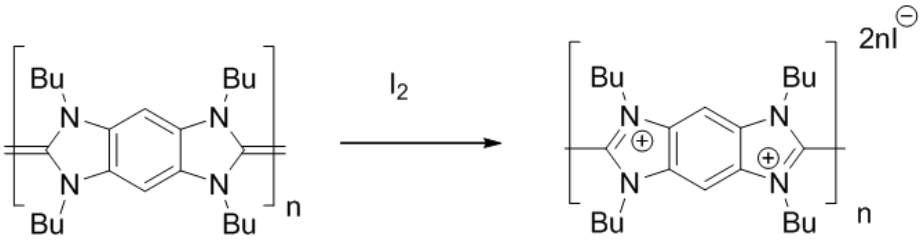

Figure 9.10. Synthesis of poly(enetetramine)s;[83] Kamplain, J. W.; Bielawski, C. W. *Chem. Comm.* **2006**, 1727-1729. Reproduced by permission of the Royal Society of Chemistry

Beer et al. used anion-templated assembly of novel pseudorotaxanes with imidazoliums threading through a chloride anion-based macrocycle to form interlocked structures for use in sensor design (Figure 9.11).[79] Selective anion recognition through electrostatic interactions has spurred interest in recent years.[79] Supramolecular assemblies widely used to create these interlocked structures are hydrogen bonding, pep stacking, and metal coordination.[79-85] The anion associates with two or more groups.[79-85] In 2006, Kim reviewed the synthesis of imidazolium anion recognition sites and self-assembly.[86]

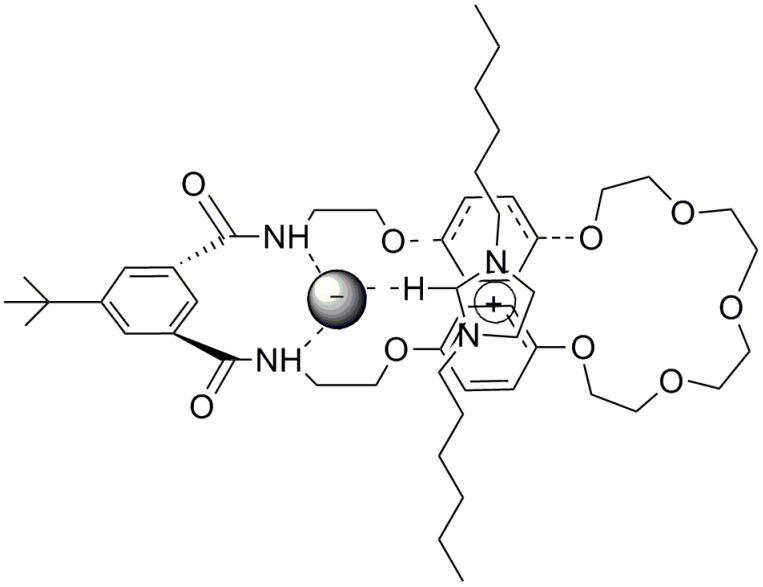

Figure 9.11. Imidazoliums threading through a chloride anion-based novel pseudorotaxanes;[79] Beer, P. D.; Sambrook, M. R.; Curiel, D. *Chem. Comm.* **2006**, 2105-2117. Adapted by permission of the Royal Society of Chemistry

9.5 Perspective for Future Studies

Imidazoles are naturally occurring in the human body, and histamine is one of the most important with formidable physiological effects.[12] Physical applications range from gas separation[25] to designed surfactants.[26] Imidazole- and imidazolium-based polymers offer new avenues for biocompatibility and antimicrobial activity.[18] Most imidazolium salts have liquid crystalline properties and possess ion conductivity.[33] Imidazole-containing polymers enable hydrogels,[19] antiarrhythmics,[21] and anti-metastic agents.[22-23] These highly-stable, imidazole-based polymers suggest a plethora of emerging biophysical applications. Imidazole-based polymers open a new avenue to functional polymers and macromolecular design. The precursor polymer 2-[(1-imidazolyl)formyloxy]ethyl methacrylate (HEMAIm) provides new routes to multiple types of functional polymers, for example (Figure 9.12).[10]

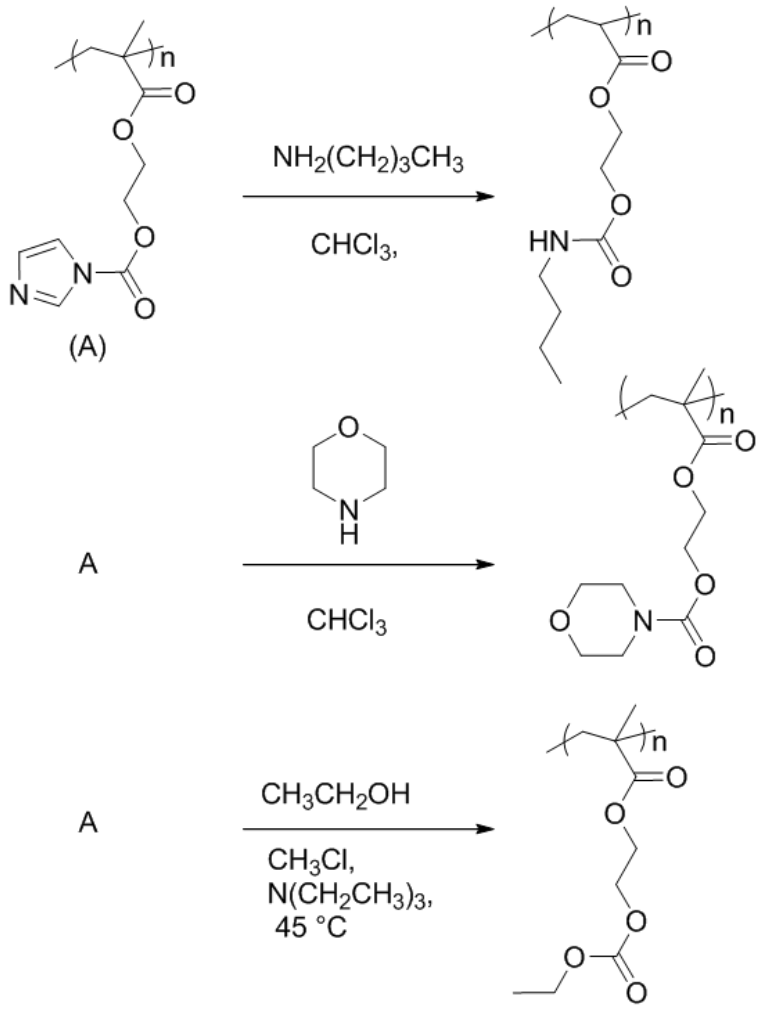

Figure 9.12. The versatile nature of the imidazolium backbone in the synthesis of functional polymers;[10] Elisabetta Ranucci, Gloria Spagnoli, Paolo Ferruti: 2-[(1-Imidazolyl)formyloxy]ethyl methacrylate as a new chemical precursor of functional polymer. *Macromolecular Rapid Communications*. 1999. Volume 20. Pages 4-5. Copyright Wiley-VCH Verlag GmbH & Co. KGaA. Reproduced with permission

Polyamides containing imidazoles that bind to the minor groove of DNA compete with transcription factors and block gene expression. A study utilizing a nude mouse xenograft model

showed that these types of polymers did inhibit the growth of estrogen receptors associated with human breast cancer cell Br 10 proliferation.[11] Sequence-specific DNA alkylation to prevent gene expression was achieved, indicating their potential use as antitumor drugs.[11]

The versatility of polymeric imidazoles and imidazolium salts extends beyond biology. Metal binding of the imidazole ring allows for oxygen transport. New steps in reversible oxygen-binding imidazole-based polymers complexed to cobalt allowed for the separation of oxygen from air. These polymer membranes achieve a high, oxygen transport of 28.[68] Furthermore, polyimidazolium electrolyte gels also show promising ionic conductivity above 1 x 10^{-3} S/cm.[67] Future development into dye-sensitized solar cells is a growing possibility. Templated assembly of imidazolium-based salts was even possible for rotaxanes with high selectivity, creating some of the first imidazolium-based interlocked catenanes.[79]

Step-growth chemistry and covalently crosslinked networks with the imidazolium functionality are especially sparse in the literature. Current efforts in our research group include using imidazolium diols (Figure 9.13) and bisacetoacetate-containing imidazolium salts (Figure 9.14) as monomers for both polyurethanes and networks from Michael addition reactions, respectively. These polyurethanes exhibited an ionic cluster transition in DMA, and increasing ionic hard segment content increasingly disrupted the flow region to produce highly physically crosslinked polymers.

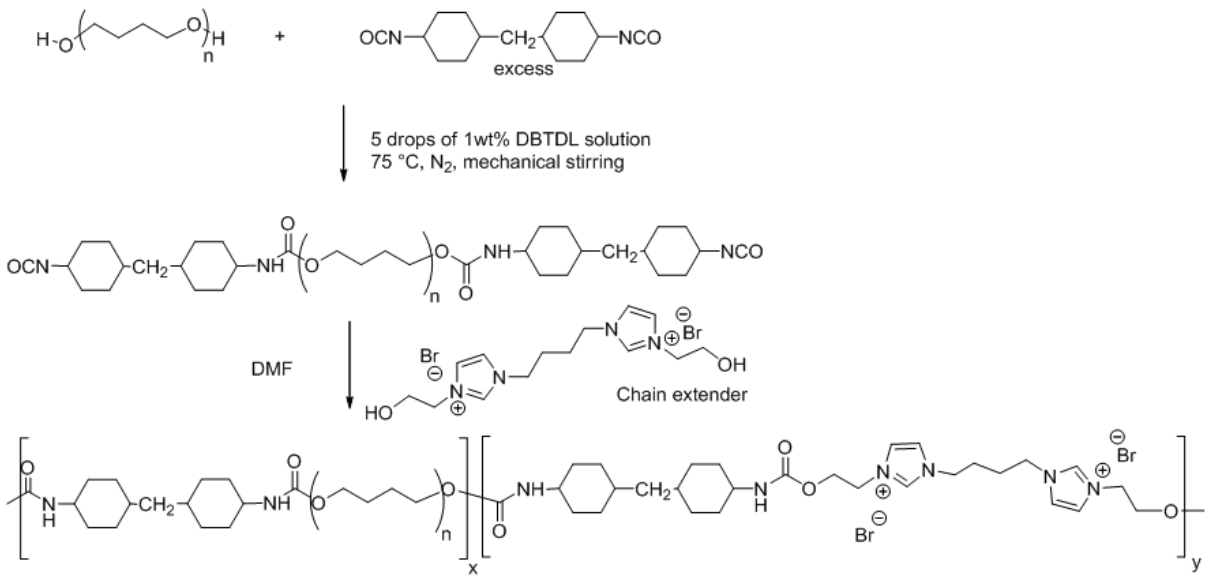

Figure 9.13. Polyurethane synthesis with an imidazolium diol as a chain extender

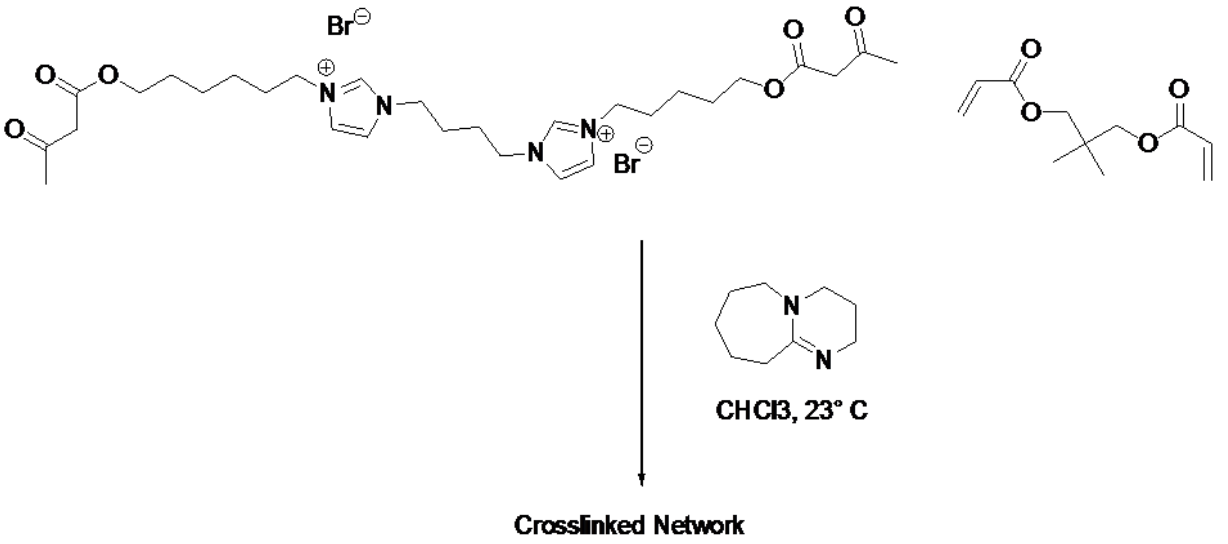

Figure 9.14. Bisacetoacetate-imidazolium salts used to synthesize networks from Michael addition reactions

We have recently demonstrated the synthesis of imidazolium-containing ionene segmented block copolymers from 1,10-(1,4-butanediyl)bis(imidazole) and 1,12-dibromododecane and 2000 g/mole PTMO dibromide (Figure 9.9).[76-78] The non-segmented imidazolium ionenes originated from Yanagida et al.[87] and Chen et al.[88] who used alkyl bis(imidazoles) and alkyl diiodides. The target for these original ethylene oxide-based ionenes was dye-sensitized solar cells. Our work involves examining the structure-property relationships of segmented-based imidazolium ionenes when changing charge density. These PTMO-based imidazolium ionenes possessed crystallinity, melting points near room temperature, and a glass transition temperature of -80 °C. Dynamic mechanical analysis (DMA) and small angle X-ray scattering (SAXS) also indicated microphase separation. The imidazolium ionene control that was not segmented with PTMO sequences had a glass transition of 27 °C.[76-78]

In addition to imidazolium-based polyurethanes and ionenes, we also pioneered the synthesis of imidazole-containing epoxide-based monomers and their subsequent ring-opening polymerization for electro-active devices. We have demonstrated the synthesis of *N*-tritylimidazole-2-ethylene oxide and *N*-tritylimidazole-4-ethylene oxide. Polymerization of these monomers was successfully initiated with potassium *t*-butoxide, and the trityl protecting group was quantitatively removed after polymerization with trifluoroacidic acid (TFA) (Figures 9.15 and 9.16).[89]

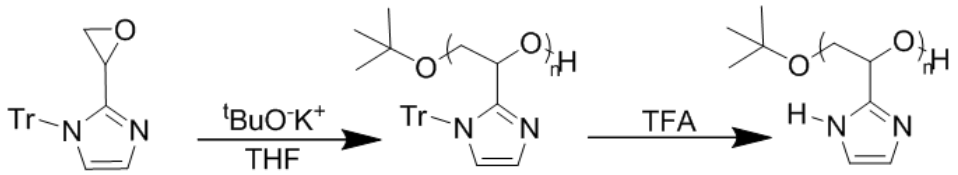

Figure 9.15. Anionic ring-opening polymerization of novel *N*-tritylimidazole-2-ethylene oxide;[89] Reproduced with permission from Ramirez, S. M.; Layman, J. M.; Bissel, P.; Long, T. E. *Macromolecules* **2009**, *42(21)*, 8010-8012. Copyright 2009 American Chemical Society

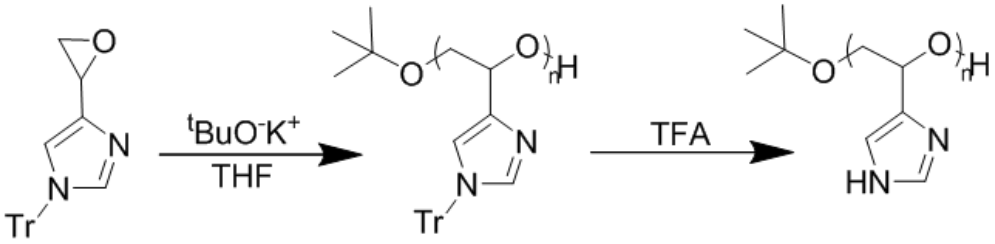

Figure 9.16. Anionic ring-opening polymerization of novel *N*-tritylimidazole-4-ethylene oxide;[89] Reproduced with permission from Ramirez, S. M.; Layman, J. M.; Bissel, P.; Long, T. E. *Macromolecules* **2009**, *42(21)*, 8010-8012. Copyright 2009 American Chemical Society

Upon deprotection, the imidazole-2-ethylene oxide polymer had a glass transition of 65 °C, slightly higher than the imidazole-4-ethylene oxide containing polymer with a glass transition of 50 °C. We are currently investigating the alkylation of the imidazole backbone with various bromoalkyls to determine structure-property relationships with various levels of alkylation to imidazolium salts. We are also investigating the effect of different vinyl group positions on the thermo-mechanical properties, fiber formation, biological binding, and conductivity. Additionally, we are exploring the synthesis of linear, living 1-vinylimidazolium,

2-vinylimidazolium, and 4-vinylimidazolium polymers and block copolymers using Blockbuilder® for nitroxide-mediated polymerization (Figure 9.17).

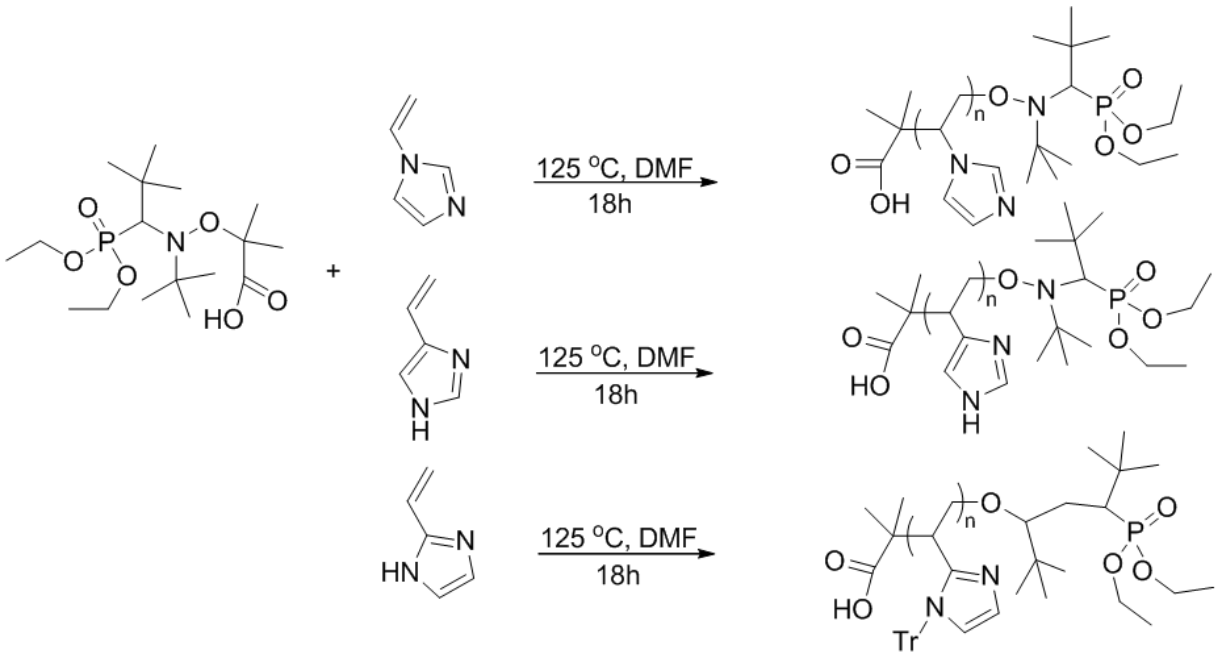

Figure 9.17. Synthesis of linear, 1-,4-, and 2-vinylimidazole-based polymers via living nitroxide-mediated polymerization

In summary, the design of imidazole derivatives and imidazolium-containing polymers enables many new applications. Imidazole-based polymers readily associate with biological molecules, drugs, metals, and proteins through hydrogen-bonding, and imidazolium derivatives offer electrostatic interactions, aggregation, and structured self-assembly. The authors hope to encourage the design of novel imidazole- and imidazolium-based polymers as a fascinating and promising field. Many applications exist in biology and material science for these polymers. Studies have investigated the cytotoxicity, antifibrotic, and anti-metastic properties of several small molecule imidazolium salts or ionic liquids *in vitro*,[30-32] but *in vitro* study of polymeric

imidazolium salts is a new area requiring much research. Investigation of imidazolium-based polymers as transfection agents also is an unexplored area. In material science, imidazolium-based polymers expand the scope of ionic polymers for transducers, actuators, and all other types of responsive applications. Although conductivity measurements indicate that imidazolium-based polymers do improve performance, continued device studies are needed. Overall, a wealth of potential applications and further research exists for imidazolium-based polymers.

9.6 References

1. Kolb, H. C.; Sharpless, K. B. *Drug Discovery Today* **2003**, *8(24)*, 1128-1137.
2. Keppler, B. K.; Wehe, D; Endres, H; Rupp, W. *Inorg. Chem.* **1987**, *26*, 844-846.
3. Brédas, J. L.; Poskin, M. P.; Delhalle, J.; André, J. M.; Chojnacki, H. *J. Phys. Chem.* **1984**, *88*, 5882-5887.
4. Hofmann, K. The Chemistry of Heterocyclic Compounds, Imidazole and Derivatives Part 1. New York: Interscience Publishers, Inc.; 1953.
5. Organ, M. G.; Avola, S.; Dubovyk, I.; Hadei, N.; Kantchev, E. A. B.; O'Brien, C. J.; et al. *Chem. Eur. J.* **2006**, *12*, 4749-4755.
6. Catalano, V. J.; Etogo, A. O. *Inorg. Chem.* **2007**, *46*, 5608-5615.
7. Samantaray, M. K.; Katiyar, V.; Pang, K.; Nanavati, H.; Ghosh, P. *J. Organomet. Chem.* **2007**, *692*, 1672-1682.
8. Preethi, N.; Shinohara, H.; Nishide, H. *Reactive Funct. Polym.* **2006**, *66*, 851-855.
9. Le Poul, N.; Campion, M.; Douziech, B.; Rondelez, Y.; Le Clainche, L.; Reinaud, O.; et al. *J. Am. Chem. Soc.* **2007**, *129*, 8801-8810.
10. Ranucci, E.; Spagnoli, G.; Ferruti, P. *Macromol. Rapid Comm.* **1998**, *20*, 1-6.
11. Bando, T.; Sugiyama, H. *Acc. Chem. Res.* **2006**, *39*, 935-944.
12. De Luca, L. *Curr. Med. Chem.* **2006**,*13*, 1-23.
13. Hamilton, C. A. *Pharmacol. Ther.* **1992**, *54(3)*, 231-248.
14. Grimmett, M. R. Imidazole and Benzimidazole Synthesis. Academic Press, Inc.; 1997.
15. Lee, S.-G. *Chem. Comm*. **2006**,1049-1063.
16. El Seoud, O. A.; Koschella, A.; Fidale, L. C.; Dorn, S.; Heinze, T. *Biomacromolecules* **2007**, *8(9)*, 2629-2647.
17. Yu, B.; Zhou, F.; Hu, H.; Wang, C.; Liu, W. *Electrochimica Acta* **2007**, *53*, 487-494.
18. Demberelnyamba, D.; Kim, K.-S.; Choi, S.; Park, S.-Y.; Lee, H.; Kim, C.-J.; et al. *Bioorg. Med. Chem.* **2004**, *12*, 853-857.
19. Batra, D.; Hay, D. N. T.; Firestone, M. A. *Chem. Mater.* **2007**, *19*, 4423-4431.
20. Batra, D. Seifert, S.; Firestone, M. A. *Macromol. Chem. Phys.* **2007**, *208*, 1416-1427.
21. Lis, R.; Davey, D. D.; Morgan, T. K.; Lumma, W. C.; Wohl, R. A.; Jain, V. K.; et al. *J. Med. Chem.* **1987**, *30*, 2303-2309.

22. Sanna, B.; Debidda, M.; Pintus, G.; Tadolini, B.; Posadino, A. M.; Bennardini, F. et al. *Arch. Biochem. Biophys.* **2002**, *403*, 209-218.
23. Sarna, S.; Bhola, R. K. *Toxicol. Int.* **2007**, *14(1)*, 83-87.
24. Liu, Z. C.; Zhou, C. H.; Xie, R. G. *Chin. Chem. Lett.* **1997**, *8(5)*, 387-388.
25. Blasig, A.; Tang, J.; Hu, X.; Tan, S. P.; Shen, Y.; Radosz, M. *Ind. Eng. Chem. Res.* **2007**, *46*, 5542-5547.
26. Evans, K. O. *Colloid Surface Physicochem. Eng. Aspect* **2006**, *274*, 11-17.
27. Cho, M. S.; Seo, H. J.; Nam, J. D.; Choi, H. R.; Koo, J. C.; Lee, Y. *Smart Mater. Struct.* **2007**, *16*, S237-242.
28. Durant, G. J.; Ganellin, C. R.; Parsons, M. E. *J. Med. Chem.* **1975**, *18(9)*, 905-909.
29. He, X.; Chan, T. H. *Synthesis* **2006**, 1645-1651.
30. Frade, R. F. M.; Rosatella, A. A.; Marques, C. S.; Branco, L. C.; Kulkarni, P. S.; Mateus, N. M. M.; et al. *Green Chem.* **2009**, 11, 1660-1665.
31. Zhang, C.; Ding, Z.; Suhaimi, N. M.; Kng, Y. L.; Zhang, Y.; Zhuo, L. A Class of Imidazolium Salts is Anti-oxidative and Anti-fibrotic in Hepatic Stellate Cells. *Free Radic. Res.* **2009**, *43(10)*, 899-912. First published on 07 August 2009 (iFirst).
32. Gava B, Zorzet S, Spessotto P, Cocchietto M, Sava G. JPET 2006;317(1):284e91.
33. Dupont J.; Suarez, P. A. Z. *Phys. Chem. Chem. Phys.* **2006**, *8*, 2441-2452.
34. Welton, T. Coord. *Chem. Rev.* **2004**, *248*, 2459-2477.
35. Welton, T. *Chem. Rev.* **1999**, *99*, 2071-2083.
36. Wasserscheid, P.; Keim, W. *Angew. Chem. Int. Ed.* **2000**, *39*, 3773-3789.
37. Dupont, J.; de Souza, R. F.; Suarez, P. A. Z. *Chem. Rev.* **2002**, *102*, 3667-3691.
38. Cang, H.; Li, J.; Fayer, M. D. *J. Chem. Phys.* **2003**, *119(34)*, 13017-13023.
39. Beste, Y.; Eggersmann, M.; Schoenmakers, H. *Chem. Ing. Tech.* **2005**, *77(11)*, 1800-1808.
40. Amyes, T. L.; Diver, S. T.; Richard, J. P.; Rivas, F. M.; Toth, K. *J. Am. Chem. Soc.* **2004**, *126*, 4366-4374.
41. Arduengo, A. *J. Acc. Chem. Res.* **1999**, *32*, 913-921.
42. Aggarwal, V. K.; Emme, I.; Mereu, A. *Chem. Comm.* **2002**, 1612-1613.
43. Xu, L. J.; Chen, W. P.; Xiao, J. L. *Organometallics* **2000**, *19*, 1123-1127.
44. McLachlan, F.; Mathews, C. J.; Smith, P. J.; Welton, T. *Organometallics* **2003**, 22, 5350-5357.
45. Hasan, M.; Kozhevnikov, I. V.; Siddiqui, M. R. H.; Femoni, C.; Steiner, A.; Winterton, N. *Inorg. Chem.* **2001**, *40*, 795-800.
46. Oxley, J. D.; Prozorov, T.; Suslick, K. S. *J. Am. Chem. Soc.* **2003**, *125*, 11138-11139.
47. Dullius, J. E. L.; Suarez, P. A. Z.; Einloft, S.; de Souza, R. F.; Dupont, J.; Fischer, J.; De Cian, A. *Organometallics* **1998**, *17*, 815-819.
48. Gao, S. Y.; Zhang, H. J.; Wang, X. M.; Mai, W. P.; Peng, C. Y.; Ge, L. H. *Nanotechnology* **2005**, *16*, 1234-1237.
49. Huang, J.; Jiang, T.; Han, B. X.; Wu, W. Z.; Liu, Z. M.; Xie, Z. L.; et al. *Catal. Lett.* **2005**, *103*, 59-62.
50. Tatumi, R.; Fujihara, H. *Chem. Comm.* **2005**, 83-85.
51. Lee, B. S.; Lee, S. *Bull. Korean Chem. Soc.* **2004**, *25*, 1531-1537.
52. Mu, X. D.; Evans, D. G.; Kou, Y. A. *Catal. Lett.* **2004**, *97*, 151-154.
53. Wei, G. T.; Sang, Z.; Lee, C. Y.; Yang, H. Y.; Wang, C. R. C. *J. Am. Chem. Soc.* **2004**, *126*, 5036-5037.

54. Kim, K. S.; Demberelnyamba, D.; Lee, H. *Langmuir* **2004**, *20*, 556-560.
55. Lee, B. S.; Chi, Y. S.; Lee, J. K.; Choi, I. S.; Song, C. E.; Namgoong, S. K.; et al. *J. Am. Chem. Soc.* **2004**, 126, 480-481.
56. Huang J.; Jiang, T.; Han, B. X.; Gao, H. X.; Chang, Y. H.; Zhao, G. Y.; et al. *Chem. Comm.* **2003**, *1*, 1654-1655.
57. Zhao, D. B.; Fei, Z. F.; Scopelliti, R.; Dyson, P. *J. Inorg. Chem.* **2004**, *43*, 2197-2205.
58. Mu, X. D.; Meng, J. Q.; Li, Z. C.; Kou, Y. *J. Am. Chem. Soc.* **2005**, *127*, 9694-9695.
59. Binnemans, K. *Chem. Rev.* **2005**, *105*, 4148-4204.
60. Bowlas, C. J.; Bruce, D. W.; Seddon, K. R. *Chem. Comm.* **1996**, *1*, 1625-1626.
61. Kazarian, S. G.; Briscoe, B. J.; Welton, T. *Chem. Comm.* **2000**, *1*, 2047-2048.
62. Ott, L. S.; Cline, M. L.; Deetlefs, M.; Seddon, K. R.; Finke, R. G. *J. Am. Chem. Soc.* **2005**, *127*, 5758-5759.
63. Bacciu, D.; Cavell, K. J.; Fallis, I. A.; Ooi, L.-L. *Angew. Chem. Int. Ed.* **2005**, *44*, 5282-5284.
64. Mathews, C. J.; Smith, P. J.; Welton, T.; White, A. J. P.; Williams, D. J. *Organometallics* **2001**, *20*, 3848-3850.
65. Fonseca, G. S.; Umpierre, A. P.; Fichtner, P. F. P.; Teixeira, S. R.; Dupont, *J. Chem. Eur. J.* **2003**, 9, 3263-3269.
66. Dupont, J.; Fonseca, G. S.; Umpierre, A. P.; Fichtner, P. F. P.; Teixeira, S. R. *J. Am. Chem. Soc.* **2002**, *124*, 4228-4229.
67. Yu, B.; Zhou, F.; Wang, C.; Liu, W. *Eur. Polym. J.* **2007**, *43*, 2699-2707.
68. Shinohara, H.; Shibata, H.; Wöhrle, D.; Nishide, H. *Macromol. Rapid Comm.* **2005**, *26*, 467-470.
69. Eisenberg, A.; Hird, B.; Moore, R. B. *Macromolecules* **1990**, *23*, 4098-4107.
70. Eisenberg, A.; King, M. *Ion-Containing Polymers.* New York: Academic Press; 1977.
71. Eisenberg A., Kim, J. S. *Introduction to Ionomers.* New York: John Wiley & Sons, Inc.; 1998.
72. Litschauer, M.; Peterlik, H.; Neouze, M.-A. *J. Phys. Chem. C* **2009**, *113*, 6547-6552.
73. Batra, D.; Seifert, S.; Varela, L. M.; Liu, A. C. Y. Firestone, M. A. *Adv. Funct. Mater.* **2007**, *17*, 1279-1287.
74. Baird, E. E.; Dervan, P. B. *J. Am. Chem. Soc.* **1996**, *118*, 6141-6146.
75. Matsumi, N.; Sugai, K.; Miyake, M.; Ohno, H. *Macromolecules* **2006**, 39, 6924-6927.
76. Williams, S. R.; Cruz, D. S.; Winey, K. I., Long, T. E. Ionene segmented block copolymers containing imidazolium cations: structure-property relationships as a function of hard segment content, *Polymer*, submited for publication.
77. Williams, S. R.; Long, T. E. *Prog. Polym. Sci.* **2009**, *34(8)*, 762-782.
78. Williams, S. R. Influence of Electrostatic Interactions and Hydrogen Bonding on the Thermal and Mechanical Properties of Step-Growth Polymers, Ph.D. Thesis, Virginia Tech (Blacksburg), 2008.
79. Beer, P. D.; Sambrook, M. R.; Curiel, D. *Chem. Comm.* **2006**, 2105-2117.
80. Nakajima, H.; Ohno, H. *Polymer* **2005**, *46*, 11499-11504.
81. Narita, A.; Shibayama, W.; Matsumi, N.; Ohno, H. *Polym. Bull.* **2006**, *57*, 109-114.
82. Marwanta, E.; Mizumo, T.; Ohno, H. *Solid State Ionics* **2007**, *178*, 227-232.
83. Kamplain, J. W.; Bielawski, C. W. *Chem. Comm.* **2006**, 1727-1729.
84. Tennyson, A. G.; Kamplain, J. W.; Bielawski, C. W. *Chem. Comm*. **2009**, 2124-2126.

85. Bianchi, A.; Bowman-James, K.; Garcia-Espana, E.; Eds. *Supramolecular Chemistry of Anions.* New York: Wiley-VCH; 1997.
86. Yoon J.; Kim, S. K.; Singh, N. J.; Kim, K. S. *Chem. Soc. Rev.* **2006**, *35*, 355-360.
87. Suzuki, K.; Yamaguchi, M.; Hotta, S.; Tanabe, N.; Yanagida, S. *J. Photochem. Photobio. A Chem* **2004**, 164, 81-85.
88. Li, F.; Cheng, F.; Shi, J.; Cai, F.; Liang, M.; Chen, J. *J. Power Sourc.* **2007**, *165*, 911-915.
89. Ramirez, S. M.; Layman, J. M.; Bissel, P.; Long, T. E. *Macromolecules* **2009**, *42(21)*, 8010-8012.

Chapter 10. Synthesis and Cytotoxicity of Main-Chain Imidazolium-Based Interfacial Polyesters

10.1 Abstract

A new class of biocompatible and biodegradable polyesters for medical applications was synthesized from imidazolium-containing monomers. We report the synthesis of a novel imidazolium-based diol monomer and its incorporation into a series of aliphatic polyesters with PEG comonomer and adipoyl dichloride. The aliphatic acid chloride, adipoyl dichloride, and two diols were reacted via interfacial polymerization utilizing a water phase and a chloroform organic phase to polymerize the monomers at the interface. Acid chloride to hydroxyl molar ratio was maintained at 1:1 for all reactions. Although a 1:1 molar ratio of acid chloride to diol was maintained, the diol to diol ratio of the two diol comonomers was varied. The molar ratio of an imidazolium diol to a 200 g/mole PEG was varied in order to synthesize polyesters with 100/0, 88/12, 50/50, and 12/88 molar ratios. Cytotoxicity studies indicated that all polymers were relatively non-cytotoxic regardless of their ratio of PEG to imidazolium diol. Cell viability was greater than 90% in all cases, even with increased concentrations of ionic sites along the main chain. Including the imidazolium cation in the main-chain structure uniquely allowed these ionic polymers to remain non-toxic unlike imidazolium-based polymers with pendant ionic sites or long alkyl chains.

10.2 Introduction

Imidazolium-based polymers have numerous applications as biological macromolecules. The imidazole ring exists in the nucleic acids guanine and adenine and in the amino acids histidine and histamine.[1] Histamine is derived from decarboxylation of histidine and is involved in allergic

responses.[2-3] Imidazolium-based polymers find purpose in a variety of applications and compounds including as metal ligands,[4] biomimetic derivatives,[5] cancer therapeutics,[4] and enzyme inhibition reagents.[1] Gene therapy involves the delivery of plasmid DNA that will transfect or deliver expression of a desired or often deficient protein.[6-7] However, efficient delivery and release of DNA into the nucleus of cells is often a problem. Delivery and release of the DNA with polyelectrolyte-based polyplexes, polymer bound DNA, has been increasingly studied,[7-10] and we have examined ammonium-based polyplexes in our research group.[7] Polycations bind to DNA through electrostatic interactions with the negatively-charged phosphates. The polyelectrolytes used to help deliver DNA must also be non-cytotoxic.[7] Fundamental relationships between polymer structure, cytotoxicity, and binding capability to DNA are of great use to designing non-toxic polymers that efficiently deliver and release DNA inside cell nuclei. Study of imidazolium-based polymers is advantageous due to the biocompatibility of the imidazolium ion.[1-3, 5]

Synthesis of imidazolium salts involves alkylation of both nitrogens in the imidazole ring. These salts are able to aggregate electrostatically due to supramolecular interactions. Imidazolium salts have low melting points and are often ionic liquids due to the low energy required to break the ionic associations between large ions.[11-13] Their large cations are difficult to assemble into crystallites.[11-13] The synthesis of imidazolium-containing hydrogels led to their potential use as biomimetic cavities. These charged, physically cross-linked gels swell to set dimensions, a property critical in medical applications such as in artificial muscles.[14]

In this dissertation, we report the synthesis of imidazolium-based aliphatic polyesters and PEG-containing copolymers through interfacial reactions. We systematically varied the ratio of the two diols (PEG to imidazolium diol) while maintaining a 1:1 total hydroxyl to acid chloride molar ratio to produce a series of copolyesters with varied imidazolium content. The subsequent polymers

were analyzed for cytotoxicity and DNA binding efficiency. The main-chain imidazolium polyesters were found to be non-cytotoxic, but it is proposed that their main-chain ionic structure restricted accessibility of ionic groups for binding DNA.

10.3 Experimental

10.3.1 Materials

Adipoyl dichloride (ADCL, >99%) was purchased from Aldrich and recrystallized from ethyl acetate. Triethylamine (TEA, >99%) and chloroform from Aldrich were distilled from calcium hydride. Bisphenol A (99%), sodium hydroxide (99%), tetraethylammonium iodide (98%), 2-bromoethanol (95%), imidazole (99%), 1,4-dibromobutane (99%), chloroform (99.5%), methanol (99%), PEG (200 g/mol), and HPLC-grade water were purchased from Aldrich and used as received. Penicillin, heat-inactivated fetal bovine serum (FBS), and streptomycin were purchased from Mediatech. Dulbecco's modified Eagle medium (DMEM) was purchased from Invitrogen. 3-[4,5-Dimethylthiazol-2-yl]2,5-diphenyltetrazolium bromide (MTT), ethidium bromide, and 50X TAE buffer (which contains Trizma® base (tris base), ethylenediaminetetraacetic acid (EDTA), glacial acetic acid, and water) was purchased from Aldrich. Water was purified with a Millipore Direct-Q5 water purification system. Theresa Reineke from Virginia Tech provided African green monkey kidney fibroblast cells. Agarose powder was purchased from BioRad Laboratories.

10.3.2 Synthesis of Bisimidazole with a Butane Spacer

Synthesis of the bisimidazole followed a procedure reported in the literature[15] and described in chapter 4 of this thesis.

10.3.3 Synthesis of Bisimidazolium Diol

Synthesis of this bisimidazolium diol based on 2-bromoethanol followed a literature procedure.[16] A 1-neck, round-bottom flask with a Teflon® stir bar was flame-dried. Bisimidazole with a butane spacer (2.32 g, 0.0122 mol) was charged into the flask. The flask and contents were purged with argon for 30 min. Then 2-bromoethanol (2.57 mL, 0.0366 mol) in 3-fold excess was charged into the flask under argon, and 18 mL of dry chloroform was added. The reaction was purged with argon for an additional 30 min and then allowed to proceed at 65 °C under an argon blanket for 24 h. The product was precipitated in ethyl ether and dried under reduced pressure in a vacuum oven at 60 °C overnight. The yields were approximately 80%. ^{1}H NMR (400 MHz, 25 ºC) in CD_3OD: δ (ppm) 2.252-2.522 (m, 4H), 4.175-4.386 (m, 4H), 4.616-4.847 (m, 8H), 7.992-8.203 (m, 4H), 9.405-9.585 (m, 2H). FAB mass spectrometry m/z (+FAB, 100% M^+, exact mass, direct probe) provided 358.12 g/mol for the exact mass which matches the calculated value of 358.22 g/mol for M^+Br^- with one rather than two bromide counteranions resolved. The melting point was 129-131 °C (DSC, 20 °C/min, heat/cool/heat -80 to 190 °C nitrogen).

10.3.4 Synthesis of Imidazolium-Containing Polyesters: Interfacial Homopolymer

The imidazolium diol monomer (1.01 g, 0.00243 mol) was dissolved completely with HPLC-grade water (5 mL) in a vial with tetraethylammonium iodide (0.01 g) phase transfer catalyst. ADCL (0.444 g, 0.00243 mols) was added to a flame-dried 250-mL, 1-neck, round-bottom flask and this was followed by immediate addition of 0.25 g (0.00243 mols) of TEA. $CHCl_3$ (5 mL, 10 wt % solids) was added to the reaction flask. The mixture was allowed to dissolve completely before addition of the aqueous phase. The aqueous phase was added slowly to the reaction flask while stirring. The reaction flask was kept under nitrogen with vigorous stirring for 24 h at 25 °C. $CHCl_3$

(50 mL) and HPLC-grade water (50 mL) were added, and the product was collected and dried in a vacuum oven at 60 °C. The product remained in the aqueous phase. Dialysis in HPLC-grade water with a 1300 g/mol cut-off membrane was used to remove excess phase transfer catalyst and residual monomer, and the polymer was subsequently dried under reduced pressure for 12 h at 60 °C.

10.3.5 Synthesis of Imidazolium-Containing Copolymers with PEG

The same procedure was followed for the interfacial copolymerization except a 200 g/mol PEG was used as a comonomer. The diol to diacid stoichiometry was maintained in a 1:1 molar ratio. Polymers with 88/12, 50/50, and 12/88 molar ratio of imidazolium diol to polyethylene glycol were targeted. All final polymers were water soluble. Dialysis with a 1300 g/mol cutoff membrane for 24 to 72 hours and changing the water every 3 h for the first 12 h removed residual monomer and phase transfer catalyst. The product was dried in a vacuum oven under reduced pressure for 12 h at 60 °C before analysis.

10.3.6 Characterization

^{1}H NMR spectra were collected in $CDCl_3$ and CD_3OD on a Varian 400 MHz spectrometer. DSC was instrumented with a Perkin Elmer Pyris 1 under nitrogen with a heating rate of 20 ºC/min. Values from the second heating scan were reported. TGA was instrumented with a Perkin-Elmer TGA 7 at a heating rate of 10 °C/min under nitrogen.

10.3.7 Cell Culture

The cell culture procedure closely followed our previous work.[7, 17] Dr. Theresa Reineke (Virginia Tech) provided all African green monkey kidney fibroblast cells (COS-7) cells for these

experiments. COS-7 cells were immersed in Dulbecco's Eagle medium (DMEM) with 10% heat-inactivated fetal bovine serum (FBS), 1 mg/mL penicillin, and 100 μg/mL streptomycin. The cells were incubated at 37 °C in an atmosphere of 5% CO_2.

10.3.8 Cell Viability Assay

The cell viability assay closely followed our previous work.[7, 17] The polymers were dissolved to 1 mg/mL in ultrapure water (resistivity 18.2 MΩ·cm, purified with Millipore Direct-Q5 water purification system). Then a 200-μL addition of a 1 mg/mL polymer solution was diluted with DMEM to a concentration of 0.8 μg/mL. 3-[4,5-Dimethylthiazol-2-yl]2,5-diphenyltetrazolium bromide (MTT) assays were used to analyze cytotoxicity. COS-7 cells were plated at 5000 cells/well on 96-well plates for 24 h before each experiment and were washed with 100 μL of DMEM per well. Then 100 μL of polymer solution was added to each of the wells, and the cells were incubated for 24 h under an atmosphere with 5% CO_2 at 37 °C. Then 100 μL of DMEM with 0.5 mg/mL of MTT was added. After 4 h, the solutions were aspirated, and 100 μL of DMSO was added to dissolve the products. A Molecular Devices Corp. SPECTRAmax M2 microplate reader was used to measure the absorbance at 570 nm for each well.

10.3.9 Gel Electrophoresis of Imidazolium-Based Polyester Polyplexes with DNA

The procedure closely followed our previous work.[7] Agarose and 1X TAE buffer were used to make 0.9 weight % gels for electrophoresis. A 50X TAE stock solution is made of 1700 g tris base, 400 mL of glacial acetic acid, and 700 mL of 0.5 M EDTA with 4 L of purified water. The solution is stirred, and then water is added until a 7 L total stock solution is made. To make a 1X TAE solution, 40 mL of 50X TAE is diluted to 2 L with water. Microcentrifuge tubes (1 mL) were

used for the polymer solutions. Polymer and DNA stock solutions were made with 1X TAE buffer. Then 0.5 μL of 0.2 μg/μL DNA stock solution was stirred with 0.2 to 0.8 μL of 1μg/μL polymer stock solution maintaining a DNA to polymer N/P ratio of 4 based on the polymer repeating unit structure. The solutions were diluted with 35 μL of a mixture of 28 μL of 1X TAE buffer and 7 μL of 1X TAE containing 40 weight % sucrose. Polyplexes formed over 30 minutes before loading the agarose gels. Then 75 V were applied to the loaded gels submerged in 1X TAE buffer over a period of 90 min. Ethidium bromide was used to stain the gels and photograph them with a UV transilluminator and digital camera.

10.4 Results and Discussion

10.4.1 Synthesis of Homopolymer and Copolymers

A bisimidazolium diol was synthesized through a S_N2 reaction of excess 2-bromoethanol and bisimidazole (Figure 10.1).[16] This monomer was synthesized from bisimidazole and excess 2-bromoethanol, unlike the bisimidazolium monomer in chapter 4 which was synthesized from reaction of bisimidazole with excess 6-bromohexanol.

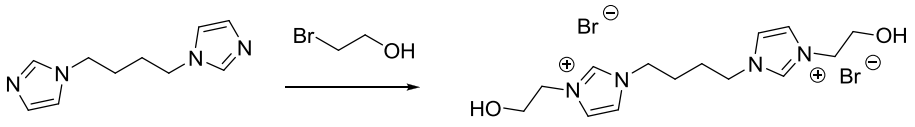

Figure 10.1. Synthesis of bisimidazolium diol monomer

The synthesis of homopolymers was facilitated through interfacial reaction conditions (Figure 10.2). The resultant polymers were separated from the water phase. After drying in a vacuum oven

overnight at 60 °C, dialysis with a molecular weight cut-off membrane of 1300 g/mole was utilized to purify the polymer and remove residual phase transfer catalyst. After dialysis, the polymers were dried under reduced pressure at 60 °C overnight before analysis. The 1:1 molar ratio of charged diacid to diol was maintained for all polymers, but the ratio of bisimidazolium diol to PEG was varied: 88/12, 50/50, and 12/88.

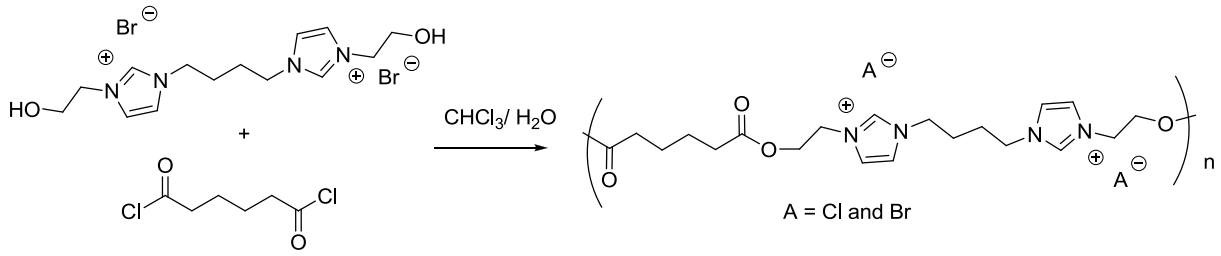

Figure 10.2. Synthesis of imidazolium-containing polyester homopolymers

Synthesis of copolymers was facilitated through interfacial reaction conditions (Figure 10.3). The final 88/12, 50/50, and 12/88 copolymers with imidazolium diol and PEG remained in the water phase. The polymers were dialyzed in water with a 1300 g/mole cut-off to remove any residual monomer or phase transfer catalyst. The polymers were lyophilized for 24 hours before performing cytotoxicity studies.

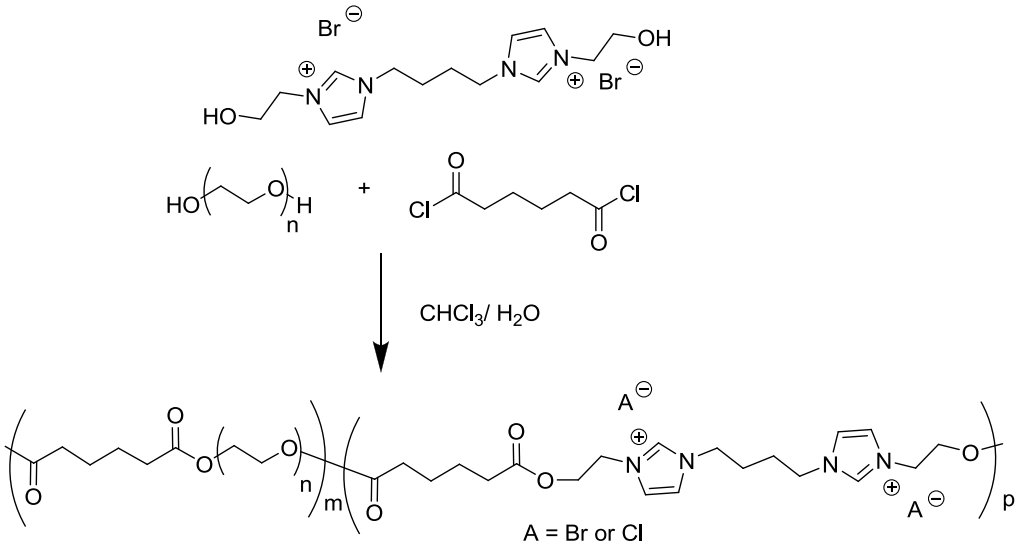

Figure 10.3. Synthesis of imidazolium-containing copolyesters

10.4.2 Thermal Analysis

Thermogravimetric analysis of imidazolium-based polyesters showed that the onset of degradation of the polymer occurred at a lower temperature than the precursor imidazolium diol. Bromide counterions were exchanged for chloride counterions during interfacial polymerization due to the use of acid chlorides. The imidazolium diol monomer had an onset of degradation of 266 °C (TGA ramp, 10 °C/minute, 25 to 800 °C) (Figure 10.4). The imidazolium homopolymer had an onset of degradation of 198 °C (TGA ramp, 10 °C/minute, 25 to 600 °C) (Figure 10.5). Future experiments to exchange the polymer counteranions post-reaction are suggested to remove inconsistencies in composition as well as improve thermal stabilities. Counteranion exchange may especially have importance for mechanical performance and electrical conductivity for future studies. In this thesis, we examined the cytotoxicity of the polymers in aqueous solution. Thermal degradation of alkylene-containing imidazolium monomers is suggested to occur through β-H elimination, producing

imidazole and vinyl products.[18] This facile elimination prevents alkylene-containing imidazole monomers from having a high thermal stability, even though the imidazole ring and imidazolium salts are known for their enhanced chemical and thermal stabilities.[19]

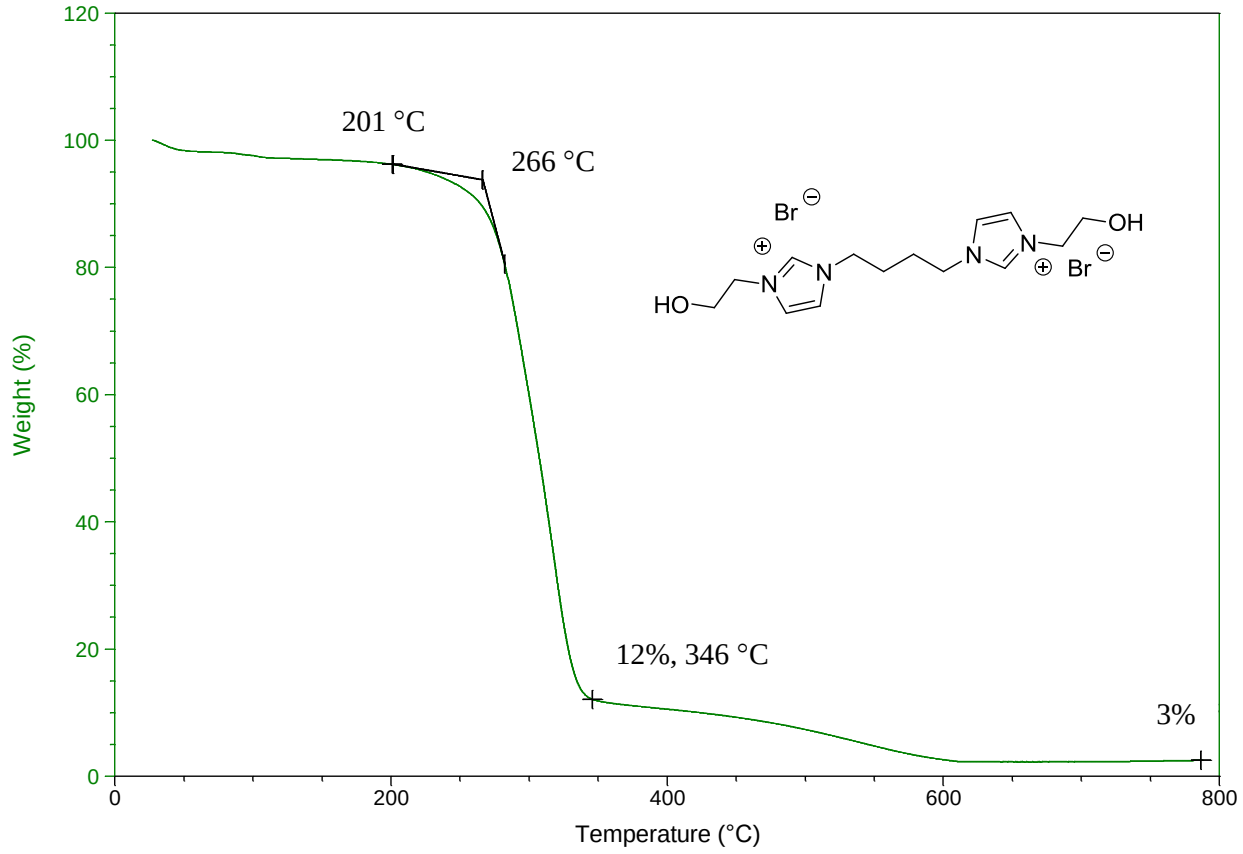

Figure 10.4. TGA thermogram of the imidazolium diol monomer; ramp 10 ºC/minute to 800 ºC, nitrogen

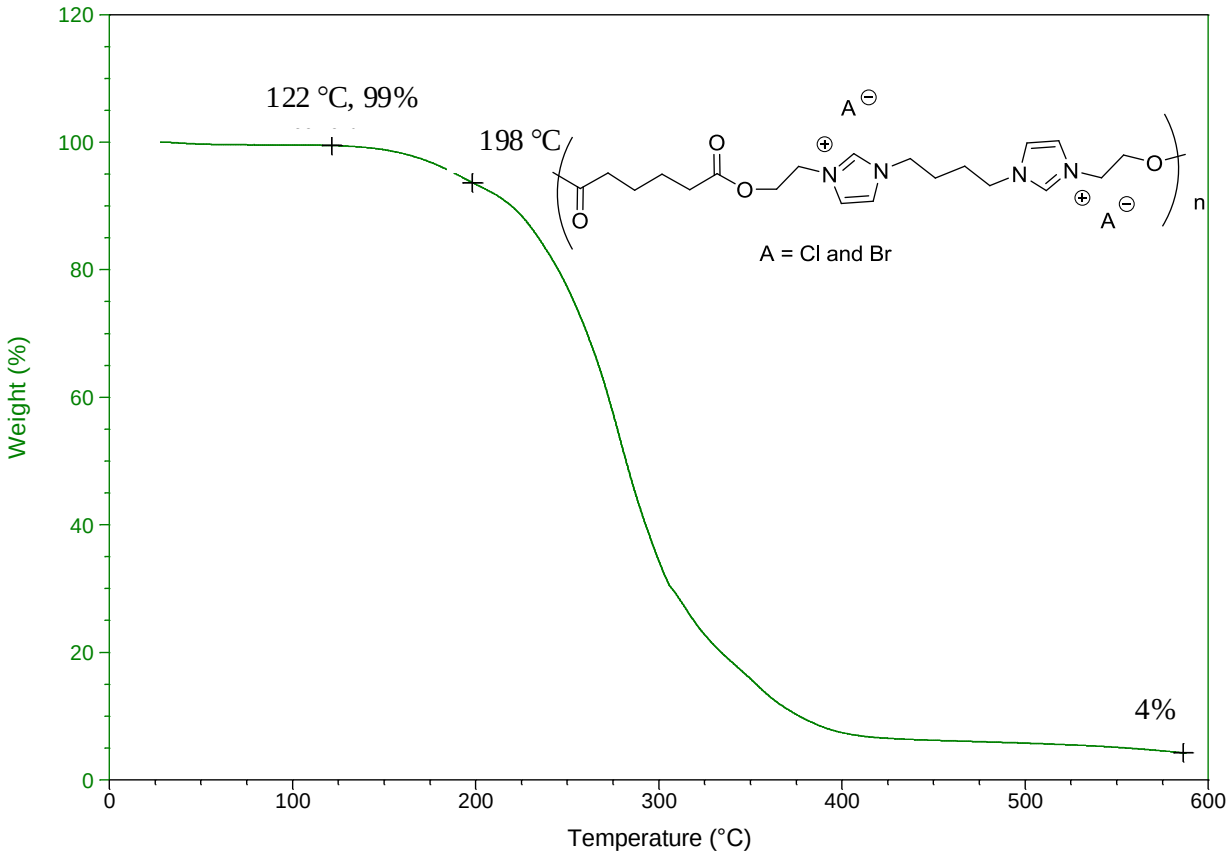

Figure 10.5. TGA thermogram of imidazolium-containing polyester homopolymers; ramp 10 ºC/minute to 600 ºC, nitrogen

The imidazolium-based homopolymer exhibited a glass transition temperature of -26 °C (Table 10.1). DSC data indicated two glass transitions for the 50/50 copolymer of -45 and -54 °C. It is hypothesized that this possibly indicated that the copolymerization resulted in block or segmented compositions with some phase separation. Typically a phase transfer catalyst is added during these reactions. The imidazolium diol itself also acts as a phase transfer catalyst and is soluble in both the chloroform and water phases, possibly causing preferential addition of the imidazolium diol before PEG. This is proposed to create a block or segmented structure in the resultant polymers, causing phase separation and the appearance of more than one glass transition temperature. However, this

result is not definitive for the segmented or block structure. Analysis with AFM and TEM images are needed to confirm this hypothesis but were difficult due to the films' rapid water absorption upon contact with air. Also, phase mixing must exist to achieve the low glass transition temperatures. All other homopolymers and copolymers possessed at least one glass transition temperature, but a second one was not observable. All other polymers displayed a glass transition temperature around or lower than -26 °C, the glass transition of the imidazolium homopolymer. The 88/12 imidazolium to PEG copolymer had a glass transition temperature at -34 °C, and the 12/88 PEG to imidazolium copolymer exhibited a glass transition at -24 °C. The variation of the glass transition temperature is dependent on molecular weight for low molar mass polymers, and SEC characterization is needed for further evaluation. Although dialysis was conducted with a 1300 g/mole cut-off bag, the actual polymer molecular weights still need to be analyzed. These ionic polymers aggregate in typical SEC solvents by dynamic light scattering, and future work will involve identification of a good solvent with little aggregation for molecular weight analysis with aqueous SEC.

Table 10.1. DSC of imidazolium-based homopolymer and copolymers

IM/PEG Ratio	DSC T_g^1 (°C)	DSC T_g^2 (°C)
100/0	-26	---
88/12	-24	---
50/50	-45	-54
12/88	-34	---

*DSC: 20 ºC/minute, nitrogen

10.4.3 Evaluation of Cytotoxicity

Cytotoxicity experiments involved culturing cells from a monkey kidney fibroblast cell line, COS-7, and MTT assays.[7, 17] The COS-7 cell line is used in our laboratories for DNA transfection studies as well as cytotoxicity investigations. Mosmann et al. founded the MTT assay, which is now used universally for analysis of cytotoxicity.[20-22] The assay involves detection of cell viability with luminescence. All polymers were non-toxic at concentrations of 0 to 200 μg/mL (Figure 10.6). A slight decrease in average cell viability is visible with increased concentration, but this decrease is within error of the experiment. Future work in this area should compare the cytotoxicity of these main-chain copolymers with imidazolium ionenes and vinyl imidazolium polymers with pendent ionic functionalities.

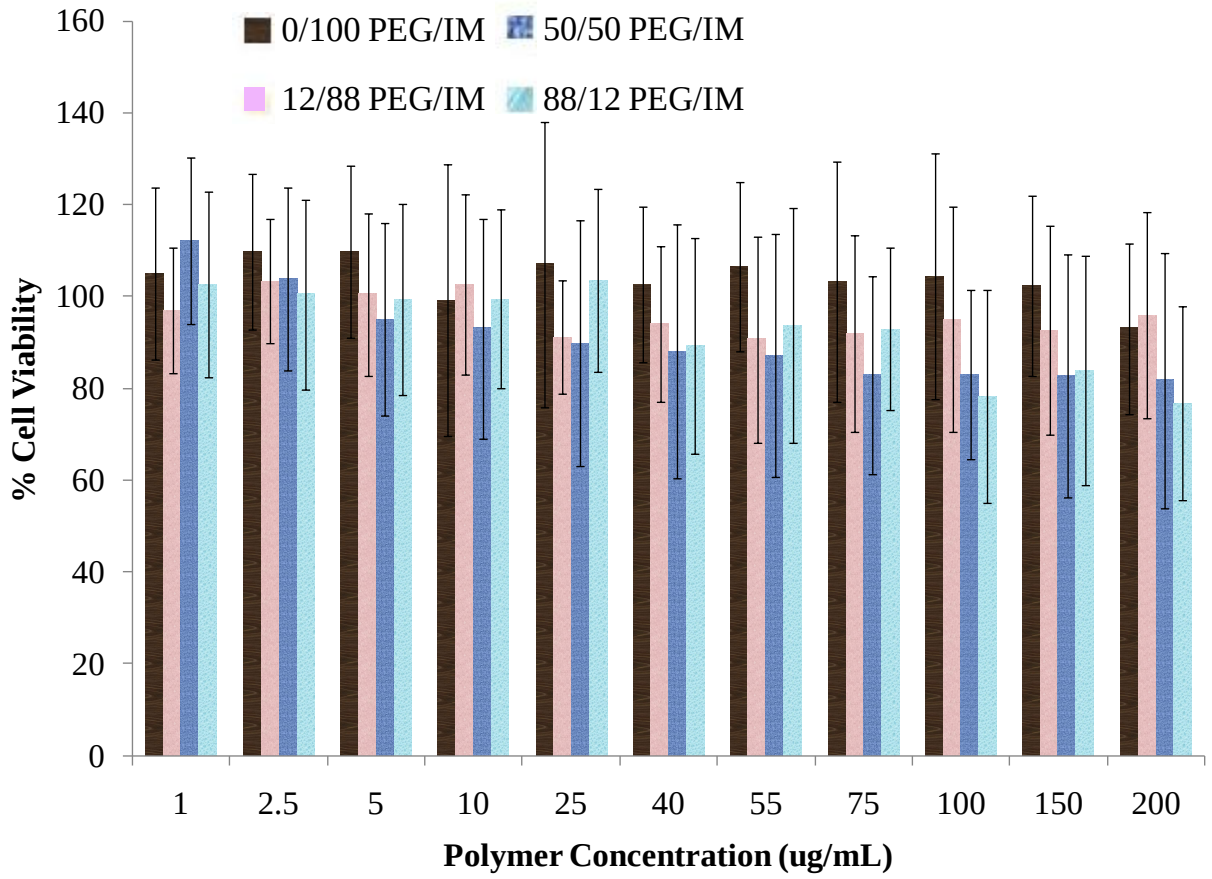

Figure 10.6. MTT assay results based on a COS-7 cell line of PEG/imidazolium copolyesters with varied molar ratio of PEG to imidazolium diol; COS-7 cells (5000 cells/well) incubated for 24 hours at 37 ºC

In addition to cytotoxicity, the capability of main-chain imidazolium-based polyesters to bind to DNA was examined (Figure 10.7). The polymers were incubated with 1X TAE solution in the presence of DNA, and electrophoresis was used to analyze whether the polymer bound to DNA. A polymer that efficiently binds to DNA to form a polyplex will not travel through the agarose gel and will remain at its starting electrode. DNA not bound to polymer will travel through the gel as 70 volts are applied across the agarose gel. Polymers with both 100% and 50% molar imidazolium diol to PEG in their polyester compositions did not bind efficiently to DNA at any concentration (Figure

10.7). It is hypothesized that including the imidazolium unit in the main chain rather than pendant to the main chain has a dramatic effect on DNA binding efficiency. When including an ionic site pendant to the main chain, the mobility of this site helps allows enhanced aggregation which in turn increases the glass transition temperature of the polymer.[23] Thus, it is hypothesized that a study of main-chain imidazolium-based polymers versus pendant imidazolium-based polymers would reveal that pendant sites would also improve DNA binding through enhanced electrostatic interaction. However, a direct comparison is not apparent in the present literature for these polymers.

Previous research in our group has evaluated ammonium-based polymers with pendant ammonium groups to the main polymer chain which effectively bind DNA.[7] If a higher N-to-P ratio or a higher amount of imidazolium polymer to DNA is used, we may eventually see some binding activity. At typical conditions or concentrations that were used in this experiment and studied previously for other polymers, these main-chain ionic polymers do not bind DNA effectively. The polymers were assumed random. Studying block versus random copolymer structure is needed to assess its effect on DNA binding. Future work should involve synthesis of pendant and main-chain imidazolium-based polyesters to compare their differences in cytotoxicity and DNA binding efficiency and confirm whether the restricted mobility of main-chain imidazolium functionalities prevents effective DNA binding and enhances biocompatibility.

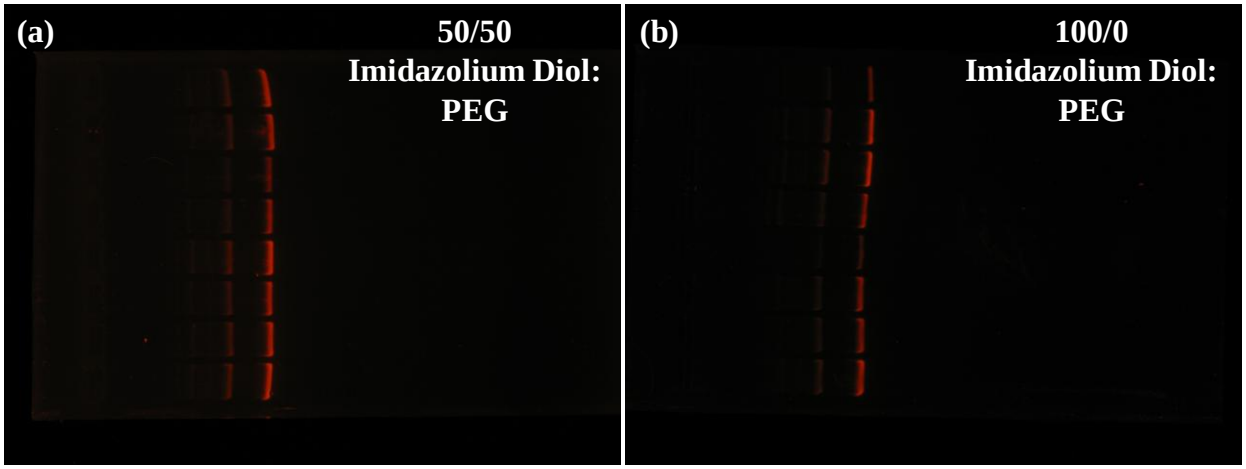

Figure 10.7. Agarose gel electrophoresis images of electrophoretic separations with (a) polyester composition of 50/50 molar ratio of imidazolium diol to PEG and (b) polyester composition with 100/0 molar ratio of imidazolium diol to PEG; N/P ratio of 4 for repeating unit structure, TAE buffer, ethidium bromide stain

10.5 Conclusions

We report the synthesis of biocompatible homopolymer and copolymer imidazolium-based polyesters via interfacial reactions. Copolymerizations with different ratios of imidazolium diol and PEG resulted in copolymers with 88/12, 50/50, and 12/88 imidazolium diol to PEG molar ratios. We evaluated the cytotoxicity of all of the polymers with MTT assays, and all polymers were non-toxic with concentrations under 200 μL/mg. Future directions will include evaluating the DNA binding efficiency of these main-chain imidazolium polymers compared to polymers with pendant imidazolium groups as well as SEC to determine molecular weights. These copolyesters will be compared to imidazolium-based ionenes and imidazolium-containing vinyl polymers in terms of cytotoxicity and DNA binding.

10.6 Acknowledgements

Research was sponsored by the Army Research Laboratory and was accomplished under Cooperative Agreement Number W911NF-06-2-0014. The views and conclusions contained in this document are those of the authors and should not be interpreted as representing official policies, either expressed or implied, of the Army Research Laboratory or the U.S. Government. The U.S. Government is authorized to reproduce and distribute reprints for Government purposes notwithstanding any copyright notation hereon. The authors would like to acknowledge Jenny B. England for help synthesizing and characterizing all water-soluble, imidazolium-based polyesters.

10.7 References

1. Luca, L.D. *Current Medicinal Chemistry* **2006**, 13, 1-23
2. Hui, David Y., Howles, Philip N. *Journal of Lipid Research* **2002**, *43*, 2017-2029
4. Bando, T.; Sugiyama, H. *Acc. Chem.Res.***2006,** *39*, 935-944.
5. Le Poul, N.; Campion, M.; Douzieche, B.; Rondelez, Y.; Le Clainche, L.; Reinaud, O.; Le Mest, Y. *J. Am. Chem. Soc.* **2007**, *129*, 8801-8810.
6. Emery, D. W. *Clinical and Applied Immunology Reviews* **2004**, *4*, 411-422.
7. Layman, J. M. Structure-Property-Transfection Relationships in Polycation-mediated Non-viral DNA Delivery. Ph.D. Thesis, Virginia Polytechnic and State University, Blacksburg, VA, 2008.
8. Palmer, D. H.; Young, L. S.; Mautner, V. *Trends in Biotechnology* **2006**, *24*, 76-82.
9. Kay, M. A.; Glorioso, J. C.; Naldini, L. *Nat. Med.* **2001**, *7*, 33-40.
10. Kaiser, J. *Science* **2007**, *317*, 580.
11. Demberelnyamba, D.; Kim, K.-S.; Choi, S.; Park, S.-Y.; Lee, H.; Kim, C.-J.; Yoo, I.-D. *Bioorganic & Medicinal Chemistry* **2004**, *12*, 853-857.
12. Dupont, J.; Suarez, P. A. Z. *Phys. Chem. Chem. Phys.* **2006**, *8*, 2441-2452.
13. Dupont, J.; Fonseca, G. S.; Umpierre, A. P.; Fichtner, P. F. P.; Teixeira, S. R. *J. Am. Chem. Soc.* **2002**, *124*, 4228-4229
14. Batra, D; Hay, D.N.T.; Firestone, M.A. *Chem. Mater.* **2007**, *19*, 4423-4431.
15. So, Y. H. *Macromolecules* **1992**, *25(2),* 516-520.
16. Nakajima, H.; Ohno, H. *Polymer* **2005**, 46, (25), 11499-11504.
17. Williams, S. R. Influence of Electrostatic Interactions and Hydrogen Bonding on the Thermal and Mechanical Properties of Step-Growth Polymers, Ph.D. Thesis, Virginia Polytechnic and State University, Blacksburg, VA, 2008.
18. Williams SR, Cruz DS, Winey KI, Long TE. "Ionene Segmented Block Copolymers Containing Imidazolium Cations: Structure-Property Relationships as a Function of Hard Segment Content," Polymer, accepted for publication.

19. Hofmann K. The Chemistry of Heterocyclic Compounds, Imidazole and Derivatives Part 1. Interscience Publishers, Inc.: New York, New York, 1953.
20. Mosmann, T. *J Immunol Methods* **1983**, 65, (1-2), 55-63.
21. Denizot, F.; Lang, R. *J Immunol Methods* **1986**, 89, (2), 271-7.
22. Carmichael, J.; DeGraff, W. G.; Gazdar, A. F.; Minna, J. D.; Mitchell, J. B. *Cancer Res* **1987**, 47, (4), 936-942.
23. Saito, T.; Mather, B. D.; Costanzo, P. J.; Beyer, F. L.; Long, T. E. *Macromolecules* **2008**, *41*, 3503-3512.

Chapter 11: Overall Conclusions

11.1 Concluding Statement

Small changes in the type, placement, and number of ionic sites pendant to or part of the main chain can result in large changes in bulk polymer thermal, mechanical, and morphological properties.[1] Physical crosslinking due to ionic aggregation can restrict mobility and enhance moduli,[1] and ionic sites in the polymers can facilitate ionic conductivity for actuation in electro-active applications[2-4] or can impart self-healing capability.[5] Random ionomers[1, 6-11] with pendant anionic sites randomly distributed along the main chain are abundant in present literature, and these anionomers frequently have carboxylate[6-7, 9, 12-14] or sulfonate[8, 15-16] ions with mobile cations not tethered to the main chain. Polymers with a cationic-containing main chain and mobile anions are less common but often involve ammonium cationic sites.[9, 17-19] Phosphonium ions also can electrostatically aggregate in polymers like ammonium ions,[20-21] and they often have greater antimicrobial activity[22] and thermal stability[23] compared to ammonium ions with similar chemical structures. Little is published on phosphonium cationomers,[25-36] but advantages of using phosphonium cations presented in this thesis should encourage future research in the field of phosphonium-containing polymers.

In this dissertation, we described syntheses of main-chain and pendant phosphonium ions in polymers and regular placement of these ionic sites. We illustrated syntheses of several phosphonium-based monomers and polymers and their potential use in composite and smart material applications. In this thesis, we examined the synthesis of various phosphonium-containing monomers and endcapping reagents to synthesize ionic polyesters, ionic networks formed from Michael addition reactions, ionomer composites with networks formed from

Michael addition, ionic polyurethanes, and ionic diblock copolymers. The amount and structure of phosphonium functionalities in the polymers influenced polymer processability, solubility, and mechanical strength. For example, in phosphonium-based polyesters with ionic concentrations less than 7.7 mole %, the large size of the phosphonium cation promoted only weak electrostatic associations within the polymers, and these weak associations prevented disadvantageous effects on processing often seen with sodiosulfonate ionomers.[8] With high ionic concentration, phosphonium-based polymers like the phosphonium-based polyurethanes physically crosslinked and were difficult to dissolve.

Most of our investigations focused on ionomers synthesized through step-growth reactions. We successfully endcapped poly(ethylene terephthalate)-*co*-poly(ethylene isophthalate) with 1.3 to 7.7 mole % phosphonium groups, controlling molecular weight and producing telechelic ionomers. The synthesis of numerous, novel phosphonium-based hydroxyl or carboxylic acid containing endcapping reagents led to a systematic study of phosphonium cation thermal stability for inclusion of these reagents in melt polyesterification at 220 °C. The phosphonium cation, butyl *p*-carboxyphenyl diphenylphosphonium bromide, survived melt reactions at temperatures above 220 ºC for several hours to produce telechelic polyester ionomers. Weak phosphonium ionic aggregation provided melt processable polymers with controlled molecular weight. Rheological results suggested that there was no appreciable ionic aggregation above 120 °C, and the glass transition temperatures were ~65 °C for number average molecular weights ranging from 5,100 to 9,900 g/mole with 7.7 to 1.3 mole % phosphonium endcapping reagent.

Additionally, we elucidated the synthesis of the first ion-containing networks from Michael addition reactions containing either a novel bisphosphonium-containing bisacetoacetate

(bisacac) or a novel bisimidazolium-based bisacac. Michael addition of bisacetoacetates and PEG diacrylates produced crosslinked films with gel fractions greater than 96 to 98% and clear, transparent films. Bisphosphonium-based, bisimidazolium-based, and non-ionic networks were compared. Bisphosphonium networks possessed the broadest glass transition temperatures and also an increased glass transition compared to the imidazolium-containing and non-ionic crosslinked films. The bisphosphonium-based networks also had greater strain at break and greater stress at break than the imidazolium-based or non-ionic networks. Equilibrium ionic liquid uptake experiments with 1-ethyl-3-methylethyl imidazolium sulfate in bisphosphonium-based, bisimidazolium-based, and non-ionic networks indicated no preferential uptake for the imidazolium ionic liquid for imidazolium versus bisphosphonium functionalities. Uptake was independent of the type of ionic group, but the non-ionic network displayed the least uptake, much lower than respective ionic films through absorbing 2.5-times less ionic liquid compared to ionic analogs. Additionally, ionic and non-ionic crosslinked fibers synthesized through Michael addition reactions were electrospun for the first time.

Composites of both bisphosphonium and non-ionic networks from through Michael addition crosslinking reactions in the presence of unfunctionalized MWCNTs had enhanced moduli and surface resistivities compared to networks without nanotubes. MWCNT composites did not possess significantly changed glass transition temperatures for polymers with 0, 1, 3, or 5 weight % MWCNTs, but the plateau moduli increased with carbon nanotube loading for both ionic and non-ionic networks as expected. Networks with bisphosphonium functionalities exhibited a 4-fold increase in Young's moduli, and non-ionic ones displayed a 3-fold increase forming composites with 0 to 5 weight % MWCNTs. Surface resistivities decreased by an order

of magnitude for all bisphosphonium films versus non-ionic analogs with the same weight % MWCNTs.

To examine the combination of phosphonium aggregation, hydrogen bonding, and crystallinity in high performance polymers, we synthesized phosphonium-based polyurethanes. The first-time synthesis of a new family of phosphonium-based ionic polyurethanes with varied hard segment and ionic contents was described. Cast films showed unique shape memory and film formation, and increasing hard segment content broadened glass transition temperatures, increased plateau moduli, and decreased the melting point of the PEG segment. SAXS was utilized to measure the inter-aggregate spacing. SAXS profiles showed a shift in the maximum scattering vector with ionic content which indicated that an increase in ionic content decreased the spacing between ionic aggregates. AFM and TEM also indicated large, circular features in phosphonium-containing polyurethanes.

Inclusion of phosphonium sites as pendant groups along the main chain through chain-growth polymerization of novel phosphonium-based monomers was also studied. Two novel, phosphonium-containing methacrylate monomers, (6-UMH)TOPBr and (2-UMH)TOPBr, were successfully synthesized. RAFT copolymerization with polystyrene macroinitiators generated microphase separated phosphonium-based diblock copolymers. AFM images showed possible microphase separation in all of the diblock copolymers with soft phases from 15-20 nm and hard phases from 20-50 nm. We also elucidated the synthesis of two novel bisphosphonium bisphenols for future use in high performance polymers, and we evaluated the cytotoxicity of several main-chain imidazolium-based polyesters with varied imidazolium content. All of the imidazolium salt-containing polymers were found to be relatively non-toxic.

Overall, we described the synthesis of a new family of phosphonium-based monomers and polymers. We included these monomers in or pendant to the main chain and studied their resultant thermal, morphological, and rheological properties. Inclusion of phosphonium functionalities broadened glass transition temperatures in various types of polymers, and ionic crosslinking provided enhanced mechanical performance, plateau moduli, and Young's moduli. Resistivities were also lowered in phosphonium-based polymers compared to non-ionic analogs, and phosphonium aggregation had a profound influence on crystalline melting points and rigidity. Through elaboration of phosphonium-based polymer syntheses and applications in this dissertation, we hope to inspire a wealth of future research with phosphonium ion-containing macromolecular materials.

11.2 References

1. Eisenberg, A.; King, M., *Ion-Containing Polymers*. Academic Press: New York, 1977.
2. Duncan, A. J.; Akle, B. J.; Long, T. E., Leo, D. J. *Smart Mater. Struct.* **2009**, *18*, 104005.
3. Duncan, A. J.; Leo, D. J.; Long, T. E. *Macromolecules* **2008**, *41(21)*, 7765-7775.
4. Brown, R. H.; Duncan, A. J.; Choi, J.-H.; Park, J. K.; Wu, T.; Leo, D. J.; Winey, K. I.; Moore, R. B.; Long, T. E. *Macromolecules* **2010**, *43(2)*, 790-796.
5. Kalista, S. J.; Ward, T. C. *J. R. Soc. Interface* **2007**, *4(13)*, 405-411.
6. Eisenberg, A.; Hird, B.; Moore, R. B. *Macromolecules* **1990**, *23*, 4098-4107.
7. Eisenberg, A.; Kim, J.-S., *Introdcution to Ionomers*. John Wiley & Sons, Inc.: New York, 1998.
8. Kang, H.; Lin, Q.; Armentrout, R. S.; Long, T. E. *Macromolecules* **2002**, *35*, 8738-8744.
9. Tant, M. R.; Mauritz, M. R.; Wilkes, G. L., *Ionomers: Synthesis, Structure, Properties and Applications*. Blackie Academic & Professional: New York, 1997.
10. Grady, B. P. *Polymer Engineering and Science* **2008**, *48(6)*, 1029-1051.
11. Berti, C.; Colonna, M.; Binassi, E.; Fiorini, M.; Karanam, S.; Brunelle, D. J. *Reactive and Functional Polymers* **2010**, *70(6)*, 366-375.
12. Buruiana, T.; Buruiana, E. C. *Journal of Applied Polymer Science* **2005**, *96*, 577–582.
13. Lahor, A.; Nithitanakul, M.; Grady, B. P. *European Polymer Journal* **2004**, *40*, 2409–2420.
14. Ibarra, L.; Alzorriz, M. *Journal of Applied Polymer Science* **2003**, *87(5)*, 805-813.
15. Saito, T., Mather, B. D.; Costanzo, P. J.; Beyer, F. L.; Long, T. E. *Macromolecules* **2008**, *41*, 3503-3512.
16. Paddison ,S. J. *Annual Review of Materials Research* **2003**, 33, 289-319.

17. Buruiana, E.C.; Buruiana, T.; Melinte, V.Reactive & Functional Polymers **2006**, *66(10)*, 1132-1140.
18. Pazhanisamy, P., Ariff, M.; Anwaruddin, Q. *Journal of Applied Polymer Science* **2005**, *98(3)*, 1100-1105.
19. Tsou, A. H.; Duvdevani, I.; Agarwal, P. K. **2004**, 45(10), 3163-3173.
20. Karaman, H.; Barton, R. J.; Robertson, B. E.; Lee, D. G. *J. Org. Chem.* **1984**, *49*, 4509-4516.
21. Jin, R. ; Aoki, S. ; Shima, K. *Chem. Commun.* **1996**, 1939-1940.
22. Xie, W.; Xie, R.; Pan, W.; Hunter, D.; Koene, B.; Tan, L.; Vaia, R. *Chem. Mater.* **2002**, *14*, 4837-4845.
23. Kanazawa, A.; Ikeda, T.; Endo, T., *Journal of Polymer Science: Part A: Polymer Chemistry* **1993**, *31*, 335-343.
24. Parent, J. S.; Penciu, A.; Guillen-Castellanos, S. A.; Liskova, A.; Whitney, R. A. *Macromolecules* **2004**, *37*, 7477-7483.
25. Zhou, P.; Blumstein, A. *Polymer* **1997**, *38(3)*, 595-604.
26. Jenkins, I. H.; Kar, A. K.; Lindsell, W. E.; Murray, C.; Preston, P. N.; Wang, C.; Wherrett, B. S. *Macromolecules* **1996**, *29(20)*, 6365-6370.
27. Seyferth, D.; Masterman, T. C. *Macromolecules* **1995**, *28*, 3055-3066.
28. Lindsell, W. E.; Radha, K.; Soutar, I.; Stewart, M. J. *Polymer* **1990**, *31*, 1374-1378.
29. Atmaca, L.; Kayihan, I.; Yagci, Y. *Polymer* **2000**, *41*, 6035-6041.
30. Kanazawa, A.; Ikeda, T. *Coordination Chemistry Reviews* **2000**, *198*, 117-131.
31. Mather, B. D.; Baker, M. B., Beyer, F. L.; Green, M. D.; Berg, M. A. G.; Long, T. E. *Macromolecules* **2007**, *40*, 4396-4398.
32. Nishikubo, T.; Koichi, A.; Uchida, J. *Makromol. Chem.* **1989**, *190*, 1471-1482.
33. Nishikubo, T.; Uchida, J.; Matsui, K.; Iizawa, T. *Macromolecules* **1988**, *21*, 1583-1589.
34. Tomoi, M.; Kori, N.; Kakiuchi, H. *Makromol. Chem.* **1986**, *187*, 2753-2761.
35. Kenawy, E.; Abdel-Hay, F. I.; El-Shanshoury, E. R.; El-Newehy, M. H. *Journal of Polymer Science: Part A: Polymer Chemistry* **2002**, *40*, 2384-2393.
36. Parent, J. S.; Liskova, A.; Resendes, R. *Polymer* **2004**, *45*, 8091-8096.